

G18970

**STUDIES ON MAGNETIC IRON OXIDE LOADED  
ACTIVATED CARBON**

**THESIS SUBMITTED TO THE  
COCHIN UNIVERSITY OF SCIENCE AND TECHNOLOGY  
IN PARTIAL FULFILMENT OF THE REQUIREMENTS  
FOR THE DEGREE OF**



**DOCTOR OF PHILOSOPHY  
IN**

**ENVIRONMENTAL STUDIES**

**UNDER THE FACULTY OF ENVIRONMENTAL STUDIES**

**BY**

**BALACHANDRAN M.**

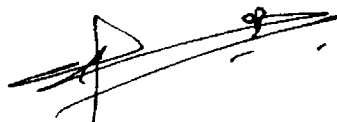
**SCHOOL OF ENVIRONMENTAL STUDIES  
COCHIN UNIVERSITY OF SCIENCE AND TECHNOLOGY  
COCHIN-682 022**

**OCTOBER 2004**

## DECLARATION

I Balachandran M. do hereby declare that the thesis entitled **“STUDIES ON MAGNETIC IRON OXIDE LOADED ACTIVATED CARBON”** is an authentic record of research work done by me under the supervision of Dr. V. N. Sivasankara Pillai, Professor, School of Rural Development and Appropriate Technology, Cochin University of Science and Technology. This work has not been previously formed the basis for the award of any degree or diploma of this or any other University/Institute.

Cochin -22,  
October 2004.



**BALACHANDRAN M.**

## CERTIFICATE

This is to certify that the thesis entitled “**STUDIES ON MAGNETIC IRON OXIDE LOADED ACTIVATED CARBON**” is an authentic record of research work carried out by **Mr. Balachandran M.** under my supervision and guidance in partial fulfilment of the requirements for the degree of Doctor of Philosophy and no part thereof has been presented for the award of any degree in any University/Institute.



Dr.V. N. Sivasankara Pillai,  
Professor,  
School of Rural Development and  
Appropriate Technology,  
Cochin University of Science and Technology,  
Cochin - 682 022.

Cochin -22  
October 2004.

## ACKNOWLEDGEMENT

*I wish to express my profound thanks and deepest sense of gratitude to **Prof. Dr. V. N. Sivasankara Pillai**, Director, School of Rural Development and Appropriate Technology, Cochin University of Science and Technology, for unfailing guidance, constant encouragement, invaluable suggestions, moral support and critical comments throughout the course of this investigation.*

*I express my gratitude to **Prof. Dr. Ammini Joseph**, Director, School of Environmental Studies, Cochin University of Science and Technology as well as to **Prof. Dr. A. Mohandas**, former Director, School of Environmental Studies for making the facilities available in the School and for their constant encouragements.*

*I place on record my sincere thanks to **Dr. V. Sivanandan Achari** for his valuable suggestions and critical evaluation towards the completion of this write up. I also thank **Dr. M. V. Hareendranathan Nair** and all the other faculty members of the School for the help and encouragement rendered by them.*

*I am beholden to **Dr. M. R. Anantharaman** of Department of Physics, CUSAT for his constant encouragement and help during the course of this work. I express my sincere thanks to **Dr. P. M. Joy**, NCL, Pune for providing me with magnetization data and **Prof. Dr. Ajay Gupta**, **Dr. D. M. Phase** and **Dr. N. P. Lalla** of IUC – DAE, Indore for Mossbauer, XRD and SEM analysis. My appreciation is due to **Mr. Amit Saraiya** and **Mr. Suresh Bharadwaj**, IUC-DAE, Indore for helping me with the physical characterization of the samples. I also acknowledge **Prof. Dr. P. Madhavan Pillai** for his encouragement and support.*

*I place on record my sincere thanks to **Dr. Abdul Rasheed**, chief manager (R&D), Sud – Chemie India ltd., Edayar, Cochin for providing me with gas adsorption data at a critical period of this study. **Mr. Joseph Thomas**, Manager, Indo German Carbon India Pvt. Ltd was kind enough to provide me with activated carbon samples and my sincere gratitude is recorded here. I am indebted to **Prof. Dr. K. E. George**, Dept. of Polymer Science and Rubber Technology for providing me with TGA data. Also express my since thanks and appreciation to **Dr. Ratheesh** and **Dr. P. D. Sasidharan**, C-MET, Athani, Thrissur for their help. A number of individuals have helped me in various ways during the course of this work*

*while it is impossible to mention all of them, I note the following in particular with appreciation: **Dr. Peeter K Varkey, Mr. Rajesh Babu V. G, Mr. Alex, P. M., Mr. Manuraj, Ms. Suja Devi Priya, Dr. Girish Gopinath, Dr. Reji Srinivas, Mr. K. R. Baiju, Mr. Laluraj, Mr. Sunil P. S, Ms. Valsamma Joseph, Mr. N. S. JayaPrakash, Mr. Anas Abdul Azeez , Mr. Abhilash, Mr. Binu and Mr. Nilof** who have helped me with immense dedication. I wish to place on record my sincere thanks to **Ms. Bindu B. K and Ms. Rema** for their support and help.*

*I thank my dear friends **Mr. Shery M. A, Manu B, Mr. Biju Chacko, Mr. Abdul Shereef and Mr. Vincent Joseph** for their moral support. I also remember with gratitude the support given to me by **Ms. Suja Sunil Thomas**. I also recall the help rendered by the staff members of the School of Environmental Studies.*

*I owe my family and **Praveena** who stood behind me in the ups and downs and gave me inspiration and moral support for the successful completion of this task.*

## PREFACE

Adsorption of organic and inorganic molecules on activated carbon is one of the classical and best studied methods in separation science and finds application in a variety of fields extending from perfumery, drug synthesis and application, waste water treatment and control of odour in emissions. The process involved is essentially phase separation of target compounds from solution or gas phase to solid. Contacting the solid with the medium under optimal flow conditions and its recovery poses engineering challenges. Many of such challenges have been solved. Unless a breakthrough in approach is evolved, the application of activated carbon is likely to become a classical subject devoid of innovations.

The application of activated carbon in the flow through mode is limited to powdered activated carbon (particle size below 149  $\mu\text{m}$ ). The adsorption dynamics are very favourable, but the challenge is in separating the fine particles after adsorption. Flocculation and settling requires additional devices, chemicals and precise control of operating conditions at the post adsorption stage. If this stage is made more operator friendly and cost effective, powdered activated carbon will be a preferred material, especially in large scale flow- through applications.

This dissertation deals with investigations in the following aspects of activated carbon:

1. Preparation of a magnetic iron oxide activated carbon composite that has magnetic properties. The idea behind a magnetized activated carbon is that it could be recovered using non-invasive methods in a flow through mode of application. It is also important to optimize the method of preparation. As part of this work procedures were evolved to prepare magnetized activated carbon samples with different iron oxide loading.

2. Physical and chemical characterization of a new material is very important to understand its desired properties. The effects of impregnation of magnetic iron oxide on the carbon matrix are made out from these studies. There are a number of standard methods used for the physical and chemical characterization of activated carbons. And this aspect of characterization forms an important section in this dissertation.
3. The preparation of any modified material requires an evaluation of its desired qualities. Any modification should not significantly sacrifice other desired qualities of the original material. The loss in adsorption capacity due to iron oxide impregnation was quantitatively evaluated to understand the influencing factors.
4. The application of a non-invasive magnetic separation for the recovery of spent activated carbon from the process stream requires system optimization. There are many critical parameters in the recovery of carbon particles. The influence of these parameters on retention efficiency was studied in the bench scale. The design parameters for a full scale set up can be derived from these bench scale experiments.

## CONTENTS

<b>Chapter 1</b>	<b>Page No.</b>
<b>Introduction</b>	1
1.1 History	1
1.2 Forms of Activated Carbons	2
1.2.1 Physical Forms	3
1.2.2 Choosing Between Two Forms	3
1.2.3 Properties of Two Forms	4
1.3 Preparation of Activated Carbon	5
1.3.1 Starting Materials	6
1.3.2 Activation Process	6
1.4 Physical and Chemical Properties	8
1.4.1 Structure	8
1.4.2 Surface Area	9
1.4.3 Porosity	9
1.4.4 Surface Functional Groups	11
1.4.4a Surface Acidity	12
1.4.4b Electrophoretic Characteristics	14
1.5 Adsorption Equilibria and Isotherms	14
1.5.1 A Review of Adsorption Fundamentals	14
1.5.2 Henry's Law - Linear Adsorption Isotherm	15
1.5.3 Langmuir Adsorption Isotherm	16
1.5.4 Freundlich Adsorption Isotherm	18

1.5.5	Brunauer Emmett Teller Adsorption Isotherm	19
1.5.6	Kinetics of Adsorption	21
1.6	Applications of Activated Carbon	23
1.6.1	Water Treatment	24
1.6.2	Odour Control	26
1.6.3	Activated Carbon Fibers	26
1.6.4	Gas Separation and Storage	27
1.6.5	Refrigeration and Heat Pumping	30
1.6.6	Recovery of Gold	30
1.6.7	Electrical Applications	31
1.6.8	In Food Industry	31
1.6.9	Miscellaneous Applications	32
1.7	Impregnated Activated Carbons	32
1.8	Comparison of GAC and PAC	35
1.9	Limitations of Activated Carbon Application	36
1.10	Scope of the Work	37

## **Chapter 2**

### **Preparation and Characterization of Magnetic Iron**

#### **Oxide Loaded Activated Carbons** 39

2.1	Introduction	39
2.2	Preparation	39
2.2.1	GAC	40
2.2.2	Magnetic Iron Oxide (MIO)	40
2.2.3	MGAC5	41

2.2.4	MGAC7	42
2.2.5	MGAC9	43
2.3	Physico-Chemical Characterization Studies	43
2.3.1	Materials	43
2.3.2	Methods	45
2.3.3	Results and Discussion	52
2.2.3a	pH	52
2.2.3b	Absolute Density	52
2.2.3c	Total Ash	53
2.2.3d	Iron Loading	54
2.2.3e	Iodine Number	56
2.2.3f	Scanning Electron Microscopy	57
2.2.3g	N <sub>2</sub> Gas Adsorption Studies	59
2.2.3h	X-Ray Diffraction Studies	63
2.2.3i	Mossbauer Spectroscopic Studies	65
2.2.3j	Magnetization Studies	66
2.2.3k	Thermal Gravimetric Analysis	68

### **Chapter 3**

	<b>Adsorption Studies on Activated Carbon - Magnetic Iron Oxide Composites</b>	70
3.1	Introduction	70
3.2	Materials	71
3.3	Methods	73
3.3.1	Adsorption Equilibrium Studies	73
3.3.2	Adsorption Kinetics Studies	74

3.3.3	Regeneration Studies on Composites	75
3.4	Results and Discussion	76
3.4.1	Adsorption of Phenol on Activated Carbon - Magnetic Iron Oxide Composites	76
3.4.1a	Adsorption Kinetics	78
3.4.1b	Adsorption Isotherm Studies	81
3.4.1c	Evaluation of Thermodynamic Parameters	86
3.4.2	Adsorption of p-Nitrophenol on Activated Carbon - Magnetic Iron Oxide composites	87
3.4.2a	Adsorption Kinetics	88
3.4.2b	Adsorption Isotherm Studies	90
3.4.2c	Evaluation of Thermodynamic Parameters	94
3.4.3	Regeneration Studies	95
3.4.4	Adsorption of Methylene Blue on Activated Carbon - Magnetic Iron Oxide Composites	96
3.4.4a	Kinetics of Adsorption	97
3.4.4b	Equilibrium Isotherm Studies using Methylene Blue	99
3.4.4c	Evaluation of Thermodynamic Parameters	103

## **Chapter 4**

### **Separation Studies on magnetic Iron Oxide**

#### **Loaded Activated Carbon** 105

4.1	Introduction	105
4.2	Materials and Methods	106
4.2.1	Materials	106
4.2.2	Methods	108
4.3	Results and Discussion	110
4.3.1	Separation Efficiency at Zero Magnetic Fields	110

4.3.2	Dependence of Retention Efficiency of Composite Samples on Iron Oxide Loading	111
4.3.3	Dependence of Retention Efficiency of Composites on Magnetic Field	112
4.3.4	Dependence of Retention Efficiency on Flow Velocity	113

## **Chapter 5**

	<b>Summary and Conclusion</b>	115
--	-------------------------------	-----

## **References**

## LIST OF TABLES

Table: 1.1	Worldwide production of activated carbon
Table: 1.2	Source materials that have been used for the production of activated carbon
Table: 1.3	Typical applications of impregnated activated carbons
Table: 1.4	List of frequently used impregnated carbons
Table: 2.1	Pore volumes of activated carbons.
Table: 2.2	Surface area of Activated carbons
Table: 2.3	Langmuir parameters for N <sub>2</sub> adsorption on carbon samples
Table: 2.4	Mossbauer parameters for binary iron oxides
Table: 3.1	Rate constants for phenol adsorption evaluated from Lagergren plots
Table: 3.2	Intraparticle diffusion rate constants for phenol adsorption
Table: 3.3	Langmuir parameters for phenol adsorption on carbon samples
Table: 3.4	Freundlich constants for the adsorption of phenol
Table: 3.5	Thermodynamic parameters for phenol adsorption
Table: 3.6	Rate constants for <i>p</i> -nitrophenol adsorption evaluated from Lagergren plots
Table: 3.7	Intraparticle diffusion rate constants for <i>p</i> -nitrophenol adsorption
Table: 3.8	Langmuir constants for the adsorption of <i>p</i> -nitrophenol
Table: 3.9	Freundlich constants for the adsorption of <i>p</i> -nitrophenol
Table: 3.10	Thermodynamic parameters for <i>p</i> -nitrophenol adsorption
Table: 3.11	Regeneration efficiency data on different carbon samples
Table: 3.12	Kinetic rate constants for methylene blue adsorption
Table: 3.13	Intraparticle diffusion rate constants for methylene blue adsorption
Table: 3.14	Langmuir constants for the adsorption of methylene blue
Table: 3.15	Freundlich constants for the adsorption of methylene blue
Table: 3.16	Thermodynamic parameters for methylene blue adsorption

## LIST OF FIGURES

- Figure 1.1.a Three dimensional structure of graphite
- Figure 1.1.b Turbostratic structure of carbon
- Figure 1.2 Schematic representation of a constituent region of the activated carbon particle
- Figure 1.3 Surface groups present on activated carbon
- Figure 1.4 Braunauer's classification of isotherms
- Figure 2.1.a Frequency curve for grain size distribution of activated carbon
- Figure 2.1.b Cumulative weight % vs Particle size of activated carbon
- Figure 2.2 A schematic representation of Mossbauer spectrometer
- Figure 2.3 A schematic of the variable sample Magnetometer
- Figure 2.4 Iron oxide loading on composite samples
- Figure 2.5.a Estimated iodine numbers for activated carbon samples
- Figure 2.5.b Reduction in iodine number with respect to the control carbon
- Figure 2.6 Isotherm plots for Nitrogen adsorption on the control carbon and the composite samples
- Figure 2.7 BET plots for the adsorption of N<sub>2</sub> on carbon samples
- Figure 2.8 Langmuir isotherm plots for N<sub>2</sub> adsorption on carbon samples at 77K
- Figure 2.9.a XRD pattern for magnetic iron oxide prepared in the laboratory
- Figure 2.9.b XRD pattern for MGAC7 at room temperature
- Figure 2.10.a Mossbauer spectrum of MIO at 298K
- Figure 2.10.b Mossbauer spectrum of MGAC7 at 298K
- Figure 2.11.a Magnetic distribution plot for iron oxide
- Figure 2.11.b Magnetic distribution plot for activated carbon iron oxide composite MGAC7
- Figure 2.12.a Hysteresis loop for MGAC5 obtained using VSM
- Figure 2.12.b Hysteresis loop for MGAC7 obtained using VSM
- Figure 2.12.c Hysteresis loop for MGAC9 obtained using VSM
- Figure 2.13 The process of magnetization in a demagnetized ferromagnet
- Figure 2.14 Plot showing the variation of saturation magnetization with iron oxide loading
- Figure 2.15.a TGA plots for GAC
- Figure 2.15.b TGA plots for MGAC5
- Figure 2.15.c TGA plots for MGAC7
- Figure 2.15.d TGA plots for MGAC9
- Figure 3.1.a Kinetic plots of phenol adsorption at 10°C
- Figure 3.1.b Kinetic plots of phenol adsorption at 20°C
- Figure 3.1.c Kinetic plots of phenol adsorption at 30°C
- Figure 3.1.d Kinetic plots of phenol adsorption at 40°C
- Figure 3.2.a Lagergren plot for phenol adsorption at 10°C
- Figure 3.2.b Lagergren plot for phenol adsorption at 20°C

- Figure 3.2.c Lagergren plot for phenol adsorption at 30°C
- Figure 3.2.d Lagergren plot for phenol adsorption at 40°C
- Figure 3.3.a Intraparticle diffusion plots for phenol adsorption on GAC
- Figure 3.3.b Intraparticle diffusion plots for phenol adsorption on MGAC5
- Figure 3.3.c Intraparticle diffusion plots for phenol adsorption on MGAC7
- Figure 3.3.d Intraparticle diffusion plots for phenol adsorption on MGAC9
- Figure 3.4.a Equilibrium adsorption isotherm plots of phenol on activated carbon composites at 10°C
- Figure 3.4.b Equilibrium adsorption isotherm plots of phenol on activated carbon composites at 20°C
- Figure 3.4.c Equilibrium adsorption isotherm plots of phenol on activated carbon composites at 30°C
- Figure 3.4.d Equilibrium adsorption isotherm plots of phenol on activated carbon composites at 40°C
- Figure 3.5.a Langmuir plots for phenol adsorption on GAC
- Figure 3.5.b Langmuir plots for phenol adsorption on MGAC5
- Figure 3.5.c Langmuir plots for phenol adsorption on MGAC7
- Figure 3.5.d Langmuir plots for phenol adsorption on MGAC9
- Figure 3.6 Reduction in the monolayer capacity for phenol adsorption for composites compared to the control carbon at different temperatures.
- Figure 3.7.a Freundlich plots of phenol adsorption on GAC
- Figure 3.7.b Freundlich plots of phenol adsorption on MGAC5
- Figure 3.7.c Freundlich plots of phenol adsorption on MGAC7
- Figure 3.7.d Freundlich plots of phenol adsorption on MGAC9
- Figure 3.8.a Plots of  $\ln KD$  vs  $1/T$  for phenol adsorption on GAC
- Figure 3.8.b Plots of  $\ln KD$  vs  $1/T$  for phenol adsorption on MGAC5
- Figure 3.8.c Plots of  $\ln KD$  vs  $1/T$  for phenol adsorption on MGAC7
- Figure 3.8.d Plots of  $\ln KD$  vs  $1/T$  for phenol adsorption on MGAC9
- Figure 3.9.a Concentration vs time graphs for *p*-nitrophenol adsorption at 10°C
- Figure 3.9.b Concentration vs time graphs for *p*-nitrophenol adsorption at 20°C
- Figure 3.10.a Lagergren plot for *p*-nitrophenol adsorption at 10°C
- Figure 3.10.b Lagergren plot for *p*-nitrophenol adsorption at 20°C
- Figure 3.10.c Lagergren plot for *p*-nitrophenol adsorption at 30°C
- Figure 3.10.d Lagergren plot for *p*-nitrophenol adsorption at 40°C
- Figure 3.11.a Intraparticle diffusion plots of *p*-nitrophenol adsorption on GAC
- Figure 3.11.b Intraparticle diffusion plots of *p*-nitrophenol adsorption on MGAC5
- Figure 3.11.c Intraparticle diffusion plots of *p*-nitrophenol adsorption on MGAC7
- Figure 3.11.d Intraparticle diffusion plots of *p*-nitrophenol adsorption on MGAC9

- Figure 3.12.a Adsorption of PNP on samples at 10°C
- Figure 3.12.b Adsorption of PNP on samples at 20°C
- Figure 3.12.c Adsorption of PNP on samples at 30°C
- Figure 3.12.d Adsorption of PNP on samples at 40°C
- Figure 3.13.a Langmuir plots of *p*-nitro phenol adsorption on GAC
- Figure 3.13.b Langmuir plots of *p*-nitro phenol adsorption on MGAC5
- Figure 3.13.c Langmuir plots of *p*-nitro phenol adsorption on MGAC7
- Figure 3.13.d Langmuir plots of *p*-nitro phenol adsorption on MGAC9
- Figure 3.14 Reduction in the monolayer capacity for *p*-nitrophenol adsorption for composite samples compared to the control carbon at different temperatures.
- Figure 3.15.a Freundlich plots of *p*-nitrophenol adsorption on GAC
- Figure 3.15.b Freundlich plots of *p*-nitrophenol adsorption on MGAC5
- Figure 3.15.c Freundlich plots of *p*-nitrophenol adsorption on MGAC7
- Figure 3.15.d Freundlich plots of *p*-nitrophenol adsorption on MGAC9
- Figure 3.16.a Plots of  $\ln KD$  vs  $1/T$  of *p*-nitrophenol adsorption on GAC
- Figure 3.16.b Plots of  $\ln KD$  vs  $1/T$  of *p*-nitrophenol adsorption on MGAC5
- Figure 3.16.c Plots of  $\ln KD$  vs  $1/T$  of *p*-nitrophenol adsorption on MGAC7
- Figure 3.16.d Plots of  $\ln KD$  vs  $1/T$  of *p*-nitrophenol adsorption on MGAC9
- Figure 3.17.a Kinetic plots for methylene blue adsorption at 10°C
- Figure 3.17.b Kinetic plots for methylene blue adsorption at 20°C
- Figure 3.17.c Kinetic plots for methylene blue adsorption at 30°C
- Figure 3.17.d Kinetic plots for methylene blue adsorption at 40°C
- Figure 3.18.a Lagergren plots for methylene blue adsorption on GCA
- Figure 3.18.b Lagergren plots for methylene blue adsorption on MGAC5
- Figure 3.18.c Lagergren plots for methylene blue adsorption on MGAC7
- Figure 3.18.d Lagergren plots for methylene blue adsorption on MGAC9
- Figure 3.19.a Intraparticle diffusion plots for methylene blue adsorption on GAC
- Figure 3.19.b Intraparticle diffusion plots for methylene blue adsorption on MGAC5
- Figure 3.19.c Intraparticle diffusion plots for methylene blue adsorption on MGAC7
- Figure 3.19.d Intraparticle diffusion plots for methylene blue adsorption on MGAC9
- Figure 3.20.a Adsorption isotherms of methylene blue at 10°C
- Figure 3.20.b Adsorption isotherms of methylene blue at 20°C
- Figure 3.20.c Adsorption isotherms of methylene blue at 30°C
- Figure 3.20.d Adsorption isotherms of methylene blue at 40°C

- Figure 3.21.a Langmuir plots for methylene blue adsorption on GAC
- Figure 3.21.b Langmuir plots for methylene blue adsorption on MGAC5
- Figure 3.21.c Langmuir plots for methylene blue adsorption on MGAC7
- Figure 3.21.d Langmuir plots for methylene blue adsorption on MGAC9
- Figure 3.22 Reduction in monolayer capacity for methylene blue adsorption for composite samples compared to the control carbon at different temperatures.
- Figure 3.23.a Freundlich plots for the adsorption of methylene blue GAC
- Figure 3.23.b Freundlich plots for the adsorption of methylene blue MGAC5
- Figure 3.23.c Freundlich plots for the adsorption of methylene blue MGAC7
- Figure 3.23.d Freundlich plots for the adsorption of methylene blue MGAC9
- Figure 3.24.a Plots of  $\ln KD$  vs  $1/T$  for methylene blue adsorption on GAC
- Figure 3.24.b Plots of  $\ln KD$  vs  $1/T$  for methylene blue adsorption on MGAC5
- Figure 3.24.c Plots of  $\ln KD$  vs  $1/T$  for methylene blue adsorption on MGAC7
- Figure 3.24.d Plots of  $\ln KD$  vs  $1/T$  for methylene blue adsorption on MGAC9
- Figure 4.1 A schematic figure of the magnetic separation set up
- Figure 4.2 Particles retained in the settling column at zero magnetic field at flow velocity of 5.67 cm/s
- Figure 4.3 Particles retained in the settling column at zero magnetic field at flow velocity of 7.4 cm/s
- Figure 4.4 Particles retained in the settling column at zero magnetic field at flow velocity of 8.98 cm/s
- Figure 4.5 Retention vs Flow velocities for different particle sizes for MGAC5 at a field strength of 49G
- Figure 4.6 Retention vs Flow velocities for different particle sizes for MGAC5 at a field strength of 99G
- Figure 4.7 Retention vs Flow velocities for different particle sizes for MGAC5 at a field strength of 147G
- Figure 4.8 Retention vs Flow velocities for different particle sizes for MGAC7 at a field strength of 49G
- Figure 4.9 Retention vs Flow velocities for different particle sizes for MGAC7 at a field strength of 99G
- Figure 4.10 Retention vs Flow velocities for different particle sizes for MGAC7 at a field strength of 147G
- Figure 4.11 Retention vs Flow velocities for different particle sizes for MGAC9 at a field strength of 49G
- Figure 4.12 Retention vs Flow velocities for different particle sizes for MGAC9 at a field strength of 99G
- Figure 4.13 Retention vs Flow velocities for different particle sizes for MGAC9 at a field strength of 147G
- Plare1**
- a) SEM of control carbon, GAC
  - b) SEM of magentic iron oxide
  - c)) SEM of iron oxide loaded GAC (MGAC7)

# CHAPTER 1

## INTRODUCTION

### 1.1 History

Adsorption processes for water treatment have had a long and productive history. The use of carbon extends so far back into history that its origin is impossible to trace. Charcoal was used for drinking water filtration by ancient inhabitants in India and carbonized wood was used as a medical adsorbent and purifying agent by the Egyptians as early as 1500 B.C. (Cheremisinoff, P.N. & Morresi, A.C., 1980). The ability of many porous substances to adsorb vapours in large quantities has been recognized since the 18<sup>th</sup> century (McBain, J. W., 1932). One of the later adsorption applications is purification, such as the removal of H<sub>2</sub>S and obnoxious fumes from air and the removal of organic compounds from liquid water. Other examples of purification are the removal of odour and colour from edible oils, decolourisation in the sugar industry, and the removal of unwanted hydrocarbons in emissions. As early as 1785, the ability of charcoal to decolorize many liquids, including brandy was discovered. This discovery led to the application of wood and bone chars in the refining of cane and beet sugars (Achaerandio, I., *et al.*, 2002). Powdered activated carbon was first produced commercially in Europe in the early 19<sup>th</sup> century, using wood as a raw material (Weber, W. J., Jr., 1972). In the United States, the first production of activated carbon used black ash as the source, after it was accidentally discovered that the ash was very effective in decolorizing liquids (Mantell, C. L., 1968). Activated carbon has since been used extensively for this purpose in many industries. In particular, it has been commonly used for the removal of organic dyes from textile wastewaters (Barton, S. S., 1987).

The modern era of the application of granular activated carbon (GAC) began in the mid 1960's at Nitro, West Virginia, where the Kanawha River contained a variety of petrochemical compounds (Faust, S. D. & Aly, O. M., 1987). Over the last few decades adsorption has gained importance as a purification and separation process on an industrial scale. An account of world production of activated carbon is given in Table 1.1.

The largest market for activated carbon is currently in the municipal water purification industry, where charcoal beds have been used for the dual purpose of physical filtration and sorption (Faust, S. D. & Aly, O. M., 1983). In fact, activated carbon filters are used today in drinking water treatment to remove the natural organic compounds (i.e. tannins) that produce carcinogenic chlorinated by-products during chlorine disinfection of water. In wastewater treatment, activated carbon is usually used as a filter medium in tertiary treatment processes (Aly, O. M. & Faust, S. D., 1972). In these applications, carbon filters are usually quite effective in removing traces of organic compounds, as well as some inorganic metals.

### **Forms of Activated Carbons**

Activated carbons can be divided in two classes:

1. Gas adsorbent carbons, which are used for vapour phase recovery of fugitive solvents, gas separation etc.;
2. Carbon for liquid phase applications, which are used to decolorize or purify liquids, solutions and liquefiable materials such as waxes.

The main distinction between gas adsorbing and liquid phase carbons lies in the pore size distribution. Gas adsorbing carbons usually have the most pore volume in the micropore (less than  $20\text{\AA}$  radius) and in the macropore (larger than  $500\text{\AA}$  radius) ranges, with little pore volume in the transitional pores ( $50$  to  $500\text{\AA}$  radius).

Table 1.1 Worldwide production of activated carbon

Countries	Tonnes
United States of America	150,000
Holland	35,000
Germany	20,000
United Kingdom	16,000
France	12,000
Belgium	10,000
Philippines	15,000
Japan	30,000
India	5,000
Italy	4,000
Sri Lanka	3,000
Taiwan	1,000

(McKay, G., 1996)

Liquid phase activated carbons have significant pore volume in the transitional pore range permitting ready access of liquids to the micropore structure resulting in rapid attainment of adsorption equilibrium for smaller adsorbates (Hutchins, R. A., 1981).

### 1.2.1 **Physical Forms**

Liquid-phase activated carbons are available in two physical forms: granular and powdered. Some adsorption problems are best handled by passing the liquid through a bed of granular activated carbon. Others are handled most effectively by stirring powdered carbons with liquid to be treated and then removing the carbon by filtration or settling. Granular carbons generally will have particle sizes larger than 20 mesh U.S. Standard Sieve size (0.84mm) while powdered carbons generally will be 100% less than 100 mesh U.S. Standard Sieve size (0.149mm) (Hutchins, R. A., 1981).

### 1.2.2 **Choosing Between Two Forms**

The choice between granular and powdered carbon for a given application depends not only on comparative carbon purchase price but also on other factors such as type of existing equipment, the carbon usage rate, variability of flow rate, nature of application, cleanliness and mode of disposal of spent carbon.

In many cases, equipment already exists which lends itself to granular or powdered carbon treatment. At low carbon usage rates (less than about 250 Kg/d), reactivation and reuse of granular activated carbon is usually not economical. Since powdered carbons are generally less expensive than granular carbon, operating costs with powdered carbon could be lower. At higher carbons usage rates, granular carbon with reactivation is usually more economical. In cases where the flow rate, impurity concentration and composition vary dramatically, granular carbon will usually be

more suitable because adequate carbon would be present to compensate for the variation (Hutchins, R. A., 1981).

With powdered carbon, adsorption selectivity can be achieved by dosage control. With granular carbon, where a large mass of carbon is in contact with a relatively small volume of wastewater at any one time, substantially all adsorbable material can be removed. At carbon usage rates of 250 Kg/d or above, granular carbon can be economically reactivated. When granular carbon is not reactivated, it can be sewer, dumped or used as a landfill. With powdered carbons disposal of the spent carbon to a sewer to a municipal or industrial waste treatment plant is usually permissible. In cases where such a mode of disposal is not permitted, the disposal is usually by landfill or dumping. In cases where carbon has been used to remove hazardous materials from wastewater, special disposal methods are required.

### 1.2.3 **Properties of Two Forms**

Adsorptive capacity is the most important property with both granular and powdered carbons because it determines how much wastewater can be treated per unit of carbon. Adsorptive capacity determines both the direct operating cost for carbon treatment and the sizing of equipment (Hutchins, R. A., 1981).

With granular carbons, pressure drop in downflow and in confined upflow columns or bed expansion in unconfined upflow columns is of primary importance. The carbons contribution to head loss is controlled by sieving during manufacture and by particle shape. Bed expansion is determined by particle size, shape and size distribution, and by particle density. Head loss and bed expansion are design factors for carbon columns (Hutchins, R. A., 1981).

Attrition resistance of granular carbons is frequently miscalled hardness. This property is important because of the harsh way granular carbons are handled and

conveyed. Since the carbon is usually transferred in slurry form by pumping and dewatered by conveyers, resistance to attrition is important if carbon losses are to be minimized. Of the analytical procedures currently in wide use, the procedure given by American Society for Testing and Materials (ASTM D 5159 – 91., 1991) gives an abrasion number which appears to be the best indicator of relative handling and regeneration losses (Hutchins, R. A., 1981).

With powdered carbon, filterability is how fast a liquid at minimum pressure can be filtered through a given cross-section and depth of filter cake at maximum clarity. This property is dependant upon the raw material and some times, manufacturing procedure, both of which determine the typical particle size and size distribution. Poor filterability will cost short filter cycles and increased carbon treatment costs. In cases where the powdered carbon will be removed by settling, the carbon must stay in suspension long enough for adequate adsorption to occur but settle rapidly enough so the liquid being decanted or overflowing will not contain significant carbon particles.

Bulk density is important when powdered carbon is removed from the treated wastewater by filtration because it determines the weight of carbon that can be contained in a filter of given volumetric solids capacity. A carbon with a higher bulk density will provide faster settling rate and the volume of sludge, which will have to be handled and dewatered, will be less.

### 1.3 Preparation of Activated Carbon

Inasmuch as the sources of material for preparing activated carbon are many and diverse, the physical and chemical properties are expected to vary considerably. Activated carbon's remarkable adsorptive properties are due to its porous nature. Surface areas of pore walls range from 400 to 1,800 m<sup>2</sup>/g in various commercial

brands. When PAC and GAC were utilized first in drinking water treatment for colour, taste and odor removal, little attention was given to material source and surface characteristics of carbon. The trend today is to vary the carbon's activation process whereupon surface properties can be altered for specific purposes.

### 1.3.1 **Starting Materials**

Activated carbons have been commercially produced from a tremendous variety of carbonaceous starting materials (Hassler, J. W., 1974). A list of materials commonly used and studied is given in Table 1.2. It should be pointed out that some materials yield products of a unique porous structure, which can lead to being favored over other carbons in application in some fields. An example of a specialized physical property is carbon made from high density coconut shells. This starting material results in a carbon, which has a considerably finer pore-size distribution and greater apparent density in the final product than that produced from raw materials such as paper-mill waste (Mantell C.L., 1968). The effects of properties of the starting material are well understood at the present time. It has been suggested that molecular structure of cellulose-like starting materials, along with the distribution of the inorganic phase, may in some way act to promote the burn-off of certain undesirable portions of the starting material, leaving highly active skeletal structure behind (Mattson, J. S. & Mark, H. B., Jr., 1971).

### 1.3.2 **Activation Process**

Activation is a term generally used to refer to the overall working process of producing an "active" carbon which is capable of chemically or physically adsorbing certain species from dilute solution, either from gas or liquid phase. Overall reactions can be split into two steps.

Table 1.2 Source materials that have been used and studied for the production of activated carbon

Bagasse	Kelp and seaweed
Beet-sugar sludges	Lampblack
Blood	Leather waste
Bones	Lignin
Carbohydrates	Lignite
Cereals	Molasses
Coal	Nut shells
Coconut shells	Oil shale
Coffee beans	Peat
Corncobs and corn stalks	Petroleum acid sludge
Cottonseed hulls	Petroleum coke
Distillery waste	Potassium ferrocyanide waste
Fish	Pulp-mill waste
Flue dust	Rice hulls
Fruit pits	Rubber waste
Graphite	Sawdust
	Wood

(Hassler, J. W., 1974)

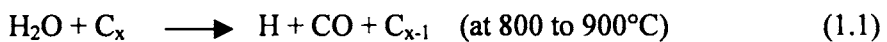
(i) *Carbonization*

The process, pyrolysis, is conducted usually in the absence of air. Temperatures below 600°C are preferable for producing chars suitable for steam activation (Hassler, J. W., 1974). . Many authors refer to activation as a process of heating a char to a sufficiently high temperature to cause the extensive burn off or degradation of non-carbon “impurities”, leaving a high surface area and highly porous product. The initial high-temperature treatment can be carried out without concomitant oxidation. However, if the heating step is carried out without the presence of oxygen, then oxidation of the material must be allowed to occur following the heating process in order to yield an “active” product.

(ii) *Oxidation*

The oxidation process, either in the gas phase or by solution reaction is very important with respect to the nature of the functional groups on the carbon surface and the equilibrium adsorption properties of activated carbons.

Many activation processes involve a reaction with oxidizing gases of steam, air, and CO<sub>2</sub> at elevated temperatures (Hassler, J. W., 1974). These reactions are as follows



Adsorptive powers and/ or capacity of the product are influenced by the chemical nature and concentration of the oxidizing gas, the reaction temperature, the extent to which the activation is conducted and the amounts and kinds of mineral ingredients in the char. In activation of many types of chars, steam is preferable to

CO<sub>2</sub> and is better than air as far as the surface area and porosity development are considered (Hassler, J. W., 1974).

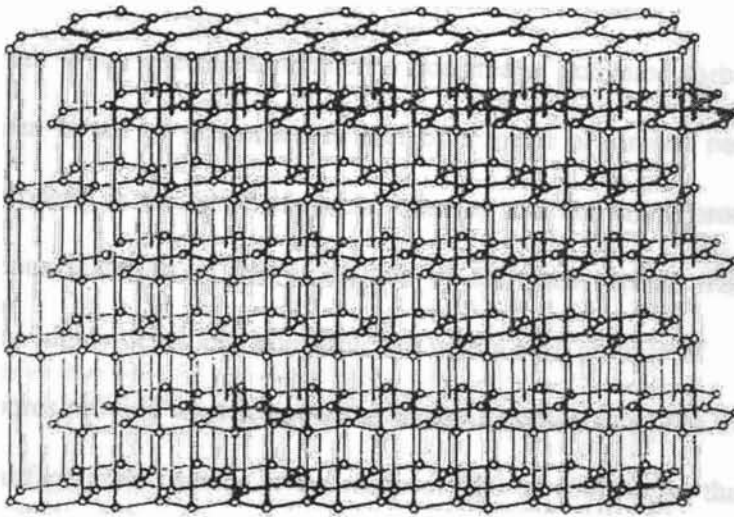
The oxidation step selectively erodes the surface, increasing the surface area and porosity and leaving the remaining atoms arranged in configurations that have specific affinities. Apparently not all adsorptive capacities develop simultaneously or at a uniform rate. A portion develops during the initial period of activation whereupon the capacity increases with time over a 60 minute period. There are many reports on kinetic studies of C-O<sub>2</sub> reaction at elevated temperatures (Wheeler, A., 1951; Gulbransen, E. A. & Andrew, K. F., 1952). When the activation was conducted at a temperature range of 600 to 800<sup>0</sup>C, the rate of reaction between carbon and oxygen was found to be one-half order with respect to the oxygen's partial pressure (Blyholder, G. & Eyring, H., 1957).

Following the activation process, carbon is washed with water for applications that require a low soluble ash. When a pH neutral carbon is needed, a suitable acid is added to remove the various basic oxides. After neutralization, the carbon is washed thoroughly with water, and Na<sub>2</sub>CO<sub>3</sub> to remove any traces of the acid.

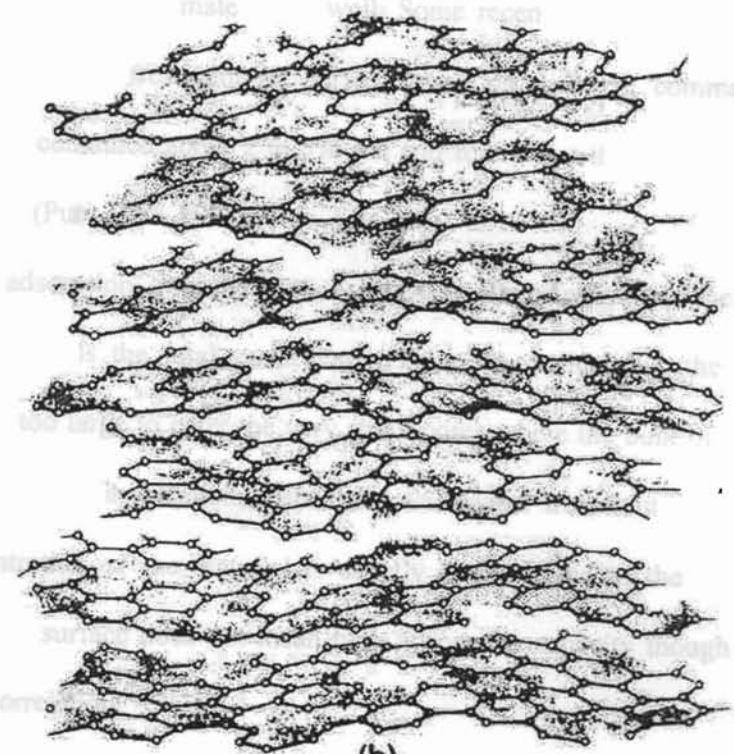
#### 1.4 **Physical and Chemical Properties**

##### 1.4.1 **Structure**

Activated carbons have a structure similar to the turbostratic carbon, having microcrystallites only a few layers in thickness and less than 100 Å in width. The level of structural imperfections in activated carbon microcrystallites is very high, which results in many possibilities for reactions of the edge carbons with their surroundings. Figure 1.1a & b illustrates the structures of graphite and turbostratic carbon of which activated carbons are similar to the latter type.



(a)



(b)

Figure 1.1 a) Three dimensional structure of graphite  
b) Turbostratic structure of carbon

#### 1.4.2 **Surface Area**

As sorption is viewed as a surface phenomenon, the surface area becomes an important parameter. Surface area is associated with the geometrical dimensions of the material. When one measures the surface area of activated carbon, the apparent surface area is out of proportion to that of a metal of similar particle size. This unusual property is the result of special charring and activation process used on all carbonaceous materials in the production of activated carbon. The result of this process is a highly developed pore structure within each granule of carbon. The walls of these pores provide what is known as internal surface area. The highly developed internal surface area, usually in the range of 500 to 1500 m<sup>2</sup>/g, that results in the extensive sorption properties of activated carbon. The surface area of GAC varies with the source of raw material as well. Some recent studies have investigated the effect of deashing treatment on surface areas on different commercial activated carbons that contained about 2 to 5% ash and found that the surface areas increased significantly (Puri, B.R., 1983).

In adsorption, only the wetted surface area is effective and the wetted surface area never equals the total surface area. In most applications, the material to be adsorbed is too large to enter the very small pores where the bulk of the surface area lays. But in many applications, especially wastewater treatment, neither the identity nor concentration of the material is exactly known. Due to the above mentioned reasons, high surface does not mean high adsorptive capacity though there is some degree of correlation.

#### 1.4.3 **Porosity**

The porous nature of carbon determines its adsorptive capacity to some extent. It is stated that over 99% of the active sites for adsorption in GAC are located in the

interior of the particle (Mattson, J. S., 1973). Figure 1.2 shows a schematic representation of a constituent region of an activated carbon particle where the macropores have diameters of 30 to 100,000 Å and the micropores are in the 10 to 30 Å range (Weber, Jr., W. J., 1967).

A cross section of a portion of an activated carbon particle might look like a maze of interconnecting channels, quiet large at the surface and terminating in small channels in the interior. Most adsorption on activated carbon takes place in the micropores with transitional and macropores providing access to the interior. Physical property such as porosity can be controlled to some degree to produce carbons suited for special applications. In a sense it can be stated that the adsorption of molecules from solution is strongly depended on the porous nature of the activated carbon. In solution adsorption case, this arises from the fact that mass transfer through the carbon pores limits the rate at which carbon can adsorb any species.

Various attempts have been made to employ physisorption measurements to determine the pore size distribution. BET (Brunauer-Emmett-Teller) nitrogen adsorption method (Brunauer, S. *et al.*, 1938) is now universally accepted as a standard procedure for the characterization of a variety of porous materials (Gregg, S. J. & Sing, K. S. W., 1982). Nitrogen is also the preferred adsorbate for the determination of mesopore size distribution. The general applicability of this method is partly dependant on the fact that the isotherm path followed by the nitrogen multilayer on a porous solid is remarkably insensitive to any change in the chemical nature of the surface (Carrott, P. J. M. *et al.*, 1982). The main disadvantage of nitrogen is that it is somewhat atypical in its molecular size, shape and micropore filling behaviour. Thus, nitrogen has been found (Roberts, A. R. *et al.*, 1987) to give consistently higher values of the effective pore volume than are obtained by the use of

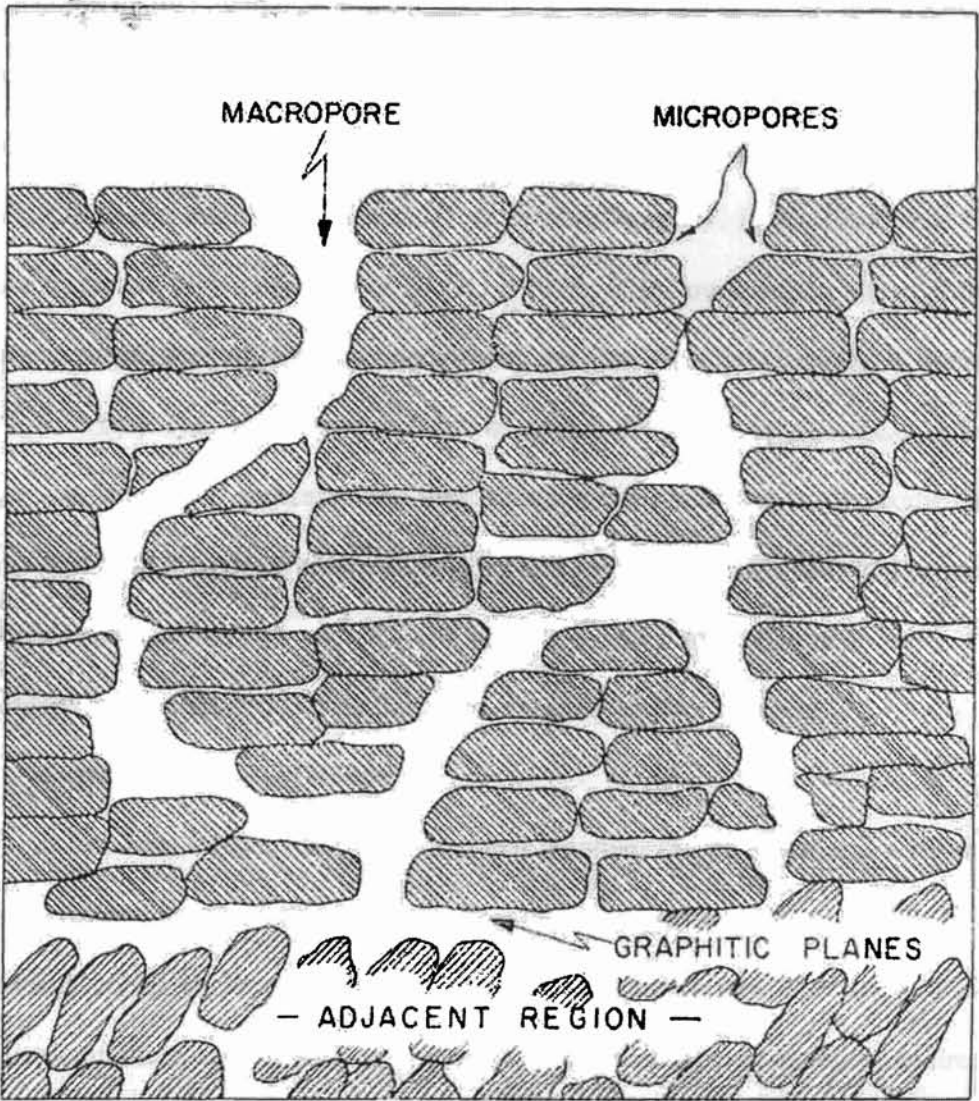


**Figure 1.2 Schematic representation of a constituent region of the activated carbon particle**

other adsorptives. The use of hydrocarbon vapors for the study of microporosity has been demonstrated on various microporous carbons having different ranges of pore size (Carrott, P. J. M. *et al.*, 1988). Some carbonaceous adsorbents have been found to give a surprisingly low uptake of nitrogen at 77 K. This is due to an “activated entry” effect (Maggs, F. A. P., 1953), which is associated with the slow diffusion of the adsorbate molecules through very narrow pore entrances or constrictions. In such cases, it has been established (Marsh, H. & Wynne-Jones, W. F. K., 1964) that the uptake of carbon dioxide (at 195 or 273 K) is likely to be much larger, although the minimum dimensions of the two molecules are not very different (for CO<sub>2</sub>, 0.28 nm; for N<sub>2</sub>, 0.30 nm). The most important factor in causing the greater uptake of CO<sub>2</sub> is the higher temperature of measurement, thus allowing the molecules to overcome the energy barrier at the pore entrance. Garrido, J and his co-workers (1987) has pointed out that the use of both N<sub>2</sub> and CO<sub>2</sub> can provide useful information concerning the micropore size distribution and the degree of access to the pore structure.

#### 1.4.4 **Surface Functional Groups**

It has been known for a long time that graphite, carbon black and activated carbon irreversibly chemisorb dioxygen (Langmuir, I., 1915; Smith, A., 1863). This chemically bound O<sub>2</sub> is removable only at elevated temperatures. The study of the chemistry of these carbon surface oxides has for the most part involved indirect methods of investigation, such as acid-base neutralization of the surface oxides (Boehm, H. P., *et al.* 1964) and the thermal removal of the surface oxides as CO and CO<sub>2</sub> (Puri, B. R. *et al.*, 1958). There has been only a small amount of direct experimental investigation of surface functional groups utilizing infrared (Mattson, J.S. *et al.*, 1969) and ESR spectroscopy (Harker, H. *et al.*, 1961). The studies employing internal reflection infrared spectroscopy (Mattson, J. S. & Mark, H. B., Jr.,

1970) provide some new information on carbon surface functional groups and their influence on adsorption.

The activation of carbon at 1,000°C in pure CO<sub>2</sub> or under vacuum followed by exposure to O<sub>2</sub> at room temperature produces a carbon surface that is capable of raising the pH value of either a neutral or an acidic solution, is hydrophobic, and has a positive electrophoretic mobility (Steenberg, B., 1944). A method of characterizing carbons that are activated and oxidized at different temperatures was developed from their acid-base properties (Kruyt, H. R. & de Kadt, G. S., 1929). Those low-temperature oxidized carbons that adsorb OH<sup>-</sup> ions primarily are called L-carbons. Those that are activated at high temperatures and adsorb H<sup>+</sup> ions are called H-carbons. These classifications have been found to divide above and below an activation-oxidation temperature of 500 to 600°C (Mattson, J. S. & Mark, H. B., 1971).

#### 1.4.4a **Surface Acidity**

All the chemisorbed oxygen on carbon evolves as three gases, CO, CO<sub>2</sub> and H<sub>2</sub>O. Quantities of CO<sub>2</sub> and CO evolved from carbon can be determined by increasing the activation temperature from 200 to 800°C. It has been suggested that surface oxides evolved as CO<sub>2</sub> are responsible for the physicochemical properties of L-carbons, whereas those oxides evolved as CO are responsible for H-carbon characteristics (Puri, B. R., 1966). Activated carbon shows either basic or acidic pH in aqueous suspensions. There are reports on a possible quantitative relationship between pH and oxygen content on the carbon surface (Studebaker, M. L., 1957). A more acidic dispersion is an indication of more oxygen content due to acidic functional groups. Such carbons have very high ion exchange capacity. Carbons with low oxygen content show basic surface properties and anion exchange behaviour (Boehm, H. P. *et al.*, 1964).

Surface groups present on carbon surface are of different functional groups. The ones suggested most often are carboxyl groups (I), phenolic hydroxyl groups (II), and quinone-type carbonyl groups (III). Other suggested groups are ether, peroxide, and ester groups in the forms of normal (IV) and fluorescein-like lactones (V), carboxylic acid anhydrides (VI) and the cyclic peroxide (VII). These are given in Figure 1.3.

Determination of adsorption isotherms for phenol on some commercial activated carbons have shown that the effect of surface oxides was to reduce adsorptive capacity in the lower concentration range (0.0 to 0.3 mmol/L) (Coughlin, R. W. & Tan, R. N., 1968). A similar effect on the adsorption of nitrobenzene was also observed when the surface of carbons was modified by wet oxidation and reduction (Coughlin, R. W. & Ezra, F. S., 1968). There are a couple of explanations (Coughlin, R. W., *et al.*, 1968) for the role of acidic surface oxygen groups in their inhibition of adsorption of phenol and nitrobenzene molecules. A major portion of these oxygen groups on carbon is located presumably on the edges of the layer planes where they are not expected to interfere markedly, in a steric sense, with adsorption of organic molecules on the basal planes. Chemically bound oxygen on the edges localizes electrons in surface states and removes them from  $\pi$  electron system of the basal planes. Depletion of electrons creates an increase in the population of holes in the conduction band of the  $\pi$  electron system. This is consistent with the concept that dispersion forces between the phenol's  $\pi$  electron system and the  $\pi$  band of the graphitic planes of the carbon are responsible for adsorption. Removal of electrons from the  $\pi$  band of the carbon by chemisorbed oxygen may interfere with and weaken the adsorptive forces.

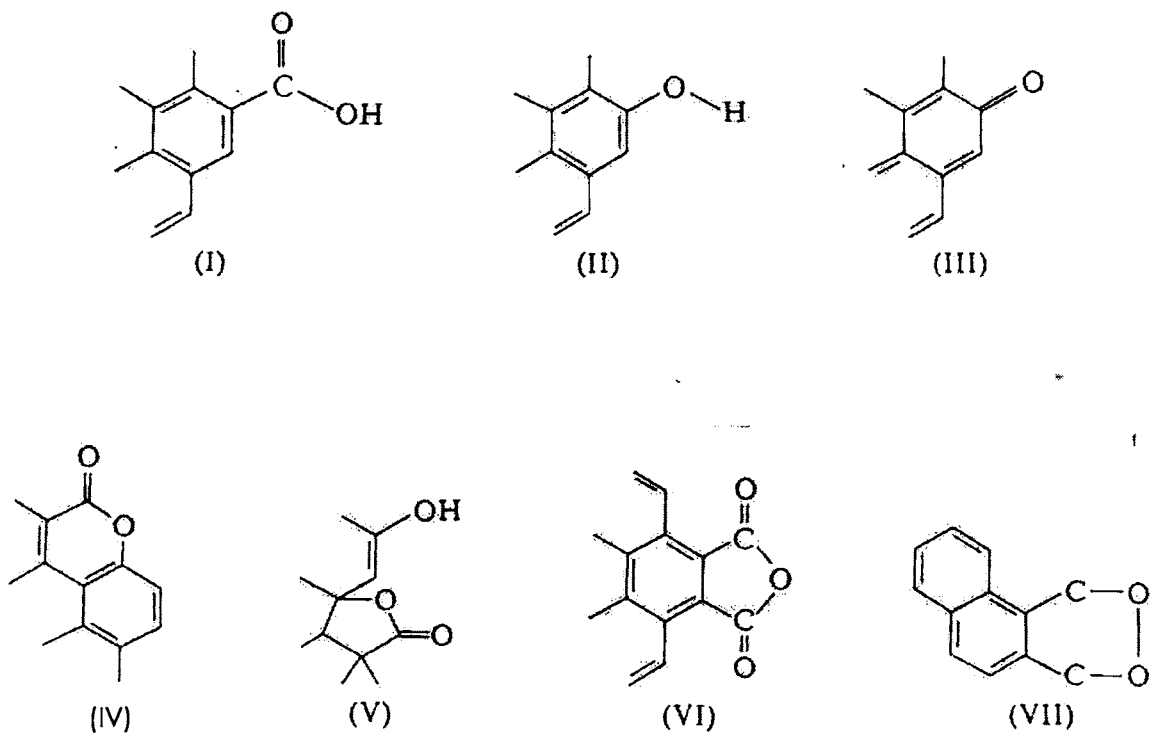


Figure 1.3 Surface groups present on activated carbon

#### .4.4b **Electrophoretic Characteristics**

Surface acidity studies on carbon surface have proved that the surface contains negative and positive sites. Huang and Ostovic have reported (1978) the electrophoretic mobility characteristics of different commercial carbons. This study also determined the intrinsic surface acidity constants of the activated carbons; that is, the acid-base behaviour of the surface hydroxyl group is expressed. The pK values obtained suggest that the carbons under investigation could be classified as weak acids and bases.

### 5 **Adsorption Equilibria and Isotherms**

#### 5.1 **A Review of Adsorption Fundamentals**

Adsorption from aqueous solutions involves concentration of the solute on the solid surface. As the adsorption proceeds, the sorbed solute tends to desorb into the solution. Equal amounts of solute eventually are being adsorbed and desorbed simultaneously. Consequently, the rates of adsorption and desorption will attain an equilibrium state, called *adsorption equilibrium*. At equilibrium, no change can be observed in the concentration of the solute on the solid surface or in the bulk of the solution. The position of equilibrium is characteristic of the entire system.

The presentation of the amount of solute adsorbed per unit of adsorbent as a function of the equilibrium concentration in bulk solution, at constant temperature, is termed the *adsorption isotherm*. The shape of adsorption isotherm gives qualitative information about the adsorption process and the extent of surface coverage by the adsorbate. Brunauer classified adsorption isotherms into five basic shapes and are given in Figure 1.4 (Brunauer, S., *et al.*, 1940). Isotherms of Type I are associated with systems where adsorption does not proceed beyond the monomolecular layer. The other types of isotherms involve multilayer formation. The isotherms for

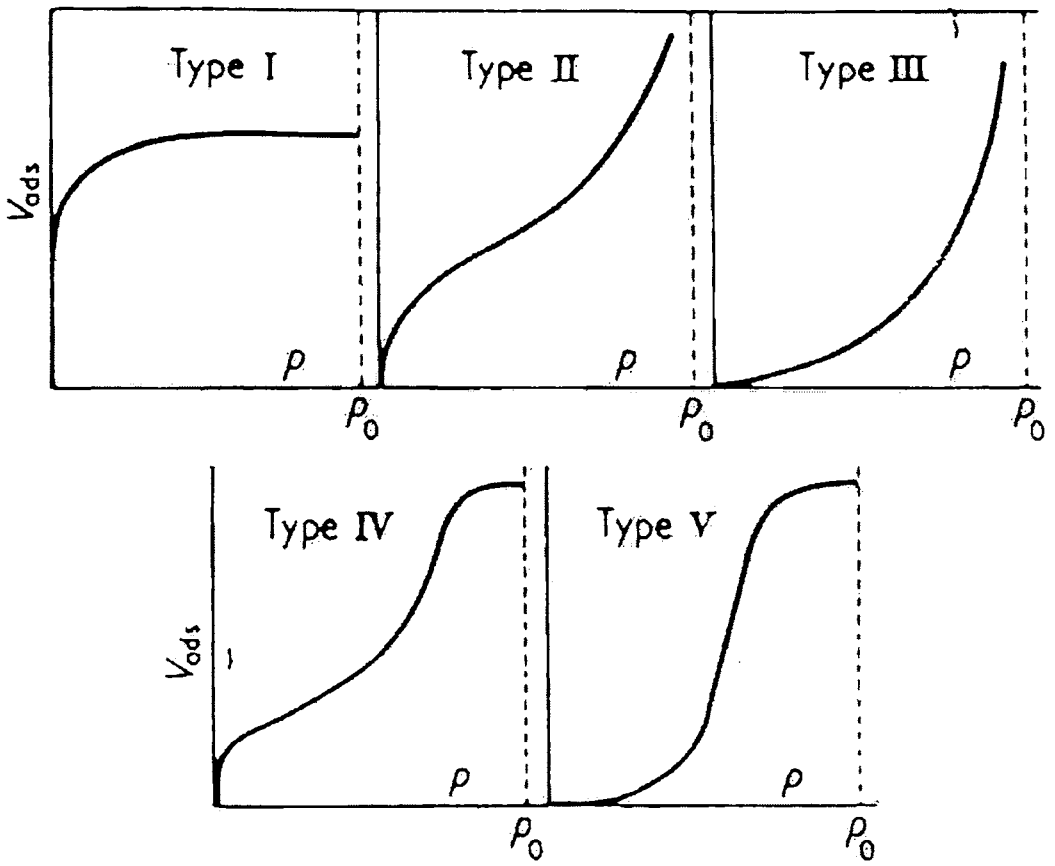


Figure 1.4 Bräuner's classification of isotherms

adsorption from solutions follow Type I, although under certain conditions multilayer adsorption may be encountered.

### 1.5.2 Henry's Law - Linear Adsorption Isotherm

This represents the simplest isotherm in which the amount adsorbed varies directly with the equilibrium concentration of the solute. It is often called Henry's Law after the analogous isotherm for the solution of gases in liquids. The isotherm is described by:

$$X = K_h C_e \quad (1.5)$$

Where  $X = x/m$ , the amount of solute adsorbed by unit mass of adsorbent (mg/g);  $C_e$  = equilibrium concentration (mg/L); and  $K_h$  = a constant.

This isotherm is obtained under conditions of low concentrations of solute. In such systems, the adsorbed layer is extremely dilute and the amount adsorbed is only a fraction of the monolayer capacity. Usually the linear relationship is observed at the lower concentration levels of a total adsorption isotherm. Therefore, the application of Henry's Law equation should be restricted to that region of the isotherm obtained from the experiment. Almost all the adsorption isotherms are reduced to Henry's Law at low concentrations.

Most of the adsorption studies reported in the literature have been conducted in distilled water systems. However, inorganic salts have been shown to affect the adsorptive capacity of activated carbon for certain solutes. Snoeyink *et al.* (1969) and Zogorski (1975) reported enhancement of adsorptive capacity of activated carbon for some phenolic compounds at high pH values (anionic species) in the presence of inorganic salts. This effect was suggested to be due to a possible reduction of the repulsive forces between adsorbed molecules and the carbon surface or between anions adsorbed on the surface. Weber *et al.* (1980) showed that the presence of low

concentrations of calcium and magnesium salts enhance the adsorption of humic acids on activated carbon possibly because of the formation of an ion-humate-carbon complex. Adsorption isotherms of humic acid in tap water in tap water systems showed higher carbon adsorption capacities than those in distilled water systems.

### 1.5.3 Langmuir Adsorption Isotherm

The basic assumptions underlying Langmuir's model, which is also called the ideal localized monolayer model, are:

1. The molecules are adsorbed on definite sites on the surface of the adsorbent.
2. Each site can accommodate only one molecule of adsorbate (monolayer).
3. The area of each site is a fixed quantity determined solely by the geometry of the surface.
4. The adsorption energy is the same at all sites.

In addition, the adsorbed molecules cannot migrate across the surface or interact with neighboring molecules. The Langmuir equation was originally derived from kinetic considerations (Langmuir, I., 1915). Later, it was derived from on the basis of statistical mechanics, thermodynamics, the law of mass action, theory of absolute reaction rates, and the Maxwell-Boltzmann distribution law (Young, D. M. & Crowell, A. D., 1962).

The kinetic derivation considered the adsorbed layer to be in dynamic equilibrium with the gas phase. A certain fraction of the molecules striking the bare sites will condense and be held by the surface forces for a finite time and are regarded as adsorbed; the remainder will be reflected. Those molecules striking sites that are already occupied will immediately re-evaporate as if they had been reflected. If the fraction of the site already filled is  $\theta$ , then:

$$\text{Rate of adsorption} = k_a P (1-\theta) \quad (1.6)$$

$$\text{Rate of desorption} = k_d \theta \quad (1.7)$$

Where  $k_a$  = rate of adsorption ( $\text{min}^{-1}$ ), and  $k_d$  = rate of desorption from a fully covered surface ( $\text{min}^{-1}$ ).

At equilibrium the number of molecules in the adsorbed state at any instant is constant; therefore:

$$k_a P (1-\theta) = k_d \theta \quad (1.8)$$

and 
$$\theta / (1-\theta) = k_a / k_d P \quad (1.9)$$

Taking  $k_a / k_d = b$ , which is the adsorption constant, Equation 1.8 becomes:

$$bP = \theta / (1-\theta) \quad (1.10)$$

or

$$\theta = bP / (1+ bP), \quad (1.11)$$

which is known as the Langmuir adsorption isotherm.

If  $V$  is the volume of gas adsorbed at pressure,  $P$ , and  $V_m$  is the volume adsorbed at infinite pressure- that is, when all the sites are occupied – then:

$$\theta = V / V_m, \quad (1.12)$$

and Equation 1.10 becomes:

$$V = V_m bP / (1+ bP) \quad (1.13)$$

For adsorption from solution by solid adsorbents, the Langmuir adsorption isotherm is expressed as:

$$X = X_m bC_e / (1+ bC_e), \quad (1.14)$$

Where  $X = x/m$ , the amount of solute adsorbed, 'x' (mg), per unit weight of adsorbent,  $m$  (g);  $C_e$  = equilibrium concentration of the solute (mg/L);  $X_m$  = amount of solute adsorbed per unit weight of adsorbent required for monolayer coverage of the surface (mg/g), also called monolayer capacity; and  $b = a \text{ constant related to the heat of adsorption, } [b \propto \exp (-\Delta H/RT)]$  (Young, D. M. & Crowell, A. D., 1962).

Equation 1.13 indicates that  $X$  approaches  $X_m$  asymptotically as  $C_e$  approaches infinity. For linearization of the data, Equation 1.13 can be written in the form:

$$C_e / X = 1 / bX_m + C_e / X_m \quad (1.15)$$

When  $C_e / X$  is plotted against  $1/C_e$ , a straight line, having a slope  $1/X_m$  and an intercept  $1/bX_m$ , is obtained. Another linear form can be obtained by dividing Equation 1.14 by  $C_e$ :

$$1 / X = 1 / X_m + (1 / C_e) (1 / bX_m) \quad (1.16)$$

Plotting  $1/X$  against  $1/C_e$ , a straight line, having a slope  $1/bX_m$  and an intercept  $1/X_m$ , is obtained.

The monolayer capacity,  $X_m$ , determined from Langmuir isotherm, defines the total capacity of the adsorbent for a specific adsorbate. Also, it may be used to determine the specific surface area of the adsorbent by utilizing a solute of known molecular area.

#### 1.5.4 Freundlich Adsorption Isotherm

The Freundlich adsorption equation is perhaps the most widely used mathematical description in aqueous systems due to its accuracy (Fritz, W. *et al.*, 1981; Peel, R. G. *et al.*, 1981; Al-Duri, B., 1988). It gives more accurate results than the Langmuir isotherm for a wide variety of heterogeneous adsorption systems. The Freundlich equation is expressed as (Freundlich, H., 1926):

$$x / m = K C_e^{1/n}, \quad (1.17)$$

where,  $x$  = amount of solute adsorbed (mg),  $m$  = the weight of adsorbent (g),  $C_e$  = the solute equilibrium concentration (mg/L), and  $K$  and  $1/n$  = constants characteristic of the system.

The Freundlich equation is an empirical expression that encompasses the heterogeneity of the surface and the exponential distribution of sites and their energies

(Young, D. M. & Crowell, A. D., 1962; Sips, R., 1948). For linearization of the data, the Freundlich equation is written in logarithmic form:

$$\log x/m = \log K + 1/n \log Ce \quad (1.18)$$

Plotting  $\log x/m$  versus  $\log Ce$ , a straight line is obtained with a slope of  $1/n$ , and  $\log K$  is the intercept of  $\log x/m$  at  $\log Ce = 0$  ( $Ce = 1$ ). The linear form of the isotherm can be conveniently obtained by plotting the data on log-log paper. The value of  $1/n$  obtained for adsorption of most organic compounds by activated carbon is  $< 1$ . Steep slopes, that is,  $1/n$  close to 1, indicate high adsorptive capacity at high equilibrium concentration that rapidly diminishes at lower equilibrium concentrations covered by the isotherm. Relatively flat slopes, that is,  $1/n \ll 1$ , indicate that the adsorptive capacity is only slightly reduced at the lower equilibrium concentrations. As the Freundlich equation indicates, the adsorptive capacity or loading factor on the carbon,  $x/m$ , is a function of the equilibrium concentration of the solute. Therefore, higher capacities are obtained at higher concentrations.

The Freundlich equation can be used for calculating the amount of activated carbon required to reduce any initial concentration to a predetermined final concentration. By substituting  $C_0 - Ce$  in Equation 1.17 for  $x$ , where  $C_0$  = the initial concentration:

$$\log [(C_0 - Ce) / m] = \log K + 1/n \log Ce \quad (1.19)$$

Equation 1.18 is useful for comparing different activated carbons in removal of different compounds.

### 1.5.5 Brunauer Emmett Teller Adsorption Isotherm

The Brunauer Emmett Teller (BET) isotherm was developed for the generalization of the ideal localized monolayer treatment (Langmuir model) to account for multilayer adsorption (Brunauer, S., *et al.*, 1940). The BET model is

based on the simplifying assumptions that each molecule in the first adsorbed layer serves as a site for the adsorption of a molecule into the second, and so on. The concept of localization, therefore, prevails throughout the layers, and the forces of mutual interactions are neglected. The heat of adsorption  $E$ , of the second and subsequent layers is assumed to be equal to the heat of liquefaction of the bulk liquid and therefore different from the heat of adsorption of the first layer. The expression of BET isotherm may be derived by an extension of the kinetic argument presented for the Langmuir isotherm or by a thermodynamic argument (Ruthven, D. M., 1984; Young, D. M. & Crowell, A. D., 1962; Sips, R., 1948). The resulting equation for the BET isotherm is:

$$V = V_m BP / (P_0 - P) [1 + (B - 1) P / P_0], \quad (1.20)$$

Where,  $V$  ( $\text{cm}^3/\text{g}$ ) and  $V_m$  ( $\text{cm}^3/\text{g}$ ) have the same meaning as in the Langmuir isotherm,  $P_0$  = saturation vapor pressure of the saturated liquid sorbate, and  $B$  = a constant:

$$B = a_1 b_2 / a_2 b_1 e^{(E_1 - E_L) / RT}, \quad (1.21)$$

which can be simplified to:

$$B = e^{(E_1 - E_L) / RT}, \quad (1.22)$$

Where  $a_1$  and  $a_2$  = rates of condensation on the first and second layers,  $b_1$  and  $b_2$  = rates of evaporation from the first and second layers,  $E_1$  = first layer heat of adsorption, and  $E_L$  = heat of liquefaction of the bulk phase.

The term  $E_1 - E_L$  is known as the net heat of adsorption. Thus, the BET equation provides a measure of both the heat of adsorption and the surface area of the solid. Application of the BET equation to the adsorption from solution takes the form:

$$X = X_m BC / (C_s - C_e) [1 + (B - 1) C_e / C_s], \quad (1.23)$$

where  $X$ ,  $X_m$  and  $C_e$  have the same meaning as in Langmuir's isotherm, and  $C_s$  = solubility of the solute in water at a specified temperature. Transforming Equation 1.22 to:

$$C_e / X(C_s - C_e) = 1 / X_m B + (B - 1) C_e / X_m B C_s \quad (1.24)$$

shows that a plot of the left side against  $C_e / C_s$  should give a straight line having slope  $(B - 1) / X_m B$  and intercept  $1 / X_m B$ .

The BET method yields a value for the volume of a monolayer of adsorbed gas on the solid surface. The surface area of one molecule of adsorbed gas may be calculated from its density and molecular weight. Using this datum the total surface area of the solid may be calculated.

#### 1.5.6 Kinetics of Adsorption

Adsorption of solutes in aqueous systems onto or into activated carbon is a time-dependant process. Adsorption kinetics is applied to the predictive modeling and design of fixed bed GAC adsorbers. Another consideration is the identification of the rate-determining step of the adsorption process.

The adsorption of organic molecules from solution by porous carbon can be described by three consecutive steps (Weber, W. J., Jr., 1972; Smith, J. M., 1968). The first step is the transport of the adsorbate from bulk solution to the outer surface of the adsorbent granule by molecular diffusion. This is called *external*, or *film diffusion*. The mass transfer coefficient,  $K_f$  (cm/s), in film theory, is related to the free liquid diffusivity of the solute,  $D_e$  (cm<sup>2</sup>/s), and thickness of the diffusional sublayer,  $\delta$ , as follows:

$$K_f = D_e / \delta \quad (1.25)$$

The concentration gradient in the liquid film around the granule is the driving force in film diffusion. The second step, termed *internal diffusion*, involves transport of the

adsorbate from the particle surface into interior sites by diffusion within the pore filled liquid and migration along the solid surface of the pore (surface diffusion) (Weber, W. J., Jr., 1972; Weber, W. J., Jr. & Rumer, R. R. Jr., 1965; Keinath, T. M. & Weber, W. J., Jr., 1968). Because these two transport processes act in parallel, the more rapid one will control the overall rate of transport. Keinath and Weber (1968) found that for typical water or wastewater sorption system, the rate parameter for surface diffusion was two to four orders of magnitude greater than the liquid phase pore diffusion. The third step is adsorption of the solute on the active sites on the interior surface of the pores. Since adsorption step is very rapid, it does not influence the overall kinetics (Weber, W. J., Jr., 1972; Smith, J. M., 1968). The overall rate of the adsorption process, therefore, will be controlled by the slowest step, which would be either film diffusion or internal diffusion.

The nature of the rate-limiting step in batch systems can be determined in a general way from properties of the solute and adsorbent. Rates of adsorption are usually measured by determining the change in concentration of the solute in contact with the carbon as a function of time. Linearization of the data is obtained by plotting the amount adsorbed per unit weight of adsorbent,  $x/m$  versus  $t^{1/2}$  for the initial fraction of the reaction. The reaction rates, determined from the slope of the line are not true reaction rates but relative rates useful for comparative purposes. For processes controlled by film diffusion, the adsorption rate is expected to be proportional to the first power of concentration. Adsorption of 2, 4-dichlorophenol by activated carbon is film diffusion controlled at concentrations less than 400  $\mu\text{mol/L}$  and a direct linear relationship exists between the initial concentration and adsorption rate (Zogorski, J. S. *et al.*, 1976). At concentrations of 2, 4-DCP greater than 500  $\mu\text{mol/L}$ , the reaction rate was shown to be intraparticle diffusion controlled. It is also

recognized that the adsorption rate is film diffusion controlled during the initial stages of the adsorption process in batch reactors and initial breakthrough in fixed bed reactors. As the carbon becomes loaded with the adsorbate, the reaction rate becomes controlled by intraparticle diffusion (Liu, K. T. & Weber, W. J., Jr., 1981; Weber, W. J., Jr. & Morris, J. C., 1963).

For processes controlled by intraparticle diffusion, the size and configuration of the adsorbate molecule should affect the overall rate of adsorption. The larger the molecule or the more branched, the lower should be the rate at which it diffuses. Hence, adsorption rate should be lower. Weber and Morris (1963) reported that a linear relationship existed between observed adsorption rates and molecular weights for a series of alkylbenzenesulfonates ranging from 2-hexyl-benzenesulfonate to 2-tetradecylbenzenesulfonate. An increase in the chain length apparently reduces mobility of the molecule and also increases its affinity to the carbon surfaces in accord with Traube's rule. Both effects result in a decrease of the surface diffusion inside the pores and, hence, an overall decrease in the observed adsorption rate. Adsorbates that exhibit high affinity to activated carbon usually cause intraparticle diffusion control of the adsorptive process. This is attributed to a decrease of surface diffusion of adsorbates that is highly held and, thus, is less flexible to migrate on the internal surfaces of the carbon. Branching of the adsorbate molecules also results in a decrease of the observed adsorption rate due to a decrease in the surface diffusion rate.

### **Applications of Activated Carbon**

Activated carbon has hundreds of different applications. In fact, virtually every product manufactured today has been improved upon at least once by the use of activated carbon. In its numerous applications, activated carbon represents a number

of different functionalities. These include adsorption, reduction, catalysis and carrier of biomass and chemicals.

#### 1.6.1 **Water Treatment**

The current water treatment technology is oriented towards the removal of contaminants, mostly organic compounds, by activated carbon. In recent years, GAC has been the predominant mode of treatment despite its many limitations. Powdered activated carbon (PAC) had been employed in a successful manner for many years for removal of taste and odor constituents from surface waters. The change in technology of carbon treatment began in the early 1960's when the Kanawha River, at Nitro, West Virginia, became highly contaminated with petrochemicals that imparted tastes and odors to the drinking water. The full-scale GAC water treatment plant was placed on-stream in 1966 (Hager, D. G., 1967). Occasionally a municipal water supply, usually from groundwater, is contaminated with hydrogen (poly) sulfides whose odor is rather familiar. This odor can be controlled rather easily with PAC and GAC. For example, the Galeta Water District, California, installed four pressurized GAC adsorbers that followed diatomaceous earth filters to tackle the problem (Lawrence, C. H., 1968). Another pioneering effort in the development of GAC for taste and odor control, as well as removal of organic compounds in general, was conducted at the Passaic Valley Water Commission's Plant at Little Falls, New Jersey (Inhoffer, W. R., 1975).

To illustrate the capacity of carbon beds to remove chloroform and Total Organic Carbon (TOC), a series of experiments were conducted by the Philadelphia Water Department (Cairo, P. R., *et al.*, 1978). The study showed that *postcontactor mode* of application of GAC outperformed filter/adsorber mode by 20 to 30% in removal of  $\text{CHCl}_3$  and 11 to 16% in removal of TOC. GAC beds are also used for

treating water polluted with haloforms and pesticides such as dieldrin (Hyde, R. A., 1980). The GAC columns employed in the Santa Clara Valley Water District's Palo Alto Reclamation Facility has successfully demonstrated the capacity of activated carbons in removing chlorinated benzenes, total organic carbon and total organic halogens (Summers, R. S. & Roberts, P. V., 1983). Activated carbon is also used for the removal of Trihalomethanes (THM's) in combination with other conventional treatment techniques (Meijers, A. P., *et al.*, 1979; Blanck, C. A., 1979).

Activated carbon is very widely used for the treatment of polluted ground water all over the world. Most of the ground water sources are contaminated by specific organics. The treatment of such waters consists of pre-aeration for removal of volatiles followed by adsorption by GAC and / or a macroporous resin. This method of treatment has been proved successful for treating ground water supply of the township of Rockaway, New Jersey, which was contaminated by several volatile organic chemicals (McKinnon, R. J. & Dyksen, J. E., 1984).

Biological Activated Carbon (BAC) has been another mode of application of activated carbon for the removal of dissolved organic impurities in water. This process consists of the sequential combination of oxygenation and / or chemical oxidation; sand, anthracite, or multimedia filtration; optional oxygenation; and GAC adsorption (Rice, R. G., *et al.*, 1978). A research group in Germany was perhaps the first to examine the beneficial effect of microbial activity on the performance of a GAC bed (Ererhardt, M., *et al.*, 1979). Benefits claimed for the BAC process are biological nitrification, biological oxidation of dissolved organic compounds, and partial biological regeneration of the GAC (Miller, G. W., *et al.*, 1980).

## 1.6.2 **Odour Control**

The increased emphasis on improved air quality and the associated control of odors has focused attention on activated carbon adsorption as a viable abatement method in many odor control problems (Lovett, W. D. & Poltorak, R. L., 1974). Due to its non-polar surface, activated carbon has the ability to adsorb organic and some inorganic materials in preference to water vapor. The amount of materials adsorbed is partially dependant upon the physical and chemical characteristics of the specific compound or compounds. In general, organics having molecular weights over 45 will be readily adsorbed. Once saturated, activated carbon can be thermally regenerated and reused. Activated carbons have been extensively used for odor control in sewage plants. The principal odor causing chemicals in sewage plants are H<sub>2</sub>S and organic compounds, which are generated by anaerobic decomposition of compounds containing nitrogen and sulfur. The odorous emissions include mercaptans, indole, skatole, organic acids and other decomposition products. The odors originating from secondary treatment systems and clarifiers can be controlled using activated carbon. Activated carbon has also been used for the removal of sulfide odor from well water (Lee, P. E., 1974).

## 1.6.3 **Activated Carbon Fibers**

Recent development of activated carbons in fiber form is increasing applications of activated carbons in various areas due to its unique characteristics (Suzuki, M., 1994). Activated carbon fibers (ACFs) have unique characteristics compared with granular or powder activated carbons. Thin-fiber shape clearly assures fast intraparticle adsorption kinetics compared with palletized or granular activated carbons commonly employed in gas phase and aqueous phase adsorption.

Carbon fibers (CFs) have been on the market since the beginning of the 1960's and are now produced to satisfy the worldwide market, especially in the areas of aeronautical and space materials technologies. CFs are expected to be in the increasing demand for composite materials in automobile, housing, sport, and leisure industries as well as airplane and space applications. The high strength type is produced from polyacrylonitrile (PAN) and the high elasticity type is manufactured from coal tar pitch (Rodgers, S. J., *et al.*, 1965).

ACFs provide much faster adsorption kinetics compared with the granular adsorbents conventionally used. Thus, the application of ACFs may lead to smaller adsorption units and effective recovery of valuable components. For environmental pollution control, volatile organic chemicals have been successfully removed from waste streams using activated carbon fibers (Sakoda, A., *et al.*, 1991). Extensive studies have been conducted on the removal of trichloroethylene and 1, 1, 1-trichloroethane on ACF derived from pitch (Tanada, S., *et al.*, 1992). In aqueous phase adsorption, Sakoda and coworkers obtained fundamental data on trichloroethylene and tetrachloroethylene adsorption on ACFs derived from phenolic resin (Sakoda, A., *et al.*, 1987). ACF also find application in the reduction of NO by ammonia gas (Mochida, I., *et al.*, 1985). The oxygen containing functional groups on ACF surfaces catalyses the reduction.

### **Gas Separation and Storage**

Separation and purification of gas mixtures by adsorption is a major unit operation in the chemical and petrochemical industries. Commercial availability of a large spectrum of microporous adsorbents and the possibility of designing many different process schemes under the generic category of pressure swing adsorption (PSA) and thermal swing adsorption (TSA) are the main reason for development in

this field. Activated carbons produced from coal, petroleum, vegetable and polymeric precursors have played a major role in this development. The separation efficiency of a gas mixture by TSA or PSA process is governed by the capacity and selectivity of adsorption of the more strongly adsorbed component of the mixture as well as by the ease of desorption of the adsorbed species (Sircar, S., *et al.*, 1996).

Packed activated carbon columns are frequently used for removing trace or dilute organic impurities, solvent vapors, odor forming compounds from air and other industrial gases by selectively adsorbing the impurity at near ambient temperature. The adsorbed impurity is then desorbed by heating the column countercurrently with an inert gas or steam. Activated carbons offer a very special advantage for this application because of their relative hydrophobicity. A significant adsorption capacity for the impurity can be achieved even when the feed gas is wet (Rudisill, F. N., *et al.*, 1992). PSA process is also used for the production of hydrogen from reformer off gas (Fuderer, A. & Rudelstorfer, E., 1976) and for the production of nitrogen from air (Juntgen, H., *et al.*, 1981). Latter is made possible by the application of a new class of activated carbons called carbon molecular sieves (CMS). These are microporous carbons in which the size of the pore mouth has been altered to allow faster diffusion of relatively smaller O<sub>2</sub> molecules (~ 3.46 Å diameter) into the internal pore structure rather than larger N<sub>2</sub> molecules (~ 3.64 Å diameter).

A new class of nanoporous activated carbon membrane for gas separation developed by Air Products and Chemicals (Rao, M. B. & Sircar, S., 1993) has been used for the recovery of H<sub>2</sub> from a low pressure petroleum refinery waste gas containing low concentrations of H<sub>2</sub>. The nanoporous carbon selective surface flow (SSF) membrane allows economic recovery of the valuable H<sub>2</sub> from a waste gas which may not otherwise be practical. Air or other gas drying by using PSA or a TSA

process is a common practice. Typically NaX zeolite or activated alumina is used as adsorbents. This method has limitations due to the difficulty in desorbing water from zeolite and the low water adsorption capacity of alumina at low partial pressures. But modified activated carbons having polar oxygen groups do possess better hydrophilic nature (Golden, T. C. & Sircar, S., 1990) and are well suited for gas drying application by PSA.

Stricter environmental regulations have renewed interest in the removal of trace hydrocarbons from contaminated air. Air Products and Chemicals Inc. has developed a novel method requiring less energy for air purification by using a cyclic sorption-reaction (SR) (Dalton, A. J. & Sircar, S., 1977). The system consists of two parallel adsorbents containing a physical mixture of an activated carbon and an oxidation catalyst. A typical SR cycle would include (a) adsorption of the trace hydrocarbon on the carbon at ambient temperature until impurity breakthrough, (b) in-situ oxidation of the hydrocarbons by directly or indirectly heating the adsorbent-catalyst mixture to about 423 K, and (c) cooling the adsorbent-catalyst mixture to ambient temperature either directly or indirectly and venting the combustion products.

Compressed Natural Gas (CNG) has been used as a popular fuel in motor vehicles. A large effort has been made to replace CNG by storing methane in a vessel packed with activated carbon. This concept of adsorbed natural gas (ANG) can potentially reduce the highest storage pressure so that light weight cylinders can be used. To achieve the net deliverable capacity of such a device compared to CNG, activated carbon with high pore volume and high surface are required.

### 1.6.5 **Refrigeration and Heat Pumping**

Adsorption cycles for refrigeration were first used in the early 1900s (Plank, R. & Kuprianoff, J., 1960). Machines using both the adsorbent-refrigerant pairs  $\text{CaCl}_2 - \text{NH}_3$  and activated carbon – methanol were successfully manufactured. Adsorption cycles have also been considered for use in heat-actuated heat pumps, as have many different absorption cycles. Methanol – activated carbon combination have been studied extensively for this purpose (Pons, M. & Grenier, Ph., 1985; Meunier, F., *et al.*, 1986). The porosity characteristics of available activated carbons give reasonable performance compared to the maximum that can be achieved with physical adsorption. Advances in heat and mass transfer to and from the carbon bed by increasing heat transfer area, use of additives to improve conductivity and producing activated carbons with inherently high conductivity would allow the use of semi continuous cycles that could improve the system performance (Critoph, R. E., 1989).

### 1.6.6 **Recovery of Gold**

Various methods are used to extract the gold from its ores, which includes gravity concentration, flotation, amalgamation and cyanidation (Lorenzen, L. & Van Deventer, J. S. J., 1993; Lorenzen, L., 1995). Cyanidation is a method of extracting gold or silver based on the solubility of these metal-cyanide complexes that form in solution. The gold is then recovered from the solution either by zinc reduction or by carbon adsorption.

The application of activated carbons to gold recovery has its origins in the patented use of wood charcoal for the recovery of gold from chlorination leach liquors in 1880 (Gray, E. L., 1940). The carbon-in pulp (CIP) process, which was developed to its present form in South Africa during the 1970s, is considered to be the most significant advance in gold recovery technology in recent years (Adamson, R. J.,

1972). CIP makes use of the tremendous physical affinity 'activated' carbon has for gold (it can attract 7% of its weight in gold), which it readily attracts to its surface in cyanide solution. The CIP process consists of three essential stages: adsorption in which the dissolved gold in the pulp is loaded on to aerated carbon: elution, in which the gold is removed from the carbon into an alkaline cyanide solution, and electro-winning, in which the gold is removed by an electrical process from the alkaline cyanide solution and deposited on steel wool electrodes (Stanley, C. G., 1988). Activated carbon is reused after treating with acid to remove contaminants.

#### 1.6.7 **Electrical Applications**

Activated carbon can conduct electricity and possesses the electrical properties of a semiconductor. Activated Carbon Cloth (ACC) provides a contiguous carbon form that is ideally suited for use in electrical applications. Studies have shown that ACC exhibits good electrical storage capacity; can be effectively heated using resistance heating; exhibits extremely fast heat-up and cool-down rates; can be maintained at any steady state temperature with good temperature uniformity; and shows no electrical degradation over thousands of heating and cooling cycles (Sze, S. M., 1985). Studies are also being conducted on using carbon black and activated carbon materials providing high surface areas and a distinct pore distribution for supercapacitor applications at frequencies < 0.5 Hz (Nishino, A., 1996).

#### 1.6.8 **In Food Industry**

Activated carbon is also very popular as decolorizing agent; taste- and odor-removing agent; purification agent in food processing (Food Chemicals Codex, 1996). Food and beverage production accounts for only about 6% of the market for liquid-phase activated carbon (Baker, F. S. *et al.*, 1992). Of this, the greatest use is for discoloring sugar. Activated carbon remains the most common method used to

decolour vinegar (Achaerandio, I. *et al.*, 2002). Activated carbon can also be used to remove ethylene from fruit storage facilities, particularly if brominated (Reid, M. S., 1985).

#### 1.6.9 **Miscellaneous Applications**

Activated carbon is a versatile material, a fact reflected in the vast number of patents taken out concerning this product. Activated carbon can be used as a slow release agent for perfumes, for instance rose oil (Kokando Co Ltd, 1978), an idea which is also applied in pharmaceuticals (Inst. Merieux S. A., 1979). Its use in toothpaste or mouthwash (Rialdi, G., 1977) seems more interesting. More up-to-date applications include the use of activated carbon in a nuclear fuel element to improve the heavy metal ion retention (U. S. AEC., 1967). Polishing a glass surface with activated carbon insures a good adhesion of a metal layer when metalizing in a vacuum (Yugov, V. A., 1957). Cementing of oil wells is improved by incorporating activated carbon to prevent shrinkage and to remove contaminants from the remaining drilling mud (Standard Oil Development Co., 1952). Activated charcoal is used in agriculture as a soil amendment (e.g. alkali-treated humates and humic acid derivatives), and as a component of nursery or transplant media (Wellen, C. W., *et al.*, 1997), as well as to remove pesticide residues (McCarty, L. B., 2002). Among the literally hundreds of other uses are agents in gas masks; pollution control devices such as car catalytic converters and flue gas desulfurization (Ashford, R. D., 1994).

#### 1.7 **Impregnated Activated Carbons**

Impregnated activated carbons are carbonaceous adsorbents which have chemicals finely distributed on their internal surface. The impregnation optimizes the existing properties of the activated carbon giving a synergism between the chemicals and the carbon. This facilitates the cost-effective removal of certain impurities from

gas streams which would be impossible otherwise. For environmental protection, various qualities of impregnated activated carbon are available and have been used for many years in the fields of gas purification, civil and military gas protection and catalysis.

For the manufacture of impregnated activated carbon, an activated carbon of suitable quality for the particular application is impregnated with solutions of salts or other chemicals which, after drying or other after-treatment steps, remain on the internal surface of the activated carbon. Homogeneous distribution of the impregnating agents on the internal surface of an activated carbon is important. Furthermore, blocking of the micropores and macropores should be avoided in order to keep the impregnation agent accessible for the reactants. Bansal *et al.* (1988) and Rebstein & Stoeckli (1992) examined a sulfur-impregnated activated carbon for mercury removal and demonstrated that the sulfur is predominantly distributed in the micropore system and that no pores are blocked.

Typical applications of impregnated activated carbon are shown in Table 1.3. and Table 1.4 shows a list of frequently used products with information on the quality and quantity of the impregnation agents, the basic activated carbon qualities used, and the relevant application fields.

It is obvious that each impregnation agent is frequently used for various purification tasks. The example of the potassium iodide impregnation shows that in these cases a variety of removal mechanisms become effective. Potassium iodide, as promoter of the oxidation catalyst 'activated carbon', allows catalytic oxidation of hydrogen sulfide to sulfur or of phosphine ( $\text{PH}_3$ ) to phosphoric acid:

Table 1.3 Typical applications of impregnated activated carbons

<b>Gas purification</b>	<b>Civil and military gas protection</b>	<b>Catalysis</b>
Application fields:	Application in gas masks, room filters and respiratory apparatus filters:	Application in catalysis:
Hydrogen sulfide	Sulfur dioxide	Vinyl acetate synthesis
Mercaptan	Hydrogen chloride	Vinyl chloride synthesis
Mercury	Hydrogen fluoride	Vinyl fluoride synthesis
Ammonia	Nitrogen oxide	
Amine	Amine	
Acid gases (HCl, SO <sub>2</sub> , HF, HCN)	Hydrogen sulfide	
Arsine	Mercury	
Phosphine	Radioactive iodine	
Aldehyde	Radioactive methyl iodide	
Radioactive iodine	Phosgene	
Radioactive methyl iodide	Hydrogen cyanide	
Nitrogen oxide	Chlorine	
	Arsine	
	Sarin and other nerve gases	

(Bansal, R. C., *et al.*, 1988; von Kienle, H. & Bader, E., 1980.)

Table 1.4 List of frequently used impregnated carbons

Impregnation			
Chemicals	Quantity (wt%)	Activated carbon <sup>a</sup>	Examples for application
Sulfuric acid	2-25	F 1-4mmØ	Ammonia, amine, mercury
Phosphoric acid	10-30	F 1-4 mm Ø	Ammonia, amine
Potassium carbonate	10-20	F 1-4 mm Ø	Acid gases (HCl, HF, SO <sub>2</sub> , H <sub>2</sub> S, NO <sub>2</sub> ), carbon disulfide
Iron oxide	10	F 1-4 mm Ø	H <sub>2</sub> S, mercaptan. COS
Potassium iodide	1-5	F 1-4 mm Ø	H <sub>2</sub> S, PH <sub>3</sub> , Hg, AsH <sub>3</sub> , radioactive gases/radioactive methyl iodide
Triethylene diamine (TEDA)	2-5	F 1-2 mm Ø G 6-16 mesh	Radioactive gases/radioactive methyl iodide
Sulfur	10-20	F 1-4 mm Ø, G	Mercury
Potassium permanganate	5	F 3+4 mm Ø	H <sub>2</sub> S from oxygen-lacking gases
Manganese IV oxide		G 6-16 mesh	Aldehyde
Silver	0.1-3	F 3+4 mm Ø G 8-30 mesh	F: phosphine, arsine G: domestic drinking water filters (oligodynamic effect)
Zinc oxide	10	F 1-4 mm Ø	Hydrogen cyanide
Chromium-copper-silver salts	10-20	F 0.8-3 mm Ø G 1 2-30 mesh G 6-16 mesh	Civil and military gas protection Phosgene, chlorine, arsine Chloropicrin, sarin and other nerve gases
Mercury II chloride	10-15	F 3+4 mm Ø	Vinyl chloride synthesis Vinyl fluoride synthesis
Zinc acetate	15-25	F 3+4 mm Ø	Vinyl acetate synthesis
Noble metals (palladium, platinum)	1-5	F, G, P	Organic synthesis, hydrogenation

F = pelletized activated carbon G=granulated activated carbon P = powdered activated carbon Ø = pellet diameter

(Henning, K. D. & Schäfer, S., 2003)



Furthermore, potassium iodide-impregnated activated carbon can be used for removal of mercury from gases (Henning, K. D., *et al.*, 1988).

If activated carbon is impregnated with sulfuric acid, the mercury elimination rate and, above all, the adsorption capacity are substantially boosted. The suitability of sulfur-impregnated activated carbon was described in 1972 by Sinha and Walker (1972). Sulfur impregnation yields a product which, from a corrosion technological viewpoint, is safe. The mercury vapour diffused into the activated carbon's pore system reacts, under the catalytic effect of the activated carbon, with the sulfur distributed on the internal surface to form mercury sulfide:



For H<sub>2</sub>S removal, activated carbon qualities impregnated with ~ 10 wt % Fe<sub>2</sub>O<sub>3</sub> are used. The use of an iron salt as promoter is judged differently from others since, on one hand, the reaction velocity of H<sub>2</sub>S oxidation is increased, but on the other hand, oxidation of the H<sub>2</sub>S via sulfur up to the production of sulfuric acid is promoted. Potassium iodide impregnation of activated carbon gained industrial importance because the promoter not only increases the reaction velocity but also inhibits the formation of sulfuric acid by unwanted side-reactions (Hedden, K., *et al.*, 1976).

Studies have been done using impregnated activated carbon for the removal of palladium from nitric acid solutions of nuclear fuel waste (Foersterling, H. U., 1990). For this, the use of activated carbons modified with the complexing agent dimethylglyoxime (DMG) has been suggested (Moore, R. H., 1974). DMG was selected as a modifying agent because of its well-known selectivity for palladium in

acid solutions, and activated carbons were investigated as substrate because of their large internal surface area resulting in a high DMG sorption capacity.

## 1.8 Comparison of GAC and PAC

Activated carbon is divided into two types with respect to its physical form, Granular Activated Carbon (GAC) and Powdered Activated Carbon (PAC). The choice between these two forms depends on the primary properties of the carbon such as adsorption capacity, pressure drop or bed expansion, attrition, filterability and bulk density. GAC and PAC possess different adsorption properties and surface characteristics. But ultimately it is the nature of adsorbate and its molecular weight that decides the overall performance of the system (Hutchins, R. A., 1981).

The mode of application of these two carbons is different as far as wastewater treatment is considered. In the powdered form, activated carbon is either added as a dry powder or slurry to the raw water, similar to the addition of any other chemical. The compounds in the water, which are adsorbable, are adsorbed on the carbon and then the carbon is removed from the water by the downstream sedimentation and filtration process. This can be employed with the existing facility in an effluent treatment plant. In the granular form, the water to be treated flows through a bed of activated carbon and the compounds in the water are adsorbed on to the carbon. Hence, the application of GAC requires a new facility. When the adsorption capacity of the GAC is exhausted, it is removed, replaced or regenerated.

For a short term usage PAC is more economical to GAC since only the required quantity is to be purchased. But on a long term usage, GAC is more advantageous since it can be regenerated and reused. PAC is usually disposed off after usage and that reduces its application on a long term basis. Also, disposal of PAC is a

problem due to possible secondary pollution from the adsorbed substances. GAC does not pose such a problem since it is regenerated and reused after every cycle of operation. The GAC filters are not effective against bacteria. In fact, they may promote bacterial growth especially when not used for a few days or when not changed at proper intervals. Research shows that silver-impregnated carbon units do not significantly reduce bacteria problems and may increase the silver content in drinking water up to 0.028 mg/l. Application of granular forms of carbon demands pre-treatment to remove suspended solids, which may otherwise clog the bed. PAC has an advantage that it does not require any pre-treatment of the wastewater.

#### 1.9 Limitations of Activated Carbon Application

Activated carbon is extensively used in water and wastewater treatment but this is limited to wastes with low inorganic (<5%) and organic (<1%) concentrations (Charles, M. L., 1968). Activated carbon is proved to be inefficient in removing highly soluble organic molecules or those with low molecular weight. Organics that are poorly adsorbed by activated carbon include alcohols, low molecular weight ketones, acids, and aldehydes, sugars and starches, very high molecular weight or colloidal organics and low molecular weight aliphatics (Tanju, K., *et al.*, 1996).

A significant drop in the contaminant level in influent water will cause a GAC filter to desorb, or slough off, adsorbed contaminants because GAC is an equilibrium process. As a result, raw water with frequently changing contaminant levels can result in treated water of unpredictable quality. Bacterial growth on the carbon is another potential problem. Excessive bacterial growth may cause clogging and higher bacterial counts in the treated water. Bacterial levels in the treated water must be

closely monitored, and the final disinfection process must be carefully controlled. GAC beds cannot tolerate suspended solids in the influent stream since they clog the bed and this demands pre-treatment of the raw water.

The powdered carbon adsorbs contaminants and natural organic matter (NOM) until it is removed downstream in the sedimentation and filtration processes. With regard to pre-chlorinated waters, the PAC adsorption capacities for disinfection by-products are too low for economical removal (Symons, J. M. *et al.*, 1981). Therefore, PAC is most often used for synthetic organic chemical or taste and odor control. But the regeneration of powdered activated carbon is typically not practical. And the spent powdered carbon that is removed from the treatment trail by filtration or sedimentation is disposed off as solid waste or slurry. Also, disposal of PAC is a problem due to possible secondary pollution from the adsorbed substances. The handling and disposal of activated carbon waste streams can pose a significant economic and logistical burden on the waste generator (Robert, C. M., 1987). The incentives for recycling spent activated carbon wastes include financial benefits and reduced liabilities associated with improper handling or disposal of the activated carbon waste stream.

#### 1.10 Scope of the Work

Though powdered activated carbon has many advantages over granular carbons, its application in large scale separation process is limited by difficulty in recovery. This can be overcome if PAC particles are rendered magnetic. Magnetization of particles offers an advantage that collection of magnetic particles can be actuated by a magnetic force outside the conduit (non-invasive collection) and released from the collection path (internal surface of conduit to a by pass loop).

In situ deposition of magnetic iron oxide on carbon particles provides a convenient way of magnetizing the GAC. The method is cost effective since the chemicals used are relatively inexpensive and readily available and non-toxic.

The conditions for the deposition of magnetic iron oxide on GAC, the chemical nature of the deposited magnetic oxide, changes in surface properties of GAC upon modification, adsorption characteristics of typical solutes and effect of operating conditions in the flow through system on the retention of particles in a magnetic field are some of the key points to be investigated. This dissertation is a compilation of such investigations.

## **CHAPTER 2**

### **PREPARATION AND CHARACTERIZATION OF MAGNETIC IRON OXIDE LOADED ACTIVATED CARBONS**

#### **2.1 Introduction**

The treatment of contaminated effluents is an increasing problem as environmental issues are of greater concern in recent times. One of the major methods for the removal of pollutants from wastewater is using porous solid adsorbents. The properties of porous solids that render them useful for water treatment include high porosity and surface area as well as the physical and chemical nature of the internal adsorptive surfaces. The mode of application of activated carbon depends on their physical forms and dimensions. The main objective of this study includes the preparation of a new activated carbon material that can be separated from treated waters using a magnetic separation procedure. This chapter contains two sections. The first section deals with the method for the preparation of magnetic iron oxide loaded activated carbons. The principal methods used to characterize the activated carbon magnetic iron oxide composites are described in the second section.

#### **2.2 Preparation**

Magnetic composites of the activated carbon were prepared by the alkaline precipitation of iron oxides using in the laboratory. The method suggested by Schwertmann & Cornell (2000) was used for preparing these composites with appropriate modifications. Composites of different iron loading were prepared by varying the ferrous ion concentration in the solution and only three of the samples were selected for further studies. Magnetic property of the composites was verified using a permanent magnet. A control carbon sample was used for comparative studies. The samples were kept in air tight PVC based containers and stored in a desiccator.

The coconut shell based activated carbons of 80 x 120 mesh size were procured from M/s. Indo German Carbons (IGCL) at Edayar, Cochin, Kerala. All the chemicals used for the preparation were of analytical quality and distilled water was employed through out the study.

#### 2.2.1 **GAC**

The carbon samples were sieved using ASTM sieve set to find out the particle size distribution results are give in figure 2.1a & b. Carbon granules collected on ASTM 120 and passing through 80 were selected for this study. The particle size of this fraction of sample ranged between 0.125 and 0.177 mm. The sample was then washed thoroughly with distilled water to remove any adhering impurities. In order to remove the alkaline impurities, the samples were further washed with dilute hydrochloric acid (0.1N) and treated with dilute sodium bicarbonate solution (0.1N) to remove any excess acid. Carbons were again washed thoroughly with distilled water until the washings gave neutral pH values. The GAC was then dried at 150°C in a hot air oven for three hours and stored in an air tight PVC based containers and kept in a desiccator.

#### 2.2.2 **Magnetic Iron Oxide (MIO)**

The pure magnetic iron oxides were prepared according to the method suggested by Schwertmann and Cornell (2000). 80g of ferrous sulphate ( $\text{FeSO}_4 \cdot 7\text{H}_2\text{O}$ ) was dissolved in 560 mL of distilled water. Approximately 1 g of hydrazine sulphate was added to this solution. Hydrazine sulphate removed traces of oxygen present in the system. The solution was kept on a hot plate to boil. 6.46g of potassium nitrate ( $\text{KNO}_3$ ) and 44.9g of potassium hydroxide (KOH) was dissolved in 240 mL of distilled water in another beaker. Approximately 1g of hydrazine sulphate were added to it to remove any traces of dissolved oxygen. This solution was slowly added to the

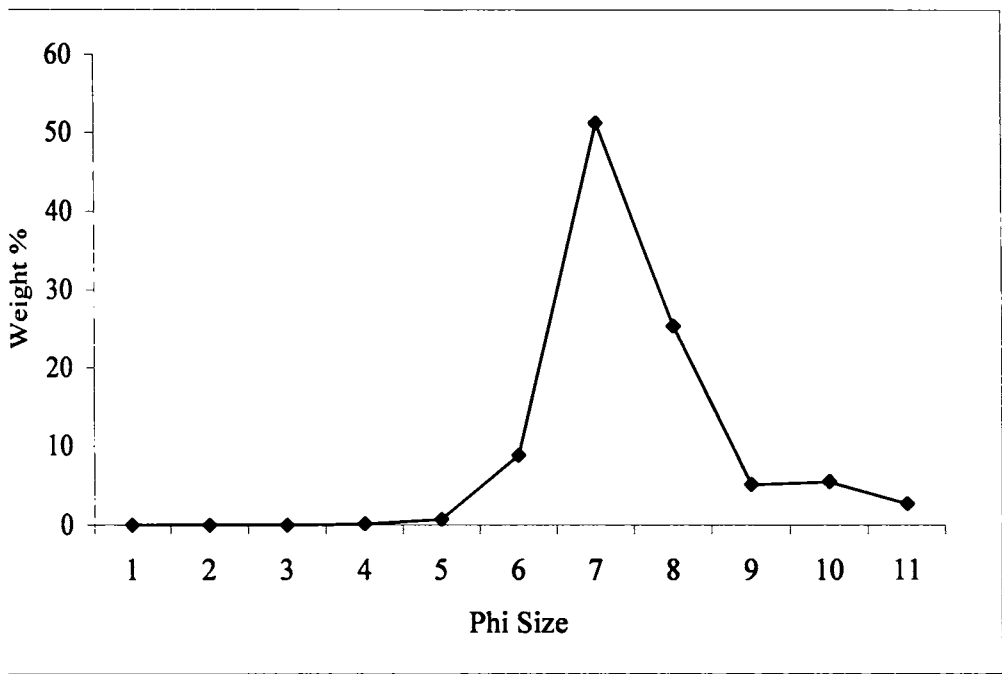


Figure 2.1a Frequency curve for grain size distribution of activated carbon.

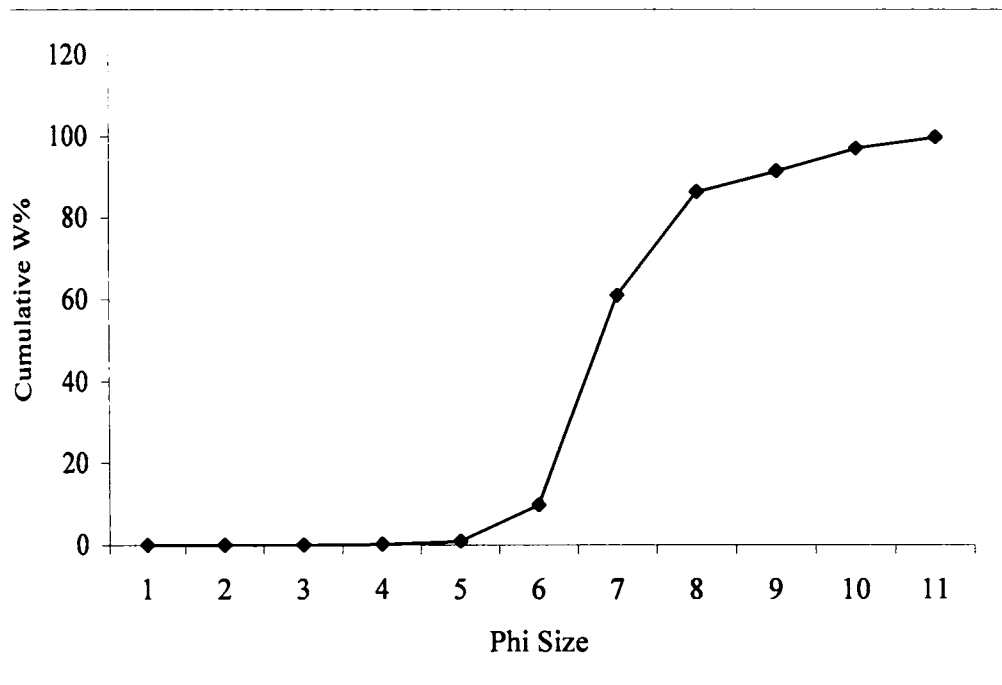


Figure 2.1b Cumulative weight % vs Particle size of activated carbon

hot ferrous sulphate solution with constant stirring. The precipitate was then kept at 80°C for one hour. The precipitate was kept over night before washing with distilled water to remove the precipitated impurities. The excess alkali was removed by passing carbon dioxide gas. The precipitate was further washed free of impurities with distilled water and stored in a PVC container.

### **MGAC5**

A magnetic activated carbon composite with iron oxide loading was coated as MGAC5 of iron oxide of activated carbon. The reagent concentrations were fixed to get a loading of 7%. The actual amount of Fe loaded was determined by gravimetric methods and the results are given in a following section.

25.2g of  $\text{FeSO}_4 \cdot 7\text{H}_2\text{O}$  were dissolved in 540 mL of distilled water. 1 g of hydrazine sulphate was added to this solution to remove any traces of oxygen. 100g of GAC was added to this solution and stirred for 2 hours. The alkali solution was prepared by dissolving 14g of KOH and 2.1g of  $\text{KNO}_3$  in 260 mL distilled water. To this solution, 1g of hydrazine sulphate was added. The activated carbon suspension in ferrous sulphate solution was kept on a hot plate and heated to 80°C. The alkali solution was slowly added to this with constant stirring. The activated carbon in precipitated iron oxide suspension was kept for one hour over at 80°C. The precipitate was kept over night before washing and drying. The precipitate was washed thoroughly with distilled water to remove impurities.

The removal of excess alkali was a major problem. The distilled water washing alone did not remove the alkali. Use of acids were not preferred due to possible leaching of deposited iron oxides. Hence, carbon dioxide was used for removing excess alkali from the precipitate. The carbon dioxide gas was bubbled through the suspension and the precipitate was washed further with distilled water.

The neutral pH values of the washings showed that the method was highly effective in removing excess alkali. Another problem was the free iron oxides that were formed outside the activated carbon matrix. Since study targeted on iron oxide that was formed *insitu* on GAC or deposited inside the pores, the removal of other free iron oxide was necessary to maintain a constant iron ratio with activated carbon matrix for characterization and batch adsorption studies. This was done by transferring the composite to a sieve of 120 mesh size followed by washing distilled water to remove free iron oxides of smaller particle size. The iron oxide carbon granules of 0.125 to .177 mm diameter were retained in the sieve.

#### 2.2.4 **MGAC7**

The ratio of ferrous ion to activated carbon was increased for the preparation of MGAC7. The reagent concentrations were adjusted to get a 15 % iron loading. The actual amount of Fe loaded on the sample was determined by gravimetric method.

Approximately 54g of  $\text{FeSO}_4 \cdot 7\text{H}_2\text{O}$  were dissolved in 540 mL of distilled water. 100g of GAC were added to this solution after removing any traces of oxygen by adding 1g of hydrazine sulphate. This suspension was stirred for 2 hours and kept over a hot plate. The alkaline solution was prepared by dissolving 30g of KOH and 4.5g of  $\text{KNO}_3$  in 260 mL distilled water. The solution was made oxygen free by adding 1g of hydrazine sulphate. The iron oxide was precipitated by similar procedure as given in 2.2.3. The precipitate was kept over night before washing with distilled water and  $\text{CO}_2$ . The sample was made free of free iron oxides by wet sieving through ASTM 120. The sample was stored in an air tight PVC container and kept in a desiccator.

## 2.2.5 **MGAC9**

MGAC9 represents the sample with the highest iron loading. The reagent concentration was adjusted so as to get an iron loading of 20%. And the actual concentration of iron loaded on the carbon matrix was determined by gravimetric procedure.

The MGAC9 was prepared by dissolving 72g of  $\text{FeSO}_4 \cdot 7\text{H}_2\text{O}$  in 540 mL distilled water to which 1g of hydrazine sulphate was added to scavenge the dissolved oxygen. 100g of granular activated carbon was added to this solution and stirred well for 2 hours. After the equilibration time, the solution was transferred onto a hot plate. The alkaline solution was prepared by dissolving 40g of KOH and 6g of  $\text{KNO}_3$  in 260 mL distilled water. Any trace of oxygen was removed by using 1g of hydrazine sulphate. The alkali solution was added to the hot activated carbon suspension in ferrous sulphate solution slowly with constant stirring. The precipitated composite was kept over night before washing and drying by similar procedures adopted for other samples. The sample was stored in PVC container and kept in airtight desiccator.

## 2.3 **Physico-Chemical Characterization Studies**

### 2.3.1 **Materials**

#### (i) **Adsorbents**

Activated carbons prepared from coconut shells having a particle size of 0.125 – 0.177 mm were used in the study. Modified carbons prepared according to the described scheme of preparation were used. A control carbon was employed for comparative studies.

(ii) Distilled Water

Distilled water having a conductivity less than 1  $\mu$  mho/cm at 303 K prepared using a glass distillation apparatus was used throughout this study. Distilled water was stored in clean glass bottles to avoid contamination from PVC containers.

(iii) Chemicals

All the chemicals used were of analytical reagent grade, with almost 99.9% purity as specified by the manufacturer and were obtained from E. Merck, BDH and Qualigens. The solutions were prepared as specified in the respective method and stored in clean glass reagent bottles.

(iv) Glassware

All the glasswares used in this study were cleaned with dilute hydrochloric acid (1+1 N) solution followed by repeated rinsing with distilled water.

(v) Instruments

*pH meter:* An Systronics model digital pH meter 335 was used for pH measurements. The instrument was calibrated using three buffer solutions (pH – 4, 7 and 9.2) daily.

*Muffle Furnace:* A Fourtech model muffle furnace was used for heat treatment steps in iron loading estimation and total ash content measurements. The temperature ranged varied between 20°C and 1000°C with an accuracy of 5°C.

*Analytical balance:* The accurate weighing of samples and chemicals was done using a Sartorius BP 211 D model analytical balance having an accuracy of  $d = 0.01$  mg (80g), 0.1 mg (210g). The balance was auto calibrated.

*X – Ray Diffraction:* For XRD studies a Rigaku model RTP 300 RC X – Ray diffractometer was used. The instrument used a rotating anode using a copper target. The accelerating voltage was set at 50 kV and cathode current was adjusted to 100

mA. The measurements were done at 298 K. The cathode current was set at a low value (100 mA) compared to normal operating current (150 mA) since the material analyzed were magnetic.

*Scanning Electron Microscope:* The morphological studies were carried using a JEOL JSM – 5600 Scanning Electron Microscope. Electron micrographs were obtained at 298 K.

*Mossbauer set up:* The Mossbauer analysis was carried out using the experimental set up at Inter University Consortium for DAE facilities at Indore. The set up used a  $\text{Co}^{57}$  as source at an accelerating voltage of 14.4 keV. A proportional counter filled with Xenon gas was used as the detector. The measurements were done at 298 K. A schematic diagram of the Mossbauer setup is shown in Figure 2.2.

*Thermogravimetric analysis:* Thermogravimetric analysis of the samples was carried out using a TGA Q50 V2.34 model Universal Thermal Analyser at a heating rate of  $10^{\circ}\text{C} / \text{min}$  under nitrogen atmosphere.

*Gas adsorption studies:* The surface area and pore volume of the carbon samples were determined by  $\text{N}_2$  adsorption using a Micromeritics, model: Gemini, surface area analyzer.

*Magnetization measurements (VSM):* The magnetization measurements on the magnetic iron oxide loaded activated carbon samples were done using a EG & G Par 4500 model Variable Sample Magnetometer.

## **Methods**

### (i) pH

pH of the magnetic iron oxide – activated carbon composites was determined by ASTM D 3838 method (ASTM D 3838., 1980). Sample of composites equivalent to 10.00 +/- 0.01g on a dry basis was weighed and transferred to a boiler flask.

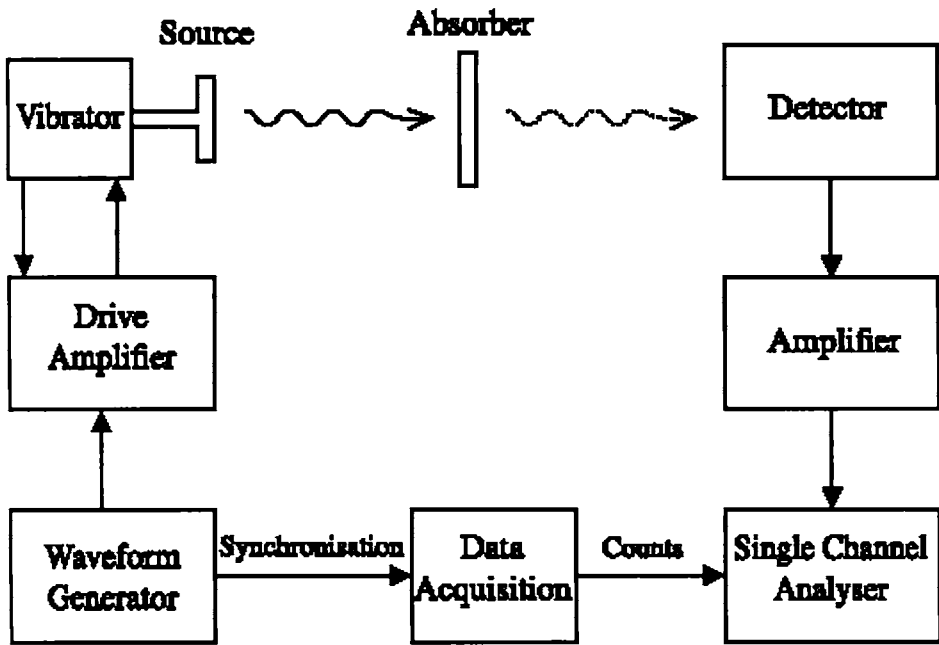


Fig 2.2 A schematic representation of Mossbauer spectrometer.

Approximately 110 mL of distilled water was brought to boiling and 100.0 +/- 0.1 mL of this was immediately added to the boiler flask containing the sample and allowed to boil for 900 +/- 10 s. The flask was then removed from the hot plate and contents were filtered immediately through the filter paper premoistened with distilled water used for the test. The filtrate was cooled to 50 +/- 5°C and pH was measured using a digital pH meter.

(ii) Total Ash

The total ash content of the samples was determined by ASTM D 2866 method (ASTM D 2866., 1994). The crucibles used for the study were pre-weighed by igniting in the muffle furnace at 650 +/- 25°C for 1h and cooling by keeping in a desiccator to room temperature followed by weighing to the nearest 0.1mg. An adequate sample of the composites was dried to constant weight. A sufficient amount of sample to get an ash content of 0.1gm was weighed out to the nearest 0.1 mg into pre-weighed crucibles and ignited in the furnace at 650 +/- 25°C for 3h. The crucibles were then cooled in a desiccator and determined the weights.

(iii) Iodine Number

Iodine number of the composites was determined by ASTM D 4607 method (ASTM D 4607., 1986). After fixing the carbon dosage, three appropriate amounts of dry carbon composites were weighed to the nearest milligram into a clean, dry 250 mL Erlenmeyer flasks equipped with a ground glass stopper. 10.0 mL of 5 wt % hydrochloric acid was added to these flasks. Each flask were then stoppered and swirled gently until the carbon is completely wetted. The stopper was then loosened to vent the flask and placed on a hot plate and brought the contents to boil gently. The contents were boiled gently for 30 +/- 2 s to remove any sulfur that may interfere with the test results. The flasks were then removed and cooled to room temperature. *This*

*step was done only for GAC sample and not for the iron oxide loaded composite samples, as hot hydrochloric acid will leach out the iron loaded on the carbon matrix.*

100.0 mL of 0.100 N standardized iodine solution was pipetted out into each flask. The flasks were immediately stoppered and the contents were shaken vigorously for 30 +/- 1 s. The mixture was filtered immediately through Whatman No. 2V into a beaker. The first 20 mL of the filtrate was discarded and only the remaining was used for estimation studies. 50.0 mL of the filtrate was pipetted into a clean 250 mL Erlenmeyer flask. It was titrated against the standardized 0.100 N sodium thiosulphate solution using starch as indicator. The iodine number was determined from a logarithmic plot of  $X/M$  versus  $C$ , the residual filtrate normality.

(iv) Absolute Density

Absolute density of the prepared samples was estimated by displacement method using nitrobenzene. A clean dry specific gravity bottle was weighed accurately using the analytical balance. Approximately one gram of the sample was added to the bottle and weighed again to find the weight of sample and specific gravity bottle together. Then the bottle with carbon sample was filled with nitrobenzene and weighed again. The bottle was then cleaned and dried and filled with nitrobenzene and weighed. These four readings were then fit into an equation to calculate the absolute density of the samples. The following equation was used for calculating the absolute density

$$A.D = W_1 - W_0 / (W_3 - W_0 / 1.2) - (W_2 - W_1 / 1.2) \quad (2.1)$$

Where,

1.2 = Specific gravity of nitrobenzene

$W_0$  = Weight of specific gravity bottle

$W_1$  = Weight of specific gravity bottle + sample

$W_2$  = Weight of specific gravity bottle + sample + nitrobenzene

$W_3$  = Weight of specific gravity bottle + nitrobenzene

(v) Iron Oxide Loading

The amount of iron oxide loaded onto different composites was determined by standard gravimetric protocol (Vogel, A. I., 1939). One gram of the sample was weighed out into a clean 250 mL glass beaker. 50.0 mL of 1+1 hydrochloric acid was added to it and stirred well to dissolve iron oxide from the composites. The mixture was then filtered through a Whatman No. 1 filter paper to separate the carbon particles. Approximately 2 mL of concentrated nitric acid was then added to the filtrate followed by 200 mL of distilled water. The contents were then kept over a hot plate and allowed to boil for approximately five minutes. To the hot solution, containing dissolved iron, concentrated ammonia solution was added till excess with constant stirring. Then the precipitate was allowed to settle. The supernatant solution was decanted and the precipitate was washed with hot 1 % ammonium nitrate solution until the washings were chloride free. The solution was then filtered through a Whatman No. 41 filter paper to collect the precipitate. The precipitate was then placed on a pre-weighed crucible and ignited to red hot temperature to get a residue of  $Fe_2O_3$  of constant composition. The amount of iron oxide loaded on each composite in terms of iron (Fe) was determined from the weight of residue obtained.

(vi) Mossbauer Analysis

The Mossbauer analysis was carried using the facility available at the Inter University Consortium for DAE facilities (IUC) at Indore. 100 mg of sample was used for the analysis of pure iron oxide whereas the quantity was fixed at 800 mg for the composite samples. A higher amount of composite sample was used due to the lower Fe concentration. The sample was made into a paste with an amorphous gel and

pasted on a glass slide. Then the sample was mounted on the holder and a processing time of 6 and 22 hrs were given for MIO and MGAC7 respectively for the spectrum generation. The spectra obtained were processed using an inbuilt NORMOS programme.

(vii) X-Ray Diffraction

The X-Ray diffraction studies were also carried out in the IUC facility. Two samples viz, pure iron oxide and composite were studied using this technique. The samples were finely ground and fitted into the slot of a holding slide before mounting on the instrument. The measurements were done at 298 K. The cathode current was set at a low value (100 mA) compared to normal operating current (150 mA) since the material analyzed was magnetic.

(viii) Scanning Electron Microscopy

Electron micrographs of pure iron oxide and composite sample were taken using a JEOL JSM – 5600 Scanning Electron Microscope available at the IUC facility. The samples were loaded onto the groove of the holding slide. Both secondary electron images and back scattered images were obtained. The images were processed using the inbuilt software available with the instrument. Images were obtained in two magnifications, 170x and 1000x. An accelerating voltage of 20 kV was used during the image capture.

(ix) N<sub>2</sub> Adsorption Studies

Nitrogen adsorption at 77 K is frequently used method to determine the equivalent monolayer capacity which is converted in an apparent surface area by using the cross sectional area of the nitrogen molecule (Molina Sabio, M. *et al.*, 1985). The sample is taken in the adsorption cell and air, water and other interfering impurities were removed by degassing the samples at 573 K for 1h. The samples were

then allowed to cool. A Dewar flask filled with liquid nitrogen was placed around the adsorption bulb. It was connected to vapour pressure manometer bulb. The nitrogen gas was then admitted to the adsorption cell and the volume of nitrogen gas adsorbed at different relative pressures was measured. The volume of nitrogen gas required for monolayer coverage ( $V_m$ ) was determined from slope of BET plots at different relative pressures.

For the purpose of characterization of porous materials, the equation is commonly used in one of its limiting forms,

$$\frac{P/P_o}{V(1 - P/P_o)} = \frac{1}{V_m C} + \frac{C - 1}{V_m C} (P/P_o) \quad (2.2)$$

where,

$P/P_o$  = relative pressure

$V$  = amount adsorbed at  $P/P_o$

$C$  = constant varying with adsorbent – adsorbate interaction  
 $= e^{(E1 - E2) / RT}$

$V_m$  = monolayer capacity

$E1$  = heat of adsorption in the first layer

$E2$  = heat of condensation of the adsorbate

The values of  $V_m$  and  $C$  are obtained from the linear plot of  $P/P_o / V (1-P/P_o)$  vs  $P/P_o$ .

The value of  $V_m$  and  $C$  can be calculated from the slope ( $S$ ) and intercept ( $Y_{int}$ ).

$$C = (S/ Y_{int}) + 1 \quad (2.3)$$

$$V_m = 1 / (S + Y_{int}) \quad (2.4)$$

If one molecule of an adsorbate occupies an area  $a$  the total number of molecules present in a volume will occupy an area,

$$S_{BET} = a V_m N / M_w \quad (2.5)$$

since the total number of molecules in volume  $V_m$  is  $V_m N / M_w$ . Actually  $a$  is the cross sectional area of the adsorbate molecule. The value of ' $a$ ' for  $N_2$  at 77 K is  $0.162 \text{ nm}^2$  (Walker, P. L. Jr., *et al.*, 1968). The value of  $V_m$  is calculated from the equation 2.4 and then on substitution in equation 2.5 gives the value of  $S_{BET}$ , the surface area of the solid.

#### (x) Magnetization Measurements

According to Faradays laws of magnetic induction, an ac voltage is induced in the electrical which is proportional to the rate of change of magnetic flux linking the circuit, and therefore to the size of the moment within the sample due to the applied magnetic field. As the sample is vibrated in the vertical direction near the detection coil, an ac signal is generated at a frequency determined by the sample oscillation. A schematic of the VSM set-up is shown in Figure 2.3. The pick up coils are situated between the pole pieces around the sample. Both the signal produced by the permanent magnet vibrating in the pick up coils and the signal induced in the sample pick up coils are fed directly into a 5210 lock-in amplifier. The permanent magnet signal is used as the reference signal input. The system is calibrated using a single crystal nickel disc whose saturation magnetisation is well documented.

The sample is placed within a uniform magnetic field, and a magnetic moment  $m$  is induced in the sample. The sample was positioned within suitably placed sample coils, and was made to undergo sinusoidal motion. The resulting magnetic flux changes induced a voltage in the sample coils that is proportional to the magnetic moment of the sample. The applied field was produced by an electromagnet. The experiment was carried out at room temperature.

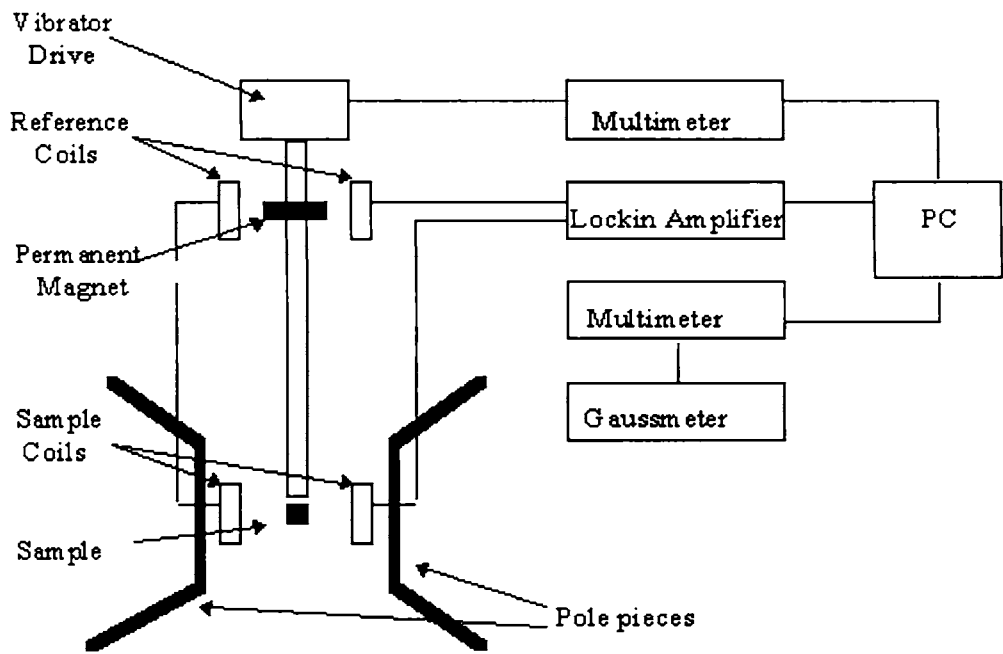


Figure 2.3 A schematic of the Vibrating Sample Magnetometer

### 2.3.3 **Results and Discussion**

#### 2.2.3a **pH**

The pH of the carbon samples was determined using a digital pH meter as per the procedure given in methods. The obtained values for GAC, MGAC5, MGAC7 and MGAC9 are 7.2, 6.8, 6.9 and 7.1 respectively. Since the carbons were neutralized during the washing process, the neutral values indicate the absence of any basic and acidic impurities. However, it is known that the adsorption of weak electrolytes such as phenol compounds depends on the pH of the carbon surface (Solar, J. M., 1987).

The pH of activated carbons have a direct relation to the concentration of oxygen bearing surface functional group present. Based on the surface pH of the carbons, they are classified as either H or L carbons. The adsorption weak electrolytes such as phenol compounds depends on the pH of the carbon surface. However, in this study chemical treatment followed by washing during the preparation setup of rendered carbons with neutral surface pH.

#### 2.2.3b **Absolute Density**

The absolute density of the adsorbents is determined using a calibrated specific gravity bottle and solvent (nitrobenzene) that is capable of penetrating the pores of the adsorbent and whose density is accurately known. The method is based on solvent displacement by an accurately weighed mass of adsorbent. The absolute density for GAC, MGAC5, MGAC7 and MGAC9 were determined to be 1.29, 1.75, 2.05 and 2.2 g/cm<sup>3</sup> respectively. Analysis of some commercial activated carbon samples has shown that the real density can be as high as 2.1 g/cc<sup>3</sup> (*Process Design Manual for Carbon Adsorption*. U.S. EPA, 1971). The apparent density is sometime used for the characterization purpose and the values are lower to that of the absolute

density. The reported apparent density values of some commercial samples range from 0.18 to 0.53 g/cm<sup>3</sup> (Netzer, A., & D. E. Hughes., 1984).

The absolute density increases with the iron loading as seen from the results. This is expected as the impregnated iron oxide will increase the density of the sample. And the increase in the absolute density is proportionate with the iron loading. And this suggests that the increase in the absolute density is due to the iron oxide impregnated inside the pores of the carbon matrix. One main disadvantage with the use of powdered activated carbon is the low density which makes it difficult to settle in the wastewater treatment system. The present use of flocculating agents will add to the contamination loading which render it a difficult material to be regenerated. Hence the increased absolute density and correspondingly better settling properties of the impregnated activated carbon composites make it more technically feasible adsorbent which can be employed in wastewater treatment.

#### 2.2.3c **Total Ash**

Activated carbon contains inorganic components as part of the source material, or the ash may originate from chemicals added during activation. It has generally seen that the total amount of inorganic constituents will vary from one adsorbent to another (Brady, M. & G. McKay., 1995). The ash content of carbon is a factor affecting performance of activated carbon in water treatment, especially the iron content (Faust, S. D. & Aly, O. M., 1987). Hence, the estimation of total ash content of the adsorbent samples is important to understand its performance in water treatment.

The total ash content of the samples was done by A.S.T.M D 2866 method. The analysis of GAC showed a total ash content of 3.72 %. The values obtained for MGAC5, MGAC7 and MGAC9 are 12.1, 18.6 and 24.7 % respectively. The control

carbon GAC has similar ash content to previously reported data on various carbons (Mantell, C. L., 1979; Ahmedna, M., *et al.*, 2000; Alaya, M. N., *et al.*, 2003). But the reports also suggest that the value can vary from 2 to 30 % in various commercial products. The low value of ash content in GAC suggests a better adsorption capacity and performance. The increase in the total ash content in MGAC5, MGAC7 and MGAC9 is expected due to the incorporation of iron into the carbon matrix. The increase in the ash content is in proportion to the iron loading in these modified samples. The final residue of ignition of these samples will constitute ash from the oxidation of carbon and iron oxide,  $\text{Fe}_2\text{O}_3$ . The increased ash content in these modified samples will have a negative influence on their adsorption capacity. The inorganic content in these modified samples can reduce adsorption compared to the control carbon.

#### 2.2.3d **Iron Loading**

The iron oxide impregnated on modified carbon samples was determined by gravimetric procedure. During the preparation setup, the concentration of chemicals ( $\text{FeSO}_4$  and  $\text{KOH}$ ) was calculated on a theoretical basis that can give an approximate loading of iron oxide for each sample. So it is important to determine the exact concentration of iron oxide actually loaded onto these samples.

The analysis of the four samples was done and the results are given in Figure 2.4. The control carbon has zero iron concentration as the traces of inorganic iron that might be present could not be determined using the gravimetric procedure used. Hence the iron loading on control carbon, GAC was taken as zero. The iron loading (in % Fe) in MGAC5, MGAC7 and MGAC 9 were determined to be 5.19, 10.2 and 13.6 respectively. The actual iron loading is much less compared to the theoretically predicted loading from the concentration of the chemicals used. This is expected as

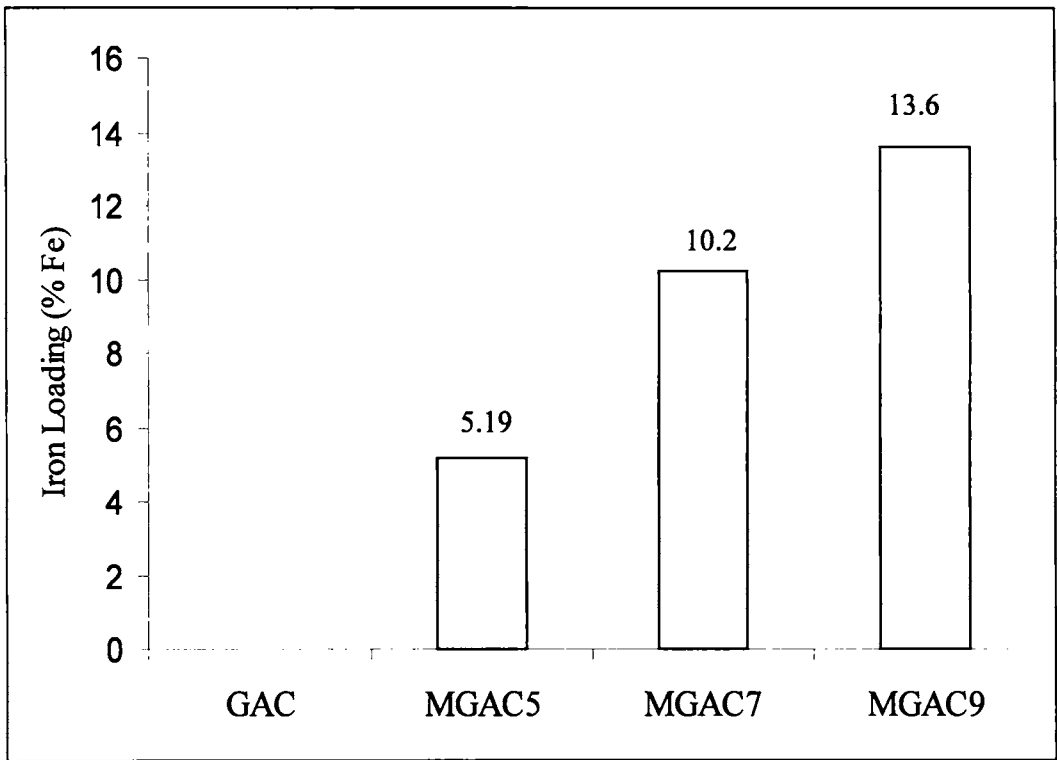


Figure 2.4 Iron oxide loading on composite samples

the amount of ferrous ion that could go into the porous structure of the carbon is less compared to what remains in the solution. Most of the ferrous ion added in the reaction vessel will remain in solution and the precipitated iron oxide is washed out during washing procedure. The wet sieving method was used to remove any free iron oxide present so that the modified sample will have a homogenous iron concentration. Only the iron oxide precipitated inside the pores of the activated carbon remain and accounts for the given values of iron loading in these three samples.

The sample identity of activated carbon and magnetic iron oxides loaded composites are defined as GAC with zero iron oxides, MGAC5 with 5.19% iron loading, MGAC7 with 10.2% iron loading and MGAC9 with 13.6% iron loading.

A previous study on magnetic composites with activated carbon has reported  $\text{Fe}_2\text{O}_3$  concentration on loaded samples to be 25 to 47 wt% (Oliveira, L. C. A. *et al.*, 2002). The high values reported should be attributed to the free iron oxide that was precipitated in the bulk of the solution. It was seen from this study that even on giving prolonged equilibration time with ferrous sulphate solution, the amount of iron loaded could not exceed the highest value reported. The equilibration was completed within 2h and an additional equilibration time never resulted in an increase in the iron oxide loaded. Also, an increased concentration of ferrous ion also failed to give an increased iron loading inside the pore structure since the pores were already saturated with the ferrous ion. So it can be reasonably assumed that the previous workers have not removed the free iron oxide that will be precipitated during the impregnation process. And these free iron oxides will contribute to the total iron loading present along with the iron oxide impregnated into the pore structure of the activated carbon matrix.

### **Iodine Number**

The iodine number is defined as the number of milligrams of iodine adsorbed by 1g adsorbent, when the iodine concentration of the residual filtrate is 0.02 N. Basically, iodine number is a measure of the iodine adsorbed in pores and, as such, is an indication of the pore volume available in the activated carbon of interest. The iodine number of the control carbon and iron oxide composite samples was done by ASTM D 4607 method. The results are given in Figure 2.5a. There is a sharp decline in the iodine number with increase in the iron loading indicating a reduction in the available pore volume. The control carbon, GAC has an iodine number of 1018.23 where as iron oxide impregnated composite samples MGAC5, MGAC7 and MGAC9 have iodine numbers of 874.7, 831.16 and 602.51 respectively. With respect to the control carbon, there is a 14.1 % reduction in iodine number in MGAC5. The corresponding reduction in iodine number for MGAC7 and MGAC9 are 18.4 % and 40.8 % respectively. The reduction in the iodine number values with % iron loading is given in Figure 2.5b. The loss in iodine number is not proportional to the iron loading. But the reduction in the values is expected as the impregnated iron oxides occupy the pores of the carbon matrix and less amount of pores are available for iodine adsorption. The higher reduction in pore volume in MGAC9 is mainly due to the increased loading of iron oxide (13.6 %), but is not proportional with reduction in other composite samples.

Typically, carbons for water treatment have iodine numbers ranging from 600 to 1100 (Wagner, N. J. & Jula, R. J., 1981). The analysis of some commercial activated carbons has also given similar figures (*Process Design Manual for Carbon Adsorption*. U.S. EPA., 1971; Netzer, A., & Hughes, D.E., 1984). The activated carbon prepared from a low rank coal using  $ZnCl_2$  as the activation agent was shown

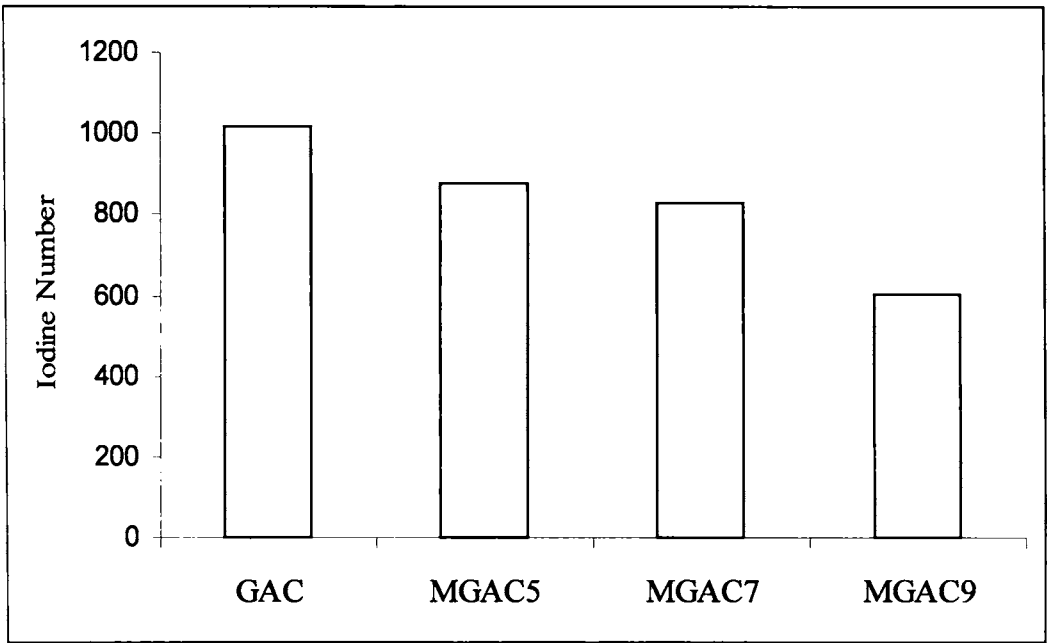


Figure 2.5a Estimated Iodine number for activated carbon samples

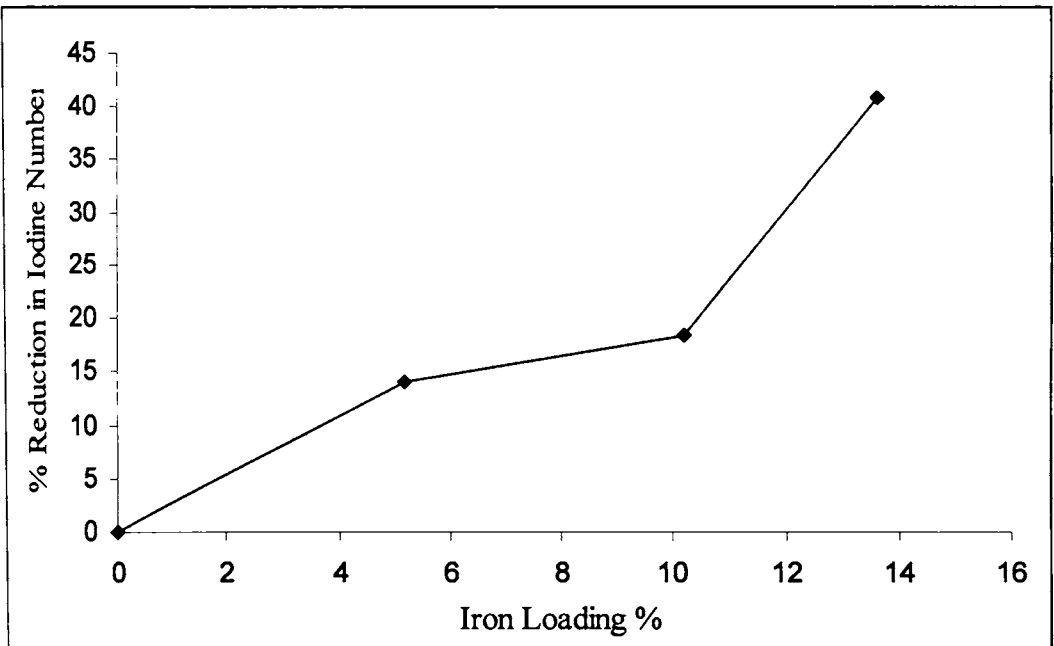


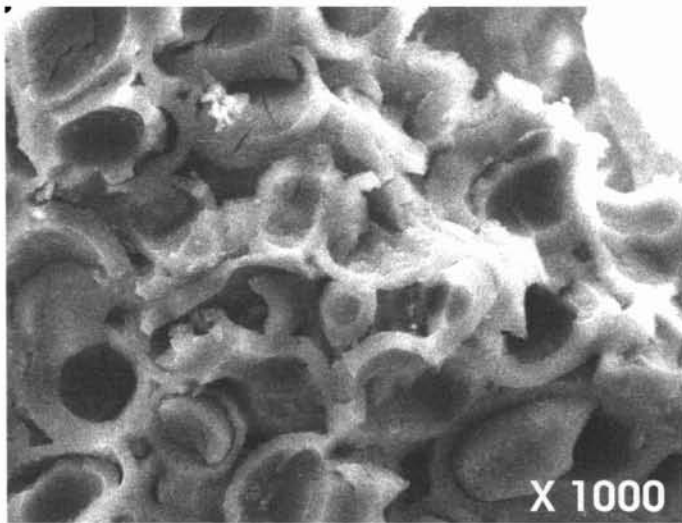
Figure 2.5b Reduction in iodine number with respect to the control carbon

to have an iodine value in the range of 15 – 856 and that the iodine number was high for samples activated at low temperature (650°C) (Usmani, T. H., *et al.*, 1996). The high value of iodine number for GAC indicates that the control carbon has high pore volume and is comparable to other commercial carbons. The loss in the iodine number and hence the pore volume will influence the adsorption capacity. The values indicate that the adsorption capacity will decrease with iron loading and the extent of reduction can be calculated from isotherm studies of typical chemical adsorbates.

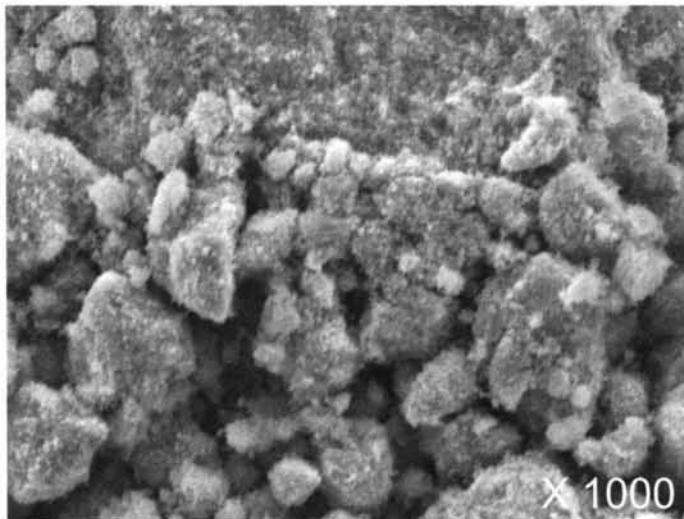
#### 2.2.3f **Scanning Electron Microscopy**

The texture of an adsorbent can be examined using scanning electron microscopy. These studies give an appreciation of the porosity of an adsorbent and hence a qualitative assessment of its ability to adsorb material in solution. The scanning electron micrographs of the samples were obtained using a JEOL JSM – 5600 Scanning Electron Microscope. The images were captured at two magnifications, x1000 and x170. Both secondary electron image and backscattered electron capture image were obtained.

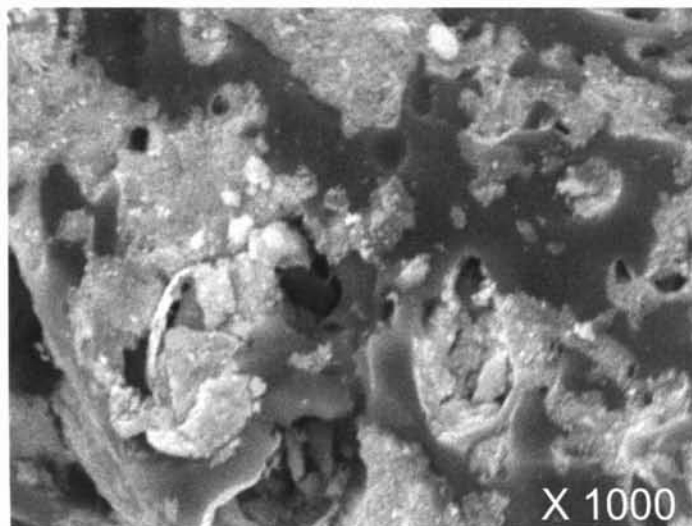
The micrographs of control carbon GAC, activated carbon – iron oxide composite MGAC7 and pure iron oxide MIO were obtained. The micrographs are shown in Plate 1. The secondary electron images of the GAC clearly explain the morphology of the control carbon as a highly porous structure with uniform distribution of the pores. The pore size was determined using an inbuilt scale and was calculated to be 10  $\mu\text{m}$ . The backscattered electron capture images are useful to give a tunnel vision to the interior of the pores but the obtained images hardly reveal any further information. The secondary electron images of the pure iron oxide reveal a non uniform distribution of the particles with sizes ranging from 3 – 20  $\mu\text{m}$ . The particle size is not uniform as the images were obtained from a compressed pellet of



a) SEM of control carbon, GAC



b) SEM of magnetic iron oxide



c) SEM of iron oxide loaded GAC (MGAC7)

the sample. The secondary electron image of the composite sample MGAC7 clearly shows the morphological changes due the impregnation of the iron oxide inside the pores of the carbon matrix. The iron oxide appears to be non uniformly distributed inside the pore structure. But the remaining pores appear to be intact. Most of the pores in the carbon matrix appear to be covered with the iron oxide. The pore size of the remaining pores is difficult to be determined from the images obtained.

The scanning electron micrographs of an activated carbon sample prepared from cherry stones (Lussier, M. G., *et al.*, 1994) give a similar pore size to that of the control carbon. The scanning electron microscopic studies on an acid treated anthracite grains (Daulan. C., *et al.*, 1998) on a macroscopic scale have shown that the diameters of the pores vary from 1 to 10  $\mu\text{m}$ . The pore diameter of the wood based Norit C granular activated carbon also falls in the similar range (Boehm, H. P., 1994). The SEM profile of Norit C carbon shows that the macropores are interconnected by the cell walls of the precursor wood at regular intervals which are meso/microporous in nature. Only the macroporosity of the carbon matrix are studied using the SEM profile. The pore diameter in GAC is 10  $\mu\text{m}$  and the particle size of the iron oxide impregnated inside the carbon matrix has to be less than that. Since the iron oxide loaded inside the carbon matrix is precipitated *in situ*, the size of the iron oxide particles will be less than 10  $\mu\text{m}$ . The electron micrograph of the composite sample shows deposition of iron oxide in the surface of the carbon granule as well. Hence, the composite sample of activated carbon with iron oxide is basically an impregnation of the iron oxide particles inside the porous structure as well as a surface coverage over the walls of the carbon granules.

### 2.2.3g **N<sub>2</sub> Gas Adsorption Studies**

Gas adsorption techniques are widely used for the characterization of carbons. The micropores (< 2.0 nm) are supposed to be the main reason for the very high adsorptive capacity. A review of publications about the characterization of activated carbons shows that there are many accepted techniques and methods available to evaluate the surface area and pore volume (especially the micropore volume) (Molina Sabio, M., 1985).

#### **Adsorption Isotherms:**

The adsorption isotherms of nitrogen gas at 77K in different adsorbent samples are obtained by plotting the volume of nitrogen ( $V_{N_2}$ ) adsorbed against the relative pressure ( $P/P_0$ ). The adsorption isotherms of nitrogen on the control carbon, GAC and composite samples MGAC5, MGAC7 and MGAC9 are given in Figure 2.6. The adsorption isotherms of all the four adsorbents are of type I, which indicates a high porosity of these activated carbons. Type I isotherms are characterized by the presence of a steep initial part followed by a gradually rising part, almost parallel to the X-axis, at higher relative pressures.

An examination of the isotherm plot shows that about 75 % of the pore volume is preferentially below  $P/P_0 = 0.10$  indicating that the samples are characterized by a large volume of very fine micropores (Matsumoto, A., *et al.*, 1997). It has been reported earlier that samples of high adsorption capacity exhibit a round knee and one with a low adsorption capacity has a sharper knee in isotherm plots (Gregg, S. J. & Sing, K. S W., 1967; Achari, V. S., 1998). The round knee of the isotherm plots for all the four samples suggest a high adsorption capacity. The presence of round knees is attributed to the presence of wider micropores in microporous solids (Sing, K. S. W., 1995; Carrot, P. J. M., *et al.*, 1988). In the lower

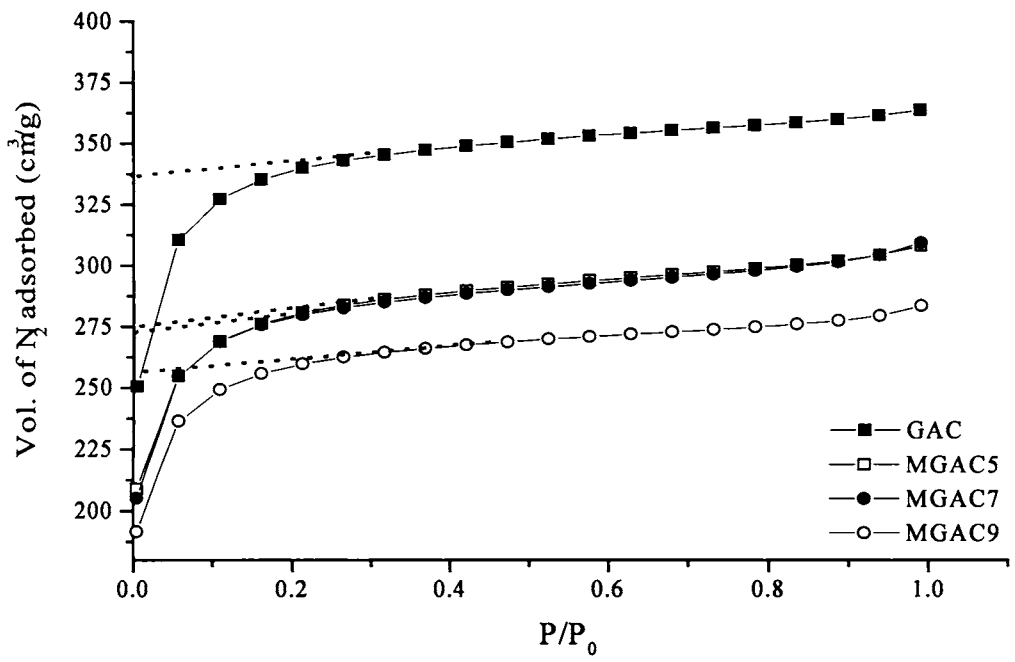


Figure 2.6 Isotherm plots for Nitrogen adsorption on the control carbon and the composite samples.

$P/P_o$ , ranges the isotherms move upward sharply up to  $P/P_o = 0.1$  and there after, bends to form the shape of a knee. The bending is completed at  $P/P_o = 0.2$  in all the cases. The adsorption of  $N_2$  is continued at smaller increments until the highest experimental relative pressure 0.95 is reached. Therefore, it can be assumed that the carbons GAC, MGAC5, MGAC7 and MGAC9 have wider pores with width of a few molecular layers (Sing, K. S. W., 1995; Carrot, P. J. M., *et al.*, 1988).

It can be seen that there is a marked reduction in the volume of nitrogen adsorbed on the control carbon GAC and composites, MGAC5, MGAC7 and MGAC9. The volume of nitrogen gas adsorbed is reduced significantly with MGAC5 compared to GAC. But the difference in the volume of nitrogen adsorbed with MGAC5 and MGAC7 are marginal. And there is again a significant reduction in the volume of nitrogen adsorbed with MGAC9.

**Analysis of Nitrogen Isotherms by BET Method:** The BET nitrogen adsorption isotherm is an extension of the Langmuir model for monolayer adsorption and it explains the multilayer adsorption of nitrogen or any other adsorbate on solid surfaces. The general form of the BET equation can be expressed as

$$\frac{V}{V_m} = \frac{C (P/P_o) [1 - (n + 1) (P/P_o)^n + n (P/P_o)^{n+1}]}{1 - (P/P_o) [1 + (C - 1) (P/P_o) - C (P/P_o)^{n+1}]} \quad (2.6)$$

For the purpose of characterization of porous materials, a limiting form of the equation is given in the section 2.3.2.

The BET plots for the adsorption isotherms for the control carbon, GAC and the magnetic iron oxide loaded activated carbon samples, MGAC5, MGAC7 and MGAC9 are given in Figure 2.7. The plots are found to be linear within a relative pressure range of 0.005 to 0.75. However, reports suggest that a relative pressure in the range of 0.10 to 0.30 is more valid for the BET analysis of carbon materials

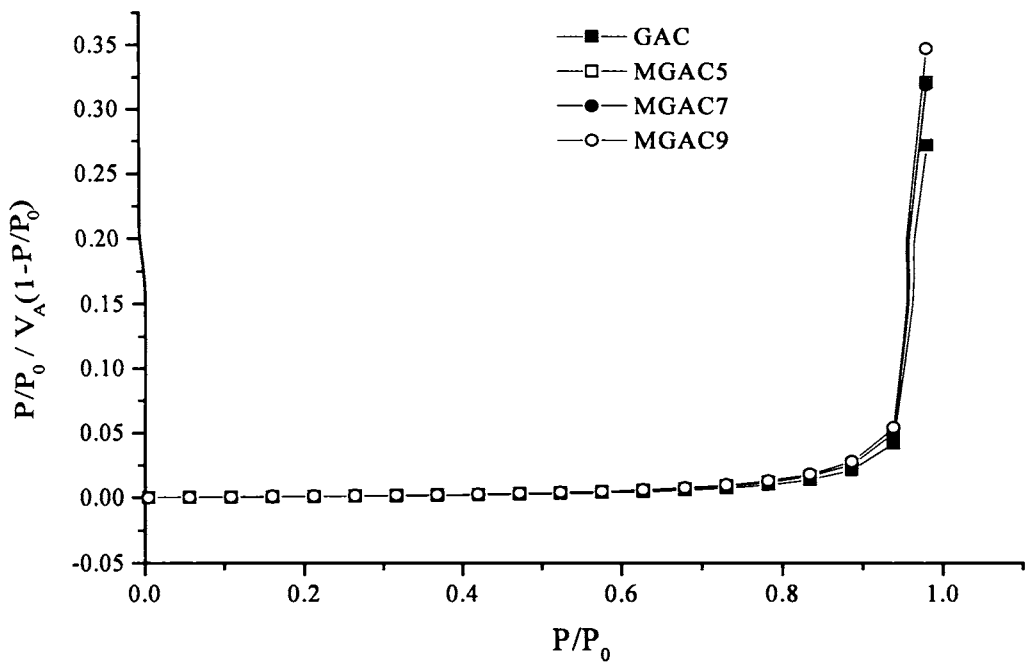


Figure 2.7 BET plots for the adsorption of  $N_2$  on carbon samples.

(Kaneko, K., *et al.*, 1992). It can be seen these plots loses their linearity on increasing the relative pressure above 0.75. Similar works reported earlier relate the initial adsorption of N<sub>2</sub> molecule in the high energy sites or micropores (Brunauer, S., *et al.*, 1938) after which adsorption proceeds on the surface of the adsorbed layer.

Porosity characteristic of the activated carbons are presented in Table 2.1. Pore volume of GAC, GAC5, GAC7 and GAC9 (cm<sup>3</sup>/g) were evaluated as 247.71, 205.15, 204.31 and 189.64. The values show a marked reduction in the pore volume with iron oxide impregnates, adsorption of N<sub>2</sub> gas on carbon is a process that occur in different phases. At first, the micropores are preferentially filled due to high potential energy followed by thickening of adsorption energy in mesopores and multiplayer adsorption in macropores. Therefore BET monolayer is taken as an indicator of micropore volume and is calculated using Dubinin- Radushkevich equation (McEnaney, B., 1987). A critical analysis of the data reveals a marked reduction in the micropore volume during surface treatment. On impregnation of GAC with iron oxide micropore volume showed a decrease 17.18% for MGAC5, 17.52% for MGAC7 and 23.44% for MGAC9. Maximum reduction in micropore volume is observed for MGAC9 and pore volume reduction for MGAC5 and MGAC7 differs by a marginal percentage of 0.34.

The total pore volume, assumed to be the sum of  $V_{mi} + V_{meso}$  was measured from adsorbed quantity at  $V_{0.95}$ . The values were determined to be for 361.69 for GAC, 304.37 for MGAC5, 304.40 for MGAC7 and 279.61 for MGAC9. The calculated decrease in total pore volume is found to be 15.84% for MGAC5, 15.83 for MGAC7 and 22.6% for MGAC9 with respect to the control GAC. This reveals a fraction of the remaining mesopores amounting to 113.98 cm<sup>3</sup>/g for GAC that were undisturbed during iron oxide impregnation. On analysis of the data, it is seen that

Table 2.1 Pore volumes of activated carbons

Carbon	$V_m$ (cm <sup>3</sup> /gm)	$V_m$ (mol/gm)	$V_{0.94}$ (cm <sup>3</sup> /gm)	$V_{0.94}$ (mol/gm)	$V_{meso}$ (cm <sup>3</sup> /gm)	$V_{meso}$ (mol/gm)
GAC	247.71	0.309	361.69	0.453	113.98	0.142
MGAC5	205.15	0.256	304.37	0.380	99.22	0.124
MGAC7	204.31	0.255	304.4	0.380	100.09	0.125
MGAC9	189.64	0.236	279.61	0.349	89.87	0.112

Table 2.2 Surface area of Activated carbons

Carbon	$S_{BET}$	$S_{tot}$	$S_{BET}/S_{tot}$	$S_{meso}$	$S_{meso}/S_{tot}$	$S_{meso}/S_{BET}$
GAC	1078.34	1574.51	0.69	496.18	0.32	0.46
MGAC5	893.05	1324.98	0.67	431.92	0.33	0.48
MGAC7	889.4	1325.11	0.67	435.71	0.33	0.49
MGAC9	825.54	1217.2	0.68	391.66	0.32	0.47

mesopore volume decreased to 99.22 (12.95% less) for MGAC5, 100.09 (12.19% less) for MGAC7 and 89.87 (21.15% less) for MGAC9. These observations make to believe that always a higher proportion of mesopores are used up in all conditions of chemical treatment. Mean while, the higher iron oxide loaded carbons showed that incorporated iron oxides occupy both micro and mesopores in almost equal proportions as evidenced by a reduction of  $V_{mi}$  by 22.6% and 23.44 % respectively. Similar porosity behaviour of MGAC5 and MGAC7, though they prepared with different Fe loading, is complicating and difficult to make a correct judgment. Under the treatment conditions the concentration of  $Fe^{2+}$  ions in the acidic medium may not be sufficient to provide a concentration gradient that could be transport  $Fe^{2+}$  ions into micro and mesopore network for optimum uptake. Equilibrium studies using phenols and dyes would answer this unusual behaviour of the carbons as higher concentrations are preferred to measure the isotherm uptake.

Surface areas of carbons were determined from BET analysis results and  $S_{BET}$ ,  $S_{tot}$ , and  $S_{meso}$  were evaluated and is given in Table 2.2. Ratio of  $S_{BET}/S_{tot}$ ,  $S_{meso}/S_{tot}$  and  $S_{meso}/S_{BET}$  were also evaluated. Surface area ( $S_{BET}$ ) of GAC, MGAC5, MGAC7 and MGAC9 were calculated to be 1078.34, 893.05, 889.40 and 825.54  $m^2/g$ . The total surface area ( $S_{tot}$ ) was calculated from the volume of  $N_2$  adsorbed at a relative pressure of 0.94. For GAC, 69% of total is contributed by micropores and for MGAC5, MGAC7 and MGAC9; the contribution is 67, 67 and 68 % respectively. This shows that the nearly equal proportion of micro and mesopores are used up for reaction. This trend is observed in the same sequence proportions reported as  $S_{meso}/S_{tot}$  and  $S_{meso}/S_{BET}$ .

**Evaluation of  $N_2$  Adsorption Using Langmuir Isotherms:** The Langmuir isotherm equation was applied for evaluating  $N_2$  adsorption by carbon samples. The

Langmuir plots were drawn by plotting  $1 / V_A \times (P_0/P)$  against  $P/P_0$  where  $V_A$  is volume of  $N_2$  adsorbed and  $P/P_0$  is the relative pressure. The Langmuir isotherm plots of nitrogen adsorption on carbon samples are shown in Figure 2.8. Important adsorption parameters such as Langmuir surface area, Langmuir constant  $b$ , and volume of nitrogen used for monolayer coverage,  $V_m$  were derived from these plots. These parameters are given in Table 2.3.

The Langmuir surface area of carbon samples were determined using data obtained within a  $P/P_0$  range of 0.05 to 0.26. It can be seen that impregnation of iron oxide has reduced the Langmuir surface area of the carbon samples. The Langmuir surface area of GAC was reduced from 1538.63 to 1276.22  $m^2/g$  for an iron oxide loading of 5.19 %. This further reduced to 1270.1 and 1178.94  $m^2/g$  for iron oxide loading of 10.2 and 13.6% respectively. The volume of nitrogen required for monolayer coverage also shows similar trend. Control carbon GAC has the highest  $V_m$  and it decreased with iron oxide loading. The values decreased from 353.45  $cm^3/g$  at STP for GAC to 293.17, 291.76 and 270.82 for MGAC5, MGAC7 and MGAC9 respectively. The reduction in monolayer volume is not proportional to the iron oxide loading.

#### 2.2.3h X-Ray Diffraction Studies

The X-Ray diffraction patterns of MIO and MGAC7 are given in Figures 2.9a & b. The X-Ray diffraction data shows a crystalline structure for MIO. The diffraction pattern of MGAC7 deviates from crystalline structure and indicates the amorphous character of the carbon matrix in which iron oxide is impregnated.

The analysis of the XRD pattern for MIO shows a sharp peak at  $2\theta = 35.641$  having a relative intensity of 100. There are weaker peaks at  $2\theta = 30.282$ ,  $62.825$ ,  $57.256$  and  $57.180^\circ$  having relative intensities of 32.38, 30.86, 25.71 and 22.6

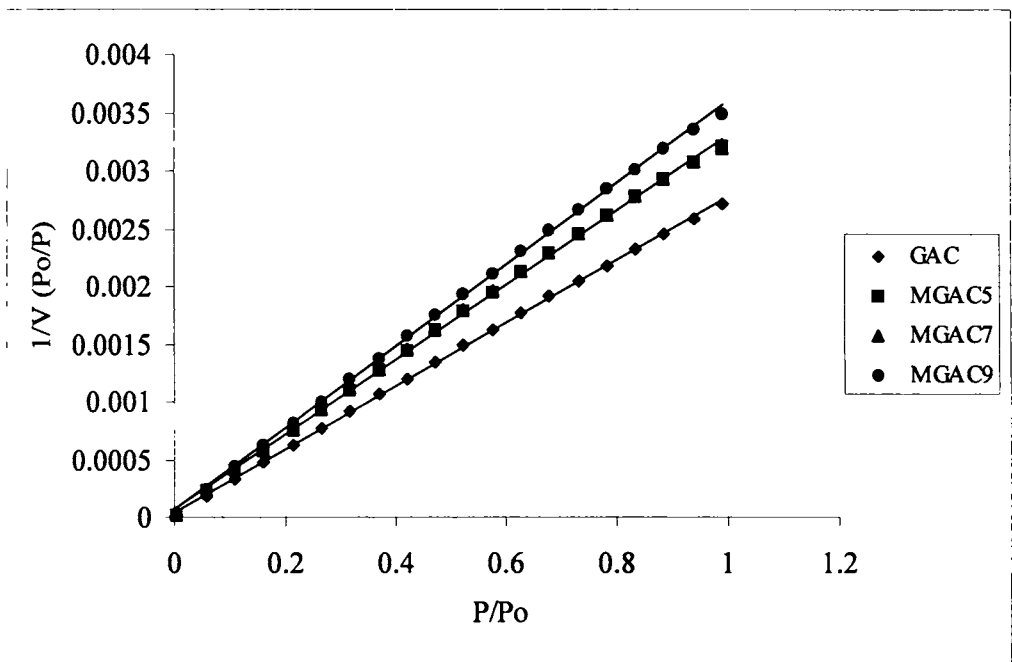


Figure 2.8 Langmuir isotherm plots for N<sub>2</sub> adsorption on carbon samples at 77 K.

Table 2.3 Langmuir parameters for N<sub>2</sub> adsorption on carbon samples

Carbon	Surface area m <sup>2</sup> /g	$V_m$ cm <sup>3</sup> /g	$b$ x 10 <sup>-3</sup>	$r^2$
GAC	1538.63	353.45	8.3	0.999
MGAC5	1276.22	293.17	9.3	0.999
MGAC7	1270.08	291.76	8.8	0.999
MGAC9	1178.94	270.82	8.9	0.999

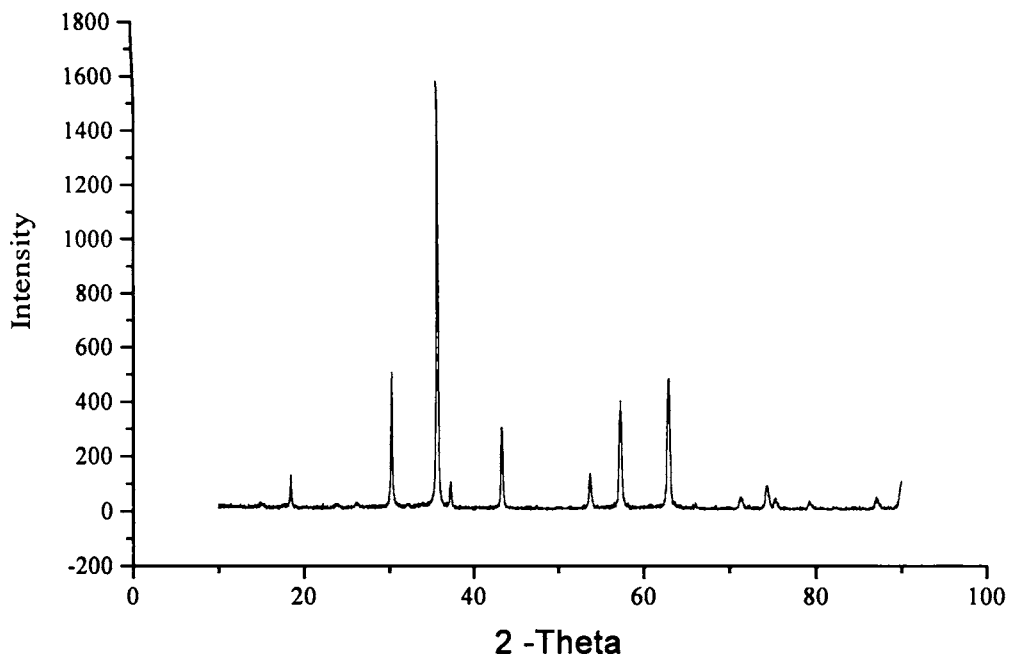


Figure 2.9a XRD pattern for magnetic iron oxide prepared in the laboratory

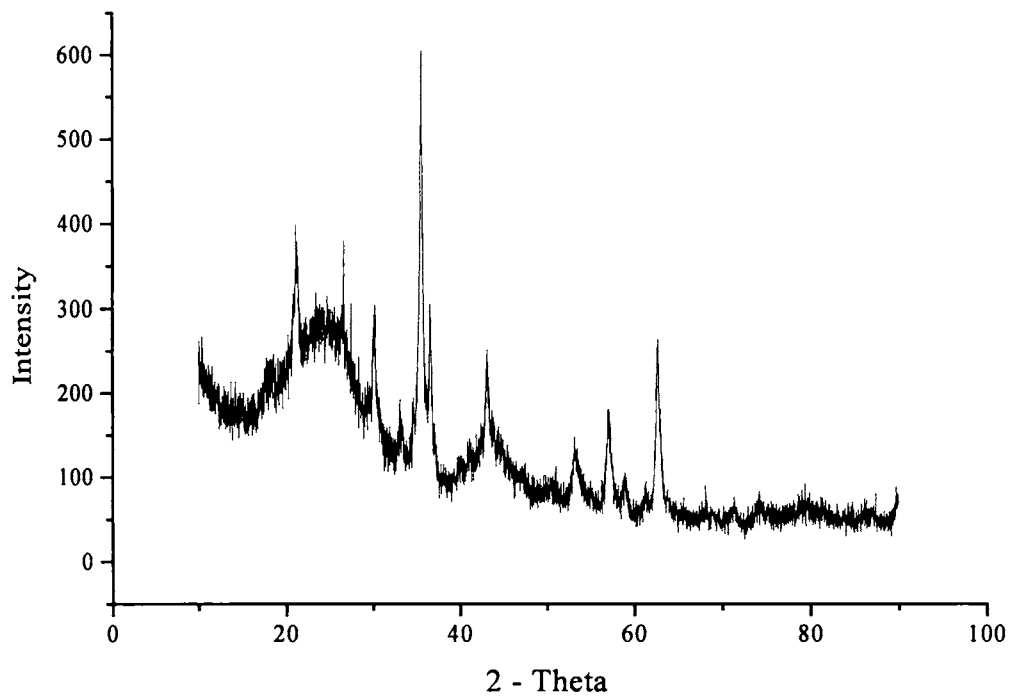


Figure 2.9b XRD pattern for MGAC7 at room temperature

respectively. The data was compared with the reference data on iron oxides. The magnetite ( $\text{Fe}_3\text{O}_4$ ) gives a peak at  $2\theta = 35.452^\circ$  and the maghemite ( $\gamma - \text{Fe}_2\text{O}_3$ ) gives a peak at  $2\theta = 35.598^\circ$ . The matching of other peaks suggests that the prepared iron oxide (MIO) has a structure similar to maghemite. But the presence of magnetite with some structural defects cannot be ruled out as some peaks correspond to that of the magnetite. A previous work on activated carbon – iron oxide composites has reported similar observations (Oliveira, L. C. A., *et al.*, 2002).

The XRD pattern of MGAC7 shows broader peaks suggesting a smaller crystallite size. The composite sample gives a sharp peak at  $2\theta = 35.5^\circ$  having a relative intensity of 100. There are weaker peaks at  $2\theta = 21.148, 26.58, 27.46$  and  $23.42^\circ$  having relative intensities of 66.17, 62.87, 50.5 and 50.17 respectively. The comparison of these data with the standard reference data on iron oxides suggests the presents of a maghemite phase in the sample. The value of  $2\theta = 35.5^\circ$  corresponds to a  $d$  value of 0.2528 nm which is characteristic of  $\gamma\text{-Fe}_2\text{O}_3$  (Shull, R. D., *et al.*, 1990). The reported  $d$  value for  $\gamma\text{-Fe}_2\text{O}_3$  is 0.252 nm. But there is slight deviation from the reference data suggesting a structural defect in the iron oxide impregnated. The XRD pattern of the composite sample is not as sharp as that of MIO due to the amorphous structure of the carbon. The presence of a diffraction peak in any shape in a carbon material is characteristic of graphite (Okabe, T., *et al.*, 1996). The grinding of composite samples for the XRD investigation should have some effect on the XRD patterns obtained. It has been shown that light grinding of a perfectly ordered graphite crystal leads to the creation of rhombohedral sequences (Bacon, G. E., 1952). The severe grinding converts pristine graphite into a material structurally identical with the disordered material obtained in pyrolyzing hydrocarbons (Tidjani, M., *et al.*,

1986). Hence, the broader peaks obtained for the composite samples can be attributed to the disordered structural alignment of graphitic planes in activated carbon.

### 2.2.3i Mossbauer Spectroscopic Studies

The Mossbauer spectra of MIO and MGAC7 were obtained using a  $\text{Co}^{57}$  source at room temperature. The spectra are given in Figures 2.10 a & b. The spectrum for MGAC7 is complex indicating the presence of several phases. But the spectrum for MIO is of a six line pattern and can be easily attributed to metallic iron. The MIO gives a hyperfine magnetic field at 49.6 T and 40.9 T with isomer shifts of 0.33 and 0.44 mm/s. The relative areas were calculated to be 0.20 and 0.026. The Mossbauer spectrum of MGAC7 shows hyperfine magnetic fields at 48.1 T and 36.1 T with isomer shifts of 0.34 and 0.49 mm/s. the relative areas were calculated as 0.2 and 0.12.

The Mossbauer parameters for binary iron oxides and hydroxides are given by Greenwood, N. N. and Gibb T. C. (Table 2.4) (1987). The magnetite gives a hyperfine field at 49.1 and 45.3 T at room temperature (300 K) (Banerjee, S. K., *et al.*, 1967) where as the maghemite ( $\gamma\text{-Fe}_2\text{O}_3$ ) gives a hyperfine field at 48.8 and 49.9 T with isomer shifts (related to Fe) 0.27 and 0.41 (Armstrong, R. J., *et al.*, 1966). The non magnetic  $\alpha\text{-Fe}_2\text{O}_3$  gives a hyperfine magnetic field of 51.5 at room temperature with an isomer shift of 0.38 mm/s (Kistner O. C., & A. W. Sunyar., 1960). The comparison of the Mossbauer spectra of the samples shows that magnetite along with maghemite is present in the MIO samples having a hyperfine field at 49.6 which is close the standard data of magnetite (49.1 T) and maghemite (49.9 T). The isomer shift values could not be compared since reference data at room temperature for magnetite was not available. The values can be related to the isomer shifts for maghemite. The analysis shows that the MGAC7 contains maghemite for having hyperfine fields at

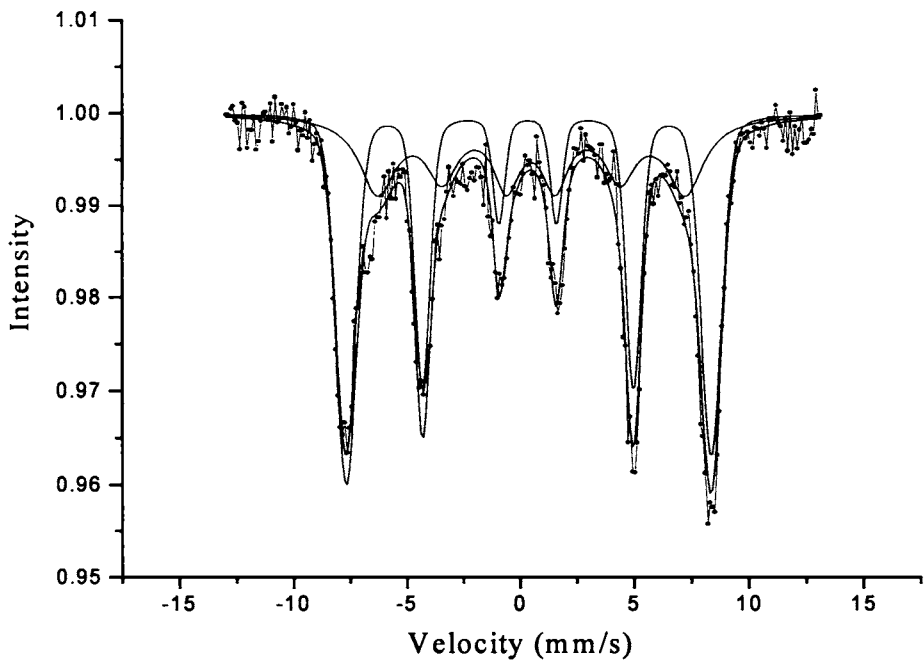


Figure 2.10a Mossbauer spectrum of MIO at 298 K.

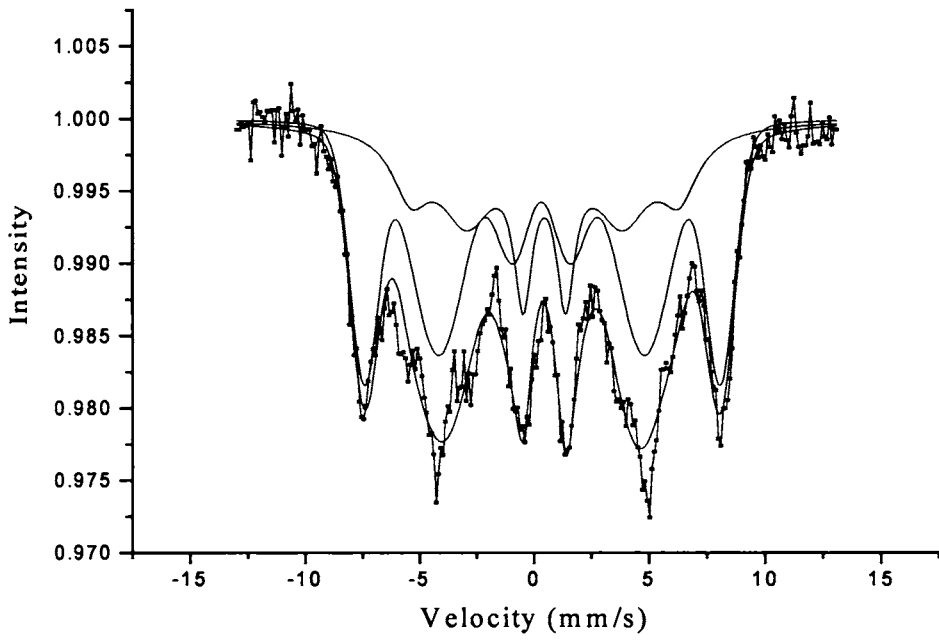


Figure 2.10b Mossbauer spectrum of MGAC7 at 298 K.

Table 2.4 Mossbauer parameters for binary iron oxides

Compound	T/K	$\Delta/(\text{mm s}^{-1})$	H/kG	$\delta(\text{mm s}^{-1})$	$\delta(\text{Fe})(\text{mm s}^{-1})$
$\alpha\text{Fe}_2\text{O}_3$	298	-0.12*	515	0.47 (SS)	0.38
	80	-0.22*	-	-	-
	(0)	-	(544)	-	-
$\gamma\text{Fe}_2\text{O}_3$	RT	-	488	0.36 (SS)	0.27
		-	499	0.50 (SS)	0.41
$\text{Fe}_{0.93}\text{O}$	297	0.46	0	0.68 (Cu)	0.91
		0.78	0	0.63 (Cu)	0.86
$\text{Fe}_3\text{O}_4$	300	-	491	A site	-
		-	453	B site	-
		-0.05	511	A site $\text{Fe}^{3+}$	0.37
	82	0.50	533	B site $\text{Fe}^{3+}$	0.77
		-0.02	516	B site $\text{Fe}^{3+}$	0.59
		0.95	473	B site $\text{Fe}^{2+}$	0.71
		-2.52	374	B site $\text{Fe}^{2+}$	1.20

48.1. The isomer shift values are close to that of the standard values for maghemite. The Mossbauer spectrum for MGAC7 is complex indicating the presence of many phases.

The distribution plots of MIO and MGAC7 are given Figures 2.11 a & b. respectively. The distribution plot for MIO indicate the presence of two phases having field strength at 49.6 T and 33.2 T. The distribution plot for MGAC7 indicates at the presence of more than two phases of iron oxides in the sample. The zero field strength peaks indicates the presence of anti ferromagnetic phases in the sample. Hence, it can be clearly seen that the MGAC7 composite sample is essentially a mixture of oxides with maghemite as the dominant phase.

### 2.2.3j **Magnetization Studies**

The response of a material to an applied field and its hysteresis is an essential tool of magnetometry. Paramagnetic and diamagnetic materials can easily be recognized, soft and hard ferromagnetic materials give different types of hysteresis curves and from these curves values such as saturation magnetization, remanent magnetization and coercivity are readily observed. The vibrating sample magnetometry is an important method used to characterize magnetic materials. VSM system measures the magnetic properties of materials as a function of magnetic field, temperature and time. The suitability of a material for a particular application is determined principally from its hysteresis loop, and VSM is the most common technique that is employed for hysteresis loop measurements.

The VSM studies were carried out on MGAC5, MGAC7 and MGAC9 to study the magnetic property of the materials. The hysteresis loops are given in Figures 2.12 a, b & c. The loop parameters  $M_S$ ,  $M_R$ , and coercivity were calculated. The saturation magnetization  $M_S$  for MGAC5, MGAC7 and MGAC9 was calculated to be

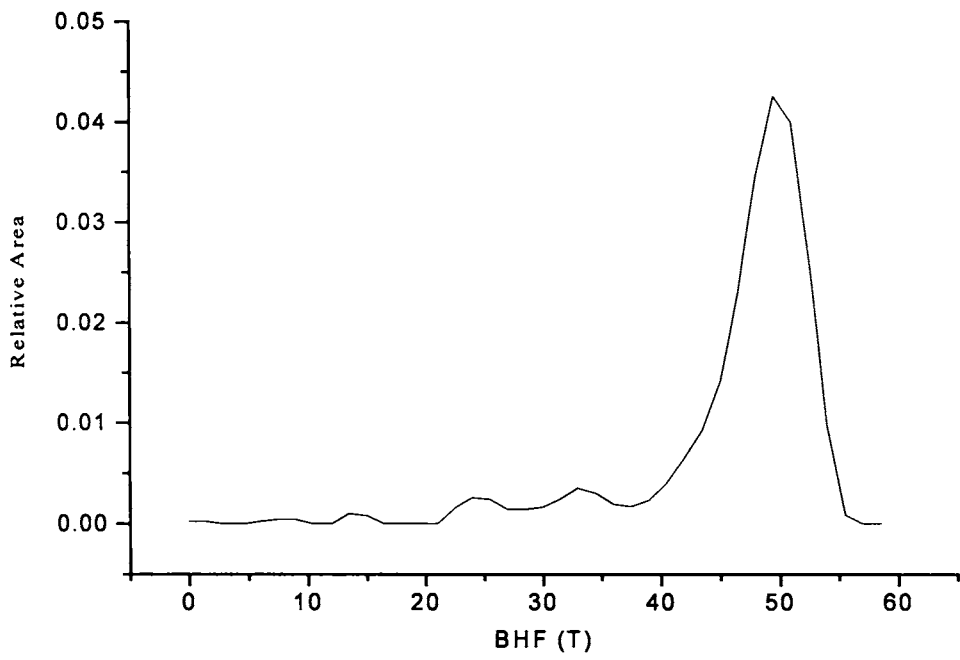


Figure 2.11a Magnetic distribution plot for iron oxide

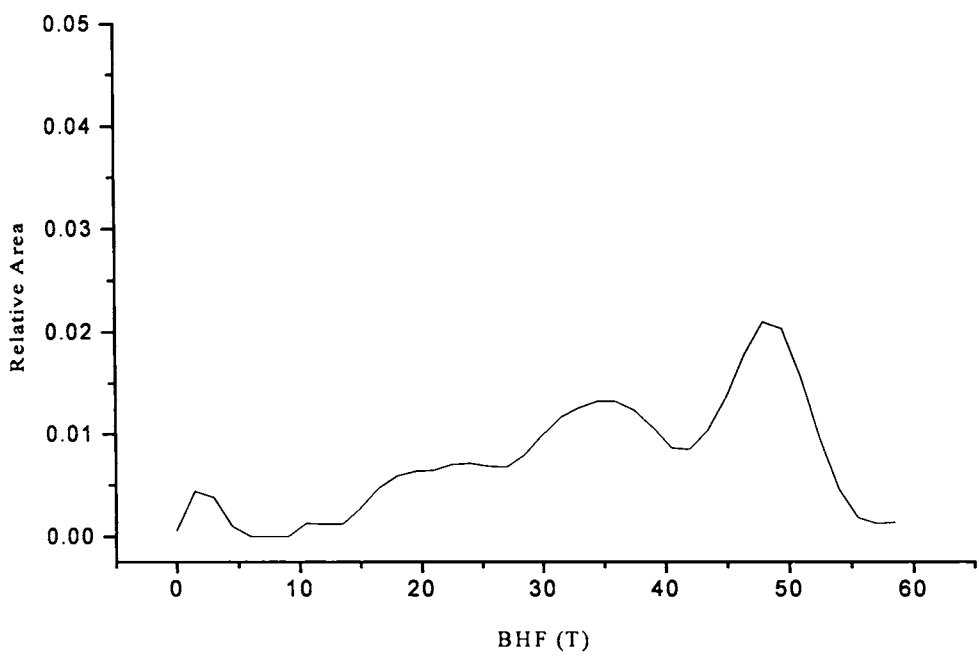


Figure 2.11b Magnetic distribution plot for activated carbon iron oxide composite, MGAC7

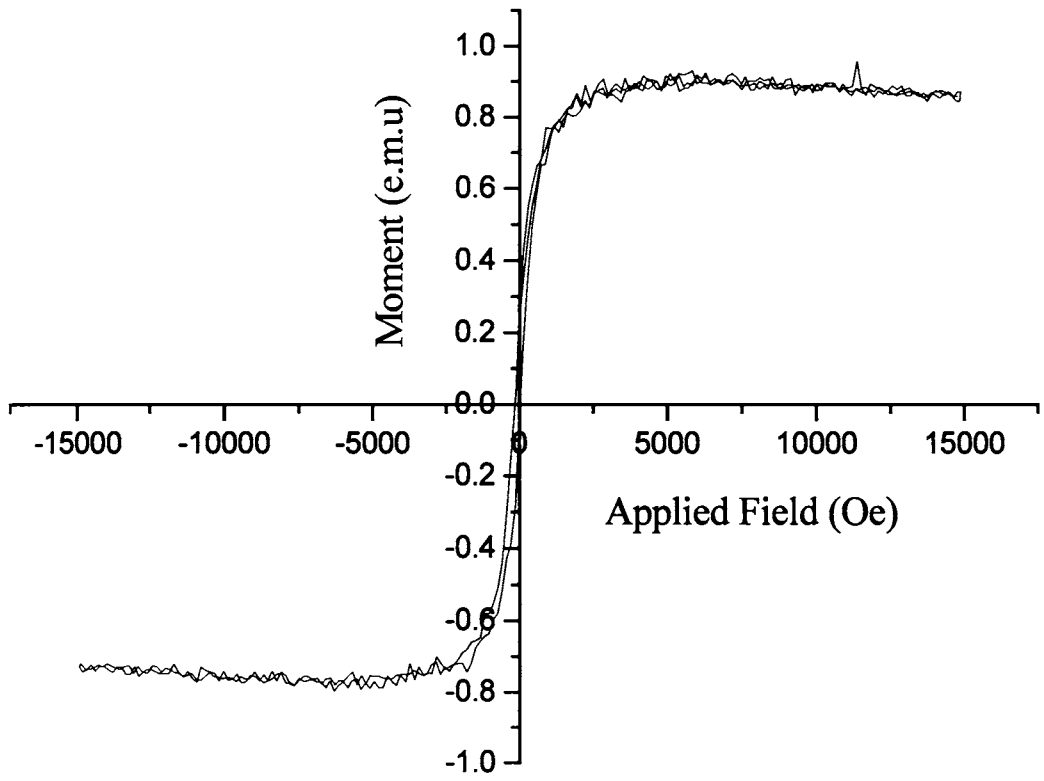


Figure 2.12a Hysteresis loop for MGAC5 obtained by VSM

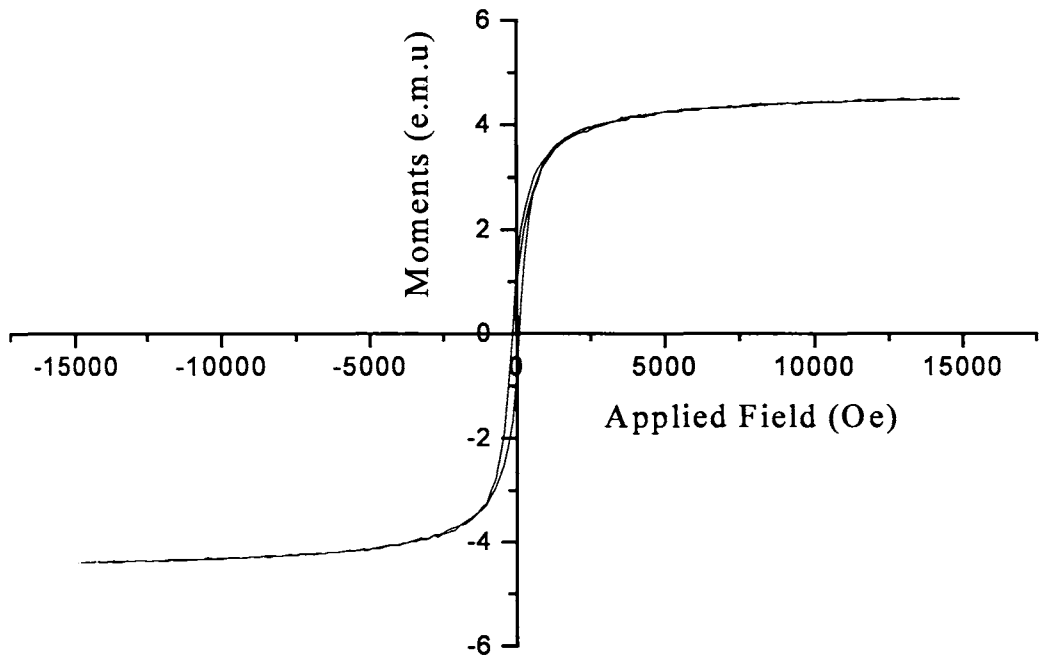


Figure 2.12b Hysteresis loop for MGAC7 obtained using VSM

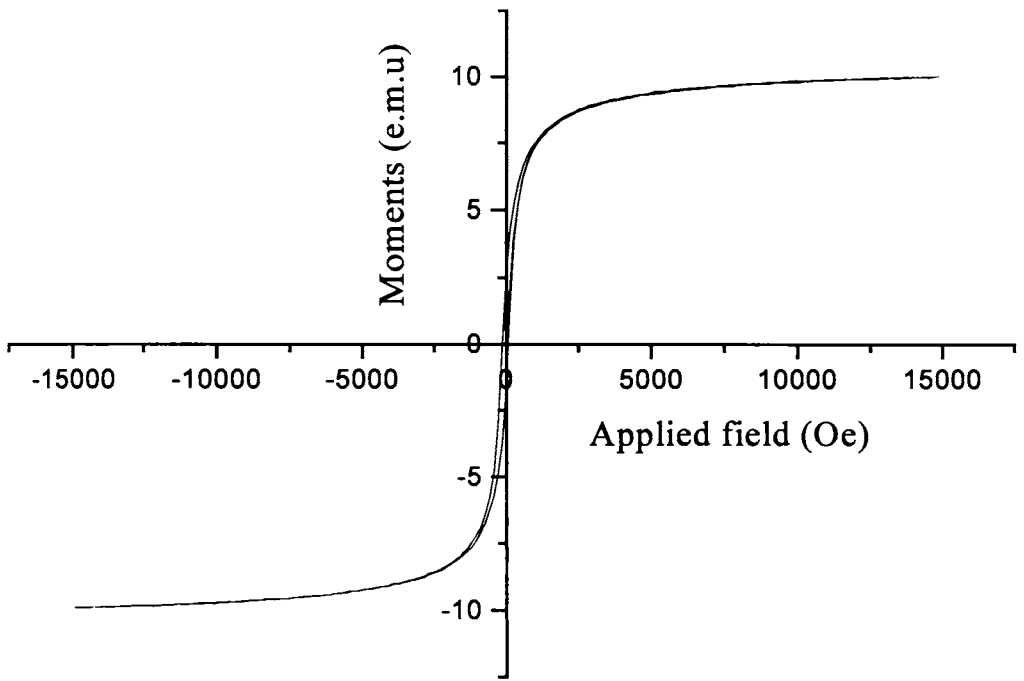


Figure 2.12c Hysteresis loop for MGAC9 obtained using VSM

0.80, 4.54 and 9.88 e.m.u/g. The remanent magnetization  $M_R$  for MGAC5, MGAC7 and MGAC9 was determined to be 0.15, 0.8, and 1.9 e.m.u/g respectively. The coercivity was also calculated from the hysteresis curve for MGAC5, MGAC7 and MGAC9 to be 96.0, 90.0 and 96.0 Oe respectively. The hysteresis curves for these composite samples are similar to that of a ferromagnetic material. Although the material is ordered ferromagnetically, it consists of a number of ordered domains arranged randomly giving no net magnetization. As the magnetic field,  $H$ , is applied those domains, which are more energetically favourable, increase in size at the expense of those whose moment lies more antiparallel to  $H$ . There is now a net magnetization,  $M$ . Eventually a field is reached where all of the material is a single domain with a moment aligned parallel, or close to parallel, with  $H$ . and, the material reaches saturation magnetization,  $M_S$ . The process of magnetization in a ferromagnet is given in Figure 2.13.

The plot of  $M_S$  versus iron loading is given in Figure 2.14. There is some correlation for the saturation magnetization and the extent of iron loading as is evident from the plot. The increase in iron concentration in the composite samples leads to a higher magnetization. As the applied field is reduced to zero after the sample has reached saturation the sample can still possess a remanent magnetization,  $M_R$ . the magnitude of this remanent magnetization is a product of the saturation magnetization, the number and orientation of easy axes and the type of anisotropy symmetry. This can be seen from the values of  $M_R$  which retains considerable magnetic property which is in proportion to the saturation magnetization values. The remanent magnetization is again proportional to the iron loading in the samples. The coercive field is the field at which the remanent magnetization is reduced to zero. This can vary from a few  $A/m$  for soft magnets to  $10^7 A/m$  for hard magnets. The coercivity is

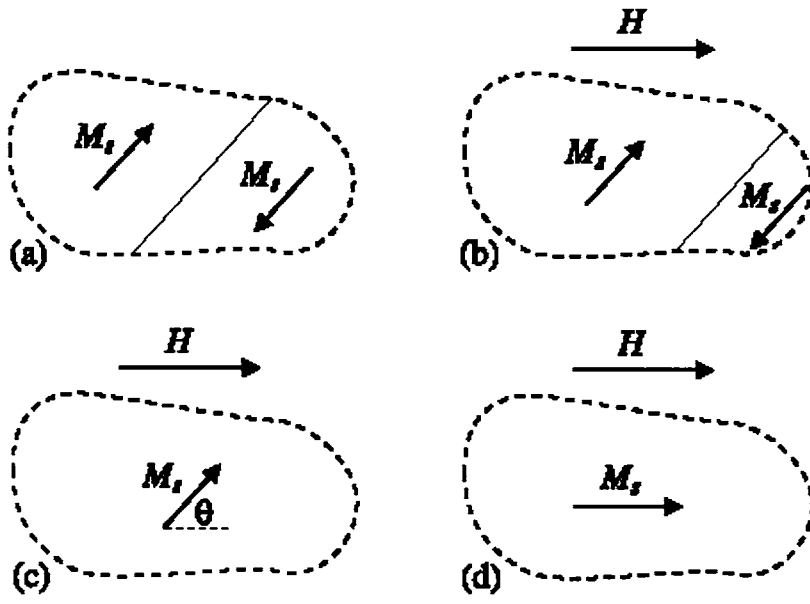


Figure 2.13 The process of magnetization in a demagnetized ferromagnet.

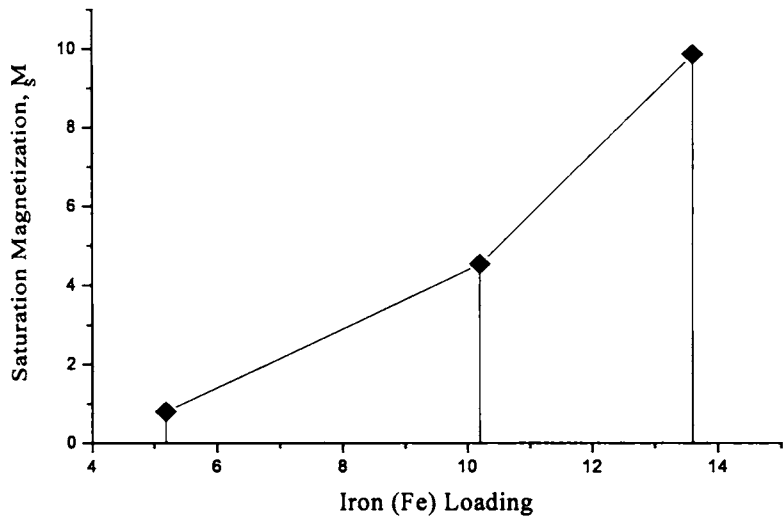


Figure 2.14 Plot showing the variation of saturation magnetization with iron oxide loading

also used to classify the magnetic materials as soft or hard. Soft materials are characterized by large permeabilities and very small coercivities, typically less than 1 Oe (Jiles., D., 1991). Hard magnetic materials are most often used in permanent magnet applications, and are characterized by large saturation magnetizations, large coercivities, typically greater than 10 kOe. Intermediate magnetic materials are generally characterized by coercivities of the order of 1 kOe, and these materials are usually used in magnetic media (Buschow, K. H. J., *et al.*, 1993). Intermediate materials include;  $\gamma\text{-Fe}_2\text{O}_3$ ,  $\text{Co}_{80}\text{Cr}_{20}$ ,  $\text{Co}_{77}\text{Ni}_{10}\text{O}_{13}$ , and thin films (Valenzuela., R., 1994). The values of coercivity obtained from the hysteresis loop suggest  $\gamma\text{-Fe}_2\text{O}_3$  present in the composite.

### 2.3k Thermo Gravimetric Analysis

TGA/DTG of activated carbons explains the thermal stability based on weight loss as a function of temperature. An evaluation of the type and nature of the thermally dissociable oxygen surface groups on activated carbon is already reported (Molina-Sabio, M., *et al.* 1994; Tremblay, G, *et al.*, 1978; Walker, P. L. Jr., 1979):

TGA of GAC is given in Figure 2.15a and shows that a distinct decomposition steps. On raising the temperature from 27°C to 100°C, a weight loss of 8.87% is observed and corresponds to the loss of moisture adhered. Further heating records a 2.6% loss in the temperature range of 100 to 365°C and relates to the thermal decomposition of oxygen surface groups. Temperature controlled decomposition in the range of (365-790°C) recorded a weight loss of 44.46%, that amounts to the carbons skeleton decomposition. A dry weight of 48.88% (discarding moisture content) is left after 800°C with a total burn off of 51.12%.

TG/DTG profile of MGAC5 is given in Figure 2.15 b and shows approximately 17.26% loss in the first phase between 0°C to 200°C, indicating a loss

Sample: GAC  
Size: 3.1200 mg  
Method: Ramp  
Comment: TGA- balachandran

TGA

File: C:\TA\DATA\TGA\balachandran\GAC a  
Operator: Thomas  
Run Date: 26-May-04 15:33  
Instrument: TGA Q50 V2.34 Build 127

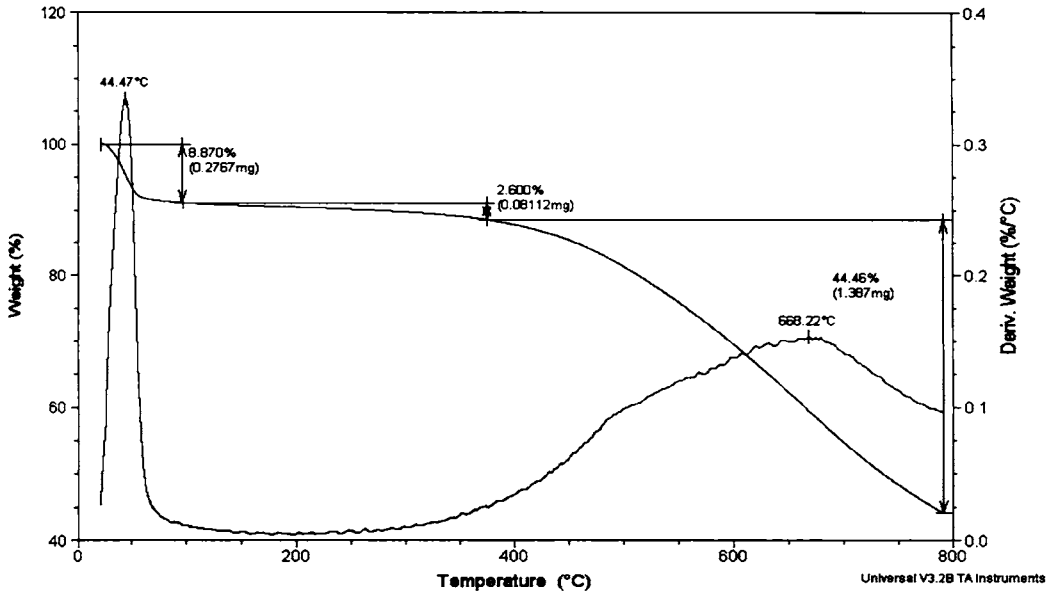


Figure 2.15a TGA plots for GAC.

Sample: MGAC -5  
Size: 5.8190 mg  
Method: Ramp  
Comment: TGA-balachandran

TGA

File: C:\TA\DATA\TGA\balachandran\MGAC -5 a  
Operator: Thomas  
Run Date: 27-May-04 15:04  
Instrument: TGA Q50 V2.34 Build 127

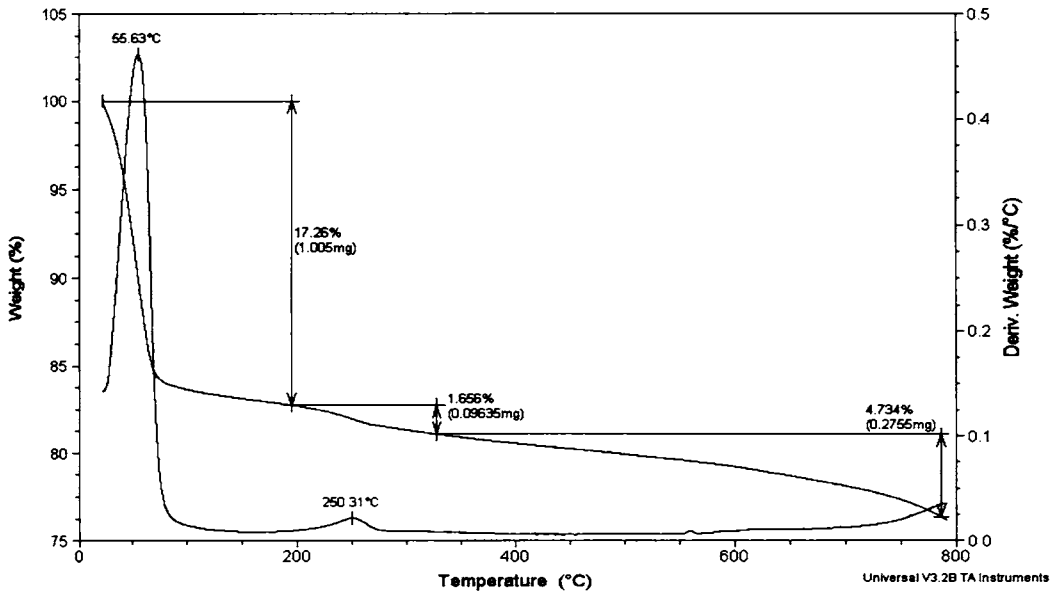


Figure 2.15b TGA plots for MGAC5.

of more entrapped water molecules (8.39%) in the pores. Decomposition of oxygen surface groups constitutes 1.66%, less by 37.5% compared to GAC. Further heating results in a weight loss of 4.7% due to carbon oxidation. At 800°C, only 8.17% of the dry mass is burnt, keeping a net weight of 91.83%.

The TGA profile for MGAC7 is given in Figure 2.15c. The moisture loss on heating amounts to 8.6% which is similar to the control carbon GAC. The weight loss is due to the thermal decomposition of  $O_2$  is further reduced to 1.47%, corresponds to a factor less by 56.34% than GAC. Weight loss at higher temperature (235 to 790°C) reconfirmed that iron oxide suppressed the carbon oxidation. At 800°C a total 94.39% of the dry mass is left as residual weight losing 5.6% the total weight.

The TGA plot for MGAC9 is given in Figure 2.15d and showed a loss of 14% weight at 100°C due to moisture adsorbed. In the second phase a loss in weight by 5.17% is observed. This constitutes the highest percentage of 19.8% among the 4 samples in the range. At 800°C a maximum burn of 18.52% was observed retaining 81.49% of the dry weight of the carbon composite.

Sample: MGAC -7  
Size: 8.6280 mg  
Method: Ramp  
Comment: TGA-balachandran

TGA

File: C:\TA\DATA\TGA\balachandran\MGAC -7 a  
Operator: Thomas  
Run Date: 27-May-04 12:35  
Instrument: TGA Q50 V2.34 Build 127

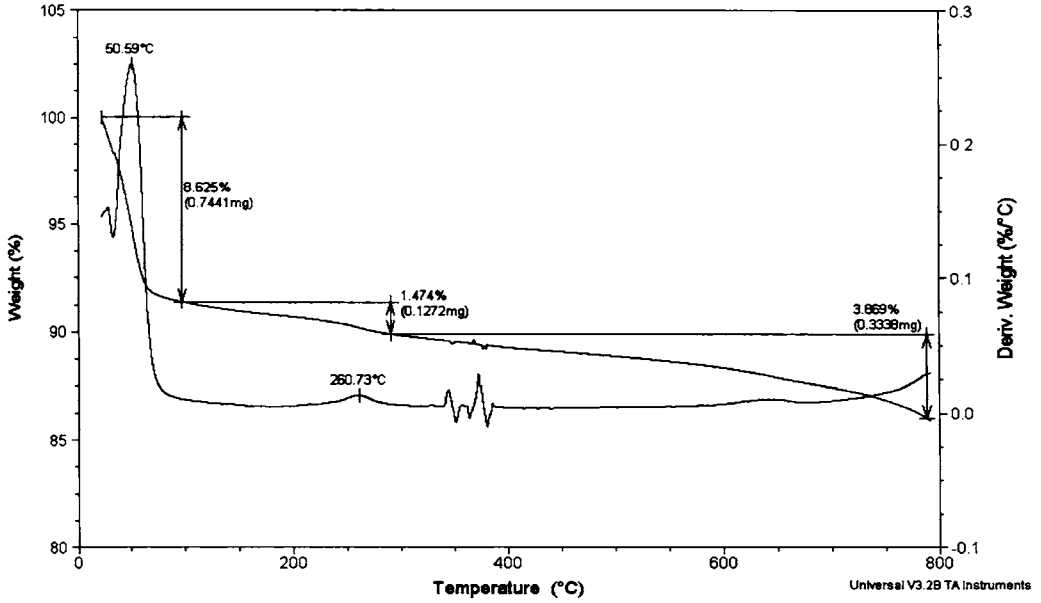


Figure 2.15c TGA plots for MGAC7.

Sample: MGAC-9  
Size: 10.9920 mg  
Method: Ramp  
Comment: TGA-balachandran

TGA

File: C:\TA\DATA\TGA\balachandran\MGAC-9 a  
Operator: Thomas  
Run Date: 27-May-04 09:26  
Instrument: TGA Q50 V2.34 Build 127

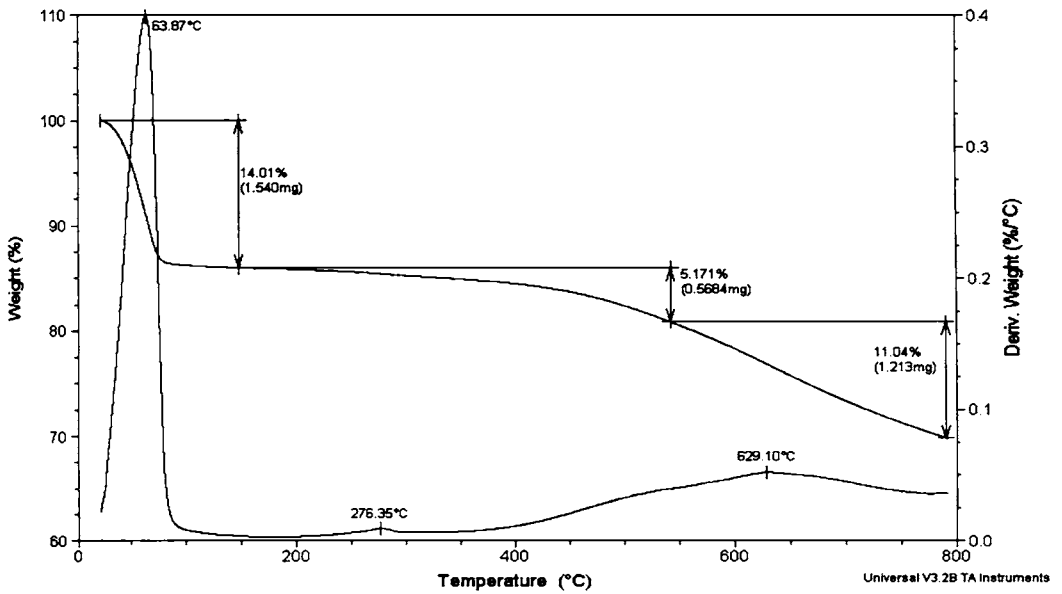


Figure 2.15d TGA plots for MGAC9.

## CHAPTER 3

### ADSORPTION STUDIES ON ACTIVATED CARBON – MAGNETIC IRON OXIDE COMPOSITES

#### 3.1 Introduction

The design of adsorption columns for industrial purpose has been done upon the evaluated parameters from a series of bench scale and pilot plant experiments. Batch adsorption systems are also well employed to evaluate the adsorption properties of new adsorbents and modified activated carbons. The results so obtained are empirical and valid for a specific system working under a set of experimental conditions. Use of adsorption models provides vital design information on extended plant wise application of a particular adsorbent – adsorbate system. Modeling is done on batch processes as they can yield accurate and reliable information that are “isolated” from the chromatographic and pseudoequilibrium effects encountered in column studies (Al Duri, B., 1995).

Rate of adsorption is provided by the study of system kinetics (or process dynamics). The concentration decay curve is important in designing of an adsorber and fixing the solution residence time. The adsorbent capacity (affinity) for the solute and thereby, the dosage of adsorbent required to remove unit mass of solute from solution is provided by equilibrium isotherm studies. Equilibrium data is described as solid phase concentration as a function of the fluid phase concentration. The most commonly used adsorption equilibrium descriptions are the Langmuir and Freundlich isotherms. A detailed description of these two expressions is already given in Chapter 1.

The adsorption properties of activated carbon magnetic iron oxide composites are evaluated and results are reported in this chapter. Batch adsorption experiments in gas and liquid phase were done to evaluate the adsorption potential of the materials.

Phenol, *p*-nitrophenol and methylene blue were used as model target solutes. Isotherms were studied at four different temperatures (10, 20, 30 and 40°C) and the kinetics of adsorption was worked out. The batch data were fitted onto Langmuir and Freundlich isotherms and adsorption constants characteristic of the system were determined. This chapter describes the effect of surface modification on the adsorption capacities of the prepared composites specific to four different adsorbates and to what extent it has differed from the control carbon. The kinetic data provides useful information on how fast these four target molecules are adsorbed on to composites samples compared to the native starting carbon.

## 3.2 Materials

### (i) Adsorbents

Magnetic iron oxide loaded activated carbon composites with different ratio of iron/carbon surface loading were used. A carbon control without modification was used to study the effect of surface modification. The descriptions of the four carbons used are GAC, MGAC5, MGAC7 and MGAC9.

### (ii) Distilled Water

Distilled water having conductivity less than 1  $\mu$  mho/cm at 303 K was used throughout this study.

### (iii) Chemicals

All the chemicals used were of analytical reagent grade, with almost 99.9% purity as specified by the manufacturers, E. Merck, BDH and Qualigens. The standard solutions of methylene blue, phenol and *p*-nitrophenol were prepared by dissolving the organic solutes in distilled water. The stock solutions of adsorbates were stored in clean glass bottles. Working standards and solutions were prepared by pipetting out

accurate volumes. Qualitative checks of stock solutions were carried out weekly by taking wavelength scan of the solution.

(iv) Glasswares

All the glasswares used for the adsorption studies were cleaned with dilute hydrochloric acid (1+1) and thoroughly washed with distilled water. Batch adsorption studies were carried out in 50 mL capacity glass tubes made of Borosil glass. Tubes were specially fabricated to satisfy the conditions of the adsorption studies. These glass tubes measured 20 cm in length and 3 cm in diameter. It has a detachable stopper through which a glass tube extends down the length of the adsorption tube. Other glasswares include beakers, conical flasks, and funnels that were used in separating the adsorbent from the solution after equilibration.

(v) Instruments

(a) Batch adsorption set up

A batch adsorption set up was fabricated for conducting the batch experiments. The experimental set up consists of a constant temperature water bath with temperature control within  $\pm 1$  °C deviation. The adsorption tubes mounted on an adjustable holding frame can be lowered into the water bath. A compressor supplied compressed air which is passed through an impinger tube containing distilled water to make it moisture equilibrated. The moisture equilibrated air passes into a sealed PVC tube which has nine side tubes with valves fitted to control the flow of the air. These tubes were fitted to the side tube of the adsorption tubes and the agitation of the adsorbent can be controlled by regulating the air supply. The air bubbles provide a method of mixing of the adsorbent and adsorbate in the solution and cause least attrition to the adsorbent.

(b) UV – Visible spectrophotometer

A Varian model Cary 50C UV – Visible spectrophotometer was used for the analysis of the adsorbate concentration. The wavelength scan was performed using this instrument to determine the  $\lambda_{\max}$  of each target adsorbate molecules.

## Methods

### Adsorption Equilibrium Studies

The adsorption batch experiments were carried out in adsorption tubes immersed in a constant temperature water bath. Adsorbent dosage was fixed at 0.05g and the adsorbate concentration varied from 100 to 2000 mg/L. A preliminary kinetic analysis with each adsorbent – adsorbate system was carried out to determine the required equilibration time. These preliminary kinetic analyses showed that 2h is sufficient to reach an equilibration between the amount adsorbed on the adsorbent and concentration of adsorbate remaining in solution. The batch experiments were then conducted as per the following procedure.

Approximately 100 mL of the adsorbate solution was pipetted out into glass tubes and immersed in water bath for 2 h to equilibrate to the experimental temperature. 0.05g of adsorbent samples was accurately weighed out into nine adsorption tubes and calculated volumes of temperature adjusted glass distilled water was added to these tubes. Accurate volumes of adsorbate solution required to give an adsorbate concentration of 100 to 2000 mg/L were pipetted out into these nine adsorption tubes at five minute intervals. The initial concentration of methylene blue was fixed at a lower range, 200 to 500 mg/L. Each tube was placed immediately inside the water bath and moisture equilibrated air was passed into these tubes to provide for uniform mixing of the adsorbent and adsorbate. A control was run simultaneously with no adsorbent sample. Each tube was taken out after 2h and the

contents were filtered through a Whatman No. 1 filter paper. First 30 mL of the filtrate was discarded to account for any adsorption onto the filter media and the rest was collected in a clean volumetric flask. The filtrates were suitably diluted and analysed for residual adsorbate concentration using the UV – VIS spectrophotometer. The  $\lambda_{\text{max}}$  of the organic adsorbates was determined by wavelength scan of a dilute solution. The  $\lambda_{\text{max}}$  for phenol, *p*-nitrophenol and methylene blue was determined to be 270, 320, and 660 nm respectively. All the batch tests were repeated thrice and the average values were used for data processing. The adsorption equilibrium studies were carried out in at four different temperatures: 10°C, 20°C, 30°C, and 40°C. All adsorption isotherms were determined without any adjustment of the pH of the adsorbate solution as variation in pH of the solution will alter the surface modification. At acidic pH the impregnated iron oxides will leach out of the composite samples and hence the influence of pH on adsorption isotherms was excluded from this study. However, the adsorption capacity of an activated carbon sample is dependant on the solution pH (Mattson, J. S. & Mark, H. B., 1971; Bansal R. C., *et al.*, 1988).

### 3.3.2 Adsorption Kinetics Studies

Kinetic studies were performed in the same glass adsorption tubes and at four different temperatures. The following procedure was used for conducting the kinetic studies on different adsorbate – adsorbent systems. 0.05g of adsorbent samples was used through out this study and the adsorbate concentration was fixed at 300 mg/L except in the case of methylene blue. The initial concentration of methylene blue was fixed at 250 mg/L.

0.05g of the adsorbent samples was accurately weighed out into the adsorption tubes and calculated volumes of distilled water were added to it. Temperature

equilibrated adsorbate solution was then added to each tube and placed in the water bath and moisture equilibrated compressed air was used for the proper mixing of the adsorbent and adsorbate in solution. A control run was performed simultaneously. Each tube was taken out at regular intervals and the solution was filtered to separate the components. The first 30 mL of the filtrate was discarded and the rest is analysed for residual concentration after suitable dilution.

### **Regeneration Studies on Composites**

The regeneration of spent adsorbent samples was done using phenol and *p*-nitrophenol as target molecules. The adsorbent – adsorbate ratio was fixed for both the adsorbate molecules. 0.1g of adsorbent samples was used for the study and the initial concentration of the adsorbate was fixed at 400 mg/L. Distilled water heated to boiling temperature was used for elution. The following procedure was used for carrying out the regeneration studies.

0.1g of the adsorbent sample was weighed out into a batch adsorption tube. Calculated volume of distilled water was added followed by required amount of the adsorbate solution. The tubes were placed inside the constant temperature water bath and the moisture equilibrated compressed air was passed through it to mix the adsorbent and adsorbate in solution. An equilibration time of 2h was given after which the solution was carefully filtered through a Whatman No. 1 filter paper. The first 30 mL of the filtrate was discarded and the rest is analysed for residual concentration after suitable dilution. The adsorbent material was completely transferred and collected on the filter media. The samples were then carefully washed with 100 mL distilled water, heated to boiling temperature, for five times with a total volume of 500mL. Samples were then dried in a hot air oven at 110°C for 3h. The batch experiment with another set of adsorbate solution of the previous concentration

(400 mg/L) was repeated after transferring the regenerated adsorbent sample into the adsorption tubes. The temperature of the adsorbent sample was adjusted to room temperature by keeping in an air tight desiccator before loading the second cycle of experiment. Five cycles of regeneration process were tried and the data is recorded. The following equation was used to calculate the % regeneration in each cycle of batch reaction.

$$\% \text{ regeneration, cycle } n = \frac{\text{Amount of adsorbate adsorbed per gram of adsorbent after regeneration, } n}{\text{Amount of adsorbate adsorbed per gram of fresh carbon}} \times 100$$

## 3.4 Results and Discussion

### 3.4.1 Adsorption of Phenol on Activated Carbon – Magnetic Iron Oxide

#### Composites

Phenolic compounds, especially the chlorinated species, impart medicinal iodine tastes to drinking water (Faust, S. D. & Aly, O. M., 1983). Most of this taste arises from the chlorination treatment for disinfection and taste and odor control. PAC and GAC have been used in water treatment for many years in a rather empirical manner for taste and odor removal (*Water Quality and Treatment*, 3<sup>rd</sup> ed., 1971).

Phenols being anionic in natural waters are highly toxic and are present in the effluents of a number of industrial units such as oil refineries, coke oven and steel plants. The concentration of phenols in wastewater varies from 10 to 3000 mg/L (Nemerow, N. L. & Dasgupta, A., 1991). In this context removal of phenols by adsorption has earned great importance in recent times. Several researchers attempted to relate the adsorption capacity of activated carbons towards phenol with the physical and chemical characteristics (Oda, H., *et al.*, 1981; Jankowska, H., *et al.*, 1986). The removal of phenol by activated carbon was first reported by Honig (1926). The porous structure of the activated carbon is an important factor in the adsorption of phenol

(Linares-Solano, A., *et al.*, 1980; Calleja, G., *et al.*, 1993). In all studies carbons with larger surface area exhibited greater adsorption capacities. It is also reported that phenol adsorption capacities of the laboratory made and commercially available carbons are not proportional to their surface area (Samaras, P., *et al.*, 1995). Kinetic experiments in combination with mathematical modeling showed fast internal diffusion of phenols into the large pores of the carbons (Samaras, P., *et al.*, 1995). These pores are formed by the catalytic activity of the mineral matter during activation.

Furthermore, as demonstrated in literature (Leon y Leon, C. A., *et al.*, 1992), there are basic sites on the surface of the carbons, probably located at  $\pi$  electron-rich regions within the basal planes of carbon crystallites, away from the crystallite edges. These regions predominate in carbon with low oxygen content (Leon y Leon, C. A., *et al.*, 1992) and may give rise to the formation of the above electron donor-acceptor complexes with the aromatic ring of the phenolic compounds. Thus, Coughlin and Ezra (1968) also suggested that phenol adsorption on carbon involves dispersive forces between the  $\pi$  electrons in phenol and the  $\pi$  electrons in carbons. Direct experimental support for this view was given by Mahajan and co-workers (1980).

Study of adsorption parameters from solution of non-electrolytes by micro porous solids is of great significance. The need for efficient removal of organic pollutants is becoming increasingly important. In this section an attempt is made to study the adsorption characteristics of phenol on the newly prepared activated carbon magnetic iron oxide composites. The objectives of this study are to evaluate the adsorption capacities of the composites towards phenol and the rate at which the adsorption proceeds.

#### 3.4.1a Adsorption Kinetics

The kinetics of adsorption of organic molecules is described by the solute uptake rate that determines the residence time required for the sorption reaction. It is well established that the sorption kinetics ultimately controls the process efficiency. The sorption of organic compounds such as phenolics from liquid phase to a solid phase can be considered as a reversible process, with equilibrium being established between the two phases.

The kinetic studies of phenol adsorption on GAC, MGAC5, MGAC7 and MGAC9 were carried out at a fixed initial concentration of 300 mg/L with an adsorbent dosage of 0.05g at different temperatures. The kinetic plots of phenol adsorption onto four adsorbents at different temperatures are given in Figure 3.1a -d. The amount of phenol adsorbed per gram of the adsorbent is plotted against time. The uptake of phenol onto these composites has two stages. The initial stage is very rapid and is followed by a slower adsorption step that gradually approaches an equilibrium condition. At 20°C, a fraction of 93 % phenol adsorbed is removed by GAC within 10 minutes where as the corresponding values for MGAC5, MGAC7 and MGAC9 are 92, 91 and 90. In the second stage, the adsorption proceeds slowly with a small fraction of phenol reaching only 98 % within 60 minutes in all the four samples. Relatively slow uptake rate on iron loaded samples compared to control carbon in the first stage can be related to narrow pores in these composite samples (Güzel, F. & Tez, Z., 1993). This is because fast internal diffusion into the carbon matrix is hindered by the presence of iron oxide in the porous structure. At 10°C, the fraction of phenol adsorbed on GAC within 10 minutes is 93 %. Corresponding values for MGAC5, MGAC7 and MGAC9 are 92, 91 and 89 %. This suggests that temperature does not have any significant influence on the fraction of adsorbate adsorbed in the

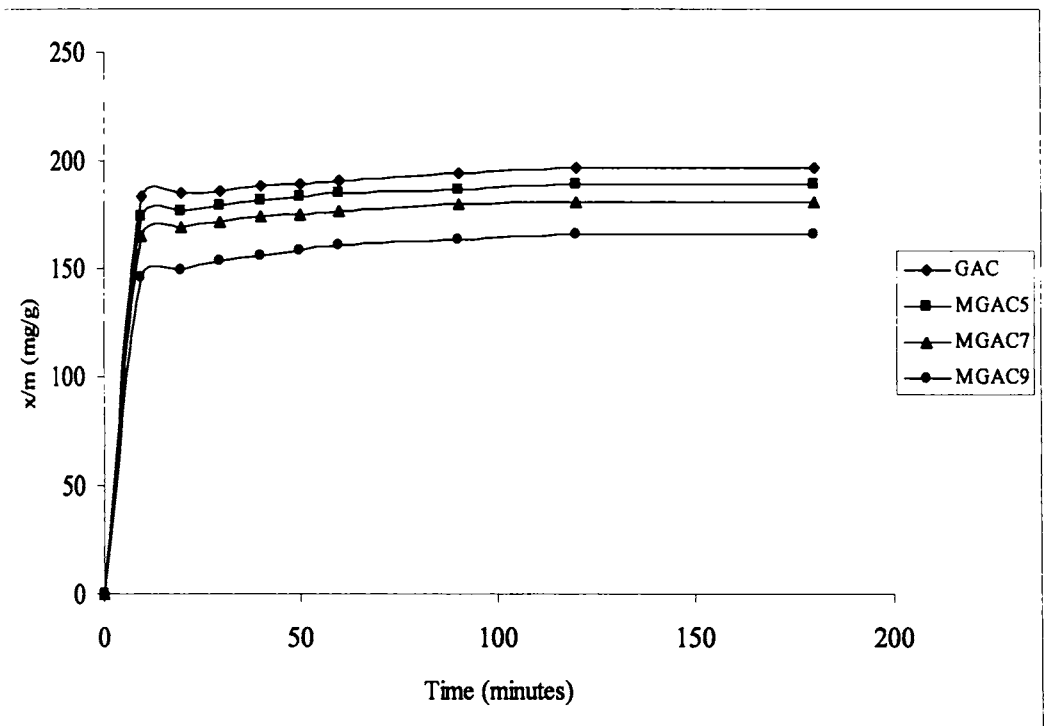


Figure 3.1a. Kinetic plots of phenol adsorption at 10 °C.

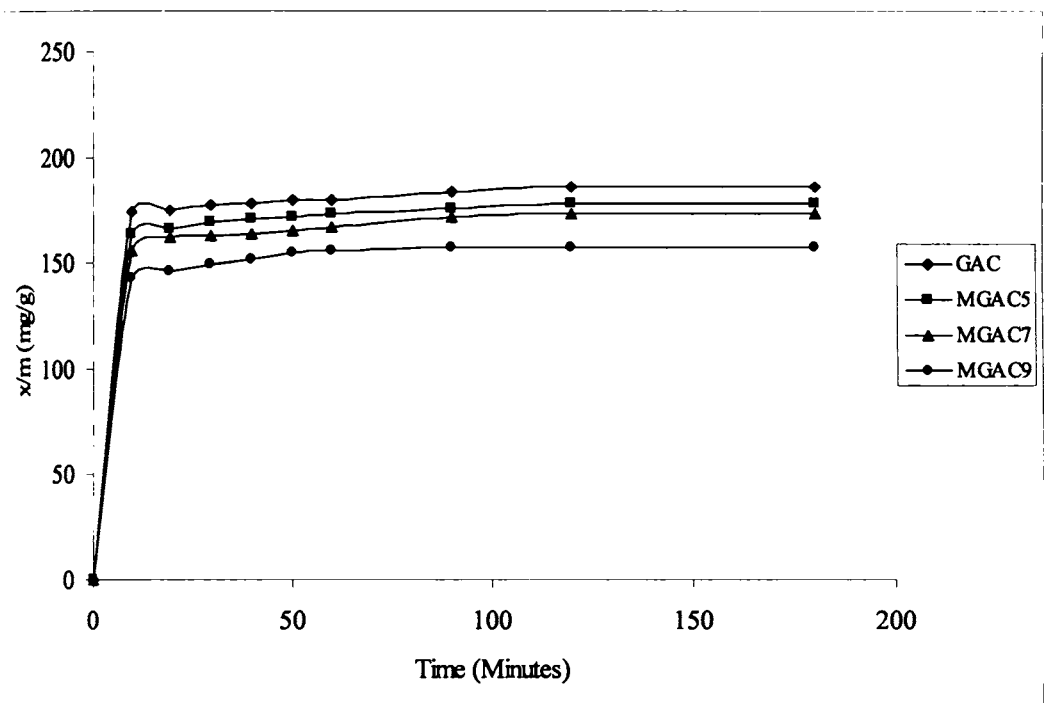


Figure 3.1b Kinetic plots of phenol adsorption at 20 °C.

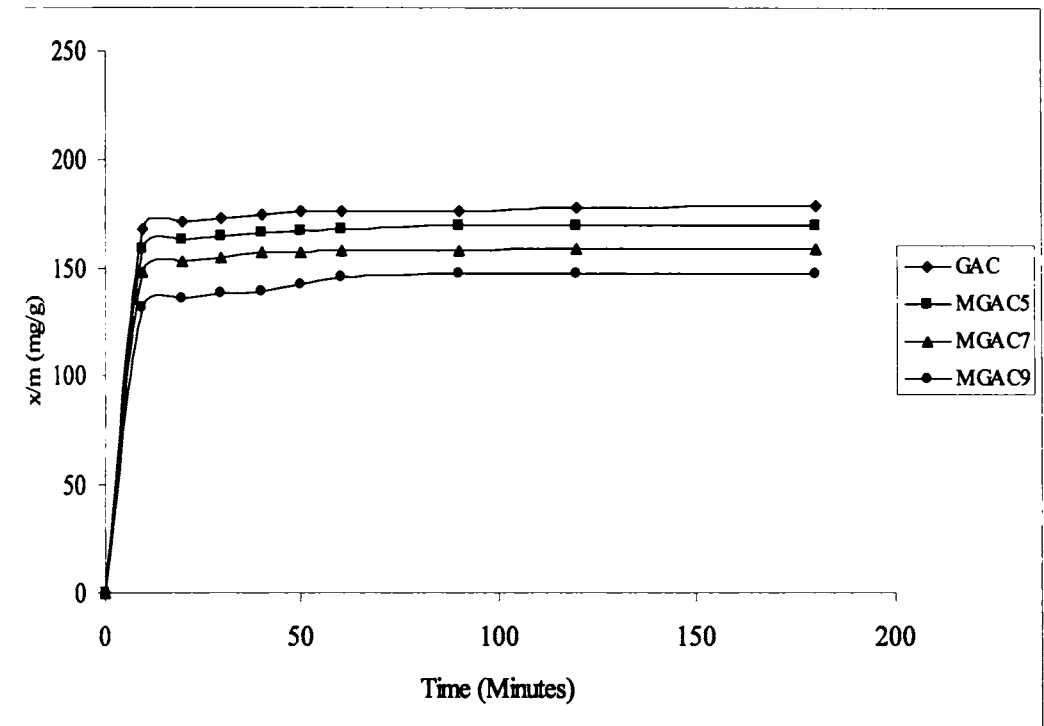


Figure 3.1c Kinetic plots of phenol adsorption at 30 °C.

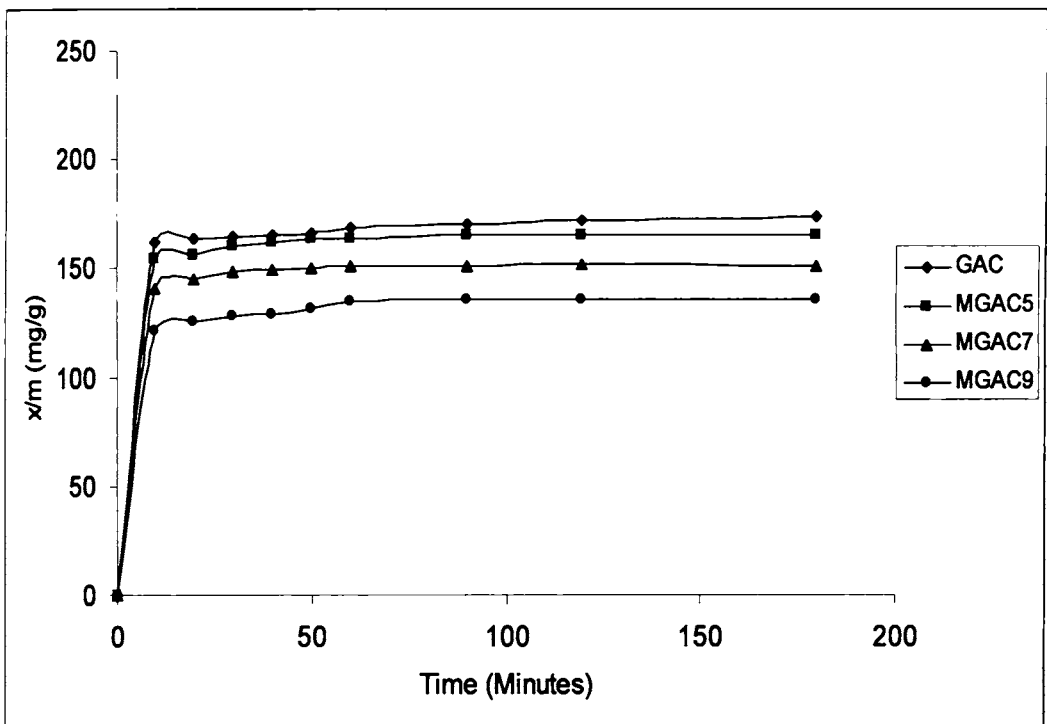


Figure 3.1d Kinetic plots of phenol adsorption at 40 °C.

initial stages of the process. But the changes in the pore structure due to iron loading do have an influence on the initial uptake of phenol.

#### **Evaluation of Rate Constants:**

The rate constants of adsorption were determined from the first order rate expression given by Lagergren (1898). The equation can be expressed as

$$\log (q_e - q) = \log q_e - k_{ad} \times t / 2.303 \quad (3.1)$$

where  $q$  and  $q_e$  are amounts of adsorbate adsorbed (mg/g) at time,  $t$  (min) and at equilibrium, respectively.  $k_{ad}$  is the rate constant for adsorption ( $\text{min}^{-1}$ ). A linear plot of  $\log (q_e - q)$  vs  $t$  indicates the applicability of the Lagergren equation. Values of  $k_{ad}$  are obtained from the slope of the linear plots.

The Lagergren plots of phenol adsorption on control carbon and composites samples at four different temperatures are given in Figure 3.2a - d. These plots clearly show that the adsorption process involves two steps, a rapid external or film diffusion step, which is completed within 10 minutes, and a slower internal diffusion, i.e. the transport of sorbate from the particle surface into interior sites. The overall rate of the adsorption process will be controlled by the slowest step (Al-Duri, B. & McKay, G., 1991). In this study the Lagergren kinetic model, is applied to the data valid for time after 10 minutes. This gave the rate constant for the limiting step in the phenol adsorption on carbon samples.  $k_{ad}$  calculated from the slope of the linear portion of Lagergren plots for phenol adsorption are given in Table 3.1. Rate constant for phenol adsorption on GAC at 20°C is  $1.26 \times 10^{-2} \text{ min}^{-1}$  and reduces progressively for iron oxide loaded samples. It can be seen from the table that the rate constant has decreased to  $1.10 \times 10^{-2} \text{ min}^{-1}$  for MGAC9. The corresponding values for MGAC5 and MGAC7 are 1.16 and  $1.11 \times 10^{-2} \text{ min}^{-1}$ . At 10°C, there is a reduction in the rate constant. The calculated rate constants for GAC, MGAC5, MGAC7 and MGAC9 are

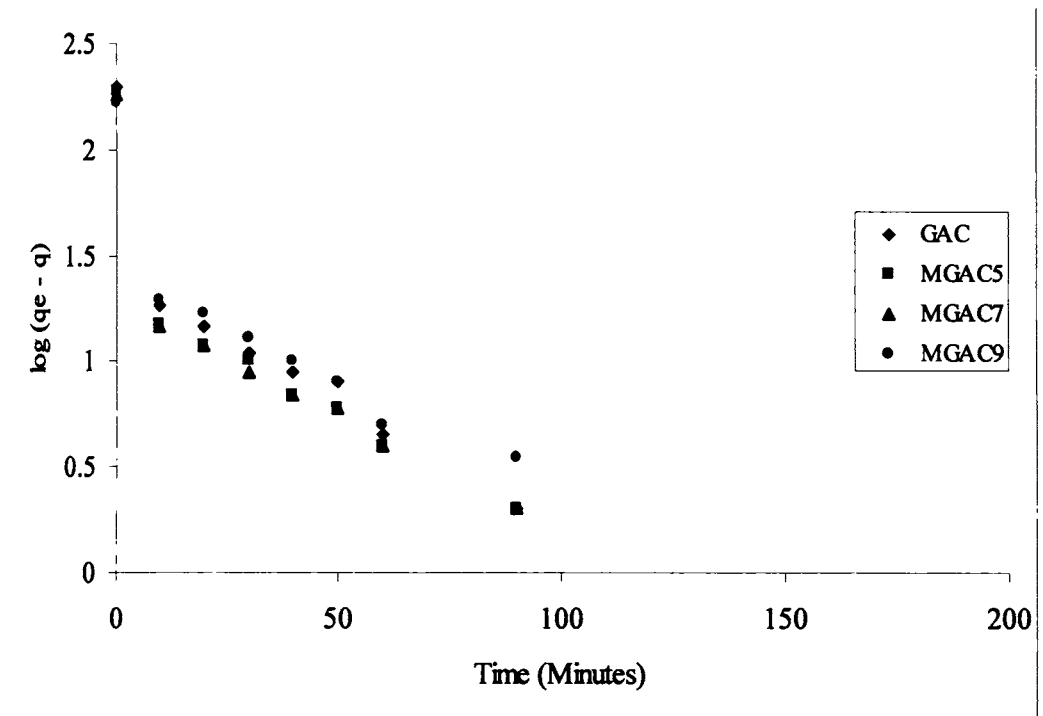


Figure 3.2a Lagergren plot for phenol adsorption at 10 °C.

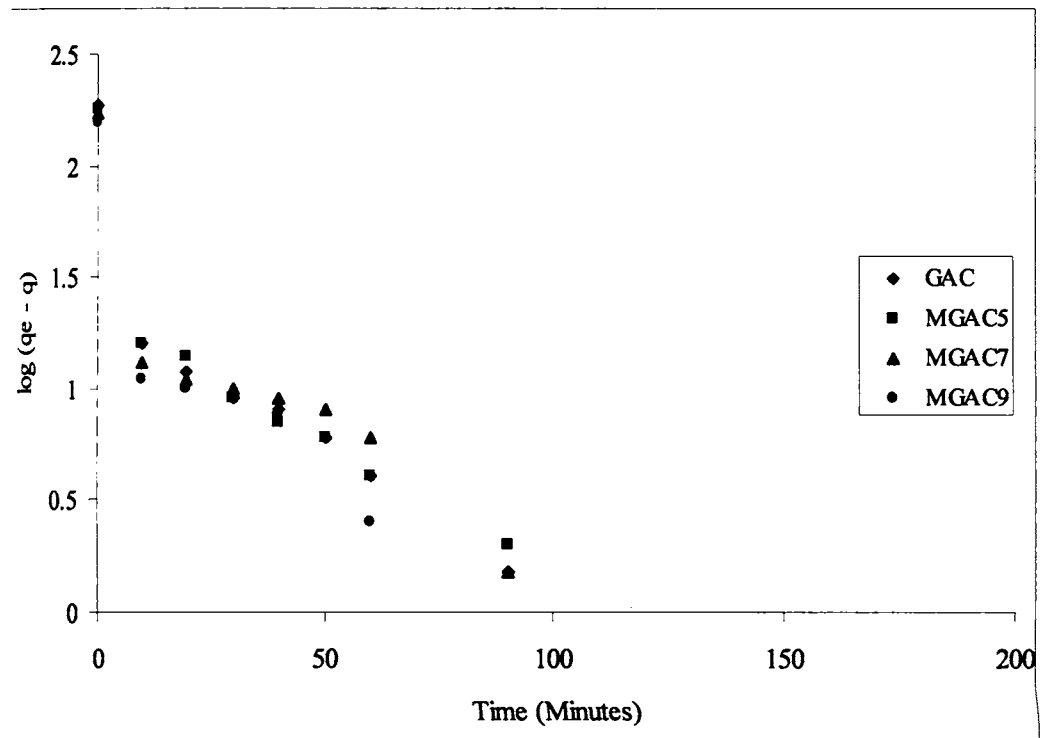


Figure 3.2b Lagergren plot for phenol adsorption at 20 °C.

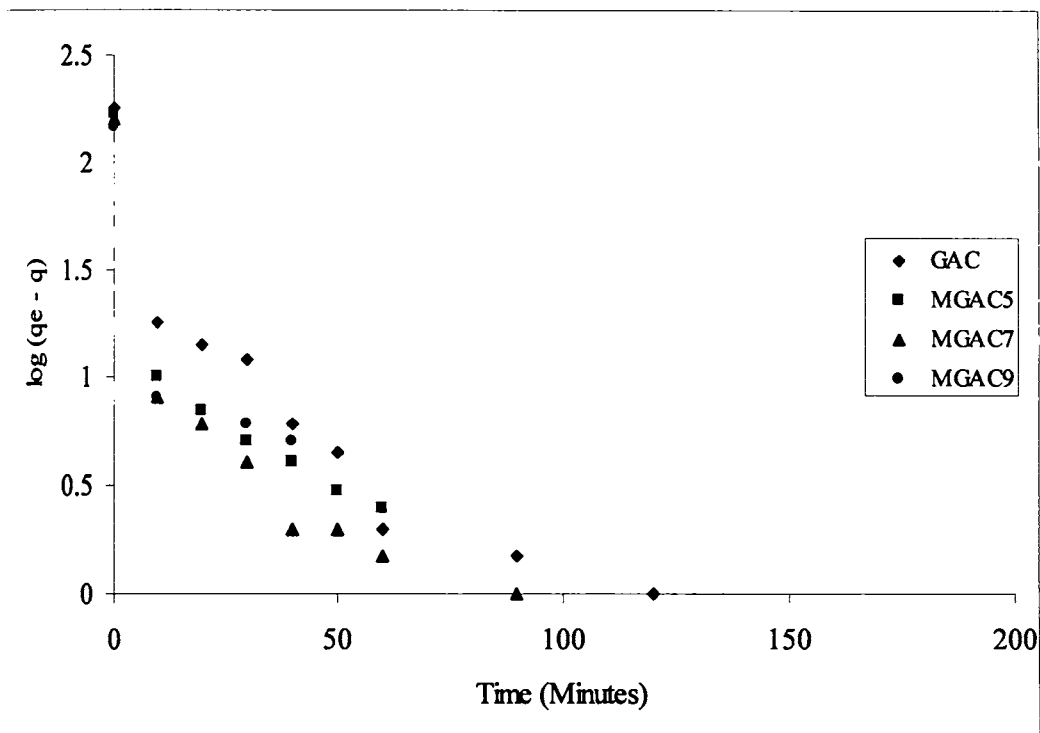


Figure 3.2c Lagergren plot for phenol adsorption at 30 °C.

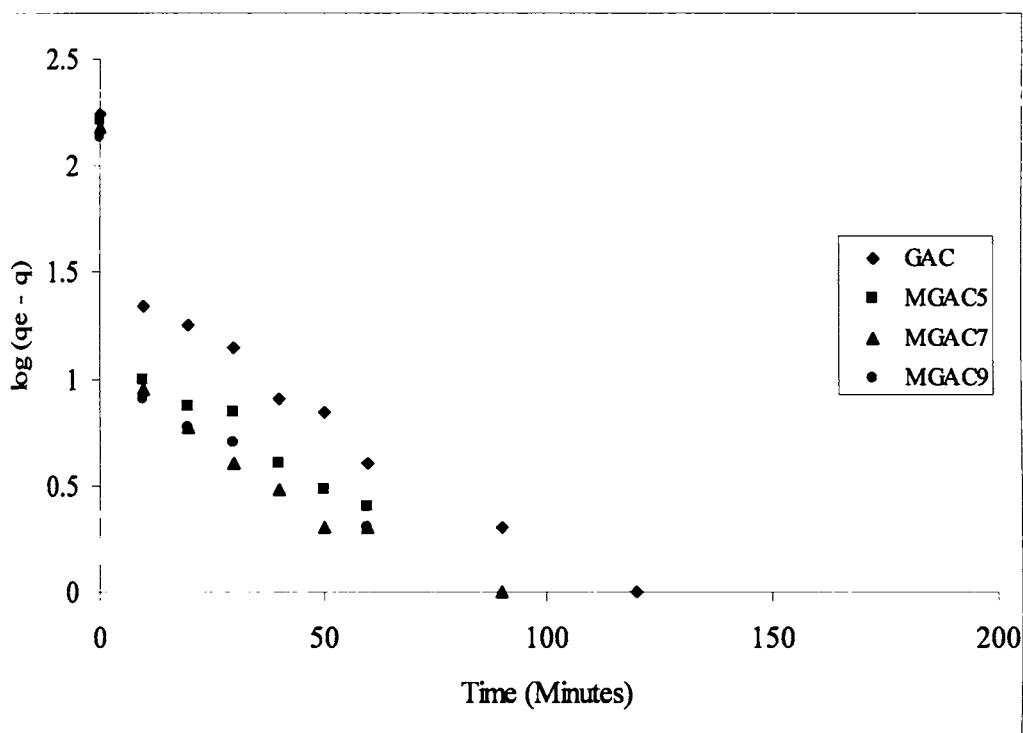


Figure 3.2d Lagergren plot for phenol adsorption at 40 °C.

Table 3.1 Rate constants for phenol adsorption evaluated from Lagergren plots

Carbon	Temperature ( <sup>o</sup> C)	Rate constant (min <sup>-1</sup> ) x 10 <sup>-2</sup>	r <sup>2</sup>
GAC	10	1.20	0.987
MGAC5	10	1.12	0.965
MGAC7	10	1.09	0.974
MGAC9	10	1.00	0.961
GAC	20	1.26	0.952
MGAC5	20	1.16	0.963
MGAC7	20	1.11	0.946
MGAC9	20	1.10	0.949
GAC	30	1.23	0.968
MGAC5	30	1.20	0.934
MGAC7	30	1.17	0.938
MGAC9	30	1.06	0.961
GAC	40	1.27	0.956
MGAC5	40	1.20	0.943
MGAC7	40	1.17	0.968
MGAC9	40	1.15	0.937

1.2, 1.12, 1.09 and  $1 \times 10^{-2} \text{ min}^{-1}$ . These results show that iron oxide impregnation has lowered phenol adsorption rate on activated carbon. There is no prominent influence of temperature on  $k_{ad}$ .

#### **Evaluation of Intraparticle Diffusion Rate Constants:**

Adsorbates that exhibit high affinity to activated carbon usually cause intraparticle diffusion control of the adsorption process (Weber, W. J., Jr. & Morris, J. C., 1963). The rate constant for intraparticle diffusion ( $k_{id}$ ) is given by Weber & Morris (1962). The equation can be expressed as

$$q = k_{id} t^{1/2} \quad (3.2)$$

where  $q$  is the amount adsorbed (mg/g) at time,  $t$  (min). Plots of  $q$  vs  $t^{1/2}$  generally have distinct features, an initial curved portion followed by linear portion and a plateau. The initial curved portion can be attributed to the bulk diffusion, the linear portion to the intraparticle diffusion and the plateau to the equilibrium.  $k_{id}$  values can be calculated from the slope of the linear portion of the curves at each temperature and concentration of the adsorbate molecule.

The plots of  $q$  vs  $t^{1/2}$  for phenol adsorption on the control carbon, GAC and the activated carbon composite samples, MGAC5, MGAC7 and MGAC9 at different temperatures are given in Figures 3.3a -d. These plots have distinct phases with an initial steep portion followed by a linear portion. The double nature of these plots may be explained by the fact that the initial steep portion is a measure of boundary layer diffusion effects (Crank, J., 1965) while the final linear portion is a result of intraparticle diffusion effects (McKay, G., *et al.*, 1980). The steep initial portion represents the bulk diffusion and corresponds to the rapid adsorption of phenol molecule onto the adsorbent samples within ten minutes. The following linear portion represents the Intraparticle diffusion. The slope of this linear portion was determined

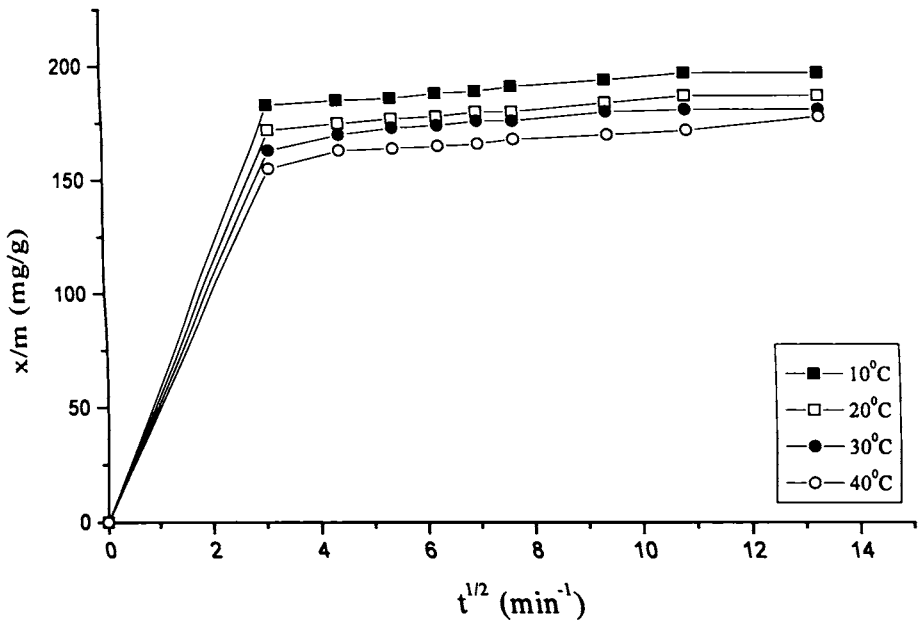


Figure 3.3a Intraparticle diffusion plots for phenol adsorption on GAC.

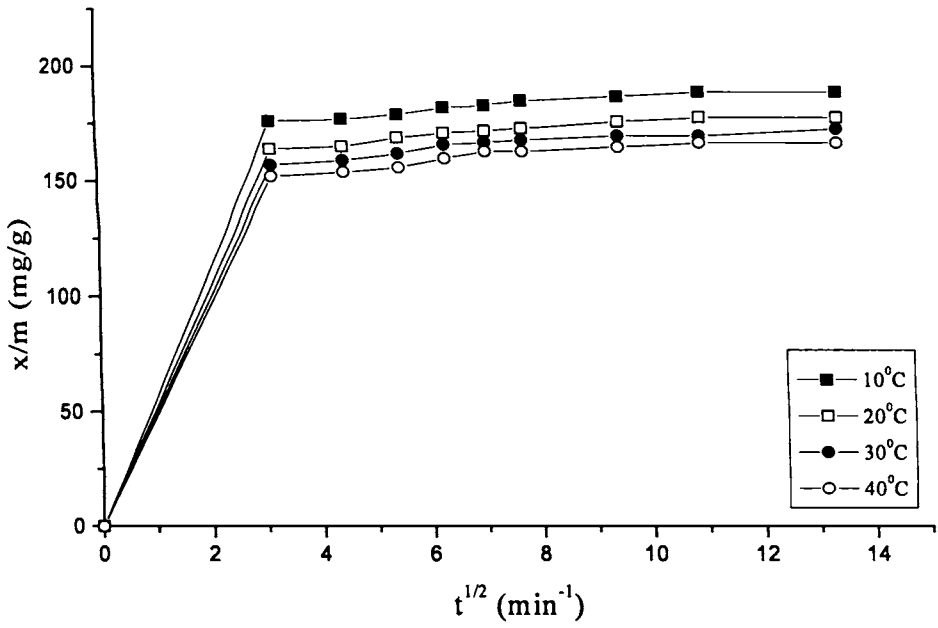


Figure 3.3b Intraparticle diffusion plots for phenol adsorption on MGAC5.

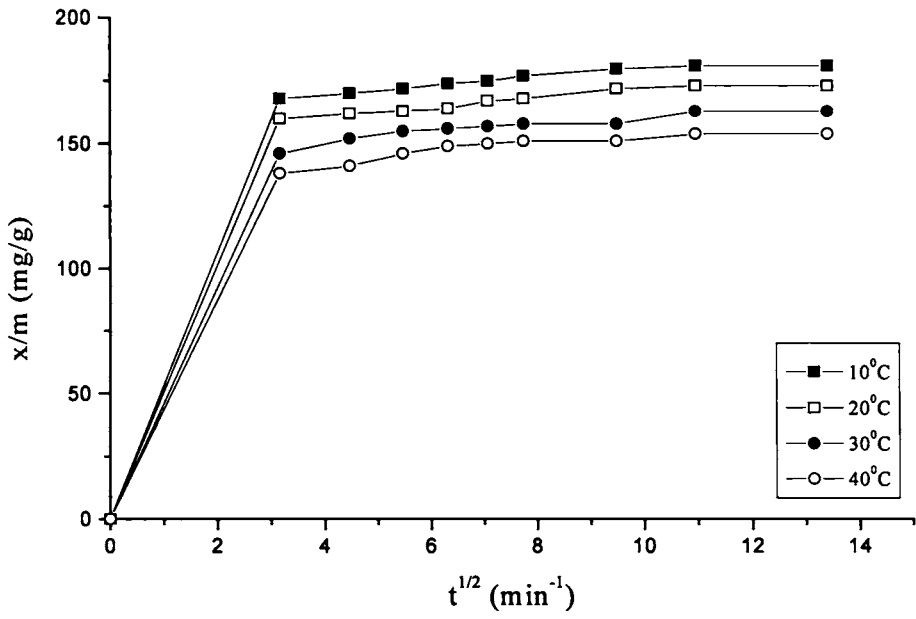


Figure 3.3c Intraparticle diffusion plots for phenol adsorption on MGAC7.

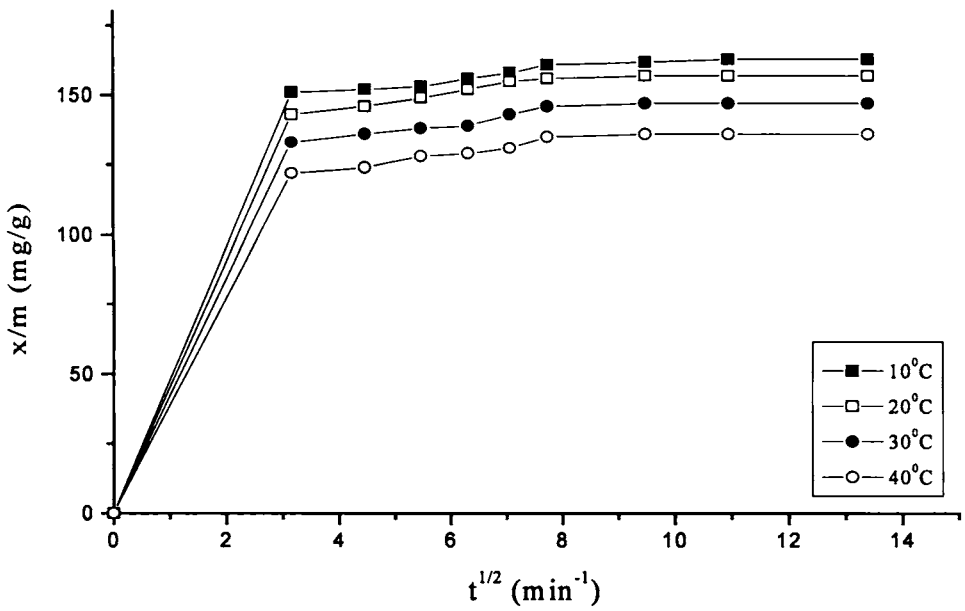


Figure 3.3d Intraparticle diffusion plots for phenol adsorption on MGAC9.

to evaluate the Intraparticle diffusion rate constant. These are not the true reaction rates, but relative rates which are useful for comparative purposes. The values of  $k_{id}$  are given in Table 3.2. The  $k_{id}$  values increase with temperature and show a decrease with the surface modification. At 20°C, the intraparticle diffusion constant reduces from 1.56 to 1.41 mg/g/min<sup>1/2</sup> for an iron oxide loading of 13.6 %. There is a gradual reduction in  $k_{id}$  with iron oxide loading on activated carbon samples. Similar trend can be seen at 20°C as well. When temperature is lowered, the  $k_{id}$  is also reduced. The decrease in  $k_{id}$  values with surface modification can be attributed to reduced pore volume in the activated carbon composite samples where by the diffusion of particle to the interiors of the carbon matrix is hindered. These are not true reaction rates, but relative rates which are useful for comparative purposes.

#### **Adsorption Isotherm Studies**

The isotherm studies of phenol adsorption on control carbon, GAC and composite samples, MGAC5, MGAC7 and MGAC9 were conducted to evaluate the adsorption capacity and other isotherm constants. Studies of the kinetics of phenol adsorption showed that the adsorption equilibrium is reached within 2h of agitation. After two hours there is no reduction in the adsorbate concentration with time. Hence, the contact time required for equilibrium with the adsorbent and phenol in solution has been fixed at 2h. This short contact time is relevant as it is feasible to use carbon for phenol and other organics removal at treatment plants where contact time is maintained in the range of 15 to 60 minutes.

Plots of phenol adsorbed on to the adsorbent (mg/g) against the equilibrium concentrations ( $C_e$ ) at four different temperatures are given in Figures 3.4a - d. Isotherms are of type 1 with a distinct slope for first phase followed by a slow adsorption phase moving somewhat parallel to the X-axis. The initial phase is almost

Table 3.2 Intraparticle diffusion rate constants for phenol adsorption

Carbon	Temperature, °C	Intraparticle rate constant, $k_{id}$ (mg/g/min <sup>1/2</sup> )
GAC	10	1.54
MGAC5	10	1.45
MGAC7	10	1.41
MGAC9	10	1.38
GAC	20	1.56
MGAC5	20	1.51
MGAC7	20	1.46
MGAC9	20	1.41
GAC	30	1.63
MGAC5	30	1.56
MGAC7	30	1.50
MGAC9	30	1.49
GAC	40	1.91
MGAC5	40	1.60
MGAC7	40	1.53
MGAC9	40	1.50

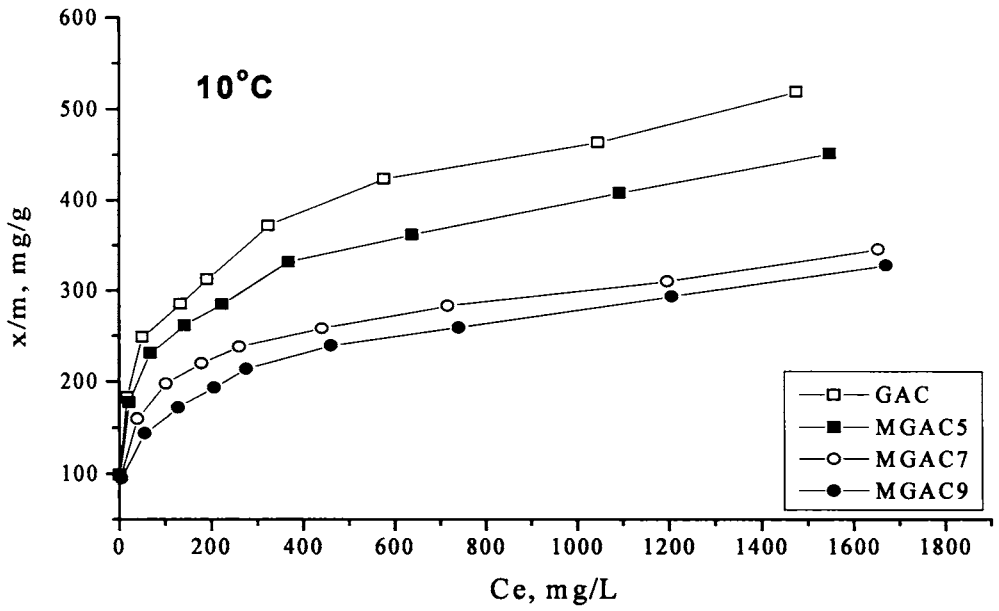


Figure 3.4a Equilibrium adsorption isotherm plots of phenol on activated carbon composites at 10°C.

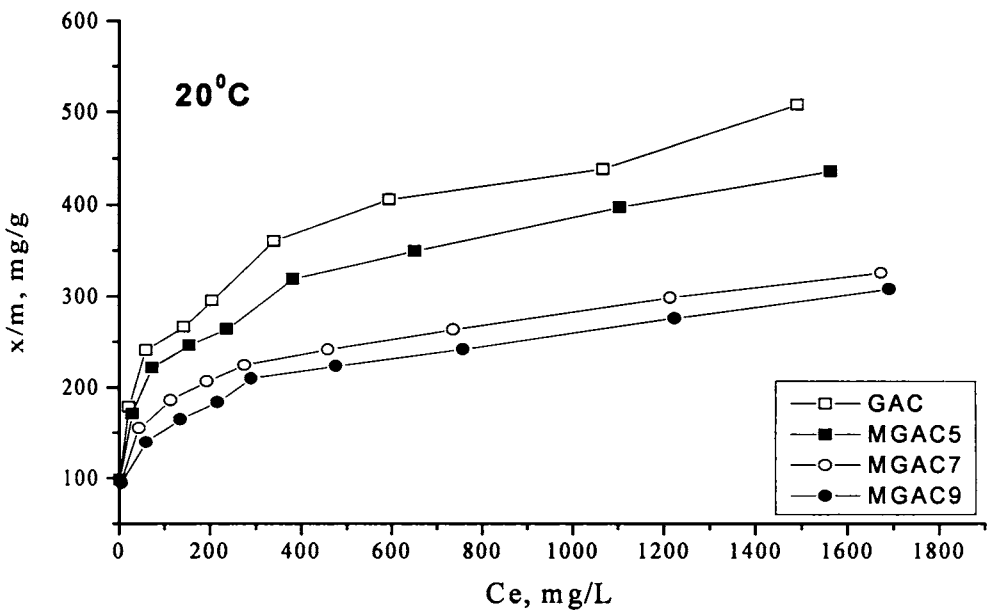


Figure 3.4b Equilibrium adsorption isotherm plots of phenol on activated carbon composites at 20°C.

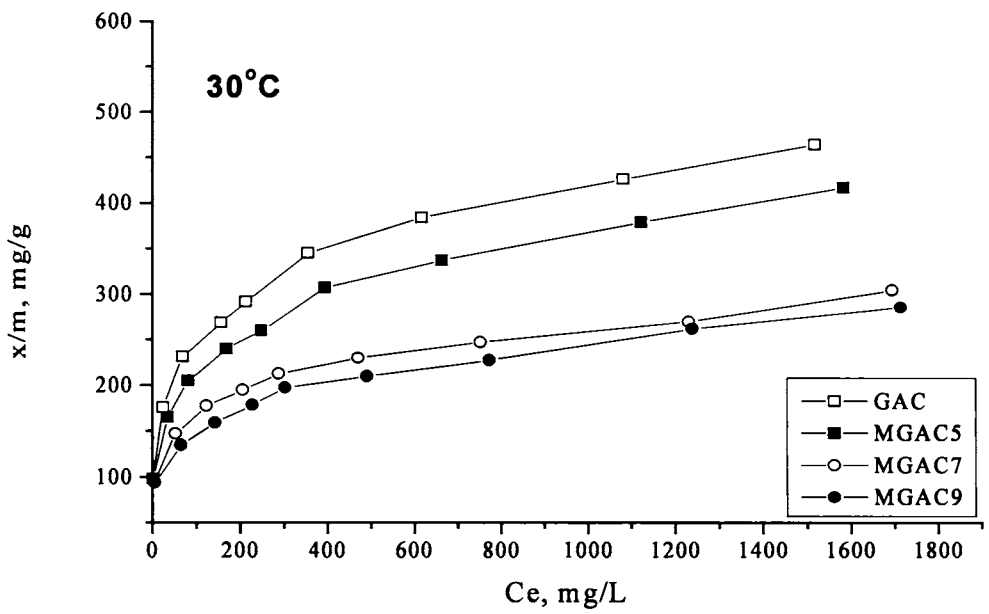


Figure 3.4c Equilibrium adsorption isotherm plots of phenol on activated carbon composites at 30°C.

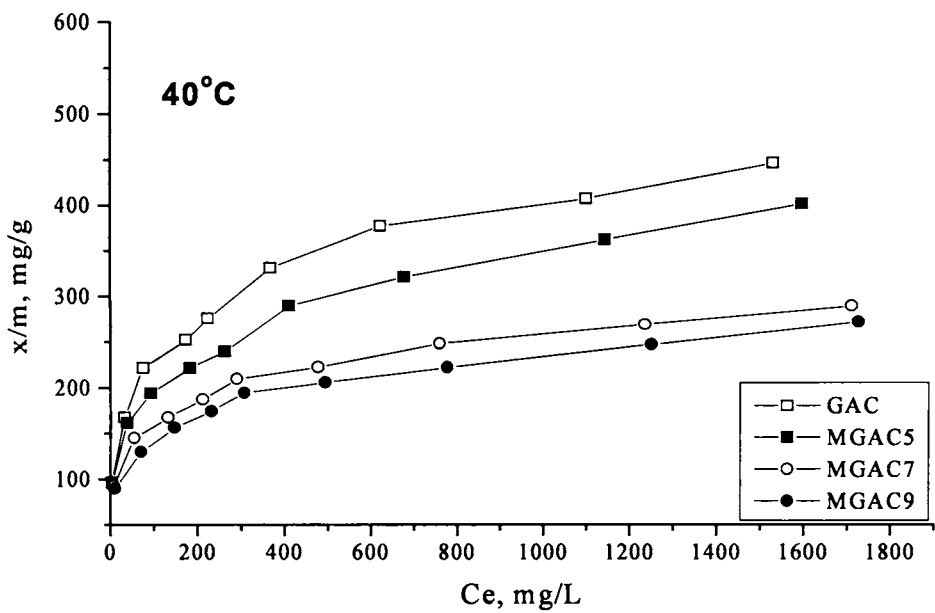


Figure 3.4d Equilibrium adsorption isotherm plots of phenol on activated carbon composites at 40°C.

completed with an equilibrium concentration of 450 mg/L in all cases, sufficient to saturate micropores (< 2 nm). There after, the saturation of mesopores occurs. The quantity of phenol adsorbed by composite grains is less compared to the control carbon and this indicates a reduction in the adsorption capacity as a result of iron oxide loading. And there is a general decrease in the surface loading of phenol with the amount of iron oxide on the carbon caused by the loss of surface area and porosity of the carbon. The isotherm studies are done to quantitatively evaluate the adsorption capacities as a result of surface modification of the carbons at different temperatures. Comparison of isotherm plots at different temperatures reveal that an increase in temperature decreases the adsorption of phenol. This suggests that the adsorption process is exothermic, where lower temperature favours the extent of adsorption. More information in this regard could be derived on subjecting the adsorption data to linear forms of mathematical models.

A number of standard isotherm equations are available to describe the distribution of organic molecules between the adsorbent and the solution at equilibrium. Among these Langmuir and Freundlich isotherms are used in this study to evaluate the adsorption parameters of phenol on control carbon and chemically modified samples, MGAC5, MGAC7 and MGAC9.

#### **Evaluation of Phenol Adsorption by Langmuir Model:**

Langmuir model and its parameters strongly indicated the monolayer behaviour of adsorption in aqueous phase. A linear form of the Langmuir equation can be written as

$$C_e/X = 1/bX_m + C_e/X_m \quad (1.15)$$

where  $C_e$  is the equilibrium concentration of the solute (mg/L),  $X = x/m$ , the amount of solute adsorbed (mg),  $x$ , per unit weight of adsorbent,  $m$  (g);  $X_m$  = amount of solute

adsorbed per unit weight of adsorbent required for monolayer surface coverage, also called monolayer capacity; and  $b =$  a constant related to the heat of adsorption, [ $b\alpha$  ( $\exp(-\Delta H/RT)$ )]. When  $C_e/X$  is plotted against  $C_e$ , a straight line, having a slope  $1/X_m$  and an intercept  $1/bX_m$ , is obtained. The monolayer capacity,  $X_m$ , determined from the plot defines the total capacity of the adsorbent for a specific adsorbate.

The Langmuir plots of phenol adsorption on control carbon, GAC and composites, MGAC5, MGAC7 and MGAC9 with respect to four temperatures are given in Figures 3.5a - d. The isotherms are plotted with respect to data at four different temperatures. The monolayer capacity,  $X_m$ , and Langmuir constant,  $b$  were calculated from the slope and intercept of the corresponding plots. The values of  $X_m$  and  $b$  are given in Table 3.3. The values for  $X_m$  decrease with temperature, suggesting that the adsorption is favoured at low temperatures. This suggests an *exothermic* adsorption mechanism (Lounici, H, *et al.*, 2004). The monolayer capacity of iron oxide loaded composite samples for phenol adsorption is significantly decreased with an increase in the iron loading. This is evident from  $X_m$  for different composites compared to the control carbon, GAC. The reduction in the monolayer capacity of the composite carbons can be attributed to the reduced porosity due to iron oxide impregnation. The phenol molecules find less potential adsorption sites on the composite samples compared to control carbon. The percentage reduction in the monolayer capacity of different composite samples compared to the control carbon at different temperatures is given in Figure 3.6. At 20°C, the  $X_m$  for MGAC5 reduced by 12 % compared to GAC. The corresponding reduction in  $X_m$  for MGAC7 and MGAC9 are 36 and 39 % respectively. Langmuir constant  $b$  is related to the equilibrium adsorption and enthalpy change. Carbon adsorbents GAC, MGAC5,

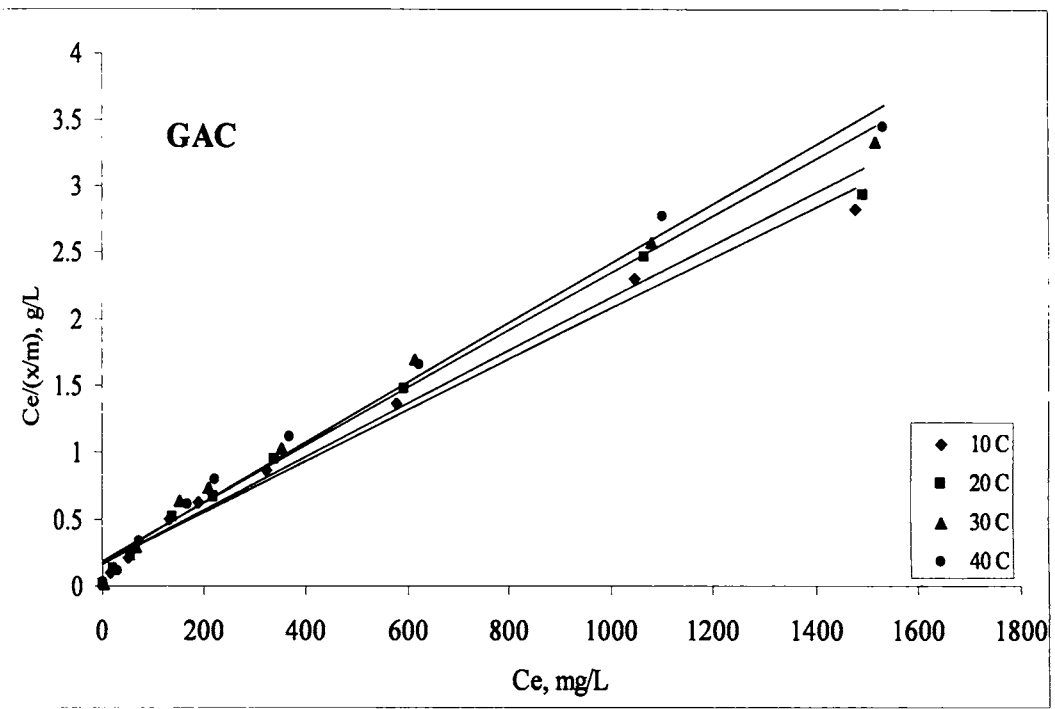


Figure 3.5a Langmuir plots for phenol adsorption on GAC.

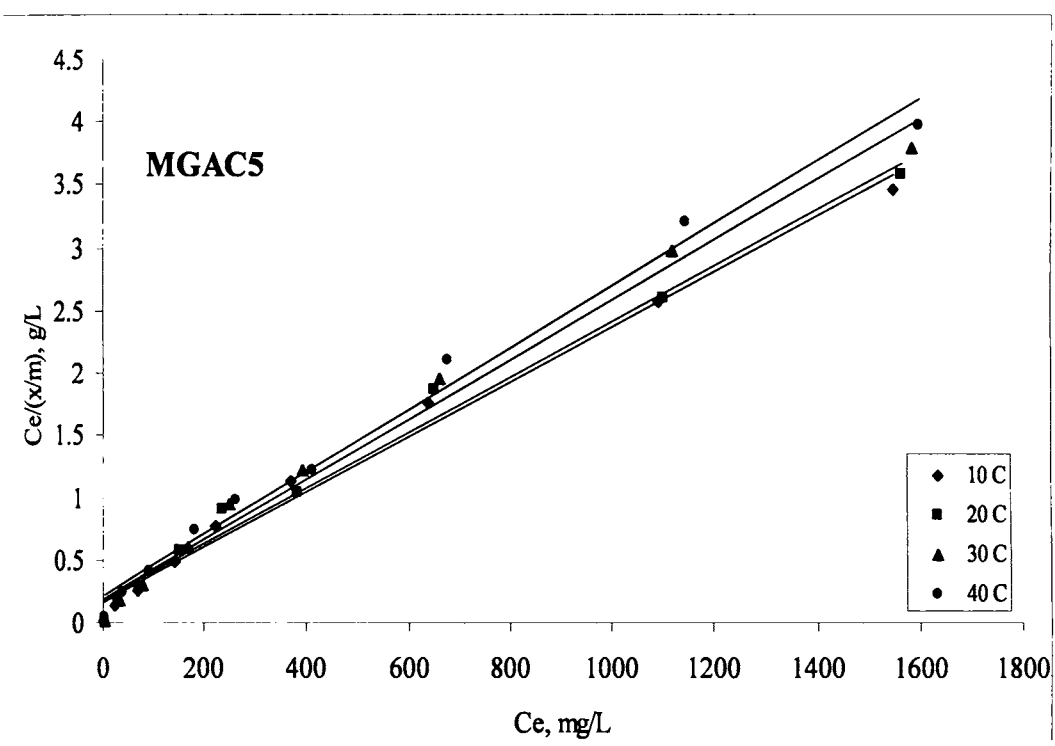


Figure 3.5b Langmuir plots for phenol adsorption on MGAC5

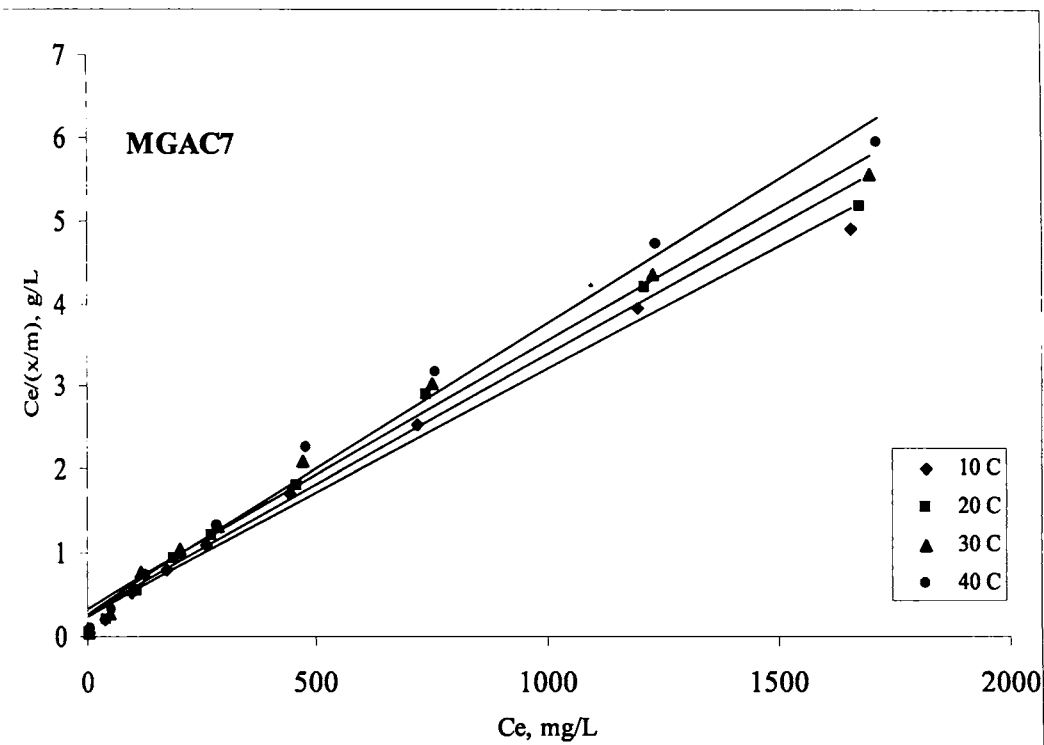


Figure 3.5c Langmuir plots for adsorption of phenol on MGAC7.

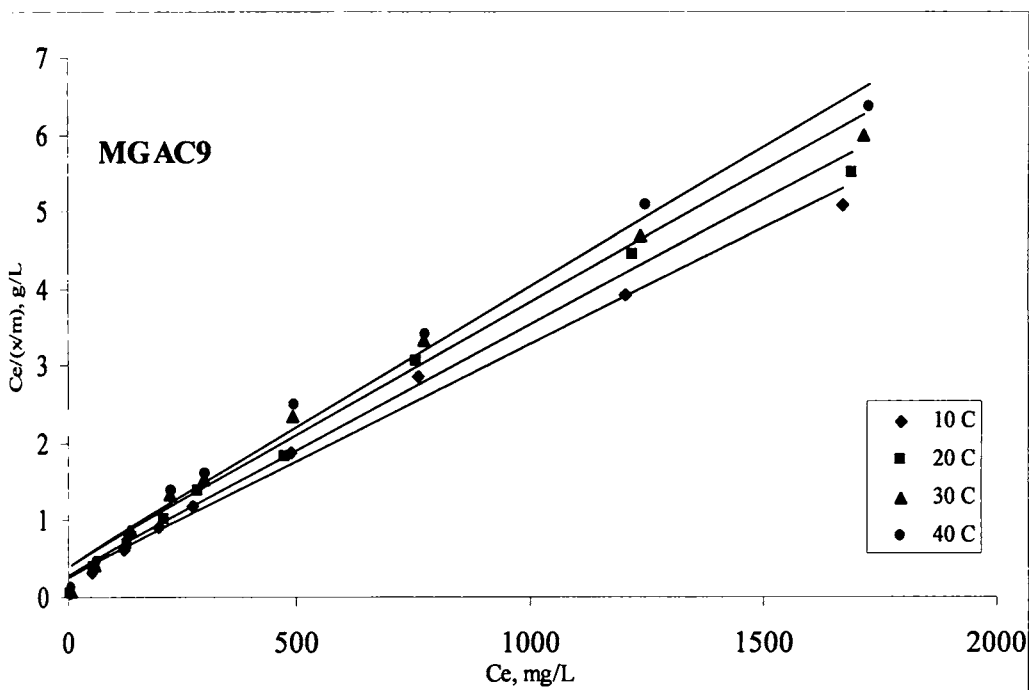


Figure 3.5d Langmuir plots for adsorption of phenol on MGAC9.

Table 3.3 Langmuir parameters for phenol adsorption

Carbon	Temperature, °C	Langmuir Constants		$X_m$ (Composite) / $X_m$ (GAC)	$r^2$
		$b$	$X_m$		
GAC	10	0.0129	526.32	1.0	0.985
MGAC5	10	0.0128	454.55	0.86	0.989
MGAC7	10	0.0126	333.33	0.63	0.991
MGAC9	10	0.0125	322.58	0.61	0.990
GAC	20	0.0126	500.00	1.0	0.984
MGAC5	20	0.0126	444.44	0.88	0.988
MGAC7	20	0.0123	322.58	0.64	0.987
MGAC9	20	0.0113	307.69	0.61	0.989
GAC	30	0.0123	444.44	1.0	0.989
MGAC5	30	0.0123	416.67	0.94	0.988
MGAC7	30	0.0117	312.50	0.70	0.987
MGAC9	30	0.0093	294.12	0.66	0.987
GAC	40	0.0120	434.78	1	0.989
MGAC5	40	0.0116	400.00	0.92	0.989
MGAC7	40	0.0113	294.12	0.68	0.990
MGAC9	40	0.0090	277.78	0.64	0.988

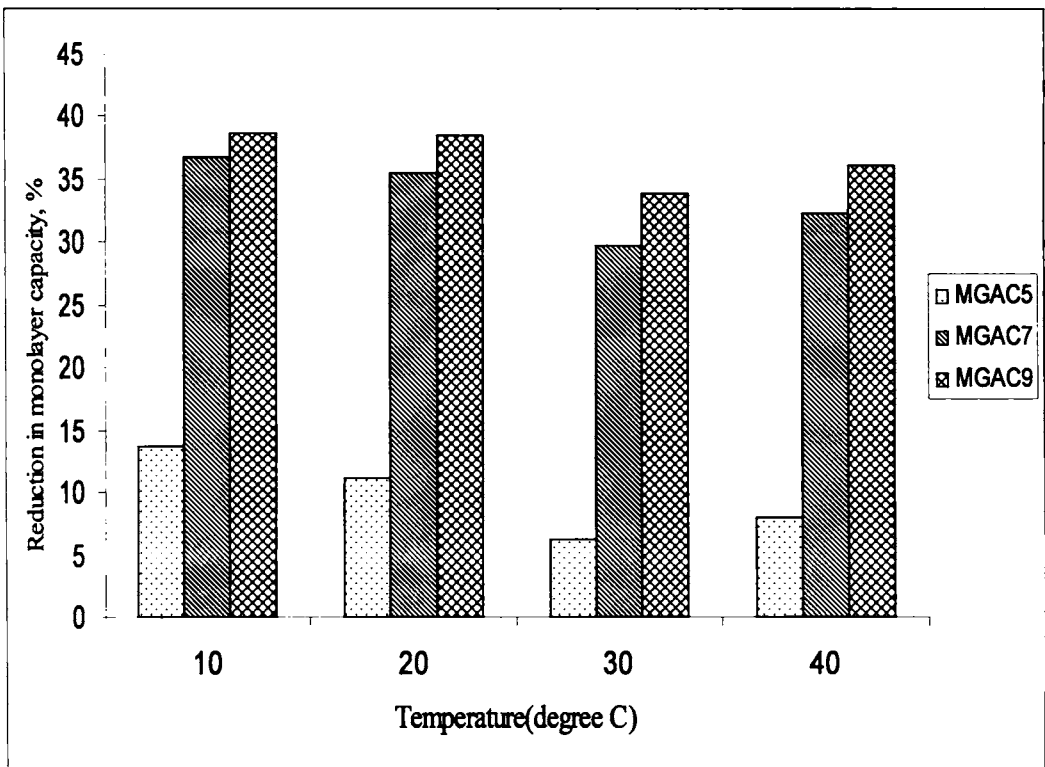


Figure 3.6 Reduction in the monolayer capacity for phenol adsorption for composites compared to the control carbon at different temperatures.

MGAC7 and MGAC9 have a  $b$  value of  $1.26 \times 10^{-2}$ ,  $1.26 \times 10^{-2}$ ,  $1.23 \times 10^{-2}$  and  $1.13 \times 10^{-2}$  respectively.

An earlier work (Oliveira, L. C. A., *et al.*, 2002) on magnetic composites reported similar adsorption profile on carbon based magnetic composites. These researchers studied the adsorption of volatile organic compounds, i.e. phenol, chloroform, and chlorobenzene, from aqueous solutions onto the 3:1 activated carbon/Fe oxide and reported that the adsorption capacity of activated carbon for phenol was reduced from 162 to 117 mg/g on surface modification. In the present study, GAC with  $X_m$  of 500 mg/g reduced to 444.4 mg/g for MGAC5, 322.6 mg/g for MGAC7 and 307.7 mg/g for MGAC9. This lower uptake of phenol corresponds to a relative affinity of 0.89, 0.65 and 0.62. However, the reported monolayer capacities are much lower than the values obtained in the present study.

#### **Freundlich Model for Phenol Adsorption**

The Freundlich adsorption equation is a widely used mathematical description of adsorption in aqueous systems. A linearised form of the Freundlich model is used to study the phenol adsorption on GAC and other modified forms. It can be expressed as

$$\log x/m = \log K + 1/n \log C_e \quad (1.18)$$

Plotting  $\log x/m$  against  $\log C_e$  will result in a straight line with a slope of  $1/n$  and an intercept of  $\log K$ , when the system follows the Freundlich type adsorption. Constants  $K$  and  $n$  are termed as the Freundlich constants.

The Freundlich plots for phenol adsorption on control carbon, GAC and MGAC5, MGAC7, and MGAC9 are given in Figures 3.7a - d. The linearity of the plots suggests that the system fits well with the Freundlich model and the constants can be evaluated with great accuracy. The  $K$  and  $n$  values were calculated from the

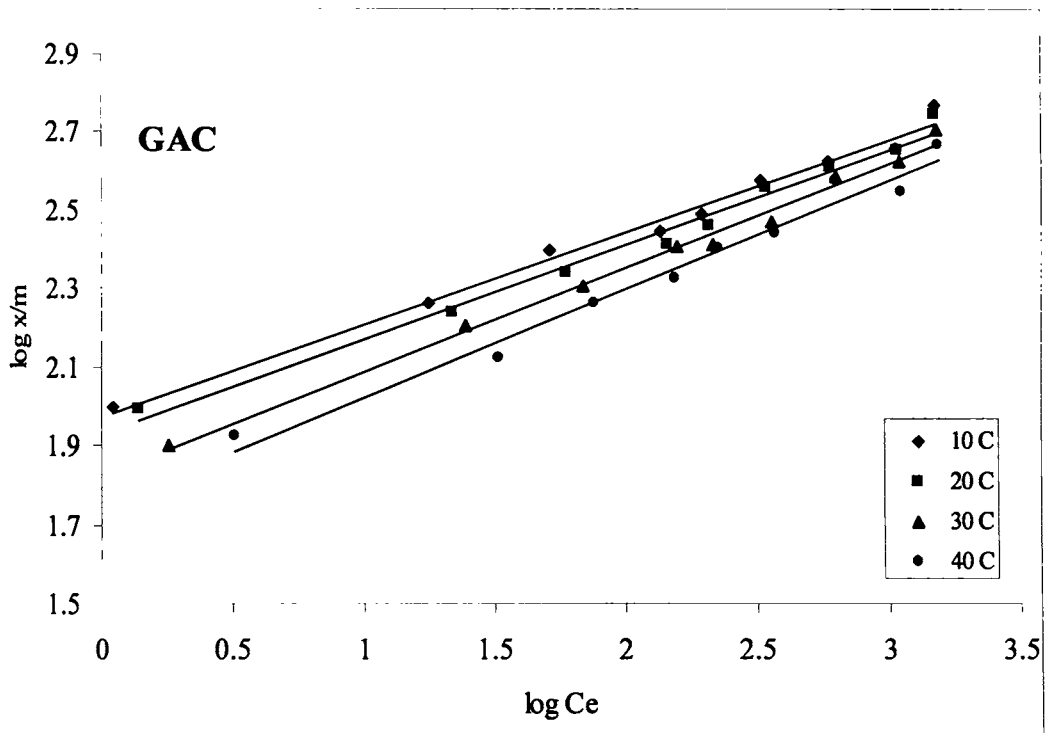


Figure 3.7a Freundlich plots of phenol adsorption on GAC.

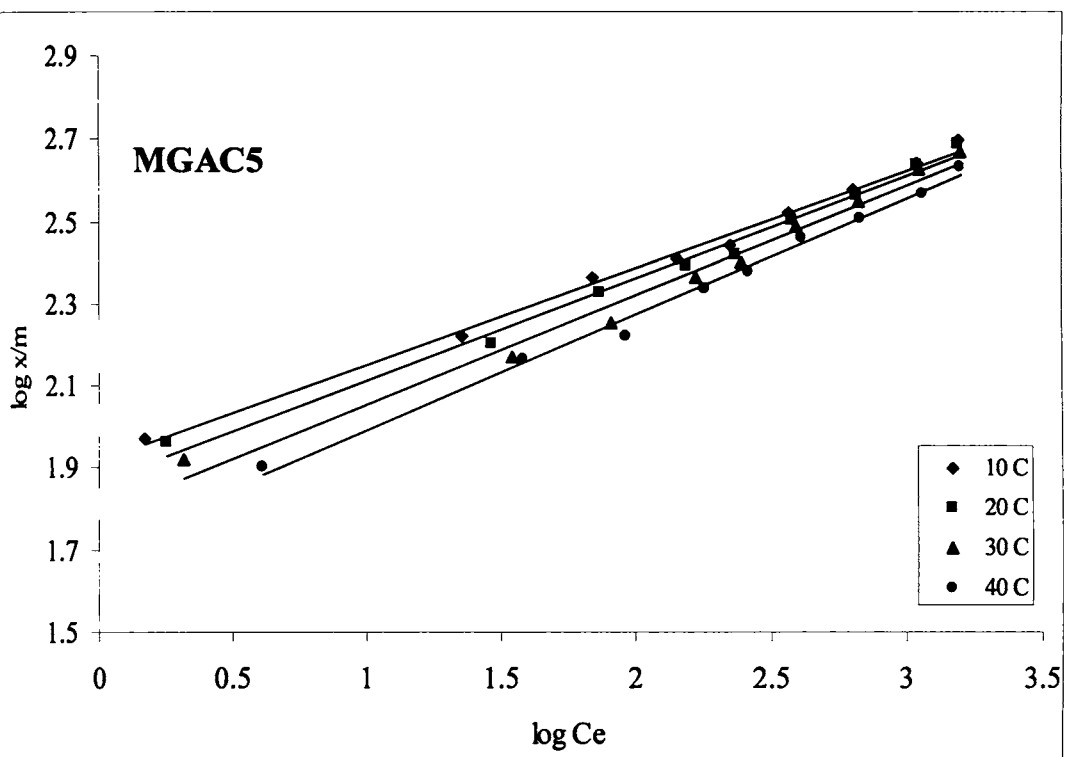


Figure 3.7b Freundlich plots of phenol adsorption on MGAC5.

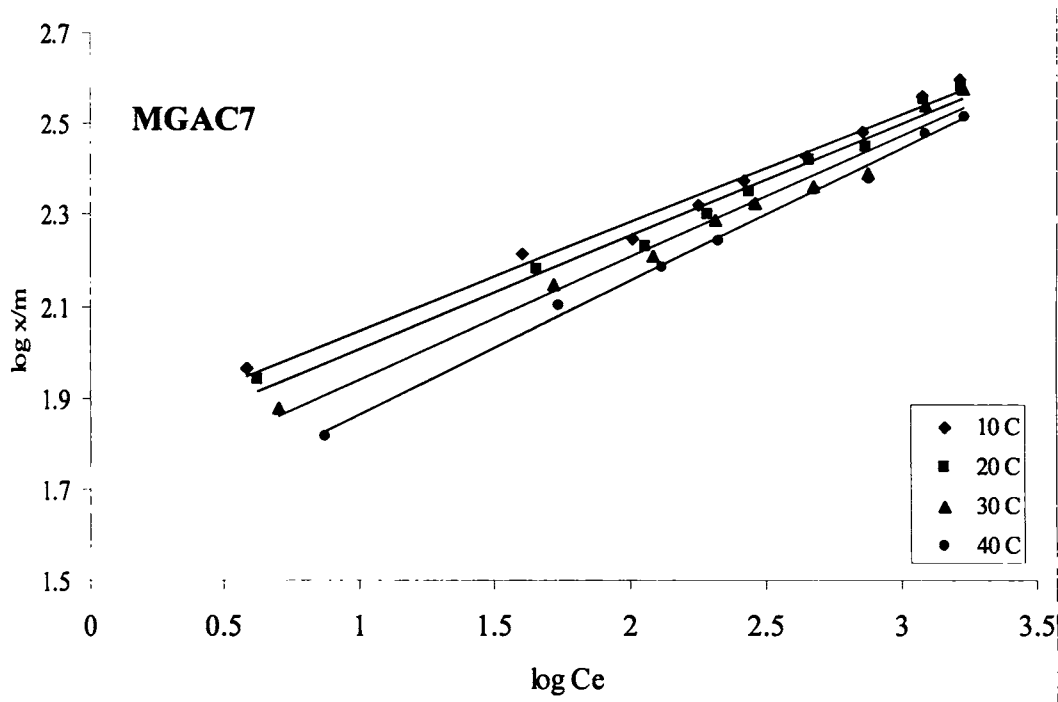


Figure 3.7c Freundlich plots of phenol adsorption on MGAC7.

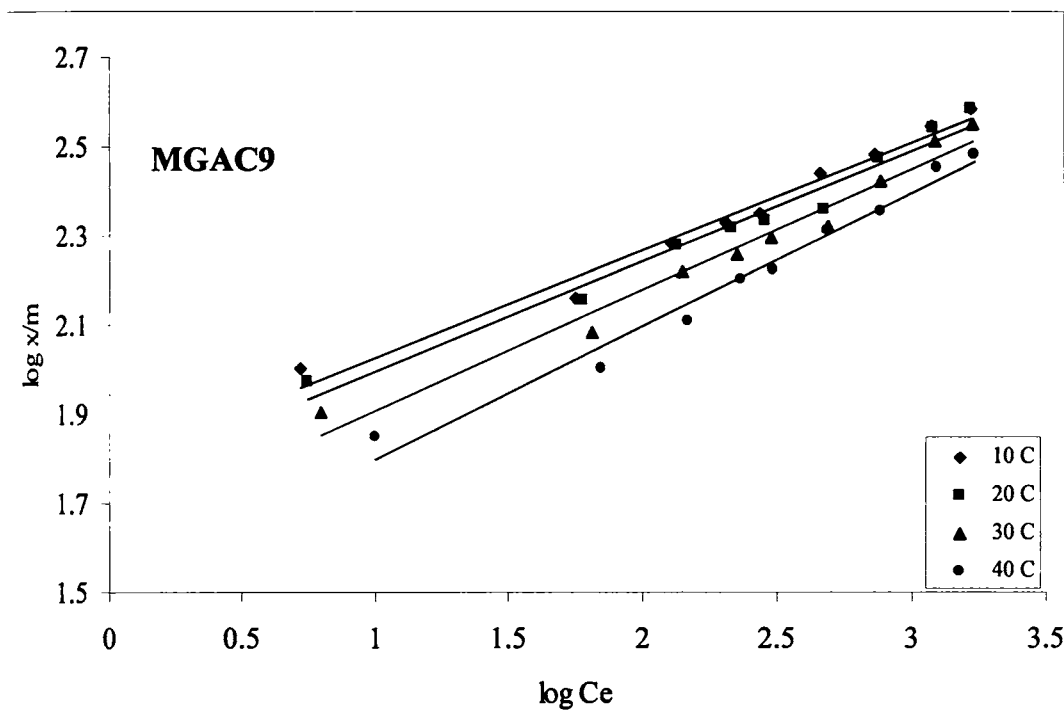


Figure 3.7d Freundlich plots of phenol adsorption on MGAC9.

intercept and slope of the linear plots and are given in Table 3.4. The decrease in the magnitude of  $K$  with temperature suggests an exothermic nature of the adsorption of phenol on these adsorbent samples. Also, the  $K$  and  $n$  values decrease with iron loading in the case of MGAC5, MGAC7 and MGAC9 compared to GAC revealing a decreased phenol uptake with composites compared to the control carbon. This can be attributed to the loss of porosity and surface area whereby less number of phenol molecules are adsorbed on surface compared to the control carbon. The values of  $K$  and  $n$  for GAC are in agreement with previously reported values for phenol adsorption on other commercially available carbons (Arbuckle, W. B., 1980; Peel, R. G. & Benedek, A., 1980; Aly, O. M. & Faust, S. D., 1972). Freundlich constant  $K$  is known as an indicator of adsorption intensity and ' $n$ ' is the adsorbent capacity (McKay, G. & Al-Duri, B., 1989). In this regard, the evaluation of the constants acts as an analytical tool to classify the adsorbents based on their relative surface loading. The native control carbon GAC has the highest affinity towards phenol as evident by a  $K$  of 84.47 mg/g and  $n$  of 4.11 at 20°C. Surface modification with iron oxide impregnation shows an overall incidence of decrease for MGAC5 ( $K = 73.62$ ,  $n = 4.04$ ), MGAC7 ( $K = 57.73$ ,  $n = 4.03$ ), MGAC9 ( $K = 56.12$ ,  $n = 4.01$ ). This shows an indirect relation between the adsorbent capacity and the iron oxide loading. Lowering of temperature improves the adsorbent capacity. GAC, MGAC5, MGAC7 and MGAC9 have higher values of  $K$  equal to 94.28, 82.11, 64.31 and 60.93 respectively at 10°C.  $K$  values decreased at higher temperatures for all the samples as can be seen from Table 3.4. The high  $K$  values of phenol adsorption on the control carbon can be ascribed to the smaller size of the phenol molecule (cross sectional area of phenol molecule is  $30.24 \times 10^{-20} \text{ m}^2$  at 25°C), and strong interaction of the electrons of the

Table 3.4 Freundlich constants for the adsorption of Phenol.

Carbon	Temperature, °C	Freundlich Constants		$r^2$
		$K$ , mg/g	$n$	
GAC	10	94.28	4.24	0.988
GAC	20	84.47	4.11	0.985
GAC	30	66.83	3.77	0.991
GAC	40	58.72	3.61	0.976
MGAC5	10	82.11	4.22	0.993
MGAC5	20	73.62	4.04	0.989
MGAC5	30	61.45	3.75	0.983
MGAC5	40	51.53	3.56	0.992
MGAC7	10	64.31	4.20	0.986
MGAC7	20	57.73	4.03	0.984
MGAC7	30	47.26	3.74	0.978
MGAC7	40	37.45	3.43	0.992
MGAC9	10	60.93	4.13	0.978
MGAC9	20	56.12	4.01	0.971
MGAC9	30	43.74	3.71	0.969
MGAC9	40	31.51	3.35	0.976

aromatic nucleus of phenol with oxygen groups present on carbon (Walker, P. L., Jr., 1970).

#### 3.4.1c Evaluation of Thermodynamic Parameters

The influence of temperature on the adsorption of phenol on GAC and composite samples, MGAC5, MGAC7 and MGAC9 were investigated. For these studies, the concentrations of phenol in the solutions used were 100, 200, 400, 700 and 1500 mg/L and the temperature was varied from 10°C to 40°C in 10°C steps. Figures 3.8a - d shows the logarithmic variation of distribution coefficient with reciprocal of temperature in Kelvin. The increase in the concentration of phenol reduced the slope of these plots. Compared to the control carbon, the composites show a decrease in  $\ln K_D$  values. The thermodynamic values of  $\Delta H$  and  $\Delta S$  for phenol adsorption on all the four adsorbents were calculated from the  $K_D$  values using the following equations:

$$\ln K_D = \Delta S / R - \Delta H / RT \quad (3.3)$$

and

$$\Delta G = \Delta H - T \Delta S \quad (3.4)$$

where, R is the universal gas constant (8.314 J/mol) and T is temperature in Kelvin.

The values of  $\Delta H$  and  $\Delta S$  were computed from the slopes and linear variation of  $\ln K_D$  with the reciprocal of temperature and are given in Table 3.5. The change in free energy for phenol adsorption was calculated from Equation 3.4. Negative values of  $\Delta G$  shows that the adsorption of phenol on adsorbents is spontaneous. The  $\Delta H$  calculated was negative for all the adsorbents and indicates that the adsorption of phenol is favoured at lower temperatures. The  $\Delta H$  values decreased with an increase in the initial concentration of phenol in solution. For GAC the values of enthalpy change calculated at solute concentrations of 100, 200, 400, 700 and 1500 mg/L were

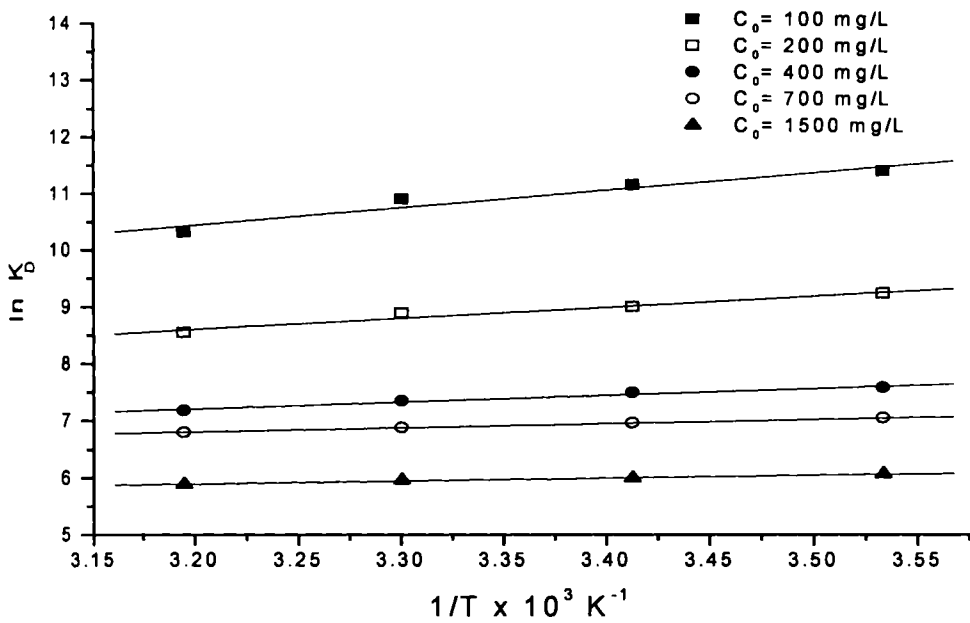


Figure 3.8a Plots of  $\ln K_D$  vs  $1/T$  for phenol adsorption on GAC.

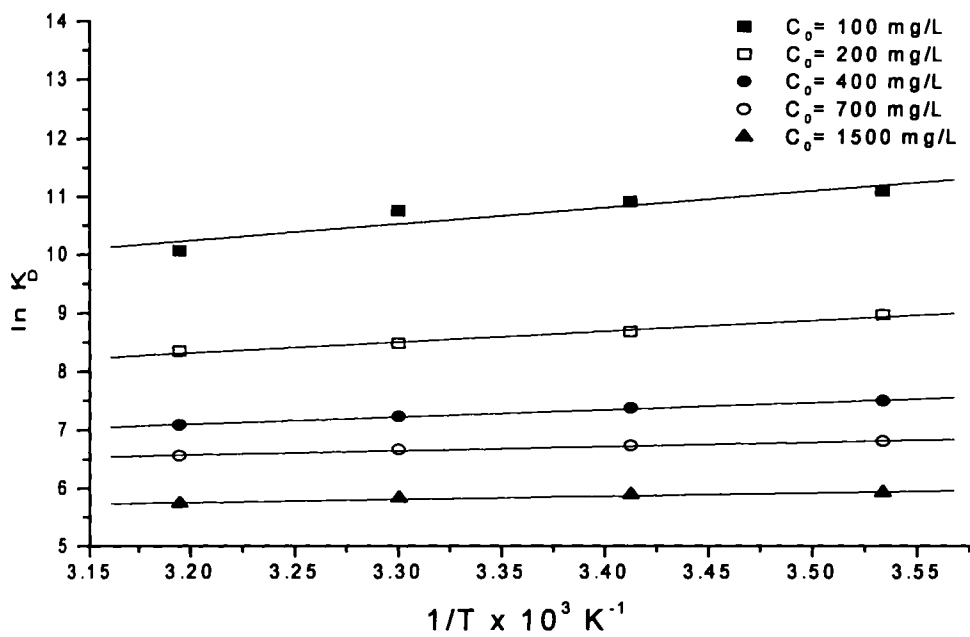


Figure 3.8b Plots of  $\ln K_D$  vs  $1/T$  for phenol adsorption on MGAC5.

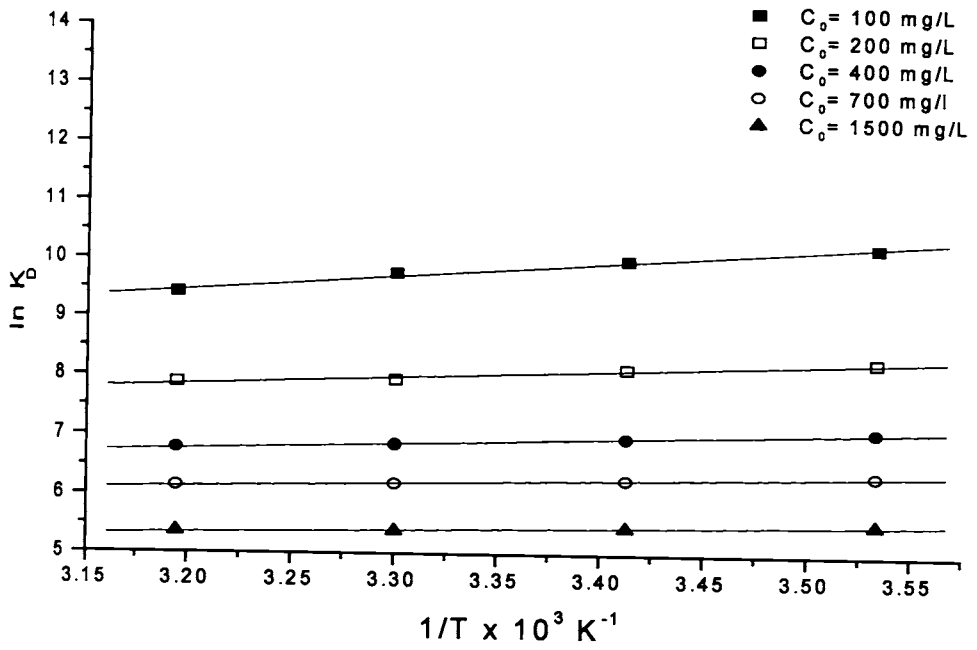


Figure 3.8c Plots of  $\ln K_D$  vs  $1/T$  of phenol adsorption on MGAC7.

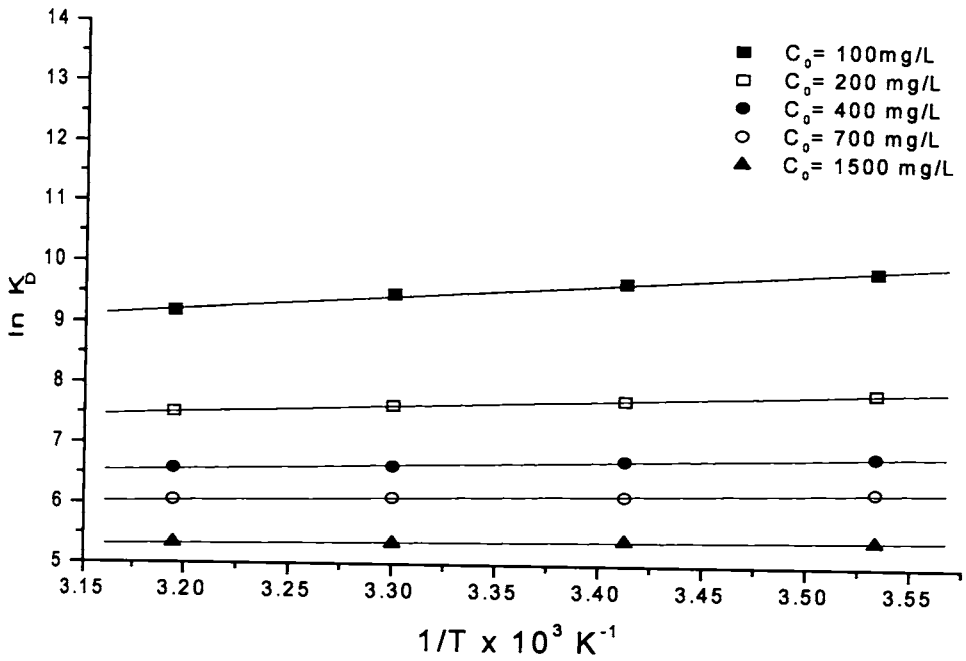


Figure 3.8d Plots of  $\ln K_D$  vs  $1/T$  of phenol adsorption on MGAC9.

Table 3.5 Thermodynamic parameters for phenol adsorption

Carbon	$C_o$ , mg/L	$\Delta H$ , kJ/mol $\times 10^{-2}$	$\Delta S$ , J/mol/K $\times 10^{-2}$	$\Delta G$ , kJ/mol			
				283	293	303	313
GAC	100	-2.6	0.4	-1.30	-1.34	-1.39	-1.43
	200	-1.64	1.9	-5.43	-5.62	-5.81	-6.00
	400	-1.01	2.7	-7.89	-8.17	-8.45	-8.73
	700	-0.6	3.5	-9.91	-10.26	-10.61	-10.96
	1500	-0.44	3.7	-10.36	-10.72	-11.10	-11.45
MGAC5	100	-2.4	0.93	-2.66	-2.75	-2.85	-2.94
	200	-1.5	2.00	-5.78	-5.98	-6.19	-6.39
	400	-1.0	2.66	-7.56	-7.83	-8.10	-8.36
	700	-0.59	3.31	-9.37	-9.70	-10.03	-10.36
	1500	-0.46	3.58	-10.12	-10.48	-10.84	-11.19
MGAC7	100	-2.03	1.39	-3.95	-4.09	-4.23	-4.37
	200	-1.06	3.08	-8.72	-9.02	-9.33	-9.64
	400	-0.81	3.14	-8.90	-9.22	-9.53	-9.84
	700	-0.56	3.31	-9.37	-9.70	-10.03	-10.36
	1500	-0.45	3.49	-9.89	-10.24	-10.58	-10.93
MGAC9	100	-1.70	2.1	-6.09	-6.30	-6.52	-6.73
	200	-0.92	3.28	-9.30	-9.63	-9.96	-10.29
	400	-0.66	3.35	-9.49	-9.82	-10.16	-10.49
	700	-0.48	3.47	-9.82	-10.16	-10.51	-10.86
	1500	-0.28	3.52	-9.96	-10.31	-10.66	-11.01

-2.6, -1.64, -1.01, -0.6 and  $-0.44 \times 10^{-2}$  kJ/mol. The enthalpy change decreased with iron oxide loading. The entropy change ( $\Delta S$ ) was also calculated for phenol adsorption on adsorbents. For GAC, the change in entropy was computed to be in the range  $0.4 - 3.7 (x 10^{-2} \text{ J/mol/K})$ . For composites  $\Delta S$  varied between  $0.93 - 3.58 (x 10^{-2} \text{ J/mol/K})$  for MGAC5,  $1.39 - 3.49 (x 10^{-2} \text{ J/mol/K})$  for MGAC7 and  $2.1 - 3.52 (x 10^{-2} \text{ J/mol/K})$  for MGAC9.

#### 3.4.2 Adsorption of *p*-Nitrophenol on Activated Carbon – Magnetic Iron Oxide Composites

Equilibrium studies using Nitrophenol as target adsorbate was used to evaluate the adsorption capacity of the modified activated carbons. Nitrophenol has  $\text{NO}_2$  groups attached to the phenolic ring at its *para* position. Nitrophenols are intermediates in the production of dyes, pigments, preservatives, pesticides, pharmaceuticals and rubber chemicals (Attia, A. A., *et al.*, 2003a). The environmental significance of this group of compounds is largely understood from the fact that molecules are produced during the hydrolytic cleavage of several organophosphorus pesticides (Boyd, S. A., 1982). The residence time of the chemical with activity in air is not known. But the breakdown takes much longer at lower soil depths and groundwater. Therefore, they are expected to stay longer in the deep soil of dump sites compared to surface soil and may even stay indefinitely.

Activated carbon treatment is identified as a viable option for the removal of this group of chemicals from aqueous systems. Adsorption on activated carbon appears to offer the best technology for the overall treatment of effluents with moderate or low concentrations (Caturia, F., *et al.*, 1988; Streat, M., *et al.*, 1995), because these carbon materials have high adsorption capacity. Attempts have been made by researchers to improve the adsorption efficiency of *p*-nitrophenol on surface modified activated carbons (Goyal, M., 2004). Batch isotherm studies for *p*-

*p*-nitrophenol adsorption were carried out on GAC, MGAC5, MGAC7 and MGAC9 to evaluate the removal efficiency.

#### 3.4.2a Adsorption Kinetics

An initial concentration of 300 mg/L of *p*-nitrophenol solution was used for the study with the adsorbent concentration fixed at 0.05 g. The rate of *p*-nitrophenol adsorption was studied at four different temperatures, 10°C, 20°C, 30°C and 40°C. Kinetic plots of adsorption were generated by plotting the amount of *p*-nitrophenol adsorbed per unit weight of carbon against time.

The kinetic plots (concentration versus time graphs) of *p*-nitrophenol adsorption on the control carbon GAC and the composite samples at different temperatures are given in Figures 3.9a & b. The plots show a two-stage kinetics with rapid adsorption of the adsorbate molecule onto the adsorbent within the first ten minutes of the adsorption process. At 20°C, 95.8 % of the fraction of *p*-nitrophenol adsorbed is removed within ten minutes and 99.1 % within 60 minutes by the control carbon. Only 3.2 % removal was observed in the second stage. And the equilibrium is reached within 120 minutes. The equilibrium concentration decreases with iron loading but not significantly. The fraction of the *p*-nitrophenol adsorbed at 10°C within an initial period of ten minutes is 95.5, 94.8 and 94 % for MGAC5, MGAC7 and MGAC9 respectively. This marginal decrease in the fraction of the adsorbate adsorbed in the initial phases of adsorption could be due to less availability of pores for the adsorption. The calculated values for the fraction of *p*-nitrophenol adsorbed within 10 minutes of the adsorption for GAC, MGAC5, MGAC7 and MGAC9 at 10°C were 95.9, 95.6, 94.6 and 94.1 %. Uptake at higher temperatures followed the same pattern suggesting that the temperature did not have any significant influence on the fraction of the adsorbate molecules removed within the initial stages of the

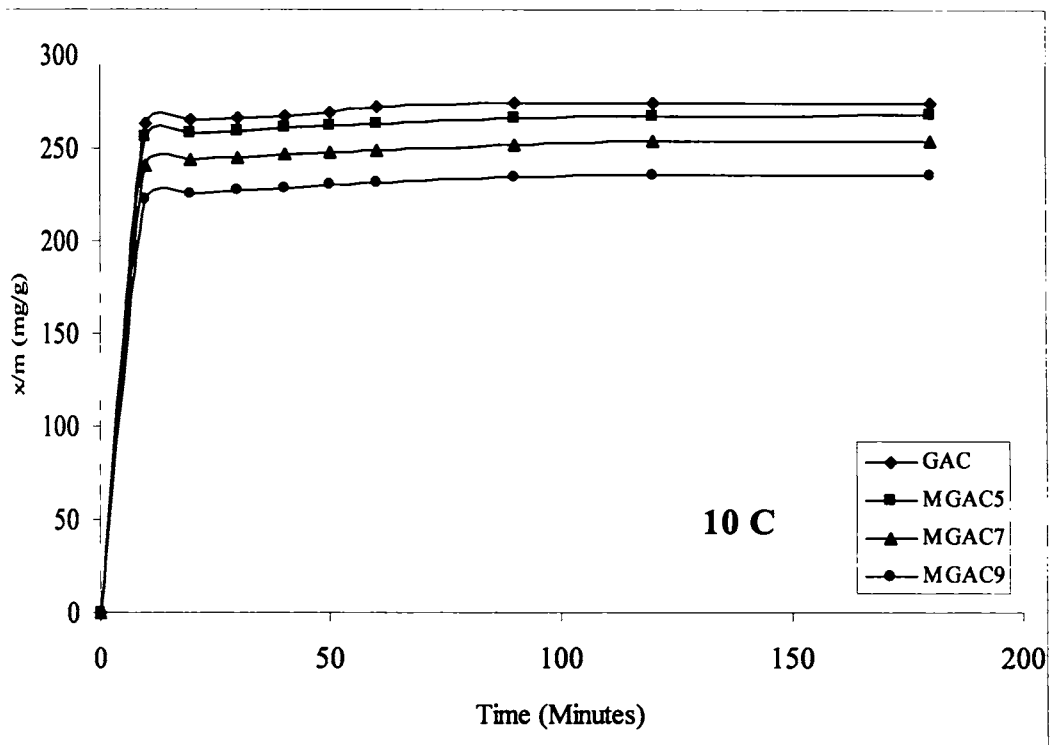


Figure 3.9a Concentration Vs time graphs for *p*-nitrophenol adsorption at 10°C.

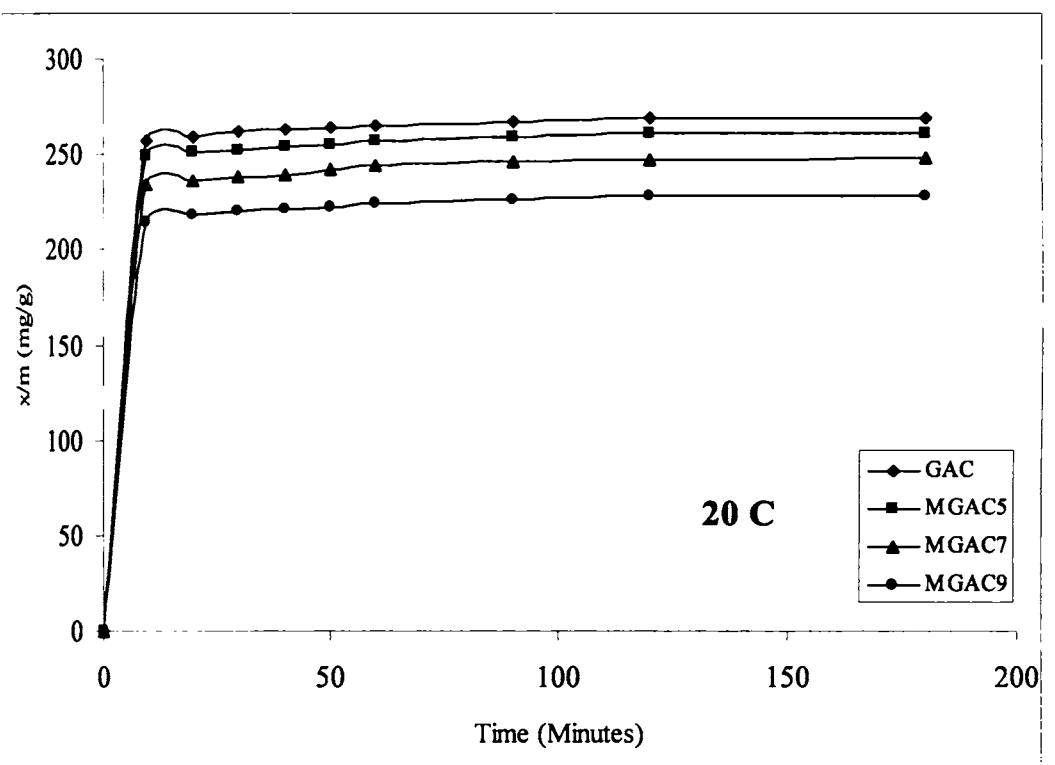


Figure 3.9b Concentration Vs time graphs for *p*-nitrophenol adsorption at 20°C.

adsorption process. But the porous structure of the adsorbent material does have an influence on the rate at which the adsorbate molecules are adsorbed onto the carbon matrix. However, there is a decrease in the amount of *p*-nitrophenol adsorbed with temperature.

#### **Evaluation of the Rate Constants for *p*-Nitrophenol Adsorption:**

The rate constants for adsorption of *p*-nitrophenol on GAC and the composites were evaluated using Lagergren equation. An expression of the equation is already given (Equation No. 3.1). The Lagergren plots for *p*-nitrophenol adsorption on the four adsorbents are given in Figures 3.10a - d. The rate constant  $k_{ad}$  is calculated from the slope of the Lagergren plots. However, the non-linearity of the plots limits the application of these kinetic plots. Since approximately 94 % of the fraction of the adsorbed molecules is removed within ten minutes of the adsorption process, the Lagergren is applied for the slowest step after the initial phase of adsorption. The rapid initial uptake of *p*-nitrophenol shows that the external or film diffusion step plays a major role in the adsorption (Al-Duri, B., 1988). As in the case of phenol, it was not practically possible to get a genuine data at a lower time frame. The rate constants calculated from the Lagergren plots are given in Table 3.6. The  $k_{ad}$  at 20°C for GAC, MGAC5, MGAC7 and MGAC9 were calculated to be  $1.25 \times 10^{-2} \text{ min}^{-1}$ ,  $1.12 \times 10^{-2} \text{ min}^{-1}$ ,  $1.09 \times 10^{-2} \text{ min}^{-1}$  and  $1.08 \times 10^{-2} \text{ min}^{-1}$  respectively. This shows that the extent of adsorption favours more effectively on GAC and less prominent on composites. There is a slight decrease in the rate constant at lower temperature. At 10°C, the calculated  $k_{ad}$  for GAC, MGAC5, MGAC7 and MGAC9 are 1.14, 1.11, 1.04 and 1.01 ( $\times 10^{-2} \text{ min}^{-1}$ ) respectively.

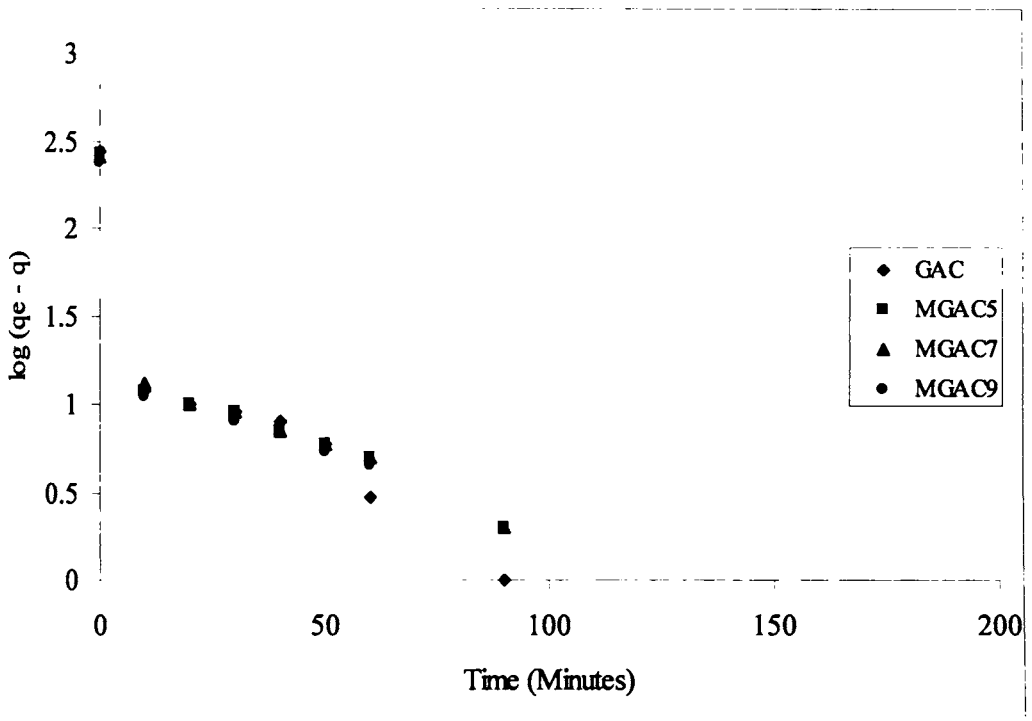


Figure 3.10a Lagergren plot for *p*-nitrophenol adsorption at 10 °C.

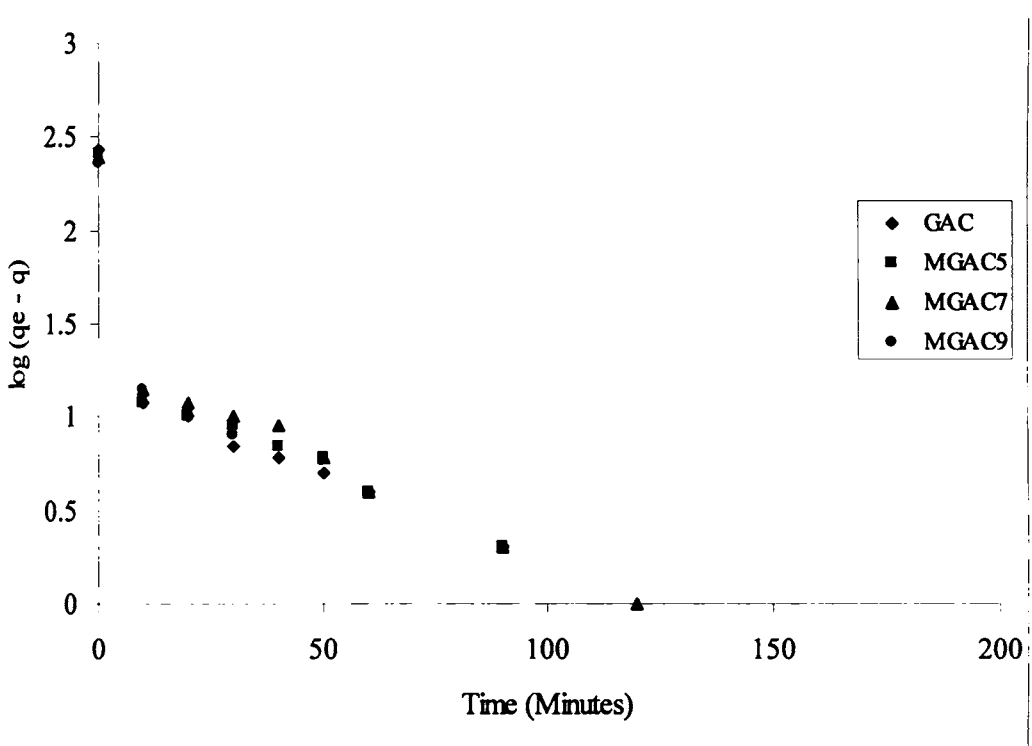


Figure 3.10b Lagergren plot for *p*-nitrophenol adsorption at 20 °C.

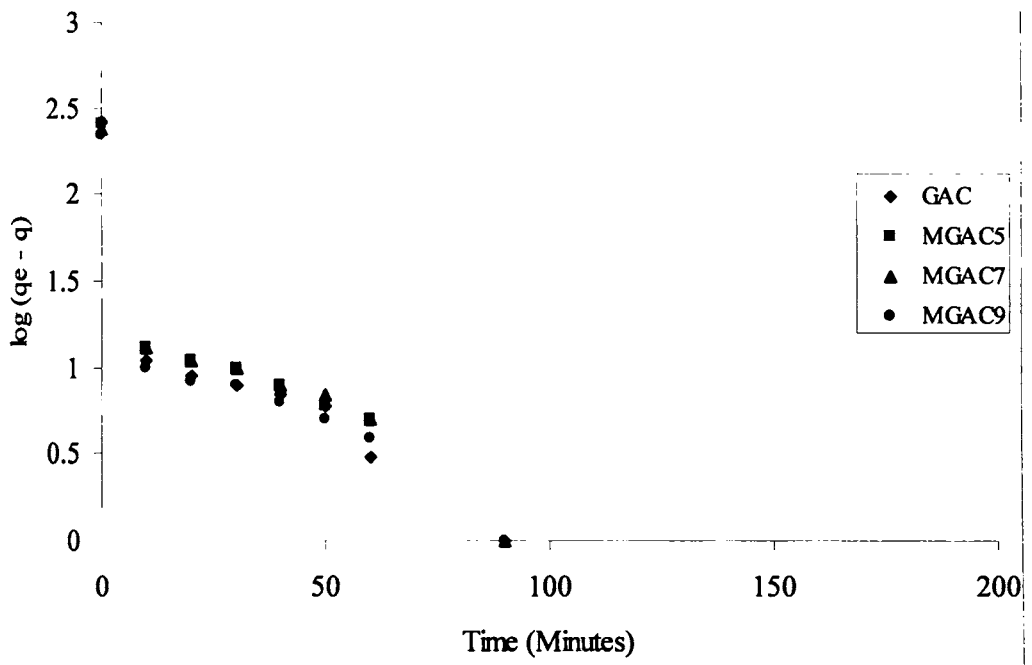


Figure 3.10c Lagergren plot for *p*-nitrophenol adsorption at 30 °C.

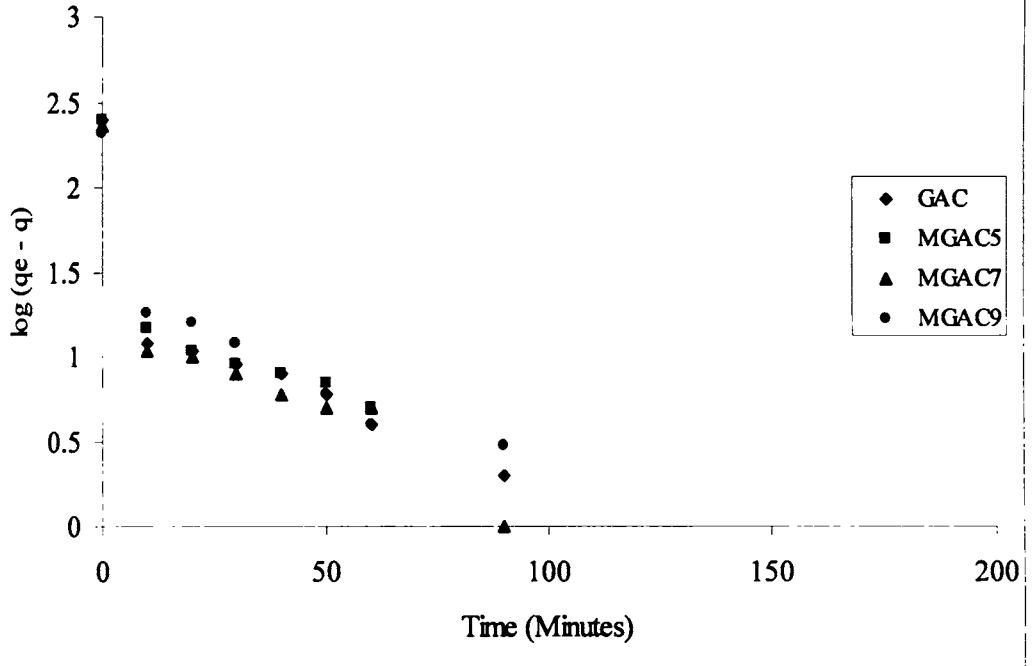


Figure 3.10.d Lagergren plot for *p*-nitrophenol adsorption at 40°C.

Table 3.6 Rate constants for *p*-nitrophenol adsorption evaluated from Lagergren plots

Carbon	Temperature (°C)	Rate constant (min <sup>-1</sup> ) x 10 <sup>-2</sup>	r <sup>2</sup>
GAC	10	1.14	0.974
MGAC5	10	1.11	0.973
MGAC7	10	1.04	0.968
MGAC9	10	1.01	0.982
GAC	20	1.25	0.981
MGAC5	20	1.12	0.967
MGAC7	20	1.09	0.979
MGAC9	20	1.08	0.961
GAC	30	1.26	0.976
MGAC5	30	1.18	0.983
MGAC7	30	1.15	0.971
MGAC9	30	1.10	0.963
GAC	40	1.26	0.973
MGAC5	40	1.19	0.988
MGAC7	40	1.16	0.964
MGAC9	40	1.12	0.974

### **Evaluation of Intraparticle Diffusion Rate Constants:**

The rate constants for intraparticle diffusion ( $k_{id}$ ) for *p*-nitrophenol adsorption on the control carbon, GAC and composite samples MGAC5, MGAC7 and MGAC9 were calculated from the equation given described earlier (Equation No. 3.2). Plots of  $q$  vs  $t^{1/2}$  at four different temperatures are given in Figures 3.11a - d. The plots show a stepwise nature with a steep first phase followed by a linear portion. The initial steep portion represents the boundary layer diffusions and the linear portion is a result of the intraparticle diffusion effects (Faust, S. D. & Aly, O. M., 1987). The intraparticle rate constant,  $k_{id}$ , was calculated from the slope of the linear portion of the plots. The values of the intraparticle diffusion rate constants calculated from these plots are given in Table 3.7. The intraparticle diffusion rate for *p*-nitrophenol adsorption at 20°C was found to be 1.37, 1.30, 1.29 and 1.27 mg/g/min<sup>1/2</sup> for GAC, MGAC5, MGAC7 and MGAC9. The  $k_{id}$  reduces with iron oxide loading and is a result of impregnation of iron oxide and reduction in porosity. There is a slight reduction in  $k_{id}$  with lowering of temperature as can be seen from the table. The  $k_{id}$  values obtained for GAC, MGAC5, MGAC7 and MGAC9 at 10°C are 1.29, 1.20, 1.17 and 1.13 mg/g/min<sup>1/2</sup> respectively.

### **3.4.2b Adsorption Isotherm Studies:**

Batch adsorption isotherm studies for *p*-nitrophenol on carbons samples GAC, MGAC5, MGAC7 and MGAC9 were conducted to evaluate the equilibrium adsorption capacities towards *p*-nitrophenol. The isotherm experiments were carried out at four different temperatures, 10°C, 20°C, 30°C and 40°C to study the influence of temperature on the extent of adsorption. Kinetics of *p*-nitrophenol adsorption has already shown that 2 h of contact time is sufficient to reach equilibrium. Hence, an equilibration time of 2 h was fixed for the batch study.

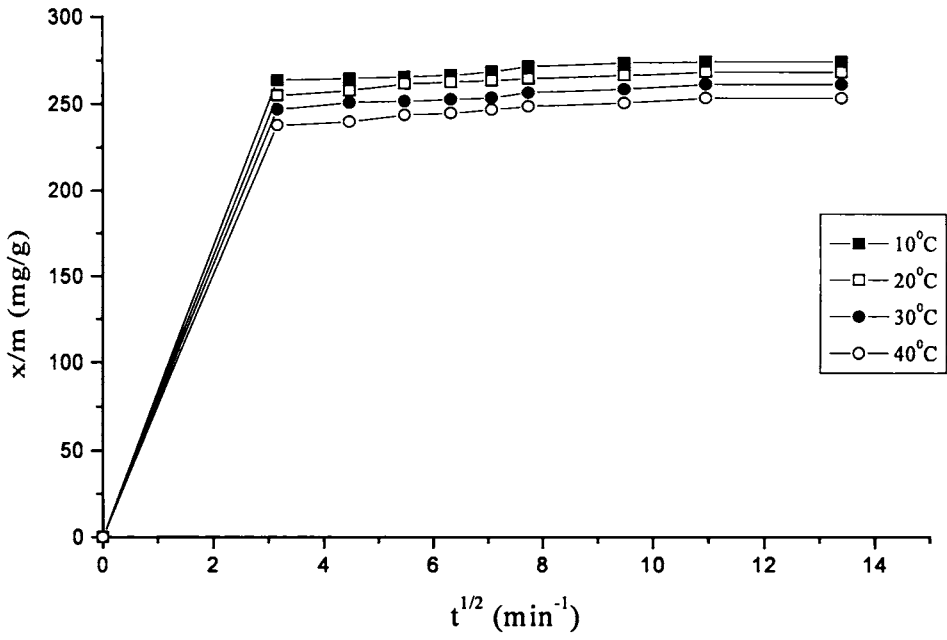


Figure 3.11a Intraparticle diffusion plots of *p*-nitrophenol adsorption on GAC.

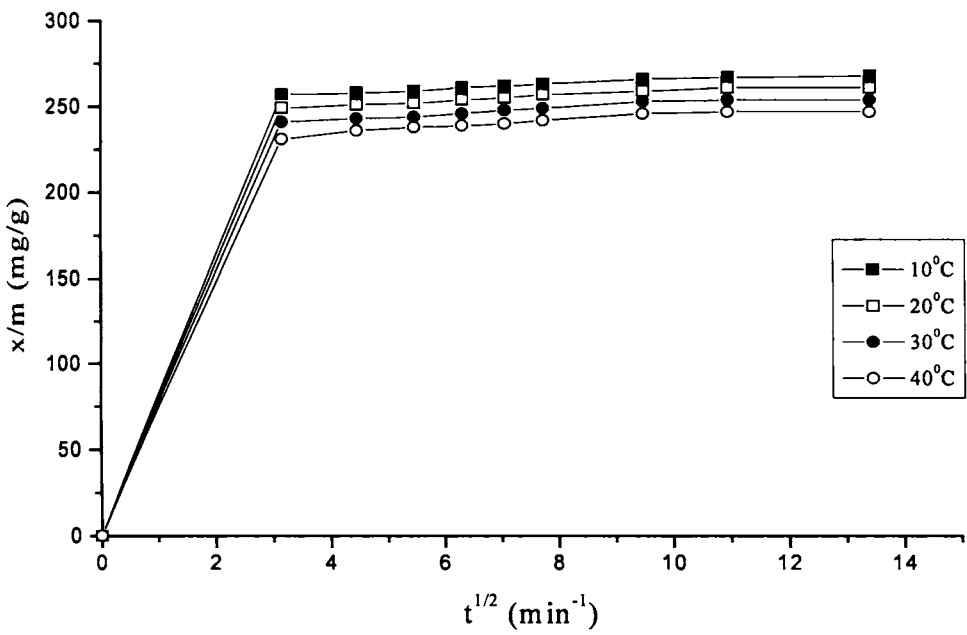


Figure 3.11b Intraparticle diffusion plots of *p*-nitrophenol adsorption on MGAC5.

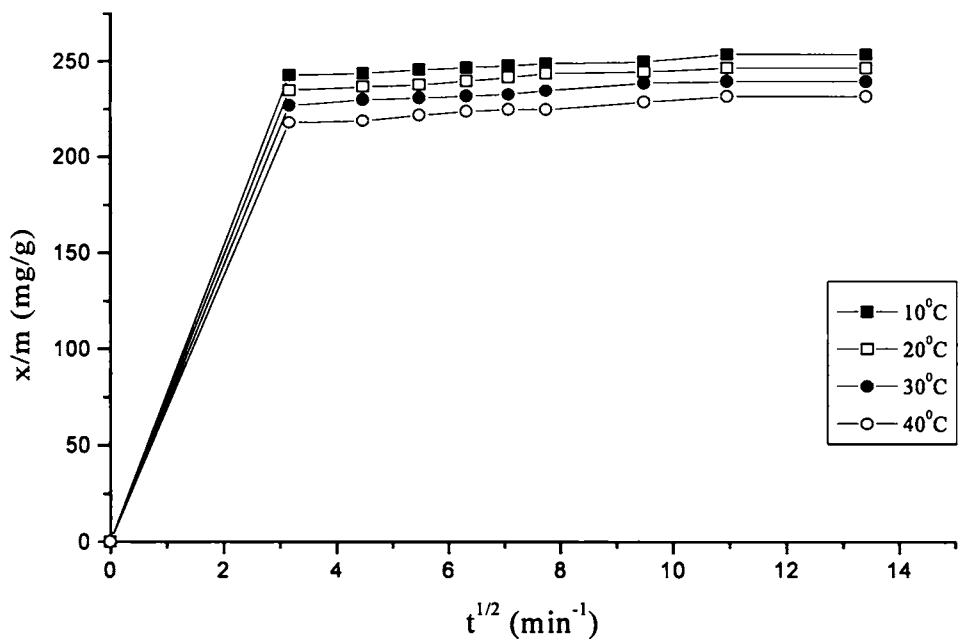


Figure 3.11c Intraparticle diffusion plots of *p*-nitrophenol adsorption on MGAC7.

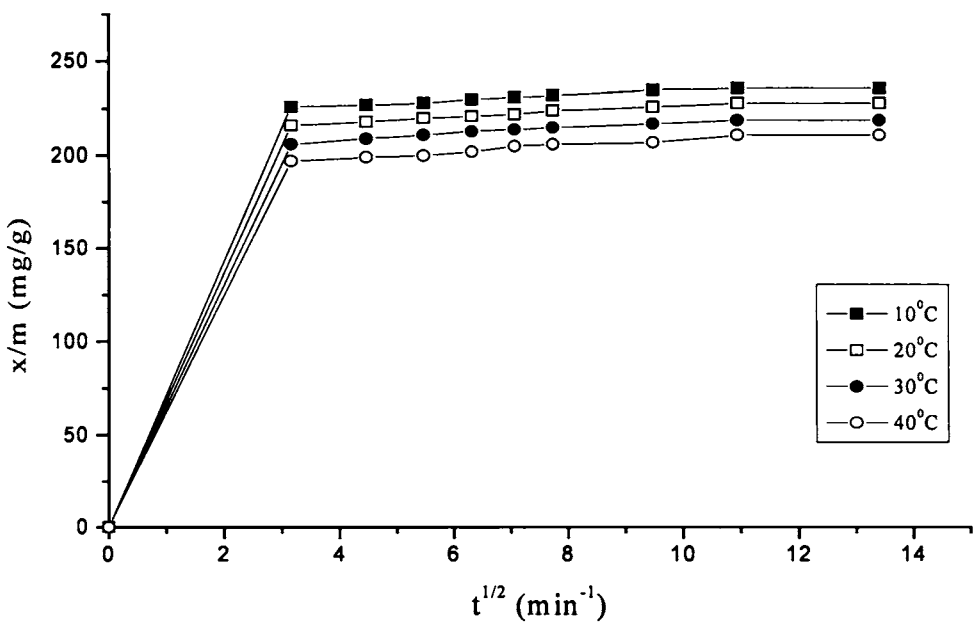


Figure 3.11d Intraparticle diffusion plots of *p*-nitrophenol adsorption on MGAC9.

Table 3.7 Intraparticle diffusion rate constants for *p*-nitrophenol adsorption

Carbon	Temperature, °C	Intraparticle rate constant, $k_{id}$ (mg/g/min <sup>1/2</sup> )	$r^2$
GAC	10	1.29	0.992
MGAC5	10	1.20	0.996
MGAC7	10	1.17	0.984
MGAC9	10	1.13	0.990
GAC	20	1.37	0.997
MGAC5	20	1.30	0.996
MGAC7	20	1.29	0.989
MGAC9	20	1.27	0.993
GAC	30	1.53	0.991
MGAC5	30	1.44	0.997
MGAC7	30	1.39	0.995
MGAC9	30	1.30	0.984
GAC	40	1.69	0.991
MGAC5	40	1.58	0.996
MGAC7	40	1.53	0.995
MGAC9	40	1.50	0.994

Equilibrium isotherm (Figures 3.12a - d) plots show that the adsorption capacity of composites towards *p*-nitrophenol is less compared to the control carbon. The surface modification reduces the adsorption capacity of the composite samples. This is expected as in the case of phenol since the iron oxide impregnation has reduced the available micropore surface area of the modified carbons. These isotherm plots were evaluated to quantitatively predict the loss in adsorption capacity of the composites towards *p*-nitrophenol. The effect of temperature on *p*-nitrophenol adsorption by carbon samples can be observed from these equilibrium plots. The amount of *p*-nitrophenol adsorbed is reduced with an increase in the temperature indicating the exothermic nature of the process.

#### **Langmuir Isotherm Plots for *p*-Nitrophenol Adsorption**

A linear form of the Langmuir equation was used to study the adsorption of *p*-nitrophenol on all carbon samples by plotting  $C_e/X$  against  $C_e$ . Linear plots with high correlation coefficients suggest that the adsorption of *p*-nitrophenol on these adsorbent samples is in agreement with the Langmuir equation. The Langmuir plots for *p*-nitrophenol adsorption on carbon samples are given in Figures 3.13a - d. The monolayer capacity,  $X_m$  and the Langmuir constant,  $b$ , were calculated from the slope and intercept these plots. The values of  $X_m$  and  $b$  are given in Table 3.8.

The monolayer capacity of the control carbon, GAC, for *p*-nitrophenol adsorption is as high as 625 mg/g at 20°C and the value decreases with temperature. The corresponding value at 10°C is 666.67 mg/g. The monolayer capacity reduces to 555.56 mg/g when the temperature is increased to 40°C. This indicates that adsorption of *p*-nitrophenol on activated carbon is favoured at lower temperatures ranges. The surface modification is shown to have significant influence on the monolayer capacity of the adsorbent samples. This reduction in the monolayer adsorption can be

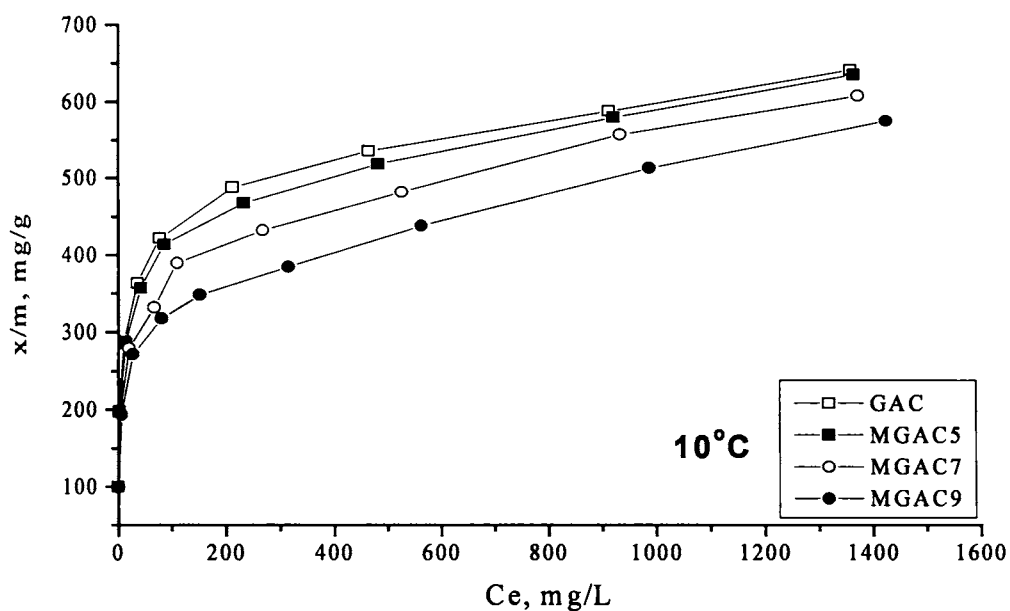


Figure 3.12a Adsorption of PNP on samples at 10°C.

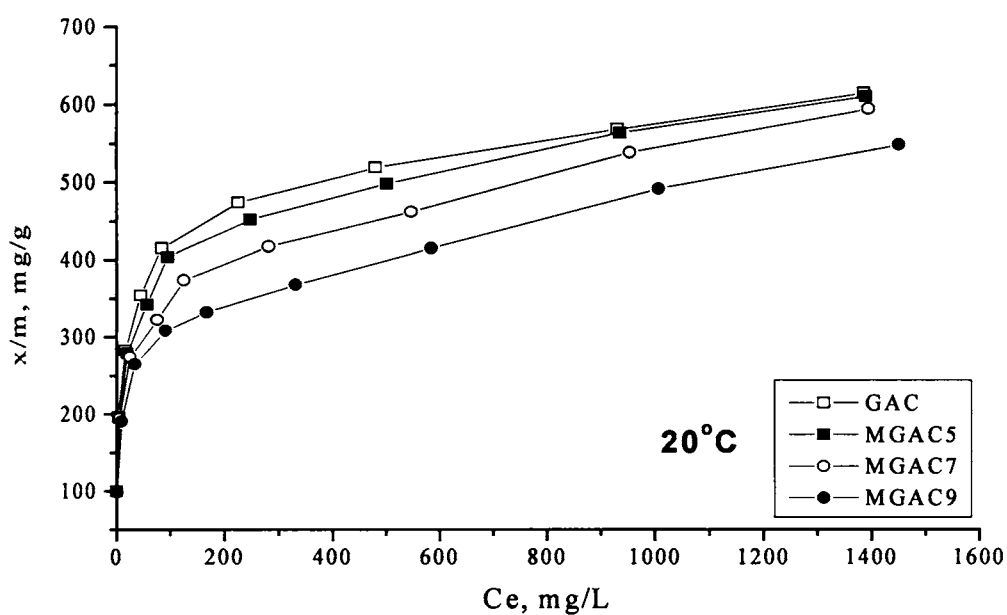


Figure 3.12b Adsorption of PNP on samples at 20°C.

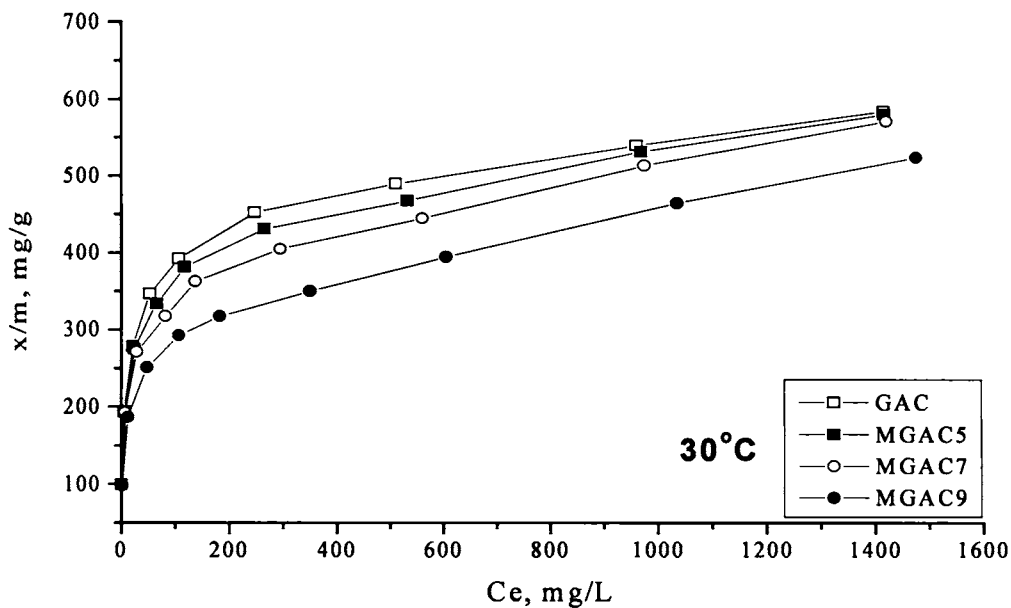


Figure 3.12c Adsorption of PNP on samples at 30°C.

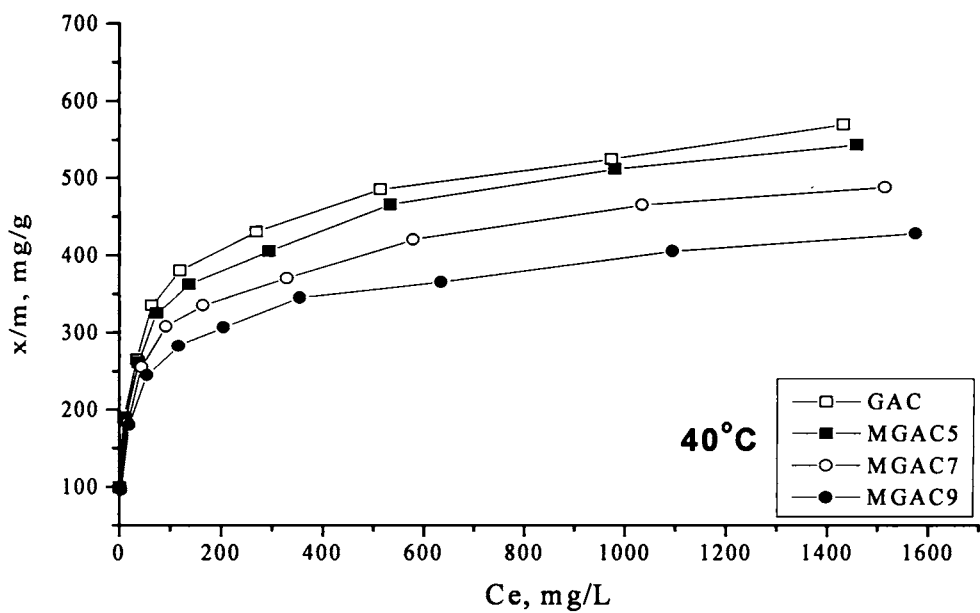


Figure 3.12d Adsorption of PNP on samples at 40°C.

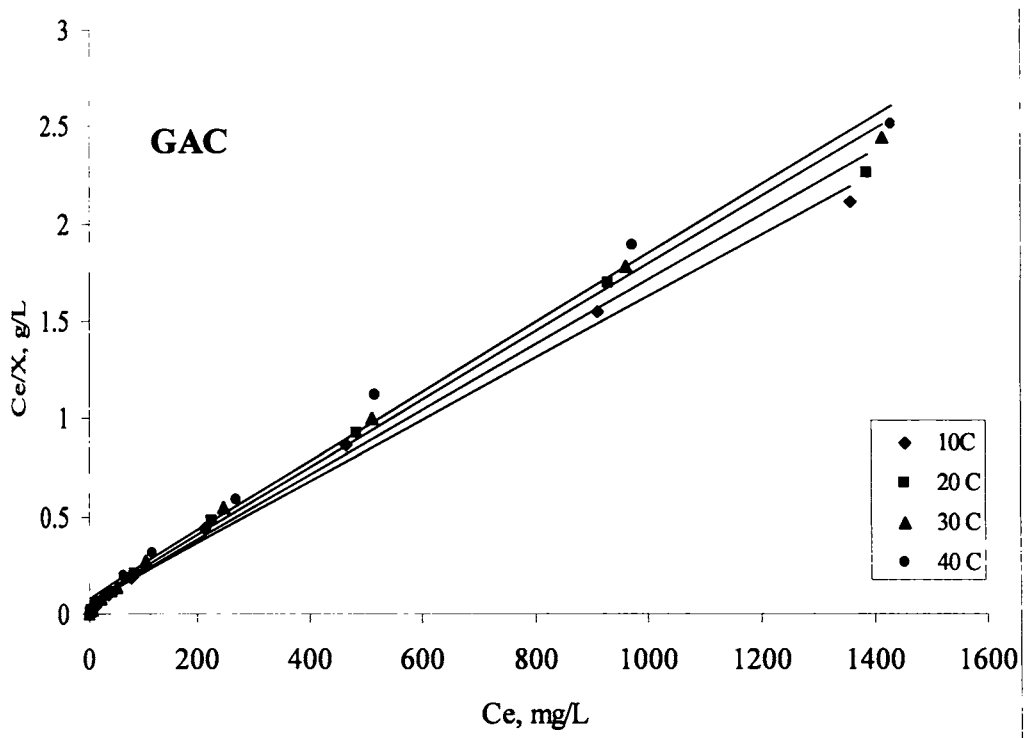


Figure 3.13a Langmuir plots of *p*-nitrophenol adsorption on GAC.

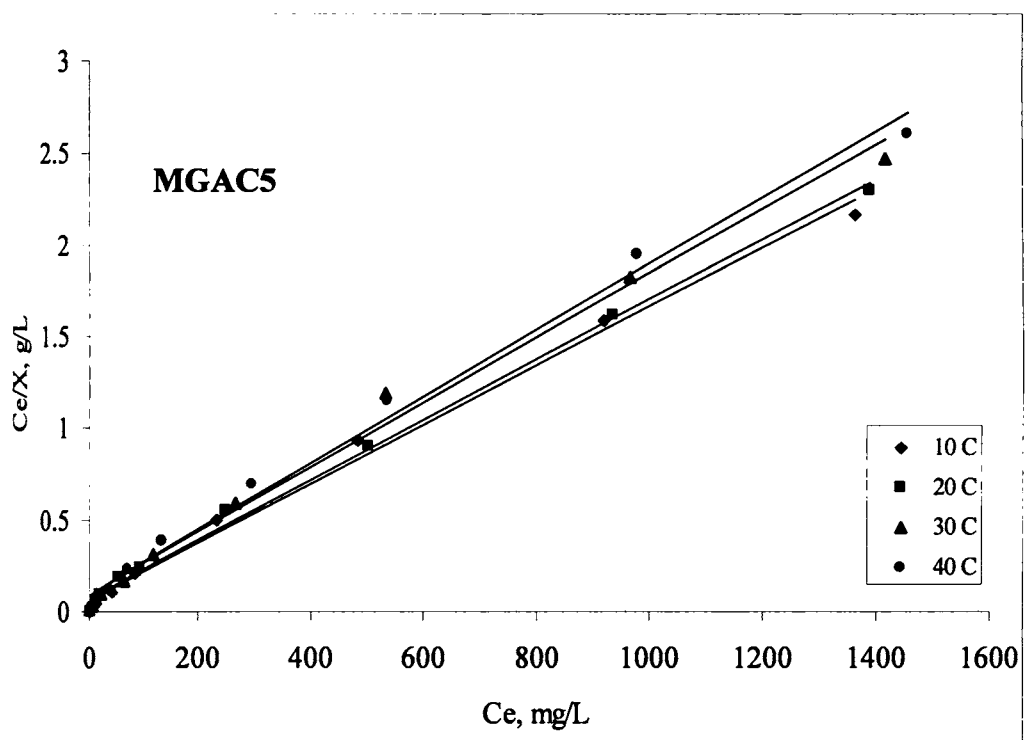


Figure 3.13b Langmuir plots of *p*-nitrophenol adsorption on MGAC5

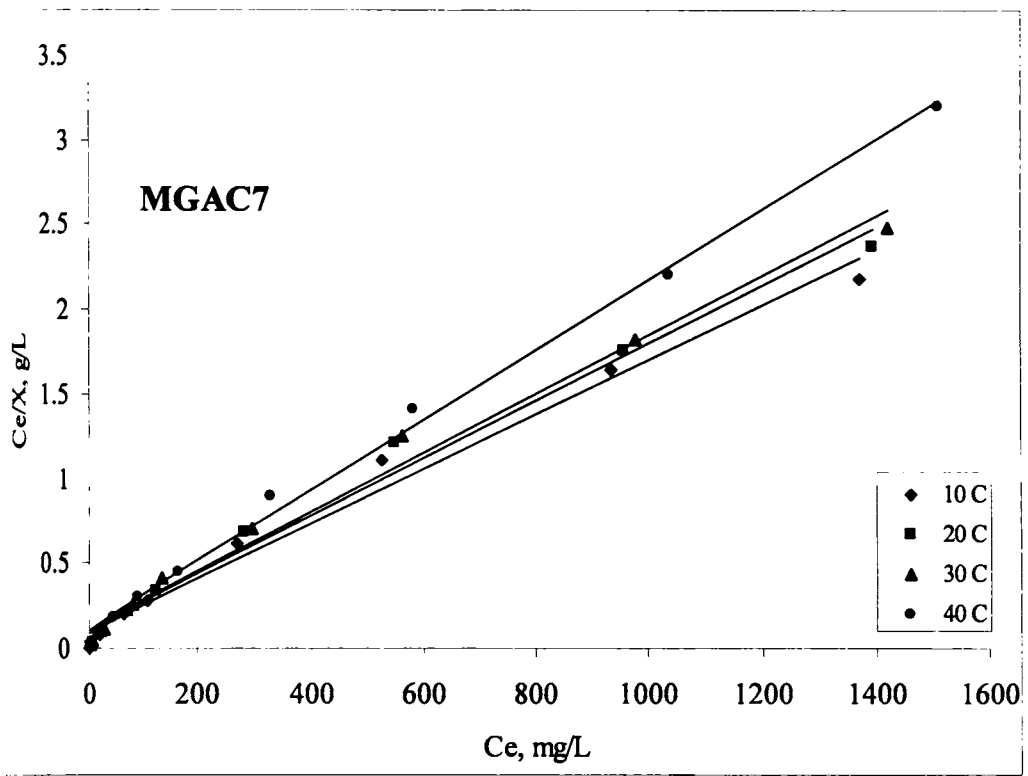


Figure 3.13c Langmuir plots of *p*-nitrophenol adsorption on MGAC7

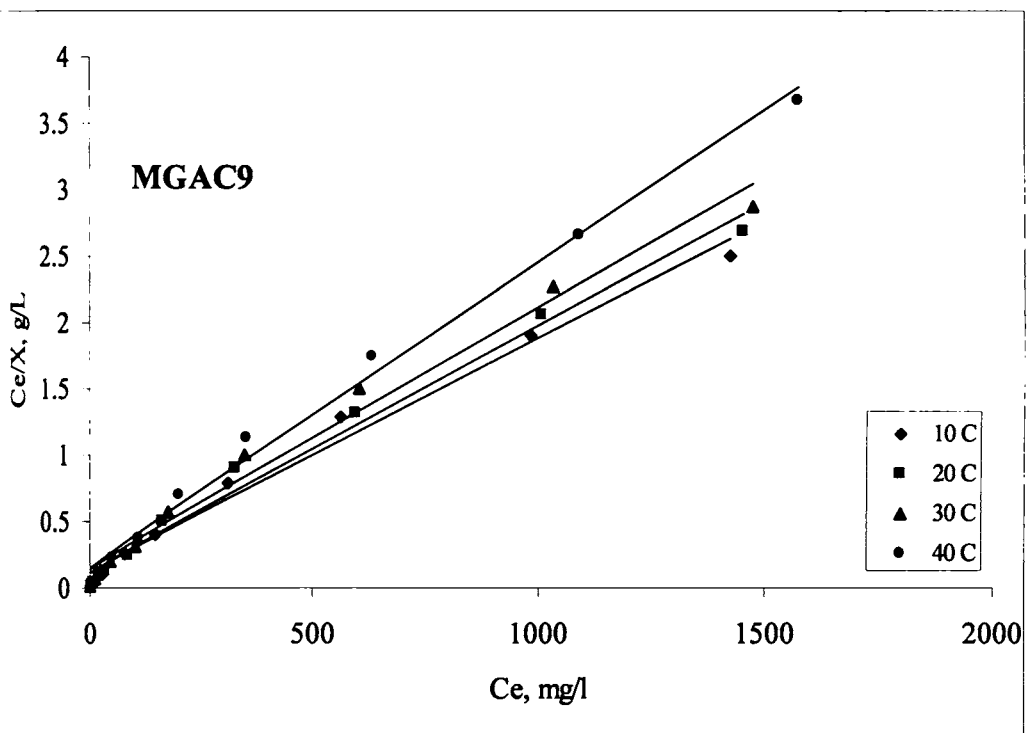


Figure 3.13d Langmuir plots of *p*-nitrophenol adsorption on MGAC9

Table 3.8 Langmuir constants for the adsorption of *p*-nitrophenol.

Carbon	Temperature, °C	Langmuir Constants		$r^2$
		$b$	$X_m$	
GAC	10	0.0298	666.67	0.9948
MGAC5	10	0.0295	625.00	0.9937
MGAC7	10	0.0186	588.24	0.9858
MGAC9	10	0.0165	555.56	0.9865
GAC	20	0.0289	625.00	0.9943
MGAC5	20	0.0250	606.06	0.9970
MGAC7	20	0.0185	555.56	0.9875
MGAC9	20	0.0163	526.32	0.9887
GAC	30	0.0285	588.24	0.9967
MGAC5	30	0.0232	555.56	0.9918
MGAC7	30	0.0168	540.54	0.9887
MGAC9	30	0.0159	465.12	0.9845
GAC	40	0.0229	555.56	0.9933
MGAC5	40	0.0205	526.32	0.9936
MGAC7	40	0.0164	476.19	0.9965
MGAC9	40	0.0158	416.67	0.9934

attributed to reduction in surface area due to iron oxide impregnation. Earlier workers have reported that the adsorption of *p*-nitrophenol from aqueous solutions is dependant on surface area and occurred in narrow pores (Gonzalez-Martin, M. I., *et al.*, 1991; Gomez-Serrano, V., *et al.*, 1994). Puri and co-workers (1976), while studying the adsorption of phenol and nitrophenol on activated carbons and carbon blacks with different surface areas and containing varying amounts of carbon oxygen surface groups observed that the adsorption was a function of surface area when carried out at moderate concentrations. The monolayer capacity is reduced with iron loading and the percentage reduction in  $X_m$  with iron loading compared to the control carbon at different temperatures is given in Figure 3.14. It can be seen that the reduction in monolayer capacity is more prominent at higher temperatures. At 20°C, percentage reduction in  $X_m$  for MGAC5, MGAC7 and MGAC9 with respect to GAC was 3.2, 11 and 15.6 respectively. The corresponding values at 10°C were 6.2, 12.5 and 16.7 respectively. The Langmuir constant '*b*' also reduces with surface modification. The variation in Langmuir constant '*b*' is influenced by the thermodynamic variables.

From the values of monolayer capacities for phenol and *p*-nitrophenol adsorption on new activated carbons, it is clear that *p*-nitrophenol is more preferably adsorbed. The increased adsorption of *p*-nitrophenol on activated carbons compared to phenol has been reported by previous workers as well (Moreno-Castilla, C. & Rivera-Utrilla, J., 1995). This higher adsorption can be related to the electron withdrawing properties of the  $-\text{NO}_2$  group at the para position in the phenol ring (Morrison, R. T. & Boyd, R. N., 1983). The electron withdrawal or deactivation of the benzene ring favours the formation of electron donor-acceptor complexes between these rings and basic groups on the surface of the activated carbons, increasing the

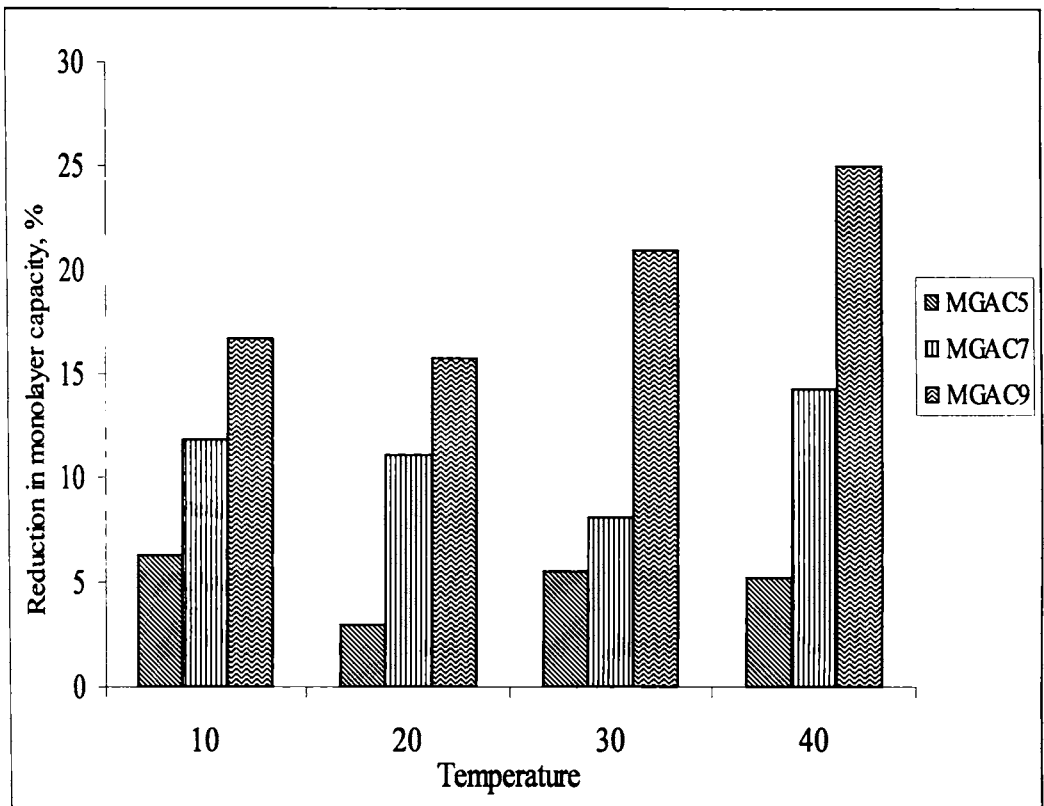


Figure 3.14 Reduction in the monolayer capacity for *p*-nitrophenol adsorption for composite samples compared to the control carbon at different temperatures.

adsorption capacity. In addition, the increased solubility of phenol compared with *p*-nitrophenol decreases its adsorbability to the carbon surface (Attia, A. A., *et al.*, 2003b).

#### **Freundlich Model for *p*-Nitrophenol Adsorption:**

The isotherm data for *p*-nitrophenol adsorption on new activated carbon composites were fitted into the Freundlich equation. The straight lines obtained show that the system obeys the Freundlich model. Plots of  $\log x/m$  versus  $\log C_e$  are linear and are given in Figures 3.15a – d. The Freundlich constants  $K$  and  $n$  were determined from the intercept and the slope of the linear plots. These are given in Table 3.9. The influence of temperature on these parameters was studied at four different temperatures.

The value for Freundlich constant,  $K$ , is 143.81 mg/g for *p*-nitrophenol adsorption on GAC at 20°C. The  $K$  value for *p*-nitrophenol adsorption on MGAC5, MGAC7 and MGAC9 was found to be 128.5, 117.3 and 95.39. The  $K$  value decreased with increase in temperature. The values of  $K$  for GAC, MGAC5, MGAC7 and MGAC9 at 10°C are 167.96, 154.45, 134.65 and 110.23 mg/g respectively. The reduction in  $K$  values can be attributed to the reduction in surface area and porosity. The reduced porosity due to impregnation of iron oxide influences the adsorption of *p*-nitrophenol as adsorption at low and moderate concentrations are very much dependant on the microporous nature and surface area of the activated carbons (Goyal, M., 2004). The reduction in  $K$  values with temperature suggests that the process is exothermic. This means the adsorption is favoured at lower temperature irrespective of surface modification. Depending on the contact time and type of carbons different values of  $K$  and  $n$  have been reported by various authors (Faust, S. D. & Aly, O. M., 1987; Nouri, S. & Haghseresht, F., 2004). The values of ' $n$ '

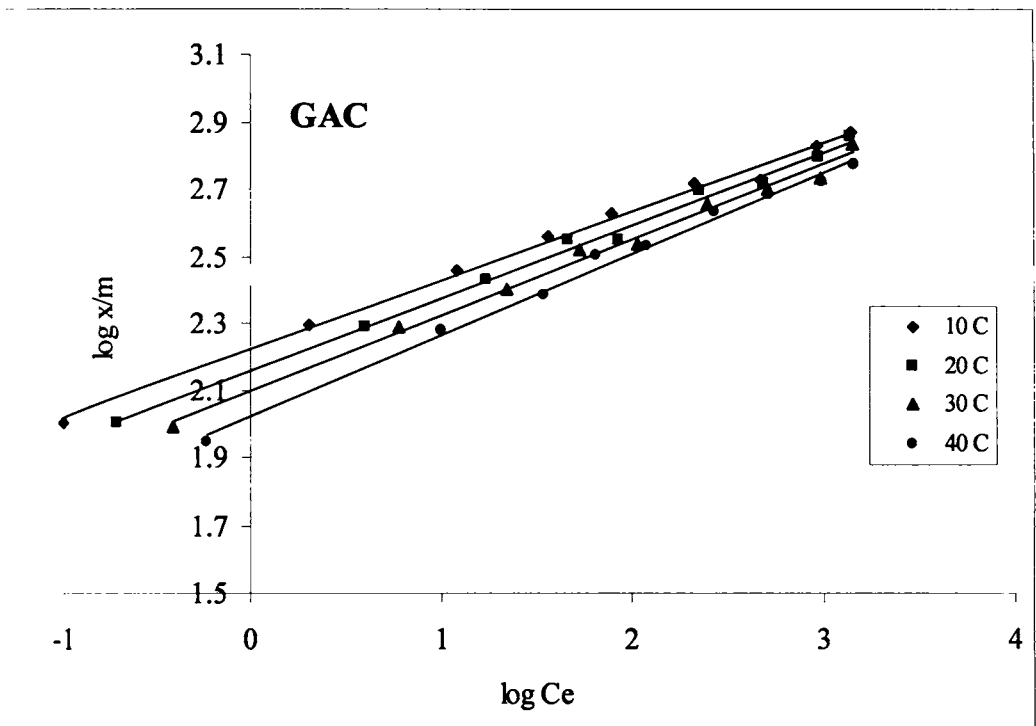


Figure 3.15a Freundlich plots of *p*-nitrophenol adsorption on GAC.

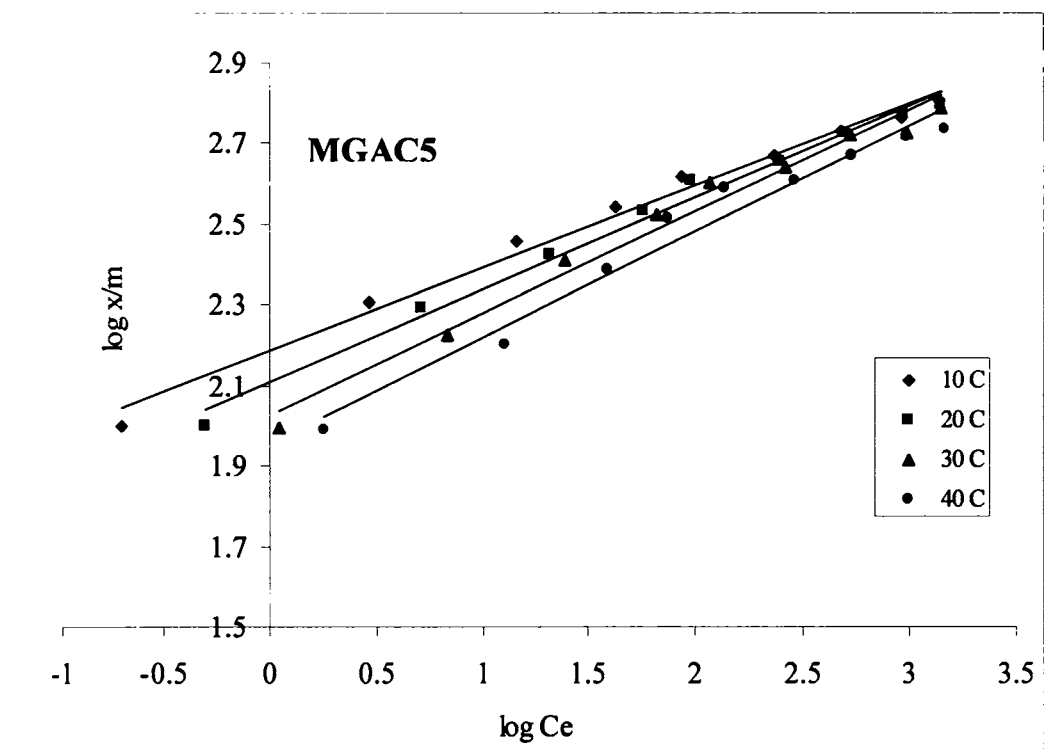


Figure 3.15b Freundlich plots of *p*-nitrophenol adsorption on MGAC5.

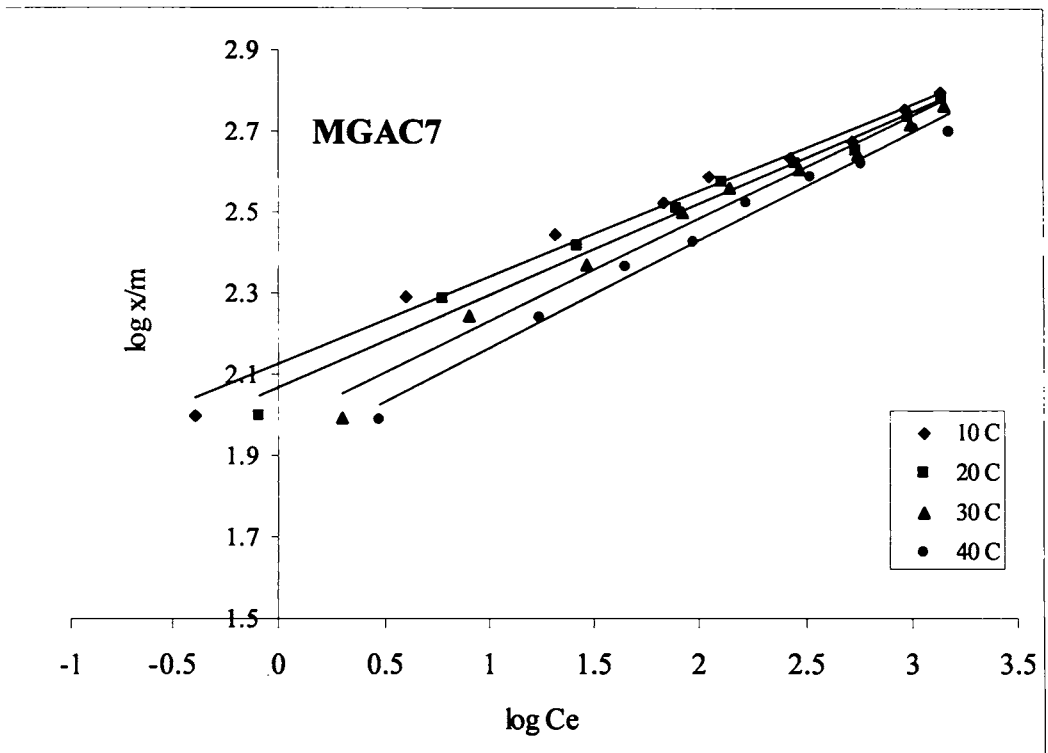


Figure 3.15c Freundlich plots of *p*-nitrophenol adsorption on MGAC7.

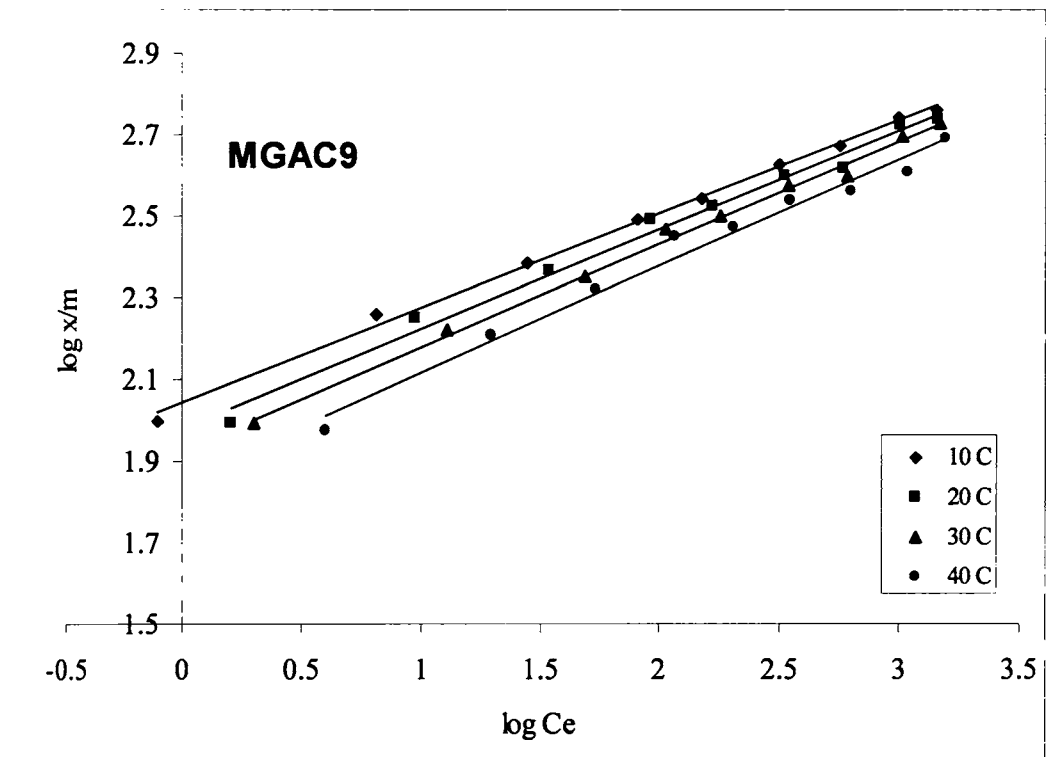


Figure 3.15d Freundlich plots of *p*-nitrophenol adsorption on MGAC9.

Table 3.9 Freundlich constants for the adsorption of *p*-nitrophenol.

Carbon	Temperature, °C	Freundlich Constants		$r^2$
		$K$ , mg/g	$n$	
GAC	10	167.96	4.88	0.9949
MGAC5	10	154.45	4.91	0.9876
MGAC7	10	134.65	4.69	0.9866
MGAC9	10	110.23	4.32	0.9968
GAC	20	143.81	4.59	0.9940
MGAC5	20	128.5	4.37	0.9888
MGAC7	20	117.3	4.4	0.9850
MGAC9	20	95.39	4.11	0.9896
GAC	30	124.77	4.41	0.9911
MGAC5	30	106.73	3.99	0.9797
MGAC7	30	95.13	3.93	0.9795
MGAC9	30	84.8	3.96	0.9951
GAC	40	105.41	4.11	0.9926
MGAC5	40	90.12	3.81	0.9690
MGAC7	40	79.4	3.76	0.9856
MGAC9	40	71.48	3.82	0.9812

obtained for GAC are comparable to previously reported values on commercial carbons (Dobbs, R. A. & Cohen, J. M., 1980; Snoeyink, V. L., *et al.*, 1969).

#### **Evaluation of Thermodynamic Parameters**

The thermodynamic parameters  $\Delta H$ ,  $\Delta G$  and  $\Delta S$  for *p*-nitrophenol adsorption on GAC, MGAC5, MGAC7 and MGAC9 were evaluated from the distribution coefficient values at four different temperatures. The logarithmic plots of  $K_D$  against reciprocal of temperature for *p*-nitrophenol adsorption on carbons are given in Figures 3.16a - d. The change in enthalpy and entropy for the system were evaluated from the distribution plots and the change in free energy was calculated using equations 3.4.

The values of  $\Delta H$ ,  $\Delta G$  and  $\Delta S$  for *p*-nitrophenol adsorption on carbons are given in Table 3.10. The values of  $\Delta H$  for *p*-nitrophenol adsorption on all the samples were negative suggesting an exothermic reaction mechanism. The change in  $\Delta H$  values for the *p*-nitrophenol adsorption on GAC was in the range  $-5.57$  and  $-0.46$  ( $\times 10^{-2}$  kJ/mol) for GAC.  $\Delta H$  shows a decrease with increase in solute concentration in solution. For magnetic iron oxide loaded composites the  $\Delta H$  shows a reduction with iron oxide loading. For MGAC5 the value of  $\Delta H$  varied between  $-5.5$  and  $-0.46$  ( $\times 10^{-2}$  kJ/mol). The corresponding values for MGAC7 and MGAC9 were  $-5.2$  to  $-0.42$  and  $-3.79$  to  $-0.24$  ( $\times 10^{-2}$  kJ/mol) respectively. The  $\Delta S$  shows an increase with concentration of *p*-nitrophenol and a decrease with iron oxide loading. The change in free energy for *p*-nitrophenol adsorption at low concentration is not useful for deriving a conclusion on the thermodynamic properties of the system and was also reported by other workers (Achari, V. S., 1998). However, at higher concentrations the  $\Delta G$  values were negative and show an endothermic reaction.

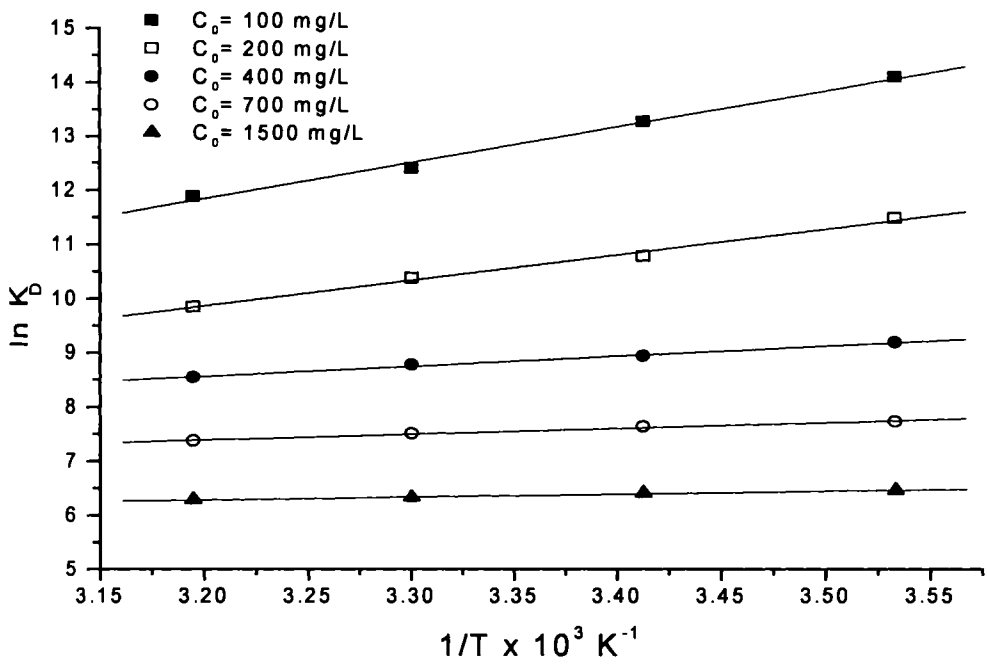


Figure 3.16a Plots of  $\ln K_D$  vs  $1/T$  of *p*-nitrophenol adsorption on GAC.

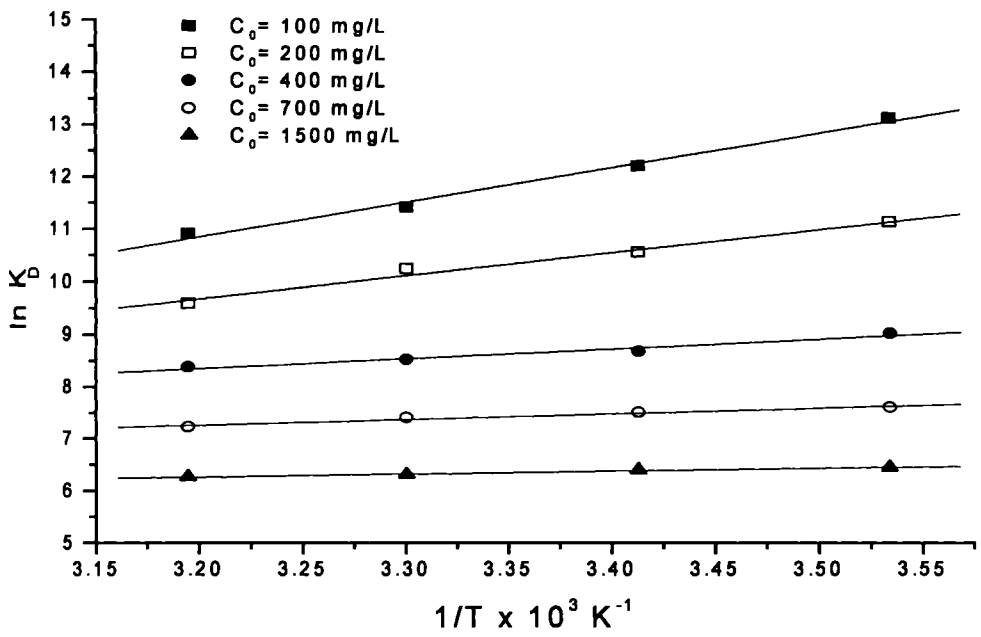


Figure 3.16b Plots of  $\ln K_D$  vs  $1/T$  of *p*-nitrophenol adsorption on MGAC5.

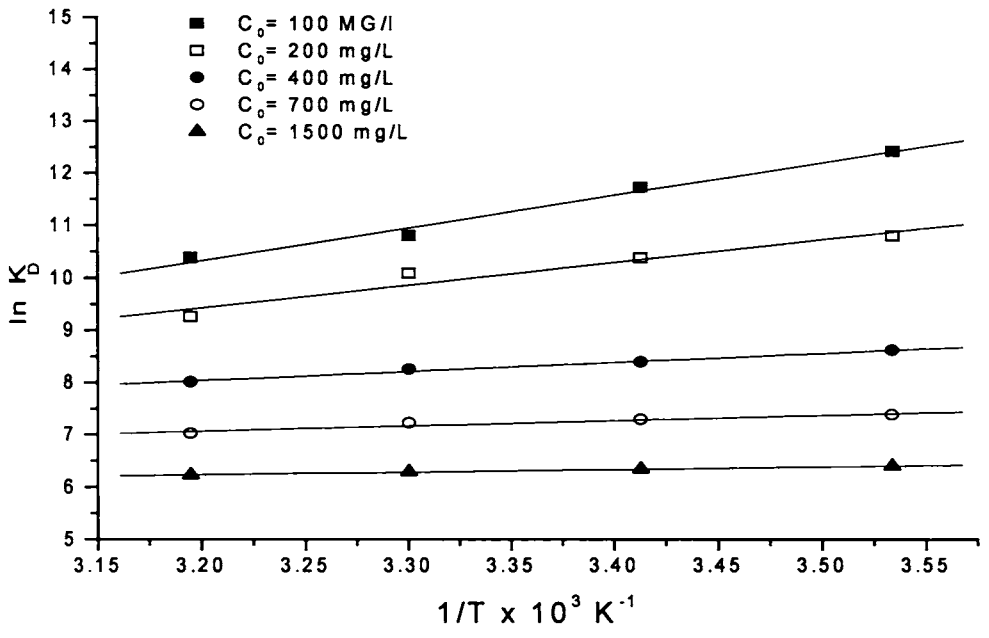


Figure 3.16c Plots of  $\ln K_D$  vs  $1/T$  of *p*-nitrophenol adsorption on MGAC7.

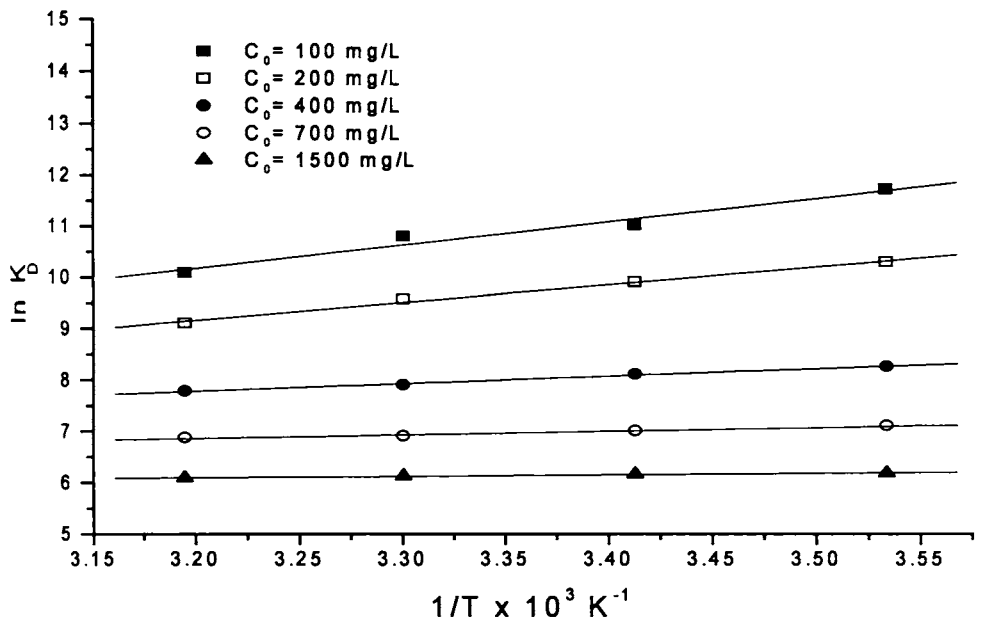


Figure 3.16d Plots of  $\ln K_D$  vs  $1/T$  of *p*-nitrophenol adsorption on MGAC9.

Table 3.10 Thermodynamic parameters for *p*-Nitrophenol adsorption

Carbon	$C_o$ , mg/L	$\Delta H$ , kJ/mol $\times 10^{-2}$	$\Delta S$ , J/mol/K $\times 10^{-2}$	$\Delta G$ , kJ/mol			
				283	293	303	313
GAC	100	-5.57	-8.56	24.15	25.01	25.87	26.72
	200	-3.96	-4.46	12.57	13.02	13.46	13.91
	400	-1.58	2.06	-5.85	-6.06	-6.26	-6.47
	700	-0.91	3.23	-9.16	-9.49	-9.81	-10.13
	1500	-0.46	3.77	-10.66	-11.04	-11.42	-11.80
MGAC5	100	-5.50	-7.80	22.57	23.38	24.18	24.98
	200	-3.62	-3.53	9.96	10.32	10.67	11.02
	400	-1.54	2.01	-5.71	-5.91	-6.11	-6.31
	700	-0.91	3.11	-8.81	-9.12	-9.43	-9.74
	1500	-0.46	3.73	-10.57	-10.94	-11.32	-11.69
MGAC7	100	-5.20	-7.90	22.30	23.90	23.88	24.70
	200	-3.61	-3.48	9.80	10.15	10.49	10.84
	400	-1.45	2.02	-5.73	-5.93	-6.14	-6.34
	700	-0.85	3.16	-8.95	-9.27	-9.58	-9.90
	1500	-0.42	3.82	-10.8	-11.19	-11.57	-11.95
MGAC9	100	-3.79	-3.68	10.36	10.73	11.10	11.46
	200	-2.88	-1.61	4.51	4.67	4.83	4.99
	400	-1.21	2.60	-7.38	-7.64	-7.90	-8.16
	700	-0.57	3.86	-10.92	-11.31	-11.69	-12.08
	1500	-0.24	4.35	-12.31	-12.74	-13.18	-13.61

### **Regeneration Studies**

Activated carbon and modified activated carbons have been extensively used for the removal of gaseous pollutants, the treatment of wastewater and the purification of drinking water. For economic reasons, the use of activated carbons is limited. The cost of carbon for single use may be so high that its use is unjustified. One procedure for reducing operational costs using activated carbon is to desorb the substances retained, thereby enabling the carbon to be reused.

The regeneration efficiency data on the control carbon and magnetic iron oxide loaded activated carbon samples were determined as per the method described in a previous section (3.3.3). The main objective of this study was to calculate the reduction in the adsorption capacity of these adsorbents with each regeneration cycles. The regeneration efficiency data on control carbon and the magnetic iron oxide loaded activated carbon samples are given in Table 3.11. The percentage regeneration efficiency on phenol saturated control carbon GAC was reduced to 83.96 % after the first regeneration cycle where as the corresponding values for MGAC5, MGAC7 and MGAC9 are 83.23, 79.60 and 79.18 respectively. Only 59.11 % of the adsorption capacity could be restored by the end of fifth cycle for GAC. Corresponding values for MGAC5, MGAC7 and MGAC9 are 55.48, 54.85 and 54.28 respectively. It can be seen that approximately half of the original adsorption capacity of the composite samples could be restored after four cycles. In the case of carbons contaminated with *p*-nitrophenol, the regeneration efficiency with boiling water is better compared to phenol contaminated carbons. For GAC, 70.33 % of the adsorption capacity could be restored by the fifth cycle of regeneration. Corresponding values for MGAC5, MGAC7 and MGAC9 was found to be 67.95, 63.40 and 55.96. It can be seen that the

Table 3.11 Regeneration efficiency data on different carbon samples

Adsorbate	Cycle	% Regeneration			
		GAC	MGAC5	MGAC7	MGAC9
Phenol	1	100	100	100	100
	2	83.96	83.23	79.60	79.18
	3	78.62	76.13	71.91	71.38
	4	69.81	67.10	60.90	60.22
	5	59.11	55.48	54.85	54.28
<i>p</i> -Nitrophenol	1	100	100	100	100
	2	91.82	90.26	84.79	76.68
	3	80.56	77.95	74.48	66.84
	4	74.68	72.31	69.60	61.66
	5	70.33	67.95	63.40	55.96

adsorption capacity of the activated carbon samples reduces by successive adsorption steps but part of this can be recovered by treating with boiling water.

#### 3.4.4 **Adsorption of Methylene Blue on Activated Carbon – Magnetic Iron Oxide Composites**

Removal of color from dye bearing wastewaters is one of the major environmental problems because of difficulty in treating such wastewaters by conventional treatment methods, as most of the dyes are stable to light and oxidizing agents (Ho, Y. S., *et al.*, 2002). Presence of even minute amount of coloring substance makes it unsuitable for drinking or other recreational purposes due to its undesirable aesthetic qualities. The most commonly adopted methods for the treatment of dye-house effluents are chemical precipitation and biological oxidation (Mall, I. D. & Upadhyay, S. N., 1998; Donmez, G. C., *et al.*, 1999; Fernandez, N. A., 1995). Activated carbon adsorption is the effective alternate for the removal of dye residues in the case of lower solute concentration. Methylene blue, a basic dye, has been selected to evaluate the adsorption behaviour of magnetic iron oxide loaded activated carbons as an indicator dye.

The adsorption of the cationic dye, methylene blue, has been used for a long time for the evaluation of the adsorption properties of activated carbons, particularly carbons for liquid phase applications. The procedure was first suggested in 1924 (Paneth, F. & Radu, A., 1924) and still described as a standard method intended for industrial use (Aygun, A., *et al.*, 2003). Methylene blue adsorption was used extensively for monitoring the production and quality of activated carbon from coal, in a fluidized bed (Kudo, K., *et al.*, 1973).

The mechanism of dye adsorption by porous solids is however, complicated by the structure and size of the dye molecule itself. Molecular behaviour is usually discussed in terms of a monomer-dimer equilibrium in aqueous phase though the

presence of higher micelles or aggregates in concentrated solutions cannot be excluded (Chambers, R. W., *et al.*, 1974; Lemin, D. R. & Vikerstaff, T., 1947). A further complicating factor is the energetically heterogeneous nature of the solid surface so that the surface available, in a geometric sense, to the large dye molecule may contain a range of adsorption sites of different adsorptive power (Barton, S. S., 1987). These factors operate so as to obscure the meaning of the isotherm describing the adsorption and complicate a thermodynamical analysis of the temperature dependence of the dye adsorption.

### **Kinetics of Adsorption**

The kinetics of methylene blue adsorption on GAC and the composites MGAC5, MGAC7 and MGAC9 were studied. The kinetic plots of methylene blue adsorption on various adsorbents are given in Figure 3.17a - d. The dependence of kinetics of methylene blue adsorption on these adsorbent samples was studied at temperatures, 10, 20, 30 and 40°C.

The kinetic plots of methylene blue adsorption on activated carbon show that adsorption is slow compared to phenol and *p*-nitrophenol adsorption. The amount of methylene blue adsorbed per gram of the adsorbent varied with iron oxide loading. For iron oxide loaded activated carbon samples the amount of methylene blue adsorbed within the contact time was less compared to fresh carbon. Temperature has a direct influence on the amount of methylene blue adsorbed with time and all the plots showed a higher adsorption for every 10°C increase in temperature. It is seen that the adsorption rate is slow and the equilibrium is not reached even within 180 minutes. Earlier workers (Barton, S. S., *et al.*, 1987) observed that a contact time as high as 72 h is required to reach a steady state for methylene blue adsorption on activated carbons. The kinetics of adsorption of methylene blue into carbon pores

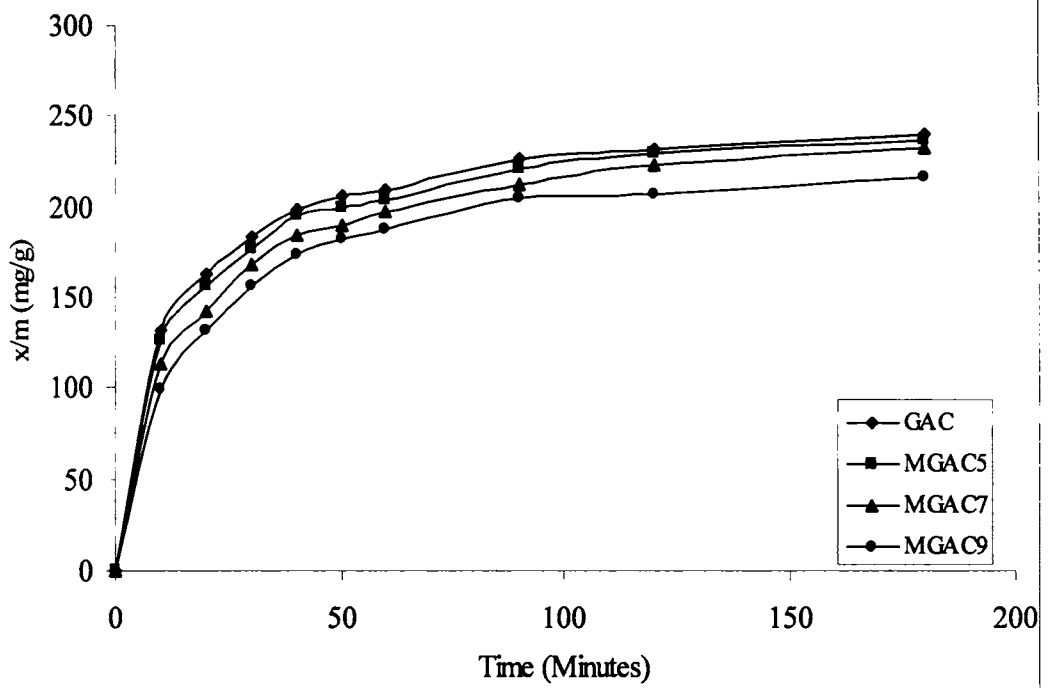


Figure 3.17a Kinetic plots for methylene blue adsorption at 10°C.

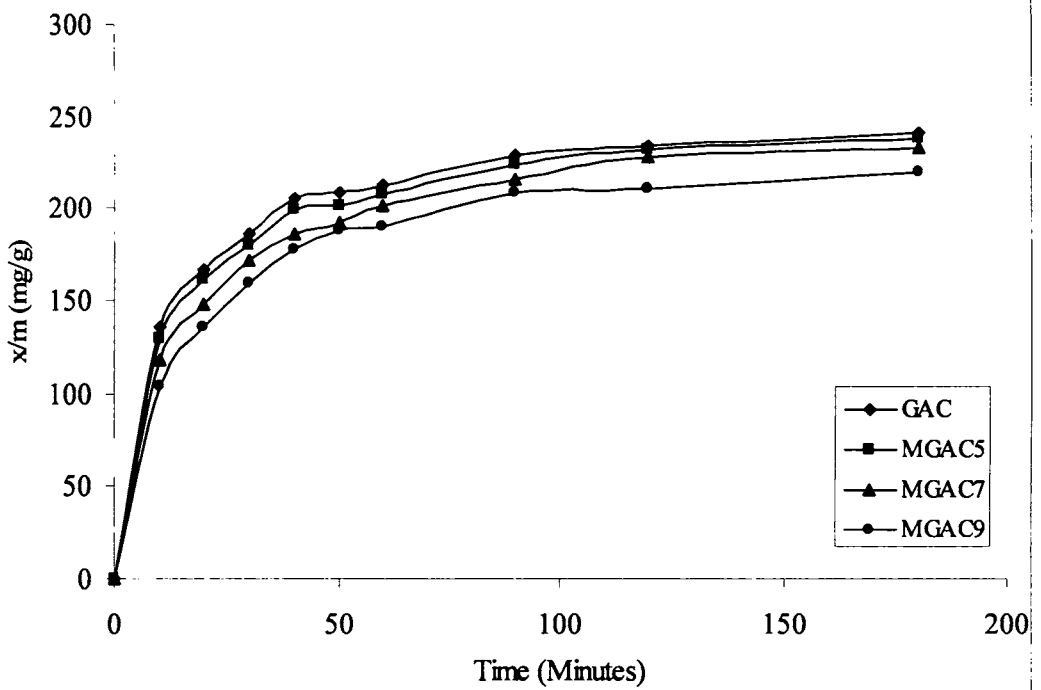


Figure 3.17b Kinetic plots for methylene blue adsorption at 20°C.

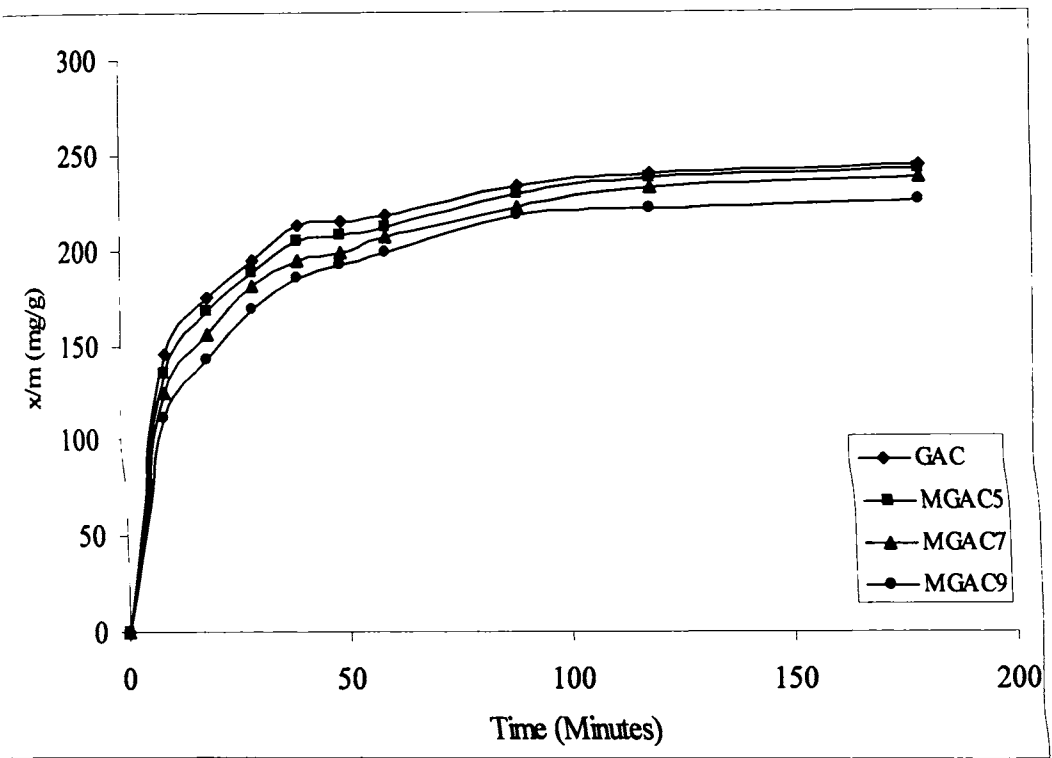


Figure 3.17c Kinetic plots for methylene blue adsorption at 30°C.

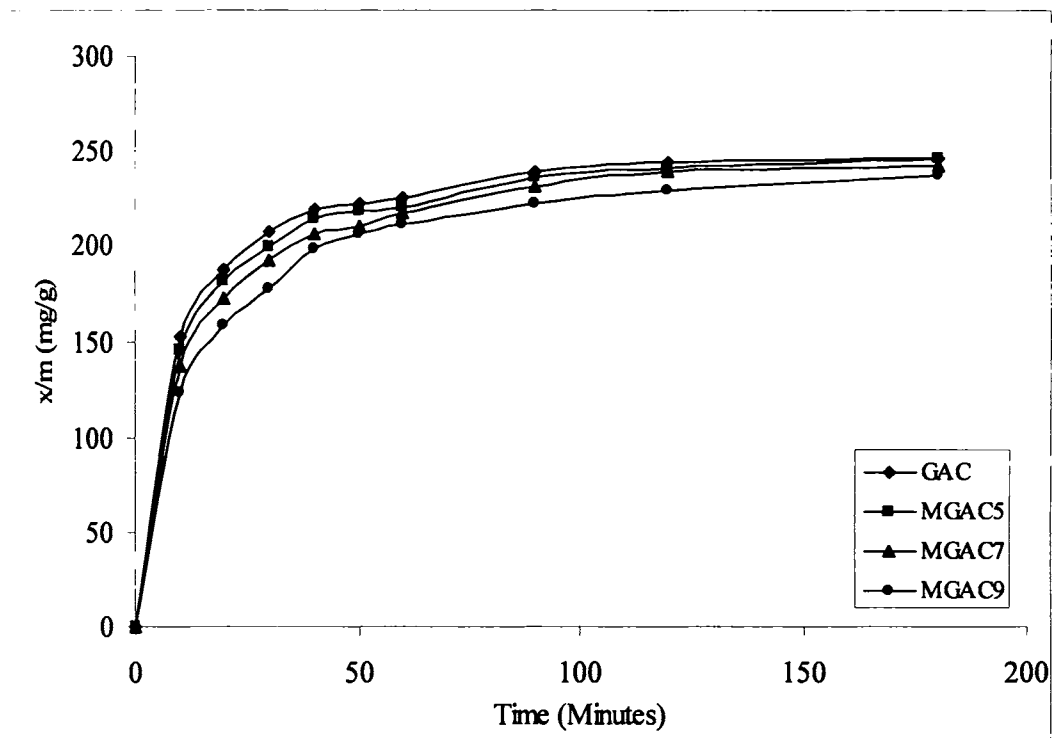


Figure 3.17d Kinetic plots for methylene blue adsorption at 40°C.

from solution is usually slow that the equilibrium state finally achieved is based on a subjective choice involving the decision in the system under consideration (Barton, S. S., 1979). Based on these observations, adsorption of methylene blue on adsorbents was measured for a contact period of 180 minutes in the present study.

#### **Evaluation of Kinetic Rate Constants:**

The kinetic rate constants of methylene blue adsorption on adsorbents GAC, MGAC5, MGAC7 and MGAC9 were determined from the constructed linear Lagergren plots. Plots of  $\log (q_e - q)$  versus time for methylene blue adsorption on each adsorbent at different temperatures are given in Figures 3.18a - d. The rate constant  $k_{ad}$  is calculated from the slope of the linear plots. Values of  $k_{ad}$  for adsorbents at different temperatures are given in Table 3.12. It can be seen that loading of magnetic iron oxide on activated carbon has a decreasing effect on the kinetics of methylene blue adsorption. But the decrease in the magnitude of kinetic rate constants is not significantly high. The kinetic rate constant values increase with rise in temperature. At 20°C, the values of lagergren  $k_{ad}$  ( $\text{min}^{-1}$ ) for GAC, MGAC5, MGAC7 and MGAC9 were calculated to be 1.17, 1.14, 1.12 and 1.08 ( $\times 10^{-2} \text{ min}^{-1}$ ) respectively. At the highest experimental temperature of 40 °C, the  $k_{ad}$  values obtained were 1.49, 1.35, 1.31 and 1.21 ( $\times 10^{-2} \text{ min}^{-1}$ ).

#### **Intraparticle Diffusion Rate Constants for Methylene Blue Adsorption:**

The rate constants for intraparticle diffusion ( $k_{id}$ ) were also determined for methylene blue adsorption. Plots of  $q$  versus  $t^{1/2}$  for methylene blue adsorption on are given in Figures 3.19a - d. Lagergren equation fit very well to the data with optimum spatial spread compared to phenol and nitrophenol adsorption. This can be attributed to slower kinetic rates at which methylene blue is adsorbed on to the activated carbons. There is an initial phase, characterized by the bulk diffusion, followed by a

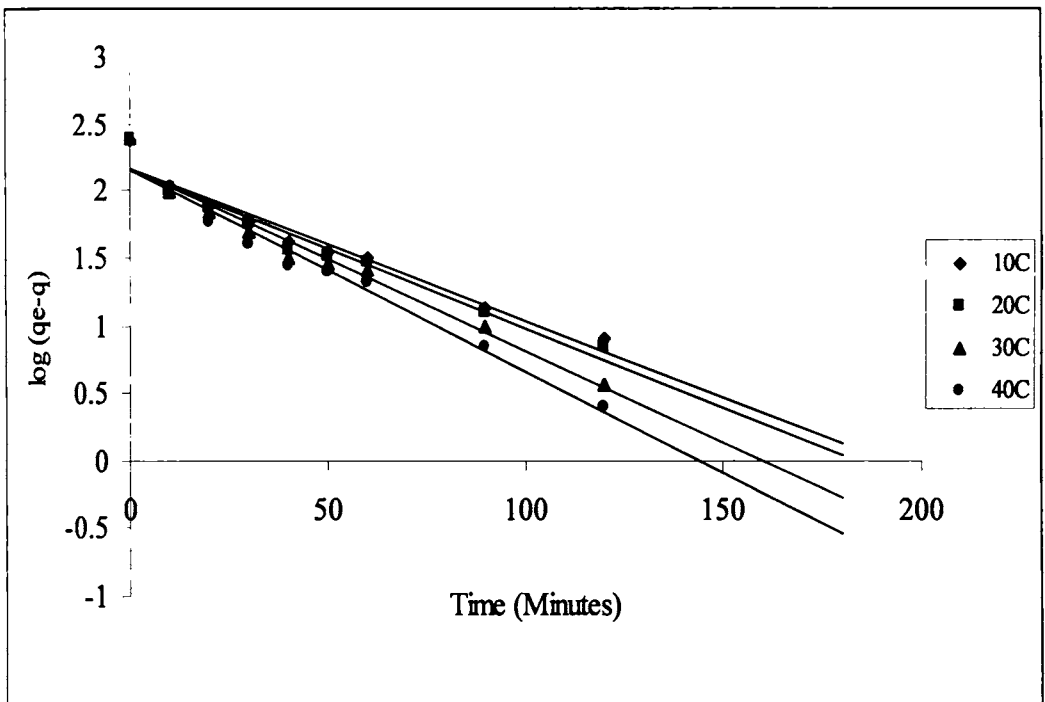


Figure 3.18a Lagergren plots for methylene blue adsorption on GAC.

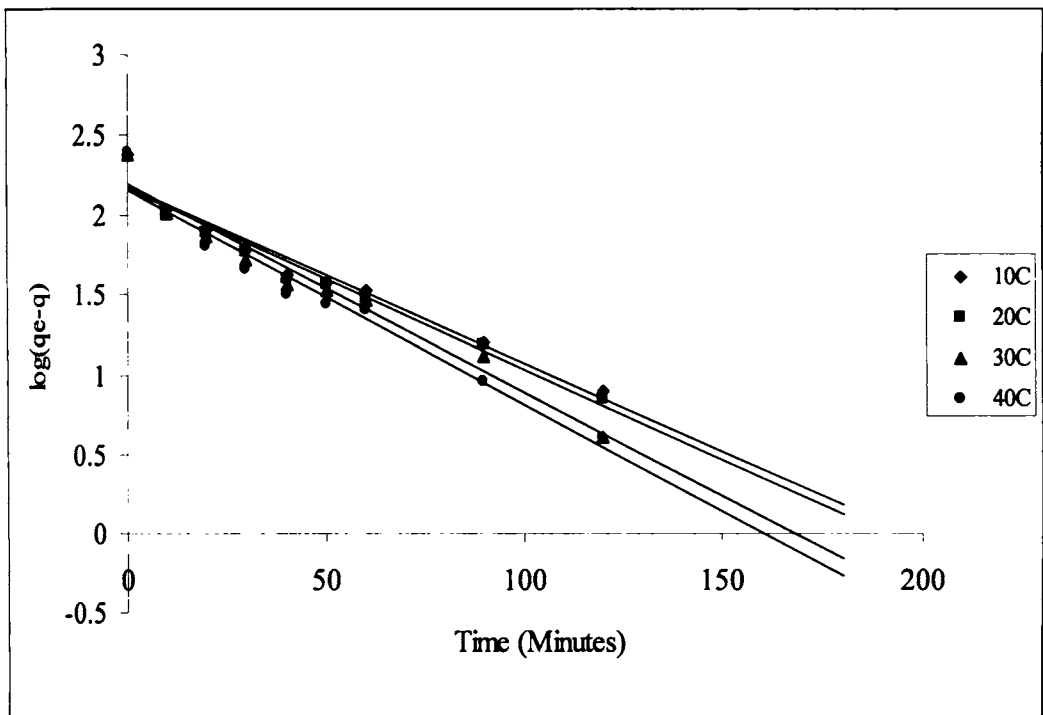


Figure 3.18b Lagergren plot for methylene blue adsorption on MGAC5.

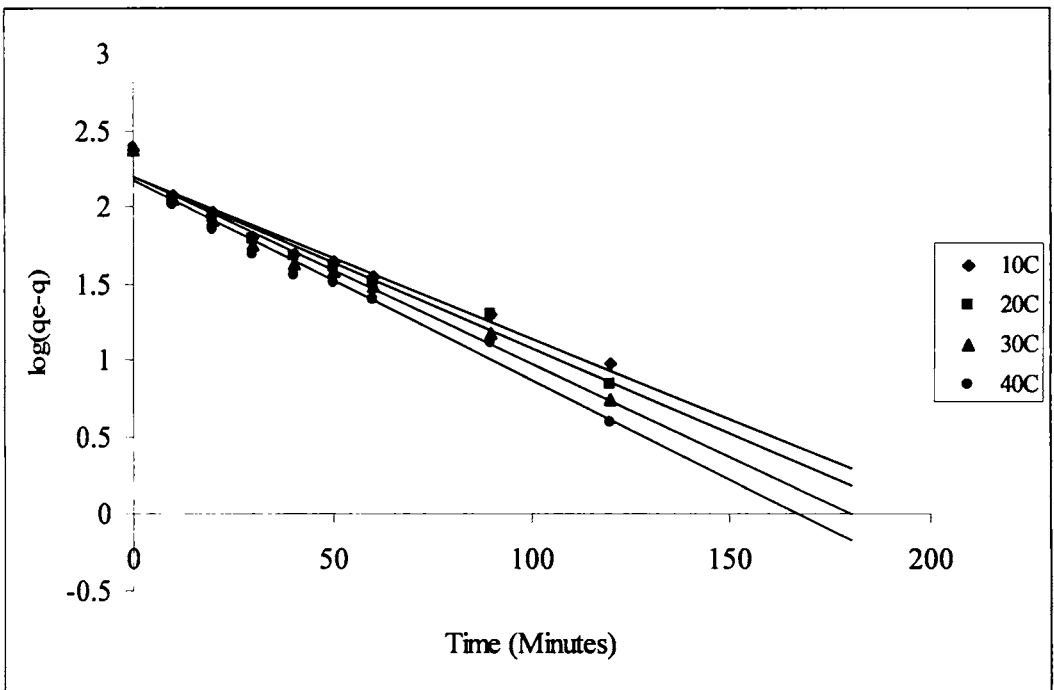


Figure 3.18c Lagergren plot for methylene blue adsorption on MGAC7.

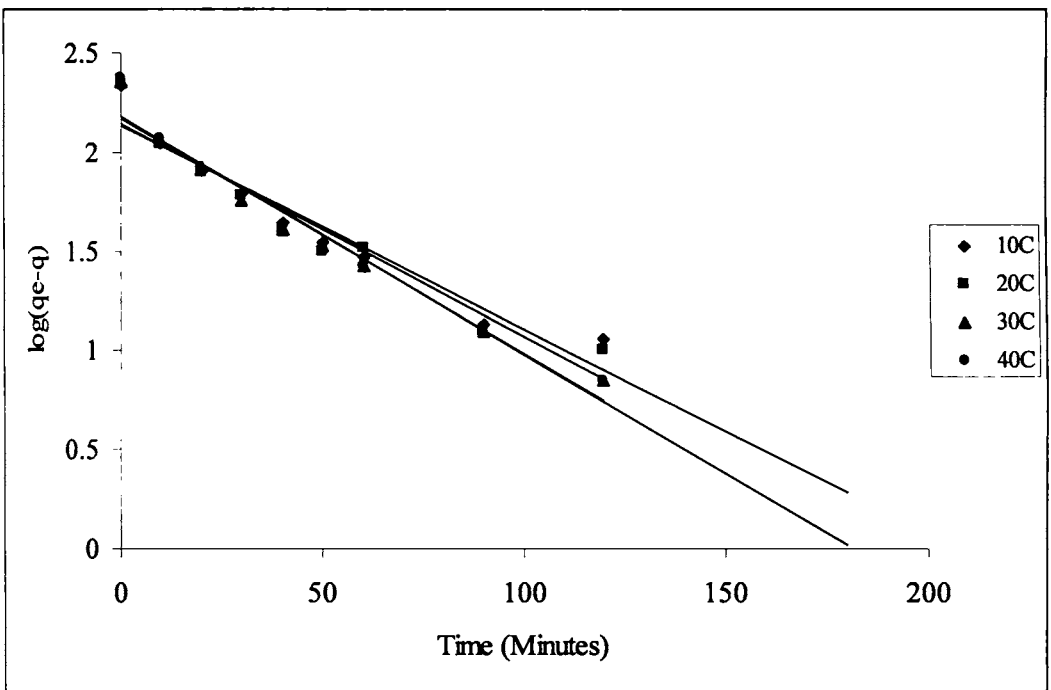


Figure 3.18d Lagergren plot for methylene blue adsorption on MGAC9.

Table 3.12 Kinetic rate constants for Methylene Blue adsorption

Carbon	Temperature, °C	$k_{ad}, \text{min}^{-1}$	$r^2$
GAC	10	$1.13 \times 10^{-2}$	0.953
MGAC5	10	$1.11 \times 10^{-2}$	0.958
MGAC7	10	$1.05 \times 10^{-2}$	0.964
MGAC9	10	$1.03 \times 10^{-2}$	0.934
GAC	20	$1.17 \times 10^{-2}$	0.949
MGAC5	20	$1.14 \times 10^{-2}$	0.959
MGAC7	20	$1.12 \times 10^{-2}$	0.964
MGAC9	20	$1.08 \times 10^{-2}$	0.938
GAC	30	$1.36 \times 10^{-2}$	0.963
MGAC5	30	$1.31 \times 10^{-2}$	0.966
MGAC7	30	$1.22 \times 10^{-2}$	0.971
MGAC9	30	$1.19 \times 10^{-2}$	0.966
GAC	40	$1.49 \times 10^{-2}$	0.964
MGAC5	40	$1.35 \times 10^{-2}$	0.960
MGAC7	40	$1.31 \times 10^{-2}$	0.964
MGAC9	40	$1.21 \times 10^{-2}$	0.961

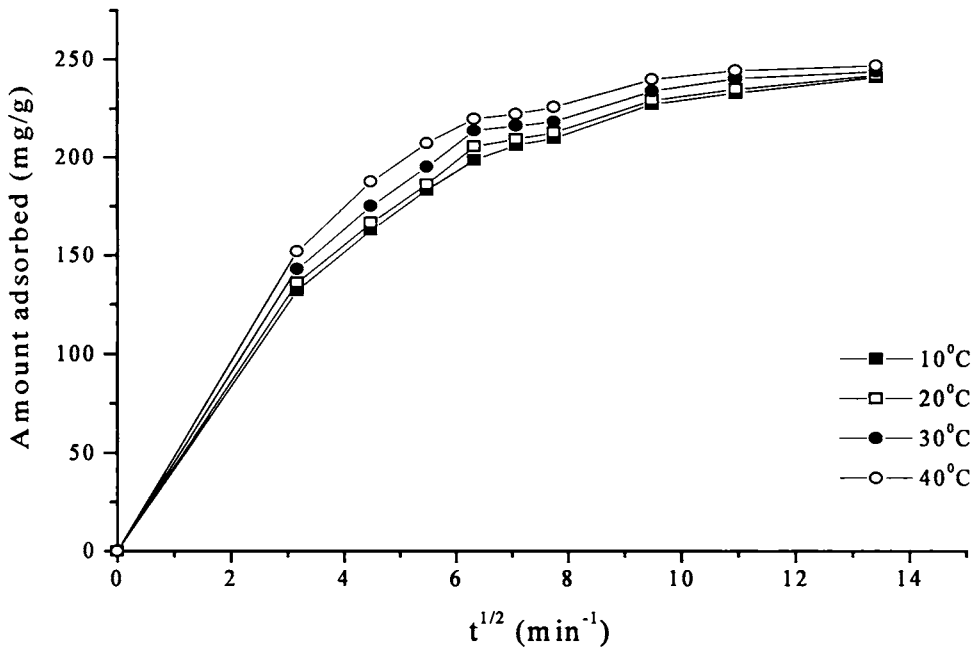


Figure 3.19a Intraparticle diffusion plots for methylene blue adsorption on GAC.

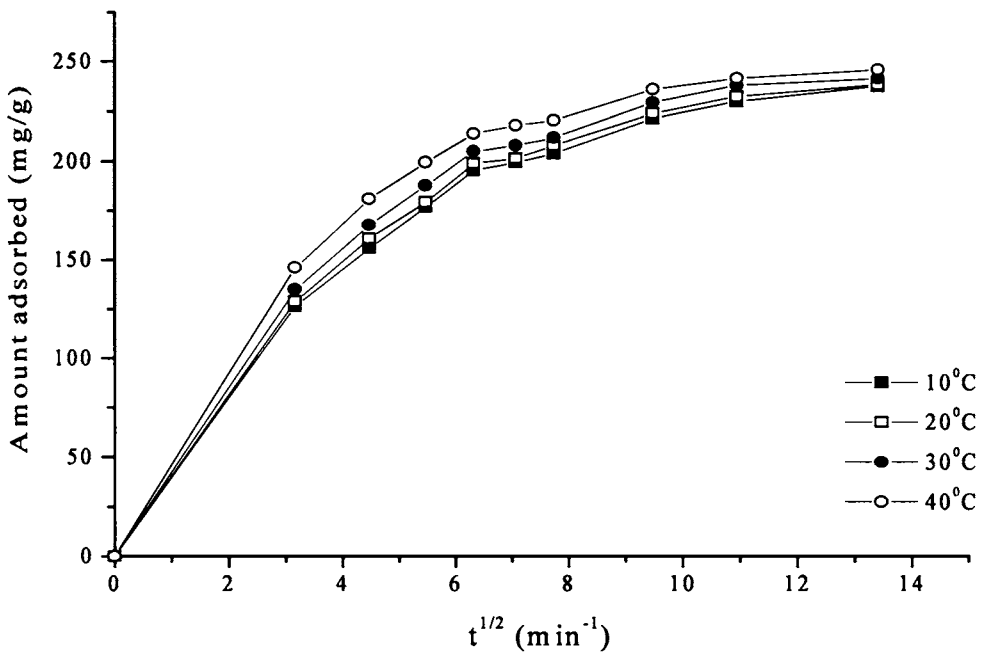


Figure 3.19b Intraparticle diffusion plots for methylene blue adsorption on MGAC5.

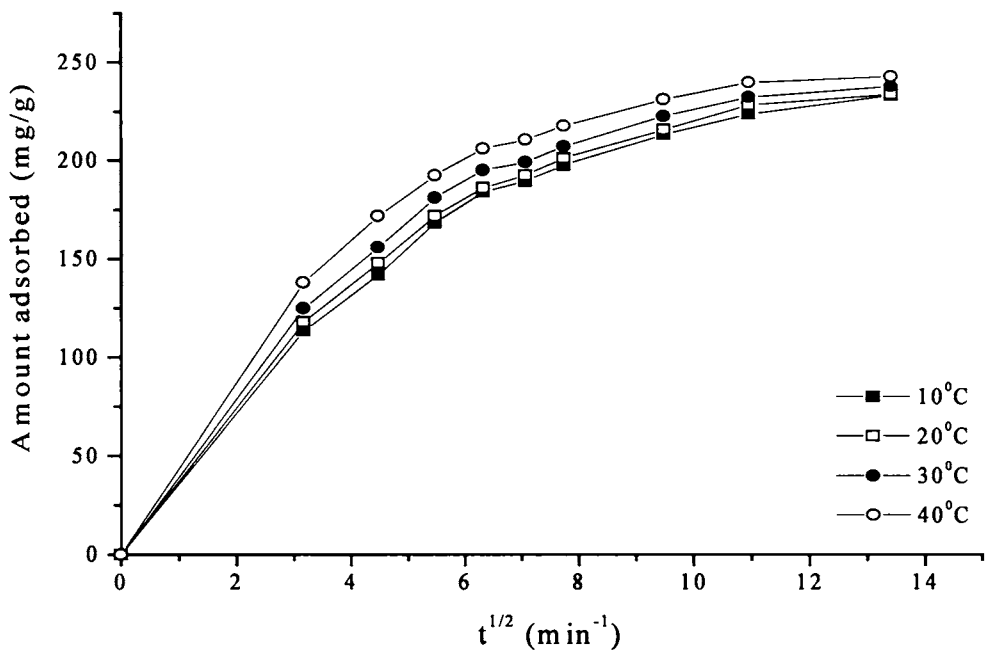


Figure 3.19c Intraparticle diffusion plots for methylene blue adsorption on MGAC7.

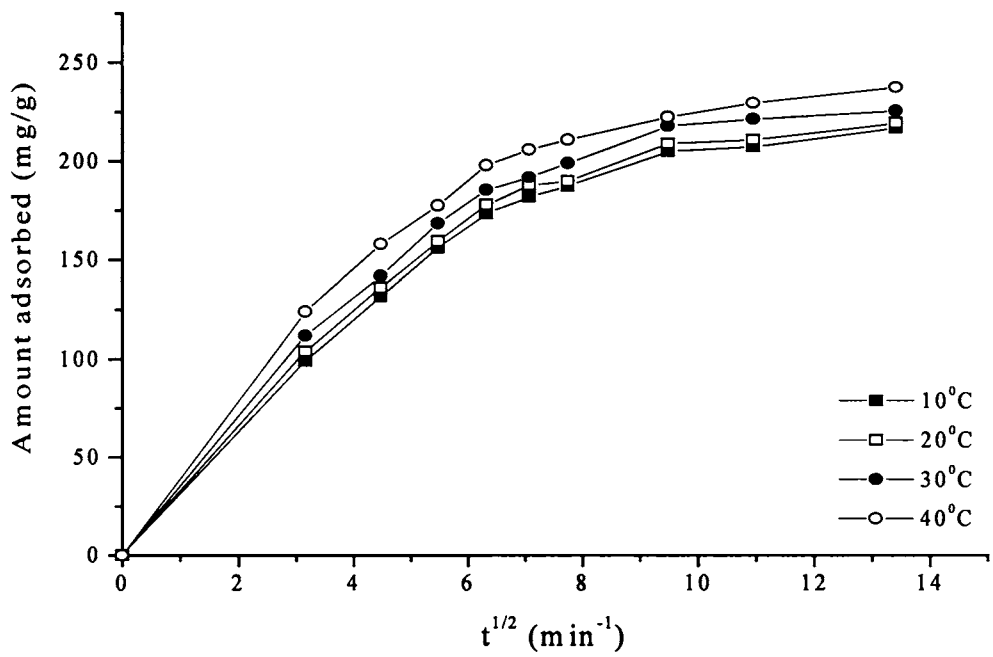


Figure 3.19d Intraparticle diffusion plots for methylene blue adsorption on MGAC9.

C8970

linear portion and then the plateau. The linear portion can be attributed to the intraparticle diffusion and the diffusion rate constants are calculated from the slope of this linear portion. The intraparticle diffusion rate constants at temperatures 10, 20, 30 and 40°C were evaluated and presented in Table 3.13. These values show an increase with temperature.  $k_{id}$  values at 20°C were found to be 19.40, 19.32, 19.28 and 19.20 mg/g/min<sup>1/2</sup> for GAC, MGAC5, MGAC7 and MGAC9 respectively. At a higher experimental temperature of 40°C,  $k_{id}$  values were calculated to be 19.52, 19.45, 19.35 and 19.32 mg/g/min<sup>1/2</sup>.

3.4.4b **Equilibrium Isotherm Studies using Methylene Blue**

The adsorption isotherms of methylene blue on GAC and the three iron oxide impregnated activated carbon composites, MGAC5, MGAC7 and MGAC9 were studied. An adsorbent concentration of 0.05g and an adsorbate concentration of 200 to 500 mg/L were used for the study. Higher concentrations of methylene blue solution were not used due to non-conformity with the Beer-Lambert's law. The contact time for equilibrium studies was fixed at 180 minutes since more than 95% of the adsorption is completed within this period.

The isotherm plots of methylene blue adsorption on the control carbon GAC, and the composites MGAC5, MGAC7 and MGAC9 are given in Figures 3.20a - d. The isotherms plots reveal that the plots are of type I, with adsorption edge parallel to the X-axis for all carbons irrespective of temperature and time. The amount of methylene blue adsorbed per gram of adsorbent decreases with iron loading as observed for MGAC5, MGAC7 and MGAC9 samples. This can be attributed to the reduction in the surface area and pore volume of the composite samples due to iron oxide impregnation. Higher the iron oxide loading, greater the reduction in the amount of methylene blue adsorbed. The graphs show that the amount of



Table 3.13 Intraparticle diffusion rate constants for Methylene Blue adsorption

Carbon	Temperature, °C	$K_{id}$ mg/g/min <sup>1/2</sup>
GAC	10	19.34
MGAC5	10	19.28
MGAC7	10	19.21
MGAC9	10	19.18
GAC	20	19.40
MGAC5	20	19.32
MGAC7	20	19.28
MGAC9	20	19.20
GAC	30	19.45
MGAC5	30	19.37
MGAC7	30	19.31
MGAC9	30	19.25
GAC	40	19.52
MGAC5	40	19.45
MGAC7	40	19.35
MGAC9	40	19.32

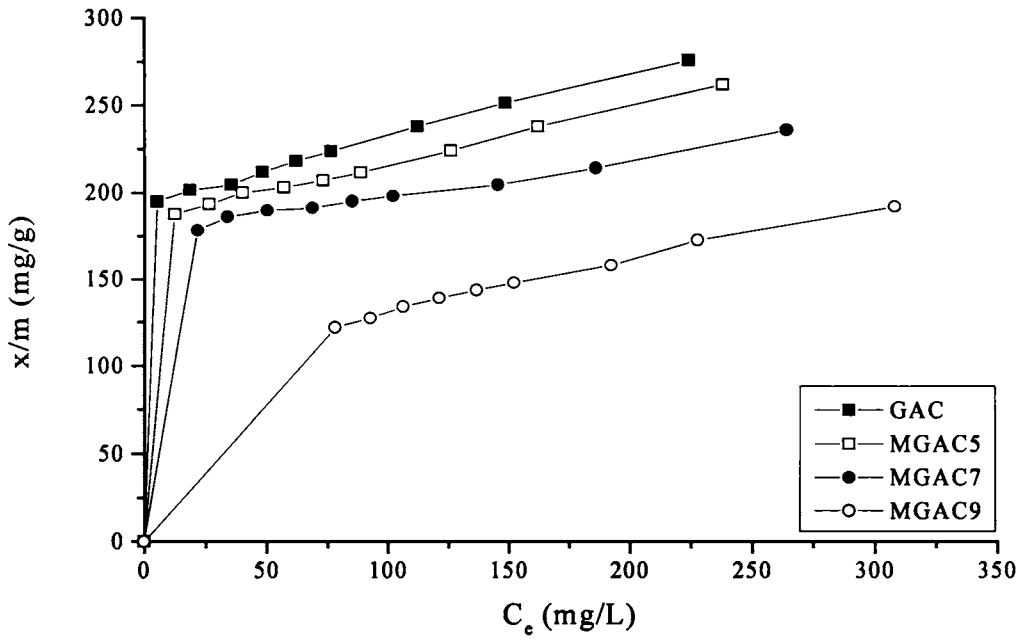


Figure 3.20a Adsorption isotherms of methylene blue at 10<sup>0</sup>C.

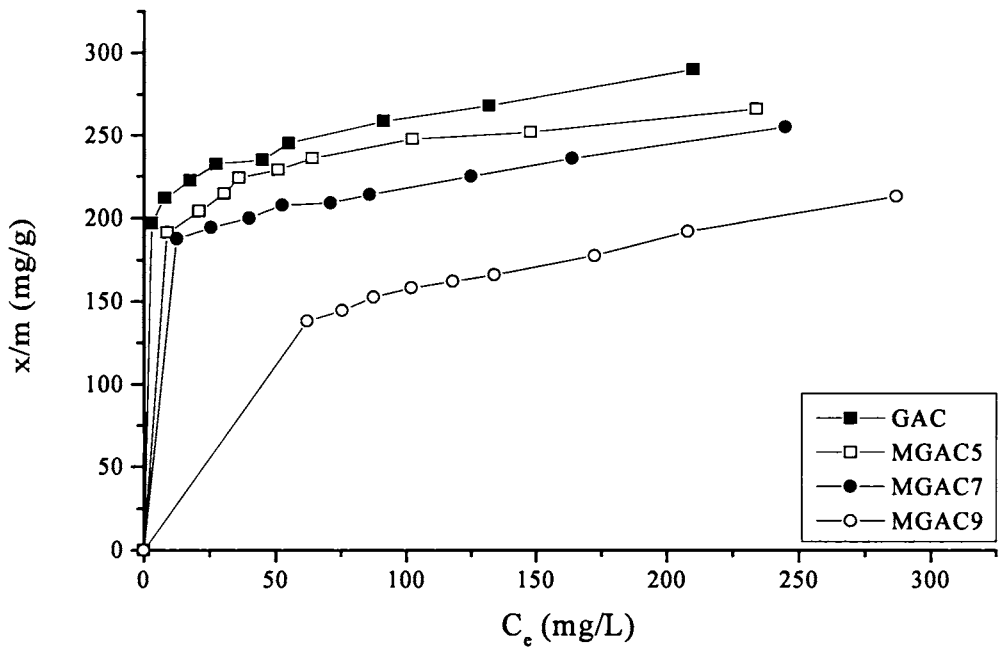


Figure 3.20b Adsorption isotherms of methylene blue at 20<sup>0</sup>C.

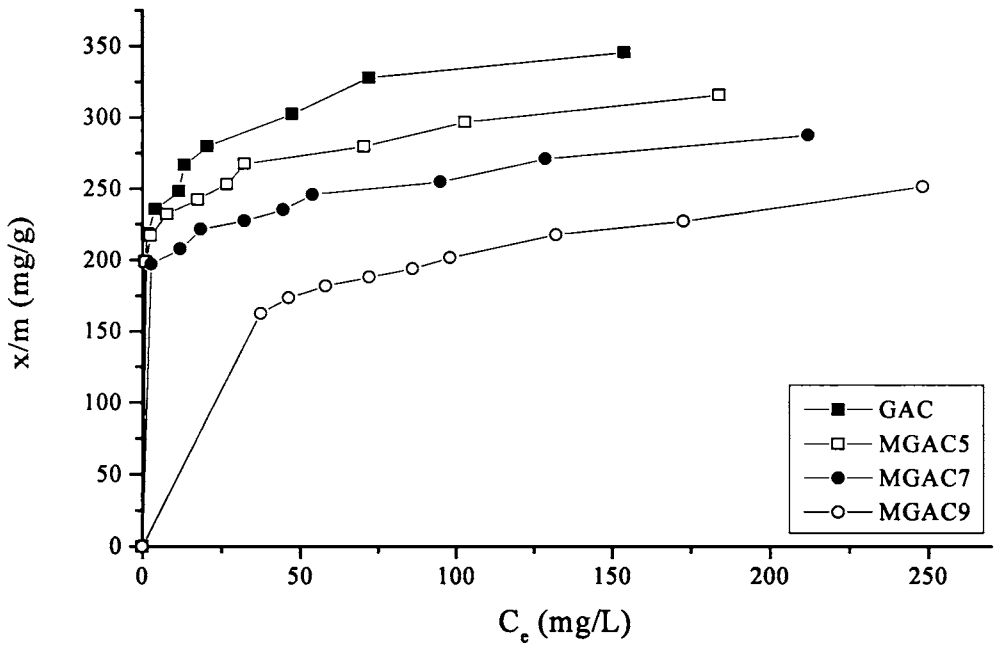


Figure 3.20c Adsorption isotherms of methylene blue at 30°C.

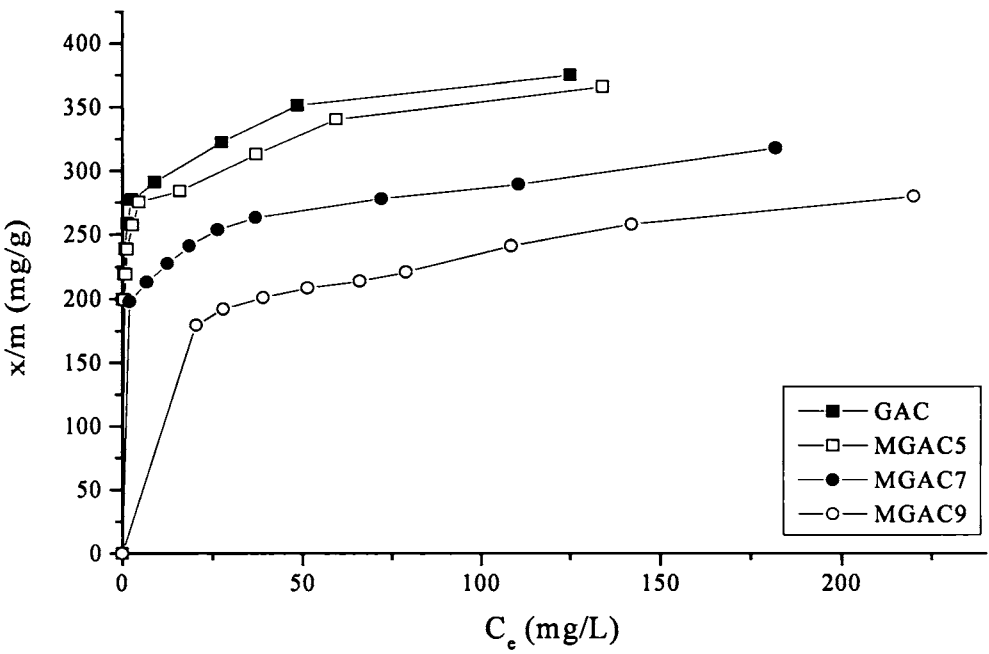


Figure 3.20d Adsorption isotherms of methylene blue at 40°C.

blue adsorbed per gram of adsorbent increases with temperature. This is in contrary to the general concept of an exothermic process encountered in physical adsorption processes where adsorption is energetically favoured at lower temperatures. This phenomenon has been reported by other workers (Barton, S. S., 1987; Kipling, J. J. & Wilson, R. B., 1960) who described this effect to the fading of methylene blue solutions at elevated temperatures. Other thermodynamic explanations are also given by these authors and will be dealt with in a later section on thermodynamic parameters.

#### **Evaluation of Adsorption Isotherms Using Langmuir Equation:**

The linear form of the Langmuir equation was applied to evaluate the adsorption characteristics of methylene blue adsorption on the equilibrium adsorption data. The plots of  $C_e/X$  versus  $C_e$  at four different temperatures are given in Figures 3.21a - d. The linearity of plots suggests that methylene blue adsorption agrees with the Langmuir model. The monolayer capacity,  $X_m$  and the Langmuir constant,  $b$ , were calculated from the slope and intercept of these plots. The values of  $X_m$  and  $b$  are given in Table 3.14.

It is seen that the monolayer capacity,  $X_m$ , increases with temperature for all the samples. But the increase is not proportional to the temperature rise. Compared to the change in monolayer capacity at lower temperatures, the variation is quite large with rise in temperature. This increased apparent adsorption at elevated temperatures can be attributed to the fading of dye at higher temperatures. More over, increased adsorption at higher temperatures indicates an endothermic reaction mechanism by which methylene blue is adsorbed on to activated carbon (Kannan, N. & Sundaram, M. M., 2001). The same phenomenon was observed for all the samples suggesting that the presence of iron oxides in the surface and pores did not alter the mechanism

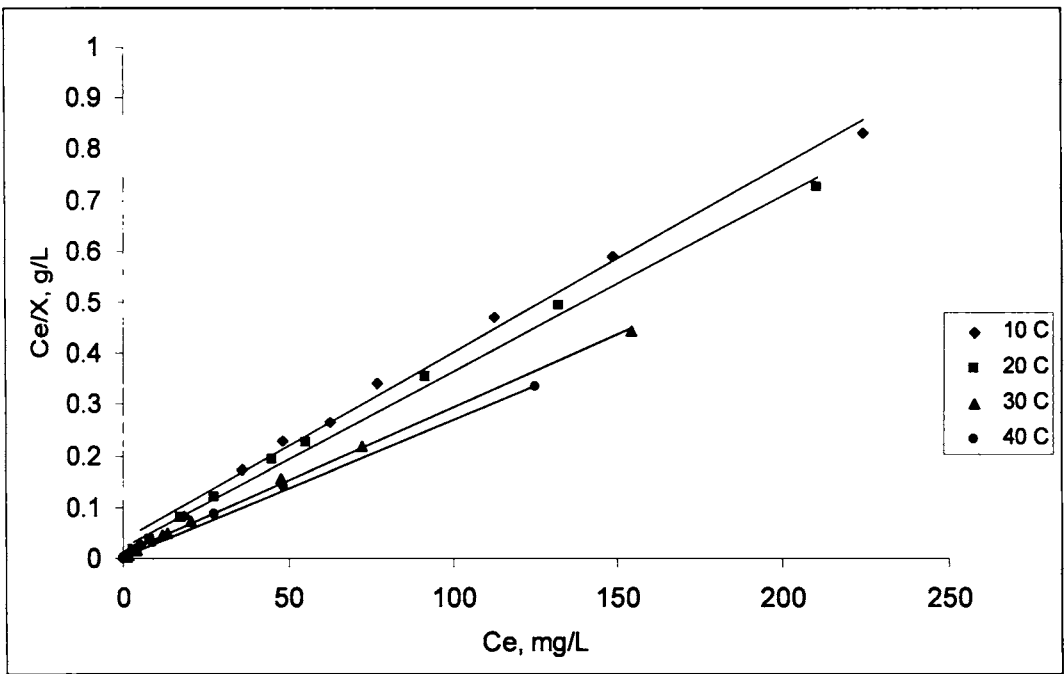


Figure 3.21a Langmuir plots for methylene blue adsorption on GAC.

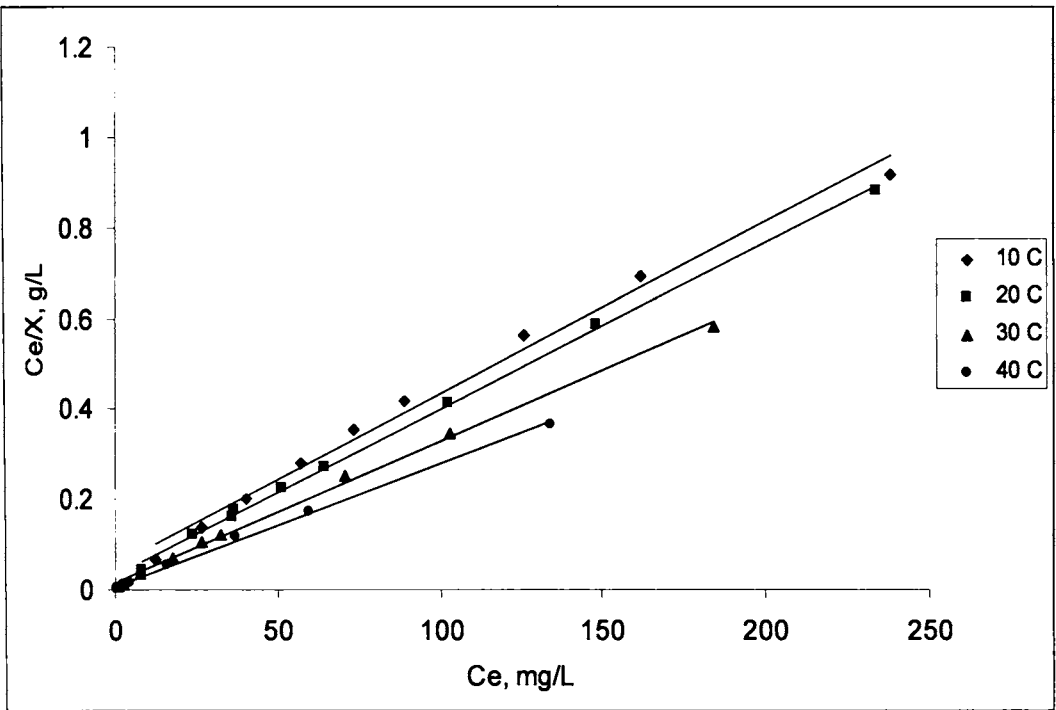


Figure 3.21b Langmuir plots for methylene blue adsorption on MGAC5.

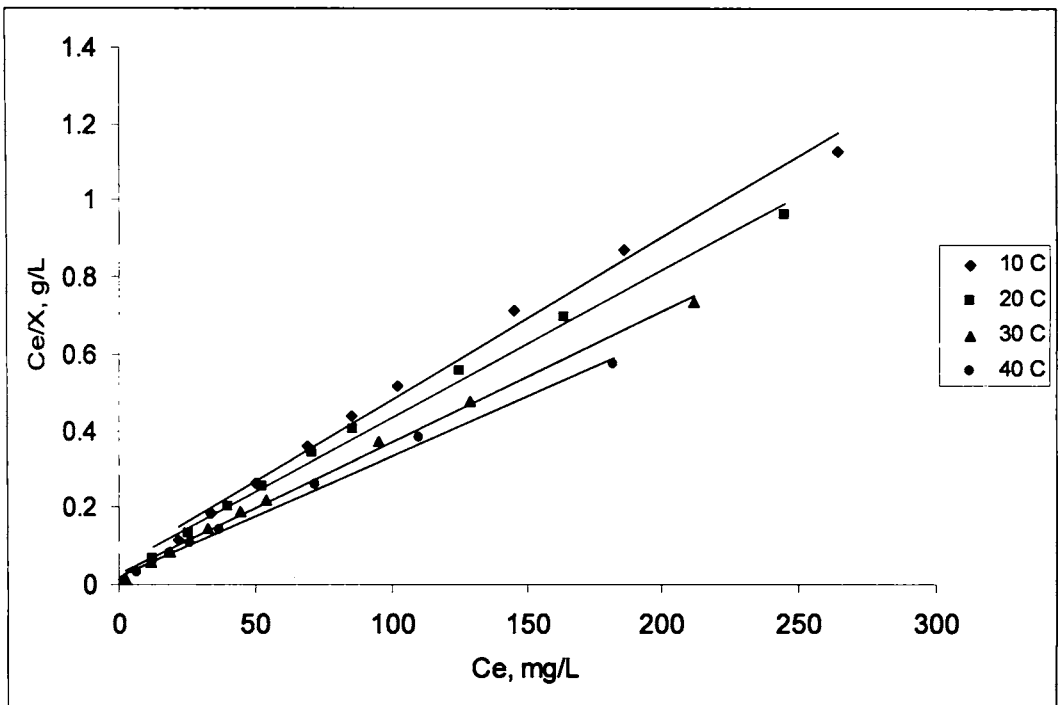


Figure 3.21c Langmuir plots for methylene blue adsorption on MGAC7.

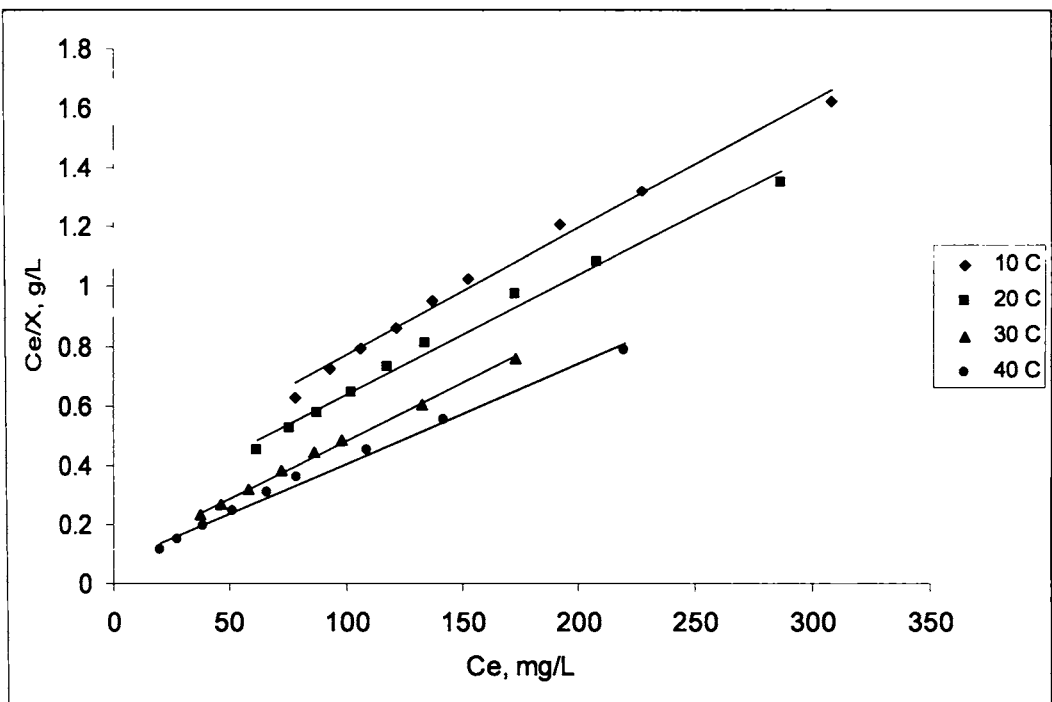


Figure 3.21d Langmuir plots for methylene blue adsorption on MGAC9.

Table 3.14 Langmuir constants for the adsorption of Methylene blue.

Carbon	Temperature, °C	Langmuir constants		$r^2$
		$b$	$X_m$	
GAC	10	0.1022	270.27	0.9933
GAC	20	0.1472	294.12	0.9960
GAC	30	0.2959	344.83	0.9979
GAC	40	0.7027	384.62	0.9985
MGAC5	10	0.0708	263.16	0.9905
MGAC5	20	0.1114	270.27	0.9985
MGAC5	30	0.2302	312.50	0.9972
MGAC5	40	0.4500	370.37	0.9974
MGAC7	10	0.0704	238.10	0.9922
MGAC7	20	0.0801	256.41	0.9943
MGAC7	30	0.1339	294.12	0.9964
MGAC7	40	0.1713	322.58	0.9961
MGAC9	10	0.0113	232.56	0.9914
MGAC9	20	0.0169	250.00	0.9900
MGAC9	30	0.0412	256.41	0.9975
MGAC9	40	0.0491	294.12	0.9932

by which the dye is adsorbed onto the activated carbon. The monolayer capacity for methylene blue dye adsorption reduces with iron oxide loading. The reduction in monolayer capacity can be attributed to reduction in surface area and pore size of iron oxide loaded samples. The percentage reduction in monolayer capacity of carbon composite samples compared to the control carbon at different temperatures is given in Figure 3.22.

The Langmuir isotherm plots for GAC, MGAC5, MGAC7 and MGAC9 are found to be smooth straight line graphs with a common composite intercept near to origin. At higher concentrations spread of the data varies widely. This may be treated as due to the preferential filling of the mesopores by the dye molecules rather than its limited accessibility to the micropores, being the molecule is larger in size or the micropores are not much exposed except in GAC. At higher equilibrium concentrations mass transfer occurs to mesopores by diffusion. At 20°C, GAC shows a monolayer capacity of 294.12 mg/g where as the MGAC5, MGAC7 and MGAC9 have 270.27, 256.41 and 250.0 mg/g respectively. At 40°C,  $X_m$  has highest value of 384.62 (GAC), 370.37 (MGAC5), 322.58 (MGAC7) and 294.12mg/g (MGAC9).

The monolayer capacity for methylene blue adsorption on all the samples is lower than that for phenol and p-nitrophenol adsorption. This can be explained by considering the size of these molecules. When a large molecule, like methylene blue, and smaller, or solvent molecules, like water, are adsorbed on a porous solid with a distribution of pore sizes the effective adsorbent surface available to the larger molecule is limited by pore screening or molecular sieving (Graham, D., 1955; Dubinin, M. M. & Zaverina, E. D., 1936). The methylene blue dye molecule has a minimum diameter of about 0.8 nm (Kipling, J. J. & Wilson, R. B., 1960) and the limiting diameter of pores that will admit the molecule is estimated to be about 1.30

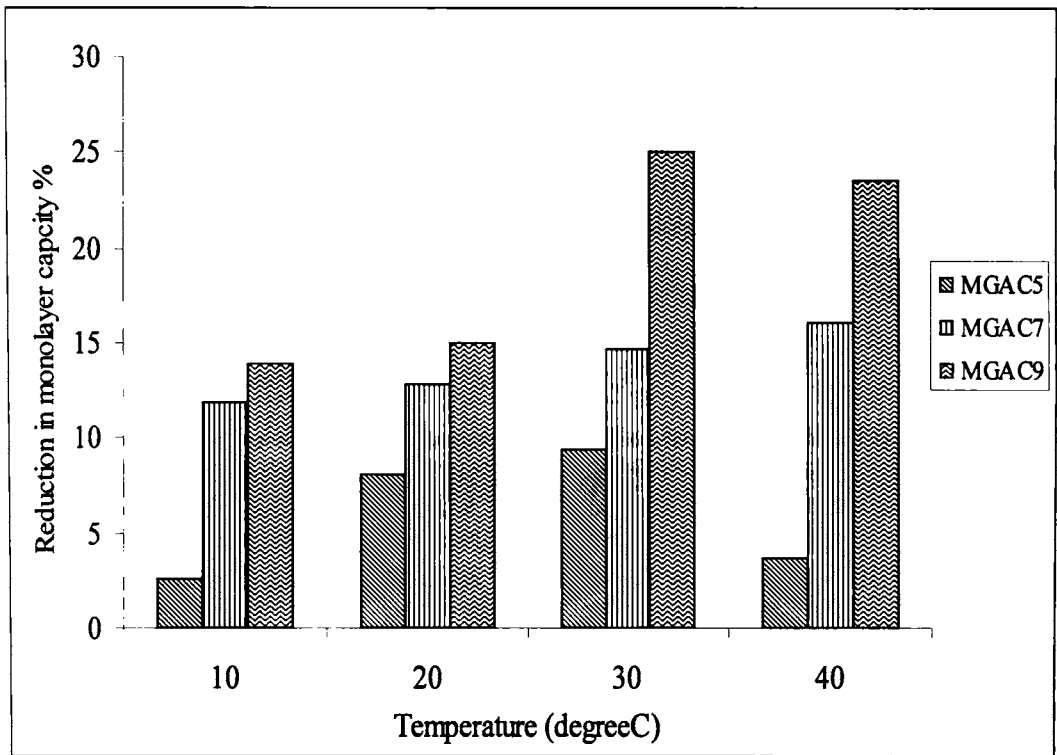


Figure 3.22 Reduction in monolayer capacity for methylene blue adsorption for composite samples compared to the control carbon at different temperatures.

nm (Graham, D., 1955). The cross sectional area occupied by a molecule of methylene blue has been reported to be  $1.2 \text{ nm}^2$  where as the value for *p*-nitrophenol is as low as  $0.525 \text{ nm}^2$  (GÜZEL, F. & UZUN, I., 2002). Hence the micropores in the activated carbon structure are not available as adsorption sites for methylene blue molecules due to their large size. This explains the reduction in the monolayer capacity of methylene blue adsorption on activated carbons compared to phenol and *p*-nitrophenol.

#### **Freundlich Model for Methylene Blue adsorption:**

The isotherm data of methylene blue adsorption was fitted to a linear form of the Freundlich equation and linearity of these plots suggest that the system agrees with the multilayer adsorption model. The plots of  $\log x/m$  versus  $\log C_e$  at different temperatures for adsorption on the control carbon and the composite samples are given in Figures 3.23a - d. The plots were critically analysed by applying least square method. Freundlich constants  $K$  and  $n$  are given in Table 3.15 and is seen that the values increases with temperature. And the  $K$  values decreases with % of surface modification. This means a higher iron oxide loading of activated carbon decreased the  $K$  for methylene blue adsorption.

Freundlich plots for GAC, MGAC5, MGAC7 and MGAC9 are characterized by straight lines with varying slopes and intercepts. But their closeness towards the Y-axis with more positive intercepts is lost on surface modification by impregnating  $\text{Fe}_2\text{O}_3$ . Freundlich isotherm constant  $K$  indicates adsorbent capacity and  $n$  treated as the intensity of adsorption. Evaluated constants show that  $n$  values for GAC, MGAC5, MGAC7 and MGAC9 were found to be 11.27, 9.43, 9.39 and 3.63 respectively. Where as the adsorbent capacity correspondingly vary as 173.70,

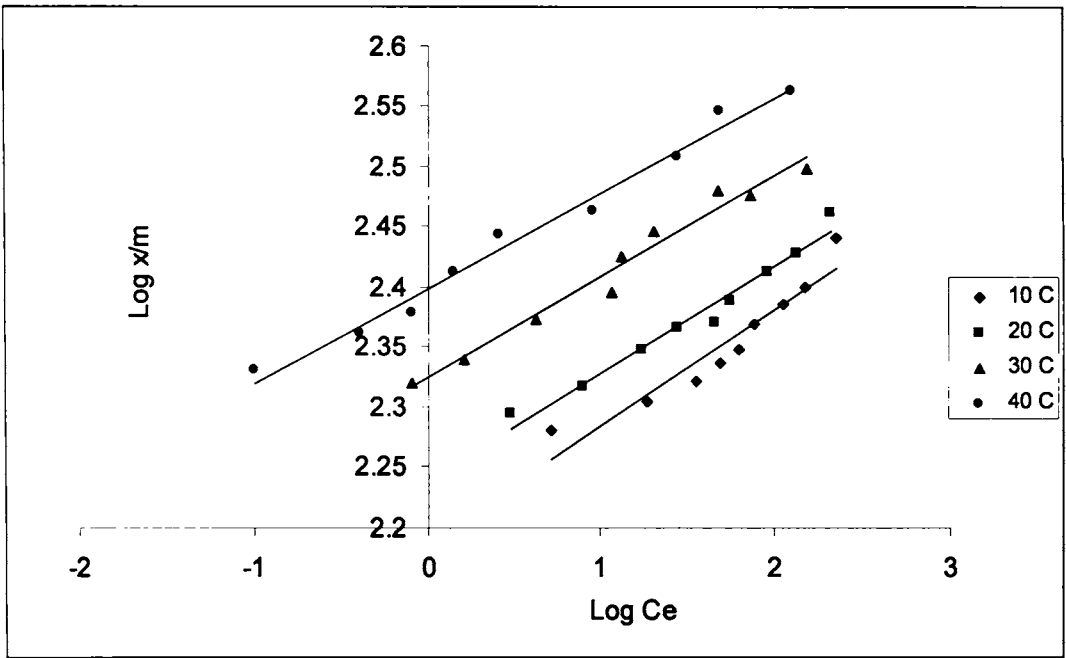


Figure 3.23a Freundlich plots for the adsorption of methylene blue on GAC.

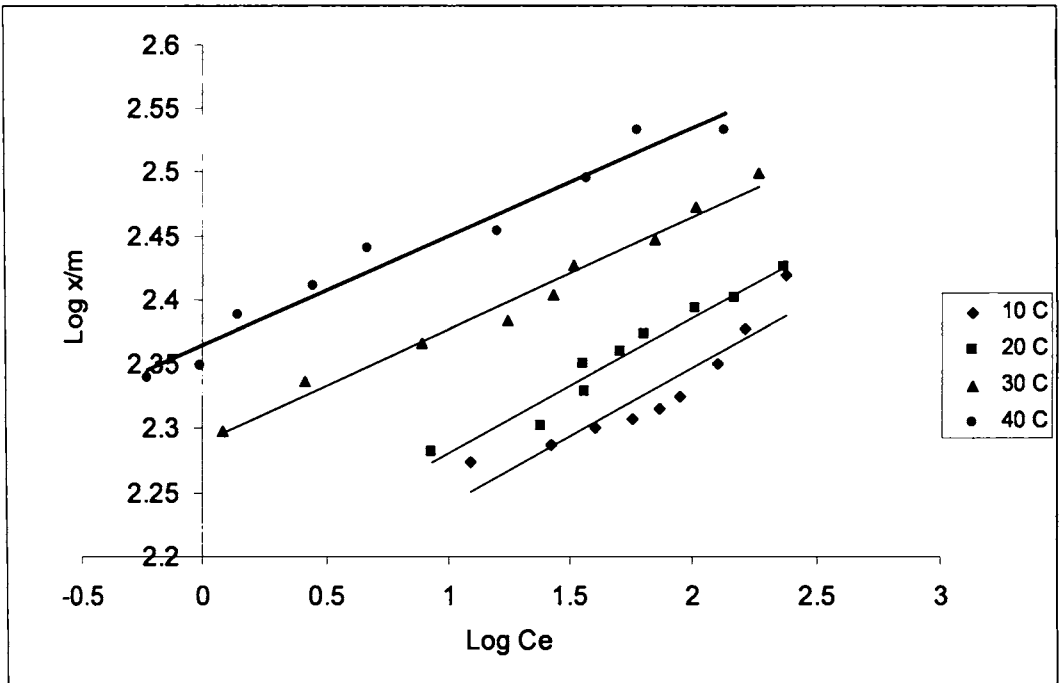


Figure 3.23b Freundlich plots for the adsorption of methylene blue on MGAC5.

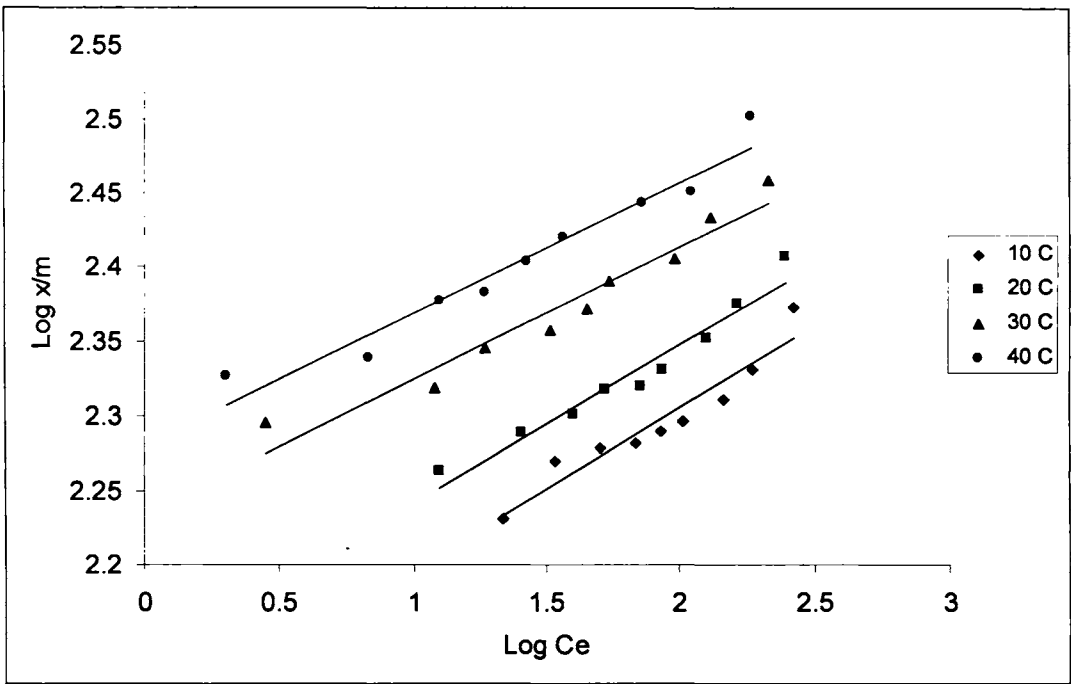


Figure 3.23c Freundlich plots for the adsorption of methylene blue on MGAC7.

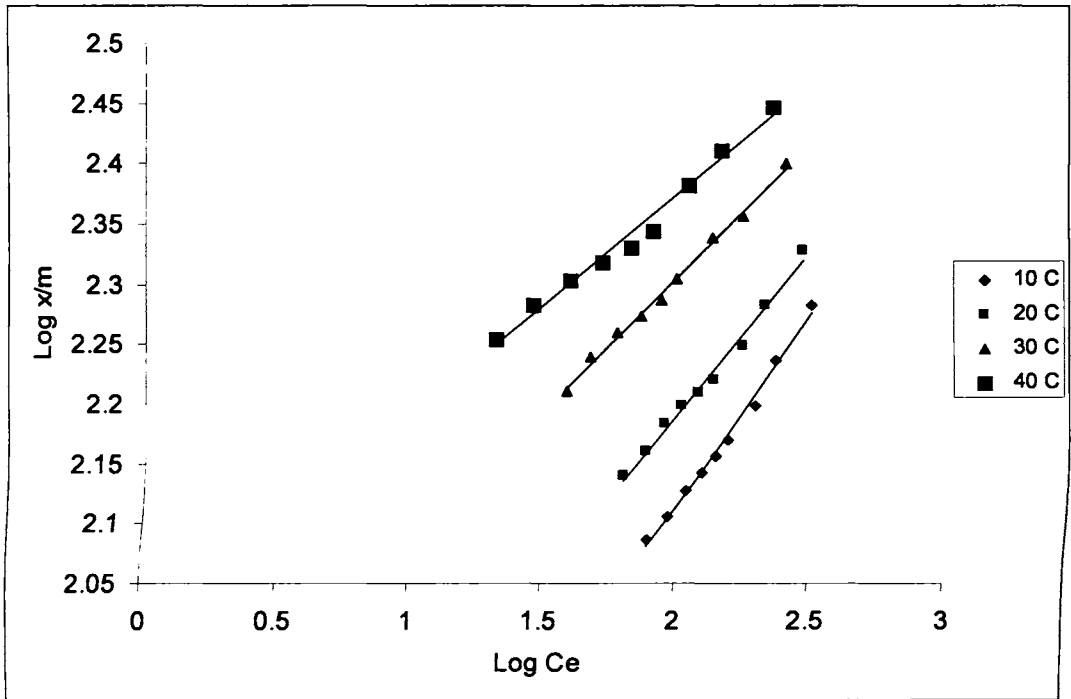


Figure 3.23d Freundlich plots for the adsorption of methylene blue on MGAC9.

Table 3.15 Freundlich constants for the adsorption of Methylene blue

Carbon	Temperature, °C	Freundlich constants		$r^2$
		$K$ , mg/g	$n$	
GAC	10	153.99	10.32	0.9079
GAC	20	173.70	11.27	0.9688
GAC	30	211.05	11.92	0.9725
GAC	40	250.84	12.64	0.9860
MGAC5	10	136.27	9.38	0.8634
MGAC5	20	149.52	9.43	0.9564
MGAC5	30	194.72	11.34	0.9793
MGAC5	40	231.90	11.79	0.9680
MGAC7	10	122.38	9.18	0.9150
MGAC7	20	136.58	9.39	0.9492
MGAC7	30	171.71	11.15	0.9445
MGAC7	40	190.77	11.25	0.9488
MGAC9	10	28.98	3.06	0.9921
MGAC9	20	43.96	3.63	0.9891
MGAC9	30	72.73	4.48	0.9949
MGAC9	40	101.95	5.43	0.9819

149.52, 136.58 and 43.96 mg/g. However, at 40°C, all the adsorbents show higher values for  $K$  and  $n$ . The modified carbons exhibit lower dye uptake.

#### 3.4.4c Evaluation of Thermodynamic Parameters

The influence of temperature on the adsorption of methylene blue on the control carbon, GAC and the composite samples, MGAC5, MGAC7 and MGAC9 was studied. The methylene blue concentrations in the solution used were 200, 240, 280, 350 and 500 mg/L and the temperature was varied from 10°C to 40°C in 10°C steps. The thermodynamic quantities, change in enthalpy ( $\Delta H$ ), change in entropy ( $\Delta S$ ), and change in free energy ( $\Delta G$ ), of methylene blue adsorption on adsorbents were calculated from the distribution coefficient ( $K_D$ ) using the equations 3.3 and 3.4.

The values of  $\Delta H$  and  $\Delta S$  were determined from the slopes and intercepts of the linear variation of  $\ln K_D$  with the reciprocal of temperature. The plots of  $\ln K_D$  with the reciprocal of temperature ( $T$ ) for methylene blue adsorption on control carbon and the composite samples are given in Figures 3.24a - d. The values for free energy change ( $\Delta G$ ) are calculated from equation 3.4. The thermodynamic parameters for methylene blue adsorption are given in Table 3.16.

The positive values of  $\Delta H$  shows that the adsorption of methylene blue on GAC and the iron oxide loaded carbons are an endothermic process. This is contrary to the usual exothermicity encountered in physical adsorption processes. Similar results were obtained by other workers for the adsorption of both anionic and cationic dyes, from aqueous solution, onto solid adsorbents (Allingham, M. M., *et al.*, 1958; Giles, C. H., *et al.*, 1961). The endothermic nature of the adsorption process is explained by the necessity of an endothermic dissociation of dye dimers, micelles, or aggregates prior to the exothermic adsorption of the dye monomer. In support of this mechanism these authors point out that adsorption from the non-associating solvent,

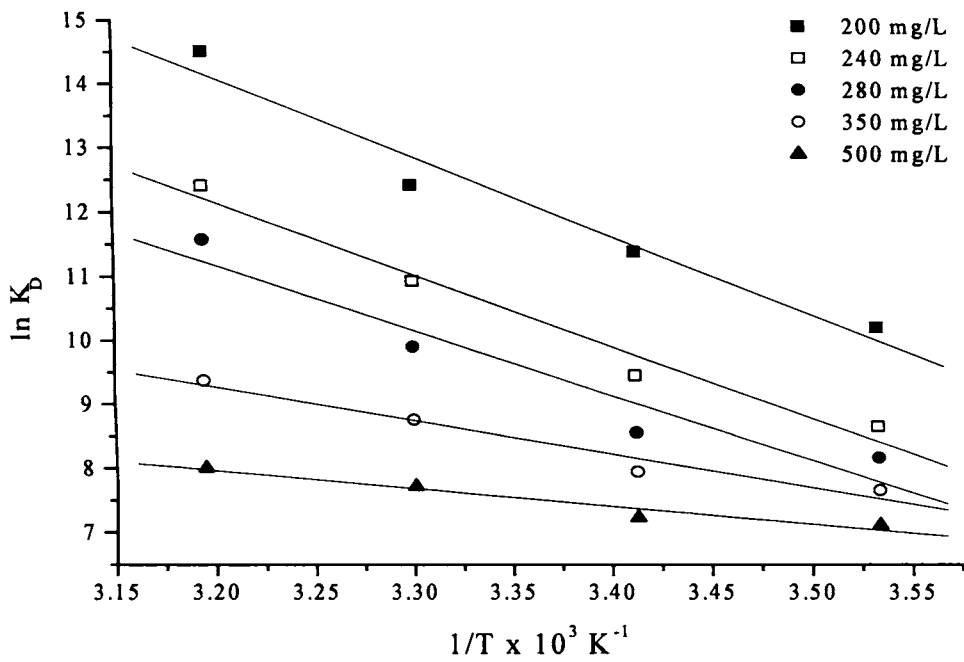


Figure 3.24a Plots of  $\ln K_D$  vs  $1/T$  for methylene blue adsorption on GAC.

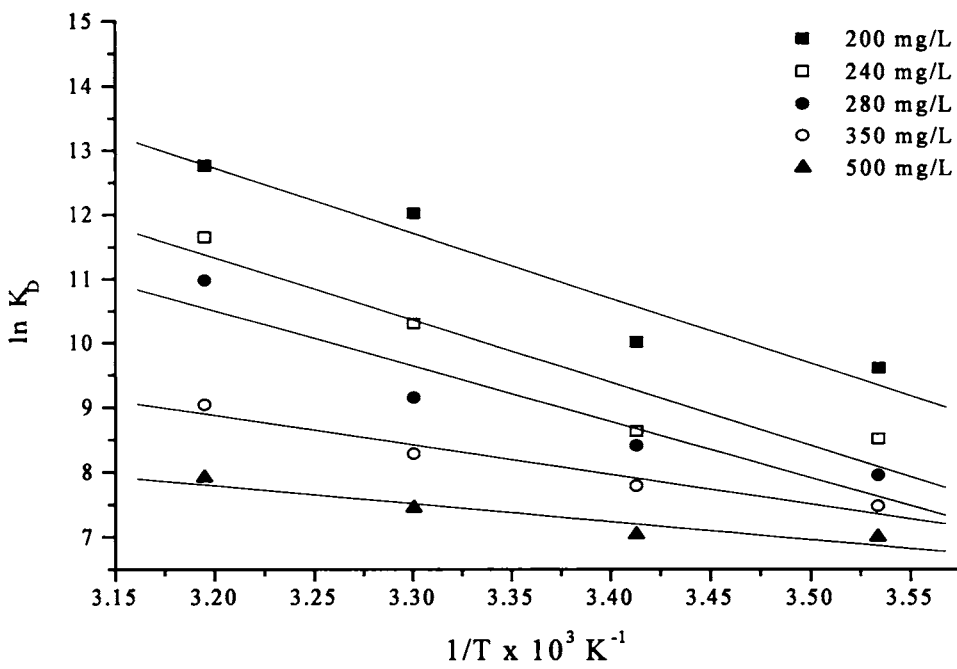


Figure 3.24b Plots of  $\ln K_D$  vs  $1/T$  for methylene blue adsorption on MGAC5.

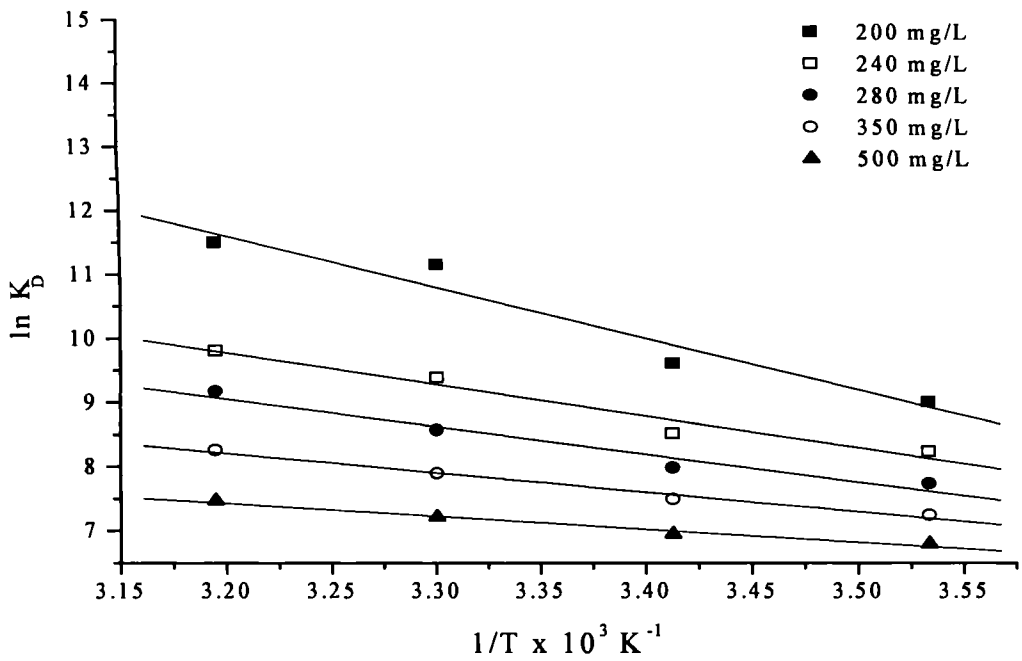


Figure 3.24c Plots of  $\ln K_D$  vs  $1/T$  for methylene blue adsorption on MGAC7.

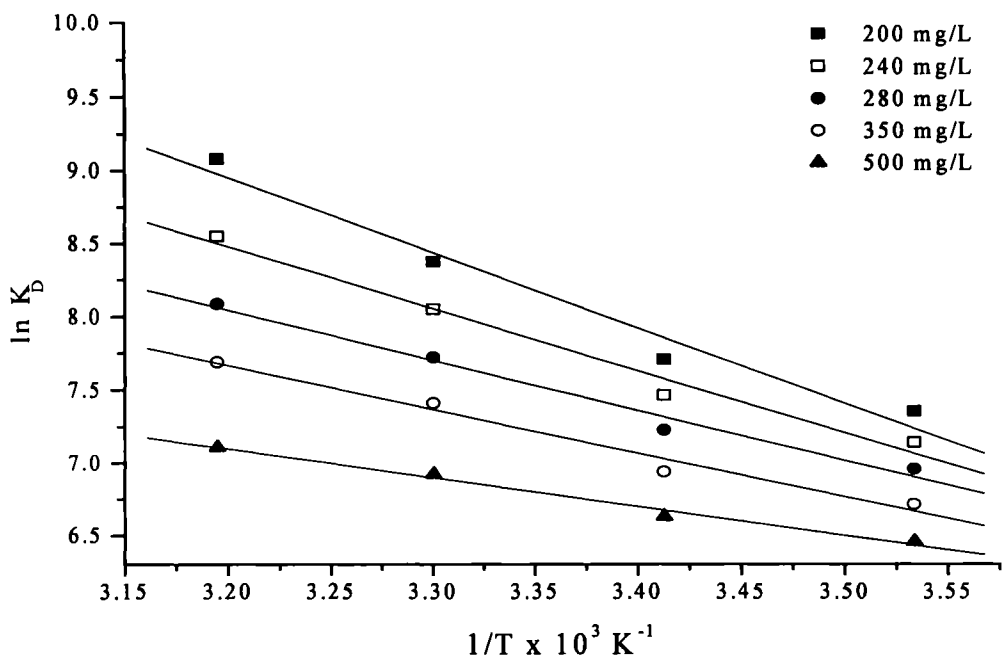


Figure 3.24d Plots of  $\ln K_D$  vs  $1/T$  for methylene blue adsorption on MGAC9.

Table 3.16 Thermodynamic parameters for Methylene blue adsorption

Carbon	$C_o$ , mg/L	$\Delta H$ , kJ/mol $\times 10^{-2}$	$\Delta S$ , J/mol/K $\times 10^{-2}$	$\Delta G$ , kJ/mol			
				283	293	303	313
GAC	200	10.20	443.80	-125.49	-129.93	-134.36	-138.81
	240	9.33	39.99	-113.08	-117.07	-121.07	-125.07
	280	8.46	36.37	-102.85	-106.49	-110.12	-113.76
	350	4.35	21.63	-61.18	-63.34	-65.50	-67.66
	500	2.31	14.03	-39.67	-41.07	-42.47	-43.87
MGAC5	200	8.44	37.57	-106.24	-109.99	-113.75	-117.51
	240	8.08	35.28	-99.77	-103.30	-106.83	-110.36
	280	7.17	31.67	-89.55	-92.71	-95.88	-99.04
	350	3.79	19.50	-55.16	-57.11	-59.06	-61.01
	500	2.29	13.80	-39.03	-40.41	-41.79	-43.17
MGAC7	200	6.64	30.91	-87.41	-90.50	-93.59	-96.68
	240	4.11	21.27	-60.15	-62.27	-64.39	-66.52
	280	3.58	18.96	-53.63	-55.53	-57.42	-59.32
	350	2.52	14.89	-42.11	-43.60	-45.09	-46.58
	500	1.67	11.52	-32.59	-33.74	-34.89	-36.05
MGAC9	200	4.27	21.13	-59.74	-61.85	-63.96	-66.08
	240	3.53	18.33	-51.84	-53.68	-55.51	-57.34
	280	2.84	15.80	-44.70	-46.28	-47.86	-49.44
	350	2.49	14.37	-40.63	-42.06	-43.51	-44.94
	500	1.65	11.21	-31.70	-32.82	-33.94	-35.06

methanol, is exothermic because the dissociation step is not required for adsorption. The surface modification of activated carbon with iron oxides reduces the magnitude of enthalpy change,  $\Delta H$ . The values of  $\Delta G$  are negative, and the process of methylene blue adsorption is spontaneous on all the adsorbents. The decrease in free energy values with increasing temperature shows that the adsorption of methylene blue is more favourable at higher temperatures. Since the adsorption process is endothermic, it follows that the process becomes spontaneous because of a positive entropy change.

## CHAPTER 4

### SEPARATION STUDIES ON MAGNETIC IRON OXIDE LOADED ACTIVATED CARBON

#### 4.1 Introduction

One of the major unit operations in any industry is the separation process. A separation operation separates a multi component input stream into two or more output streams whose compositions differ from that of the input stream or separates a multiphase stream into its constituent sub streams. To separate a multi component stream different techniques are employed such as distillation, gas absorption and stripping, liquid – liquid extraction, fractional crystallization, dialysis and pressure – swing adsorption (Robert. P & Don, G., 1997). The criteria for separation performance are based on the product purity and the fractional recovery.

The magnetic separation comes under the type where magnetic field or gradient is used. Magnetic separation is a process in which two or more solutes are separated from each other. The primary driving force of the separation is magnetization; however there are also other forces that act upon the particles as well. These forces are centripetal force and the gravitational force (Resnick, H. & Walker, P., 1997). The controlling factors include: feed rate, velocity of the particles and magnetic field strength. Conventional magnetic separation methods have been used for a long time as a standard technique in a variety of laboratory and industrial applications, including the enrichment of low grade iron ore, the removal of weakly magnetic coloured impurities from kaolinite clay, the removal of magnetic pollutants from the stack gases from several industrial processes, the desulphurization of coal and the removal of ferromagnetic impurities from large volumes of boiler water in both conventional and nuclear power plants. The magnetic separation has now been tried in wastewater treatment as well. Many effluents contain particles, ions,

molecules, etc. possessing magnetic properties (Nuñez, L. & Kaminski, M. D., 1998). The applications of magnetic separation for the efficient and economic removal of petroleum products from aqueous solutions and mixtures have been recently reported (Aplett, A. W., *et al.*, 2001). This innovative technology of using magnetic materials to solve environmental problems, such as accelerating the coagulation of sewage (Booker, N. A., *et al.*, 1991), removing radionuclides from milk (Sing, K. S.W., 1994), adsorption of organic dyes (Safarik, I., *et al.*, 1995), and oil spill remediation (Orbell, J. D., *et al.*, 1997) has gained considerable attention. A simple demonstration of the application of magnetic composites for the adsorption of water contaminants and their separation is given by Oliveira and co-workers (2004).

The non-invasive technique of separating magnetic iron oxide loaded activated carbon composites after adsorption of contaminants in solution is presented in this chapter. The main objective of this study was to find out the efficiency of separation of the prepared magnetic iron oxide activated carbon composites in a flow through system. The dependence of separation efficiency on different system parameters was studied. The dependence of separation efficiency on the gravitational force acting on a particle in a settling column, particle size of the composite samples, flow velocity of the solution and the magnetic field strength were studied.

## 4.2 **Materials and Methods**

### 4.2.1 **Materials**

#### (i) **Adsorbent samples**

The control carbon and the magnetic iron oxide loaded composite samples were used in this study. The particle size of these adsorbent samples varied from 62-88, 88-125 and 125 to 177 microns. The samples were stored in plastic containers and kept in a desiccator loaded with silica gel.

(ii) Glasswares

The study was carried out in an experimental setup made of glass. A settling column with provisions for fixing the permanent magnets was fabricated. A schematic diagram of the settling column and the separation setup is given in Figure 4.1. The settling column has a length of 14 cm and a diameter of 3 cm. The middle portion of the settling column where permanent magnets are placed has a diameter of 3.5 cm. Provisions are given in the column for the inlet and outlet of the water carrying the carbon particles. The particles retained in the column can be taken out through the tap fixed at the bottom of the settling column. The mixing of carbon particles in water was done in a 1 L glass container with a valve fitted at the bottom. This container is mounted on an adjustable stand and its height can be adjusted to deliver liquid at different flow velocities.

(iii) Instruments

*Stirrer:* A universal motor stirrer of type RQ – 122 (Remi Motors, India) was used for mixing the carbon samples in water.

*Gauss Meter:* A digital Gauss meter (Control Systems and Devices, India) was used for measuring the magnetic field strength exerted by the permanent magnets.

(iv) Permanent Magnets

Three ring type permanent magnets were used for the separation studies. Each of these magnets had an outer diameter of 5.1 cm and inner diameter of 3.6 cm. Field strength of each magnet was measured using a Gauss meter. Magnets were kept labelled and protected to prevent de-activation.

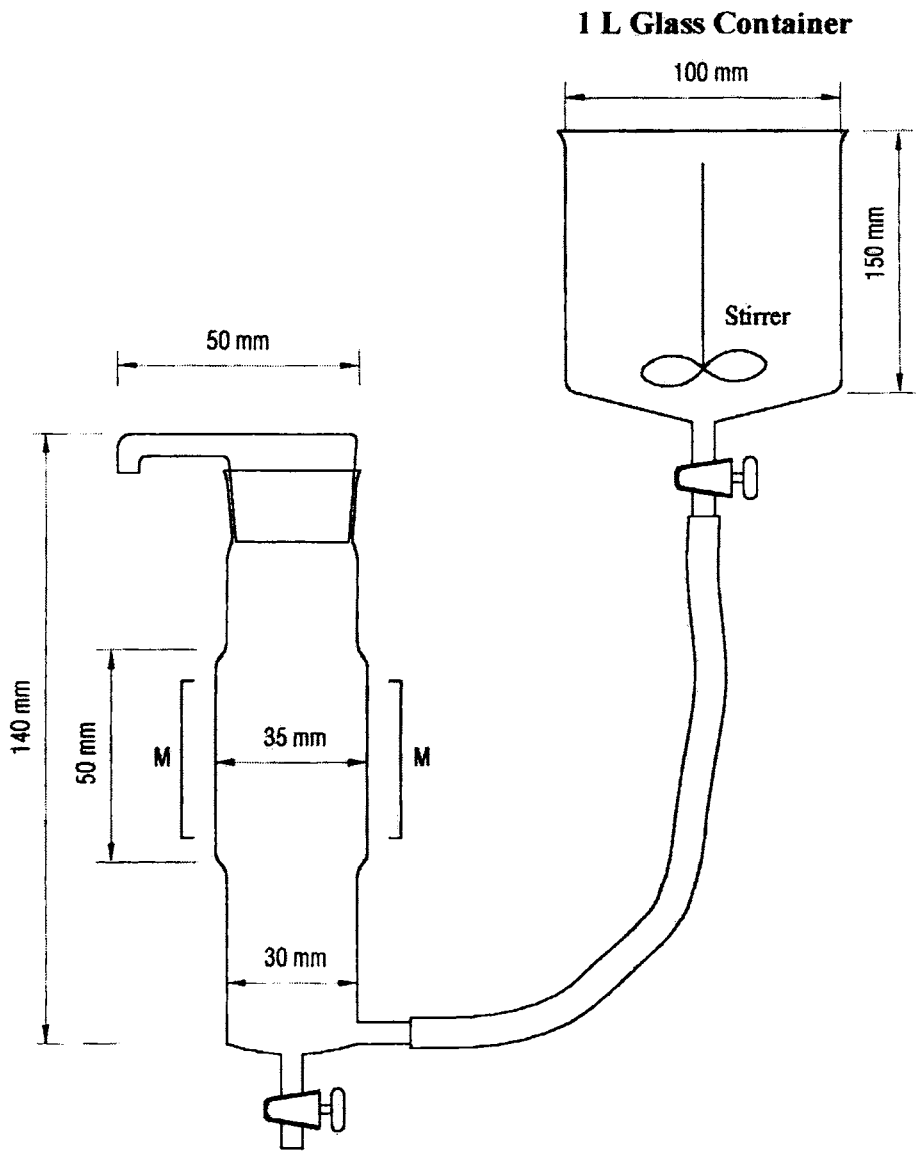


Figure 4.1 Schematic figure of the magnetic separation setup

## Methods

The removal of magnetic iron oxide loaded activated carbons from the treatment trail was studied in the settling column described above. 0.5 g of the adsorbent samples was accurately weighed and added to measured volume of (1 L) of water taken in a glass container. For this study only tap water was used, as large volumes are required. The carbon particles were well dispersed in water using a stirrer rotating at a constant speed. The beaker and the settling column were connected through a flexible tube. The valve at the bottom of the beaker is then opened to release water carrying carbon particles to flow into the settling column. The carbon particles along with water rise up the settling column and over flows through the outlet of the filter assembly. The carbon particles were collected on a previously wetted filter paper (Whatman No.1). Those particles retained in the settling column were retrieved by opening the tap at the bottom of the settling column. The filter paper containing carbon particles was then dried in a hot air oven at 110 °C for 1 hour. The weight of the carbon particles collected on the filter paper was determined. The percentage retention efficiency of the process was determined using the equation:

$$\% \text{ Retention Efficiency} = \frac{W_1 - W_2}{W_1} \times 100$$

where,  $W_1$  = Weight of the carbon added (0.5g)

$W_2$  = Weight of the carbon that flowed out of the settling column

Adjusting the head varied the flow velocity of the water that passes through the settling column carrying carbon particle. Since no attempt was made to maintain a constant water level in the storage, it was necessary to determine the average flow velocity at a particular head. The average flow velocity at a particular head was determined by measuring the volume of water discharged through the outlet tube of

the settling column for a fixed time interval when the water level in the beaker was maintained at 0.5L mark. These measurements were repeated six times and the average value was used for determining the average flow velocity of the medium.

The dependence of separation efficiency on the gravitational force and thus the settling of particles by virtue of their density were determined at zero magnetic fields. The control carbon, GAC, and the composite samples, MGAC5, MGAC7 and MGAC9 were allowed to flow through the settling column at different flow velocities. The separation efficiency due to the gravitational settling of these particles was determined by measuring the amount of particles retained in the settling column under these conditions. The influence of size of the particles on the gravitational settling was also studied at three different particle sizes of the adsorbent samples.

The dependence of separation efficiency of the composite samples on the magnetic field strength was studied at three different magnetic fields using three separate magnets. These magnets were calibrated using a Gauss meter. The field strength was adjusted by varying the number of magnets used at a time. The influence of flow velocity and particle size of the carbons at different magnetic fields on the separation efficiency of the composite samples was studied. The dependence of the flow velocity on percentage removal of the composite samples was studied by changing the hydraulic head at a constant magnetic field. Similarly the influence of particle size at a constant magnetic field on the separation efficiency was also studied by varying the size of the carbon particles.

The influence of particle size on the separation of GAC and composite samples were studied at different flow velocities and magnetic field strengths. The carbon samples had an original particle size of 125-177 microns. These particles were ground using a mortar and pestle and sieved to different size groups. The other two

size groups selected for this study were 88-125 and 62-88 microns. This study is important as activated carbons of smaller particle size, (or the powdered activated carbons) possess higher surface area and greater adsorption capacity compared to that of larger particle size (or granular activated carbon) (Metcalf & Eddy, Inc., 1991).

## **Results and Discussion**

### **Separation Efficiency at Zero Magnetic Fields**

The separation studies on the control sample and the composite samples (MGAC5, MGAC7 and MGAC9) were done under the influence of gravitational settling alone. This was to find out the extent of removal of the carbon particles due to gravitational settling alone in the settling column. The dependence of separation efficiency due to gravitational settling was studied for different particle sizes and flow velocities. The difference in the percentage retention of particles in the settling column for different size groups and flow velocities under the sole influence of gravitational settling are given in Figures 4.2 – 4.4. The percentage retention of carbon particles in the settling column was in the order  $GAC < MGAC5 < MGAC7 < MGAC9$ . This variation is attributed to the corresponding higher value for the density for these samples. The iron oxide impregnation on the activated carbon matrix has increased the absolute density of the composite sample and the increase is in proportion to the amount of iron oxide loaded. The values of absolute density of each sample are given in Chapter 2.

The dependence of settling of particles in the column on the size of the particles is clear from these graphs. It is clear that as the particle size gets smaller, less amount of carbon particles were retained in the column. The hydraulic thrust exerted by water carries away the smaller carbon particles. When the particle size becomes smaller the upward thrust exerted by the hydraulic pressure dominates over the

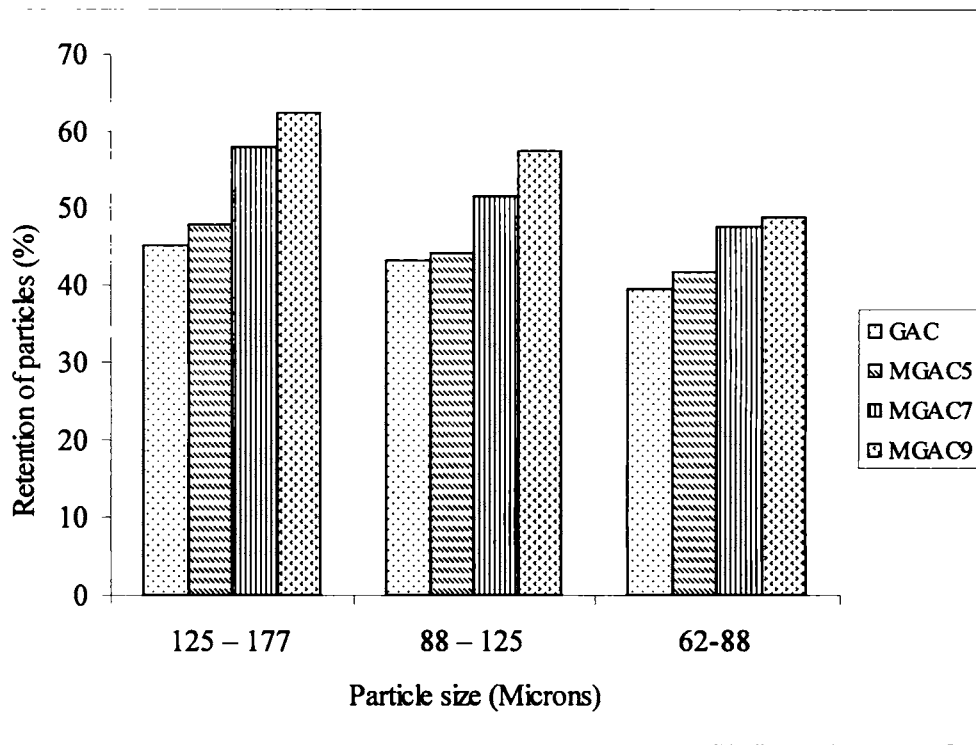


Figure 4.2 Particles retained in the settling column at zero magnetic-field at flow velocity of 5.67 cm/s.

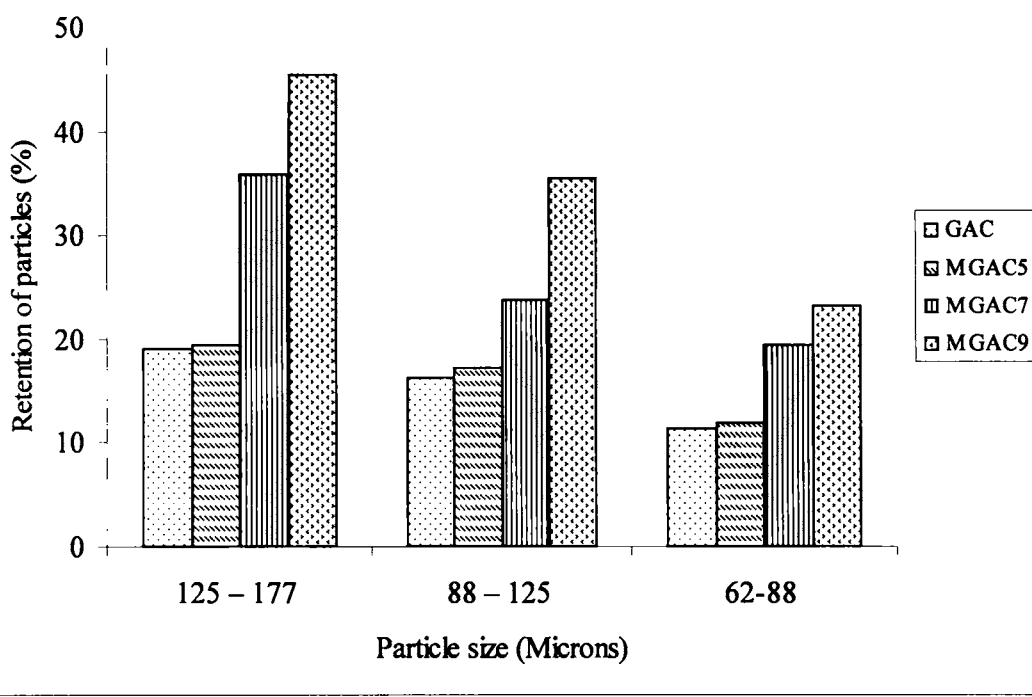


Figure 4.3 Particles retained in the settling column at zero magnetic field at flow velocity of 7.4 cm/s.

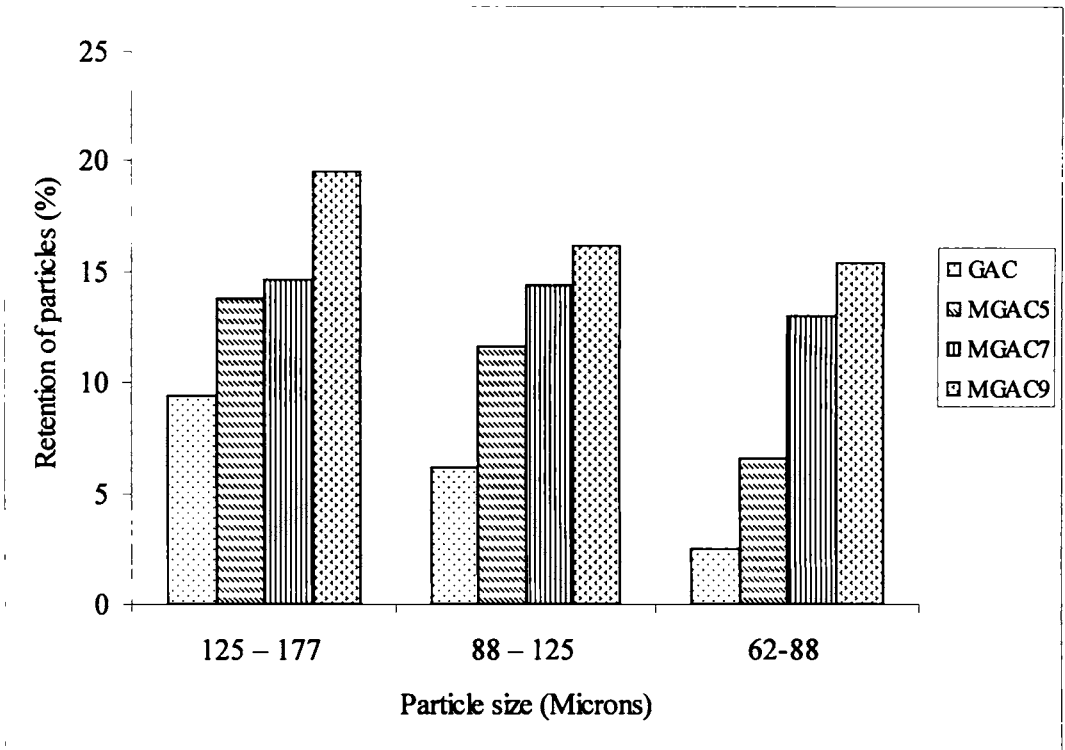


Figure 4.4 Particles retained in the settling column at zero magnetic field at flow velocity of 8.98 cm/s.

settling velocity exerted by the gravitational force. The acceleration of the particle is related to the difference between the drag and buoyancy forces. A steady velocity, terminal velocity, is reached when these forces are balanced. The terminal velocity of the particle relative to the fluid is given by the following equation

$$V_p = \frac{(\rho_P - \rho_L) \times g \times d_p^2}{18 \mu_L} \quad 4.1$$

where,

$d_p$  = diameter of the particle

$\rho_P$  = density of the particle

$\rho_L$  = density of the medium

$\mu_L$  = Viscosity of the liquid

$V_p$  = terminal velocity of the particle

The dependence of percentage retention of particles in the settling column was studied using three different particle sizes. It is evident that as the particle size decreases the influence of iron oxide loading on the retention efficiency was reduced. The percentage of particles retained in the column is drastically reduced at higher flow velocities.

#### **Dependence of Retention Efficiency of Composite Samples on Iron Oxide Loading**

The dependence of retention efficiency of composite samples under different flow velocities and magnetic fields on iron oxide loading was studied. The variation in the percentage retention of particles in the settling column under different flow velocities and magnetic field strengths are given in Figures 4.5 – 4.13. The study shows that the decrease in particle size reduced the percentage retention of carbon particles in the settling column. But the percentage loading of magnetic iron oxide on

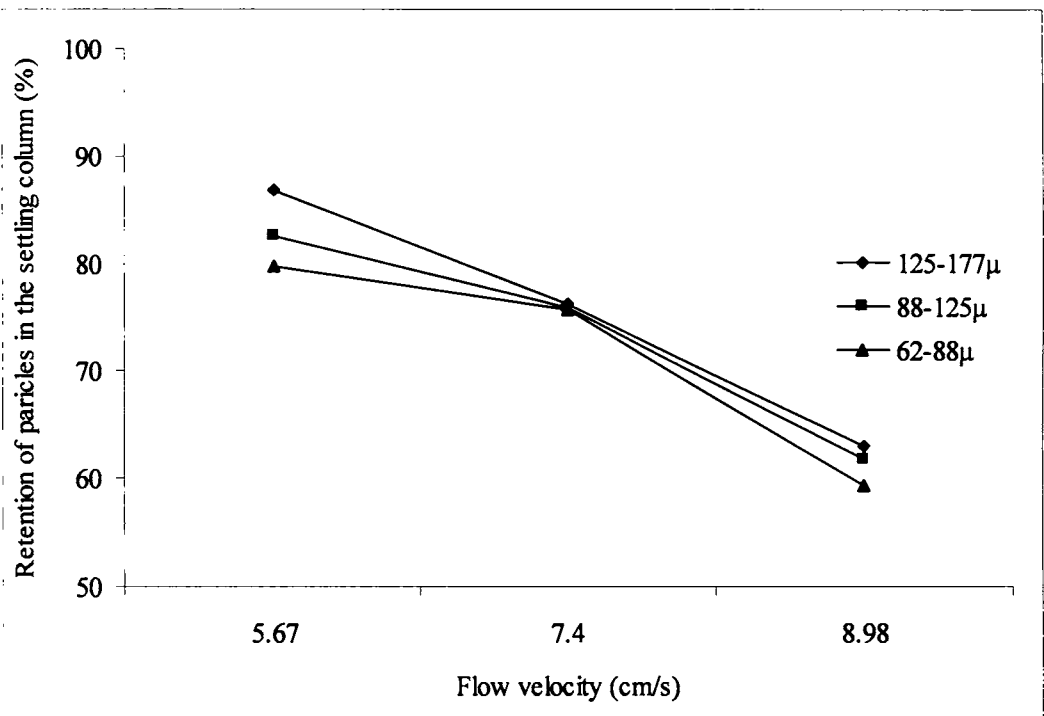


Figure 4.5 Retention vs Flow velocities for different particle sizes for MGAC5 at a field strength of 49 G.

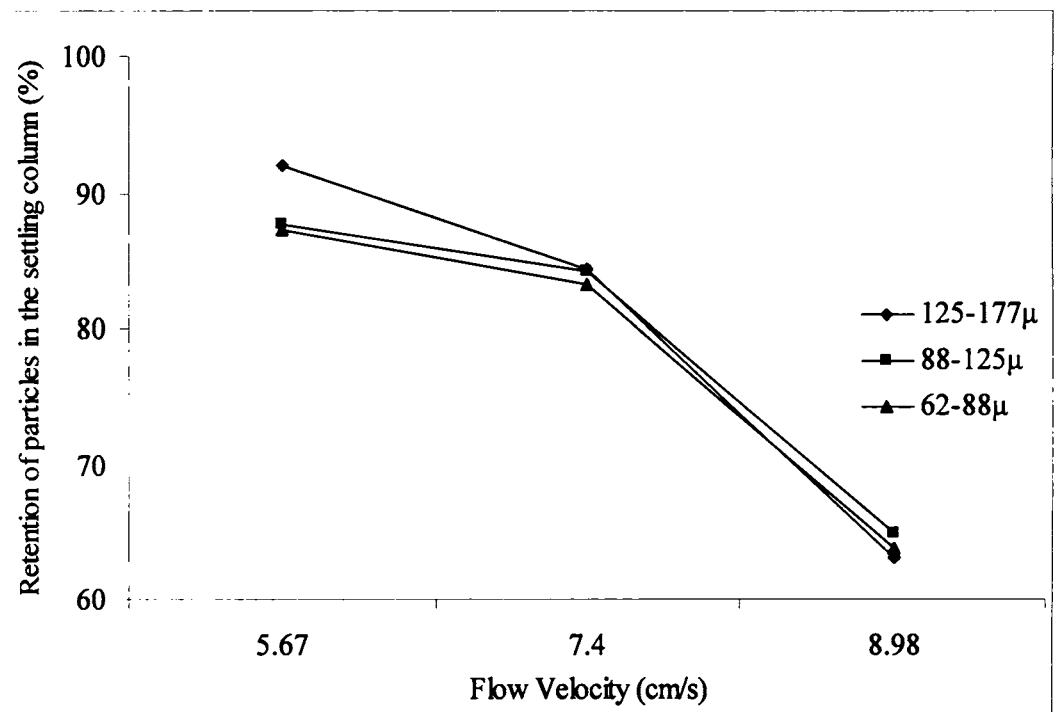


Figure 4.6 Retention vs Flow velocities for different particle sizes for MGAC5 at a field strength of 99 G.

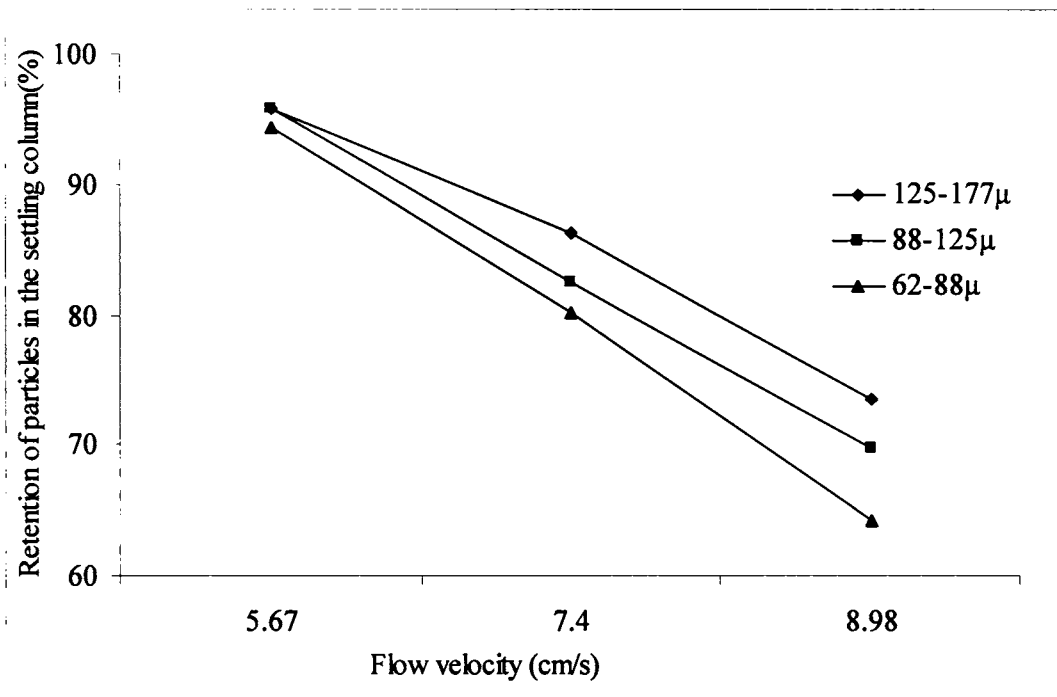


Figure 4.7 Retention vs Flow velocities for different particle sizes for MGAC 5 at a field strength of 147 G.

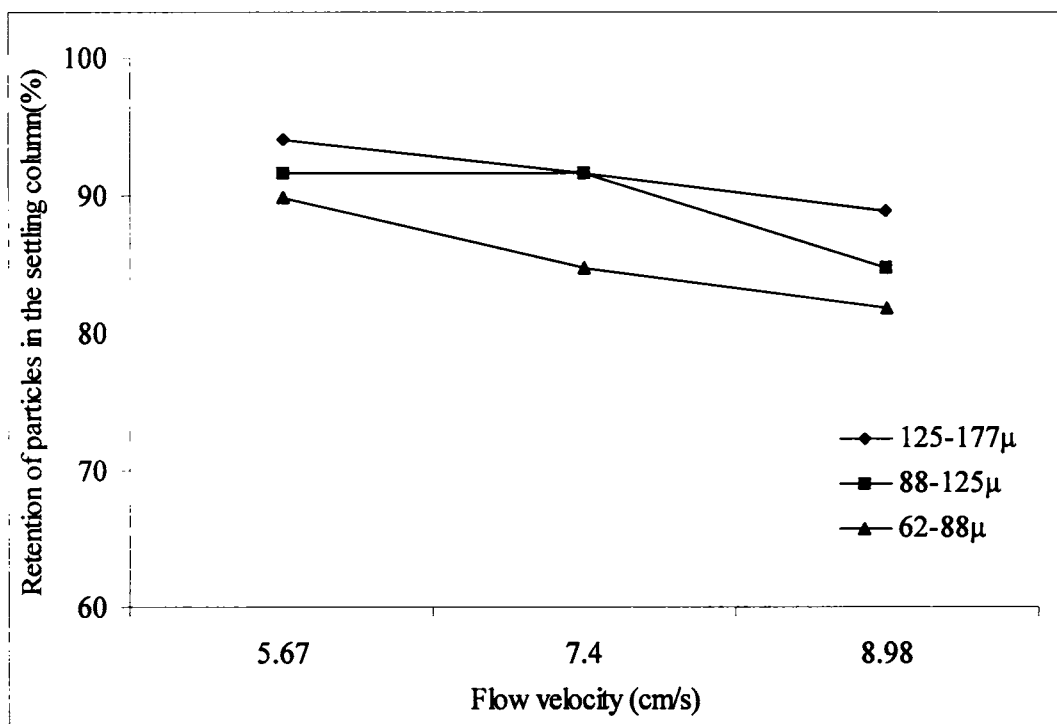


Figure 4.8 Retention vs Flow velocities for different particle sizes for MGAC 7 at a field strength of 49 G.

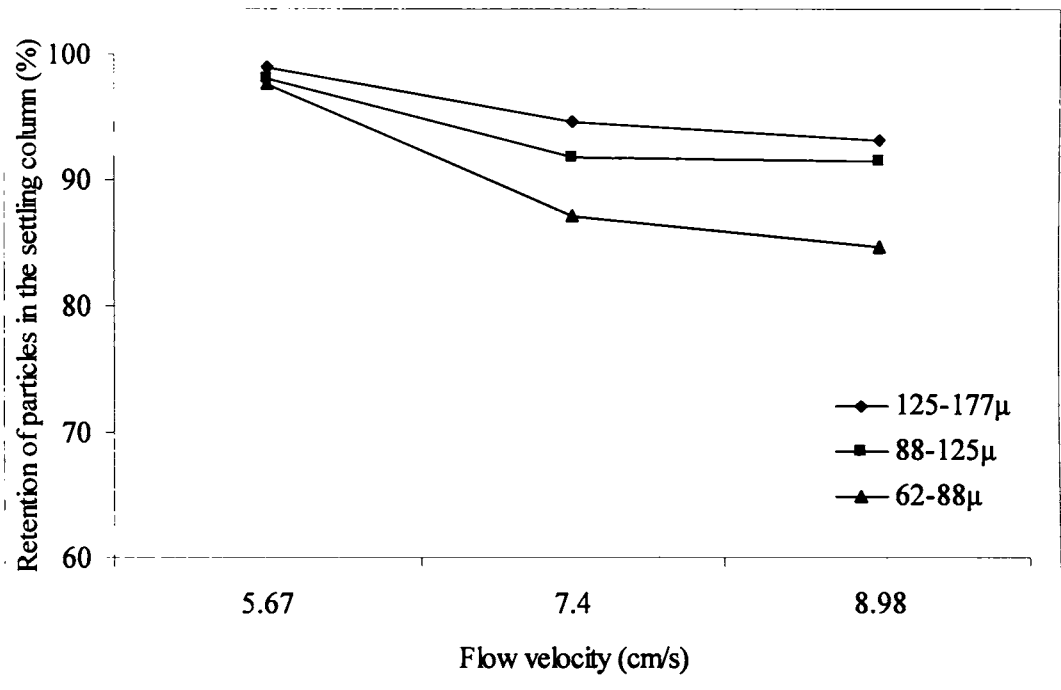


Figure 4.9 Retention vs Flow velocities for different particle sizes for MGAC 7 at a field strength of 99 G.

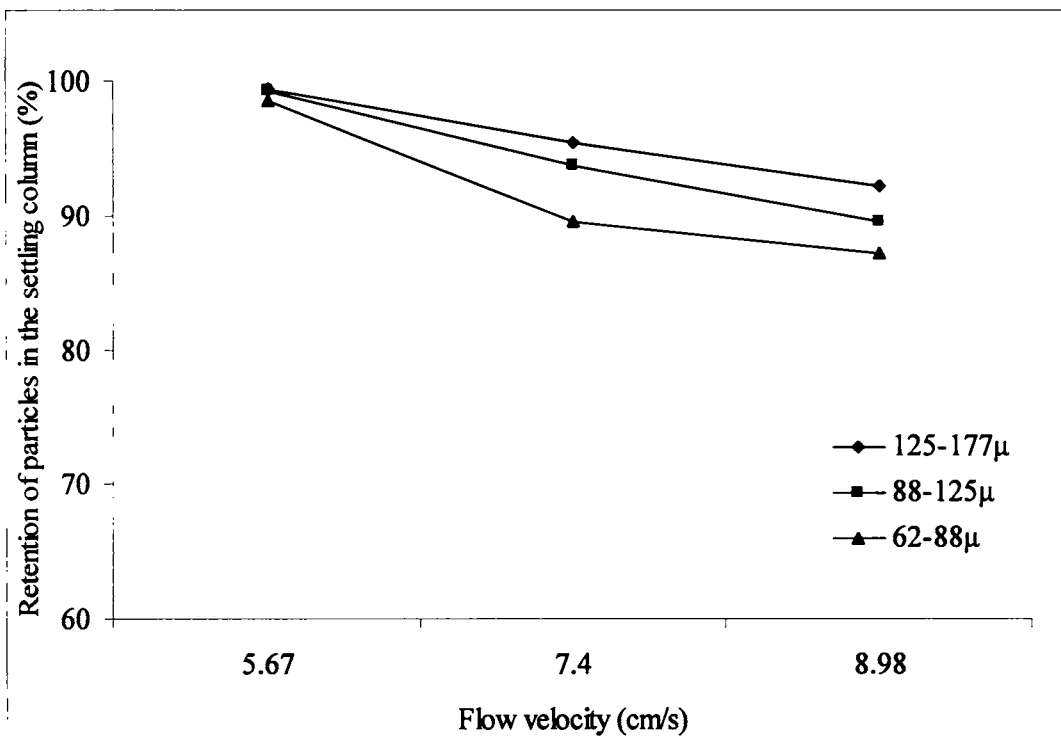


Figure 4.10 Retention vs Flow velocities for different particle sizes for MGAC 7 at a field strength of 147 G.

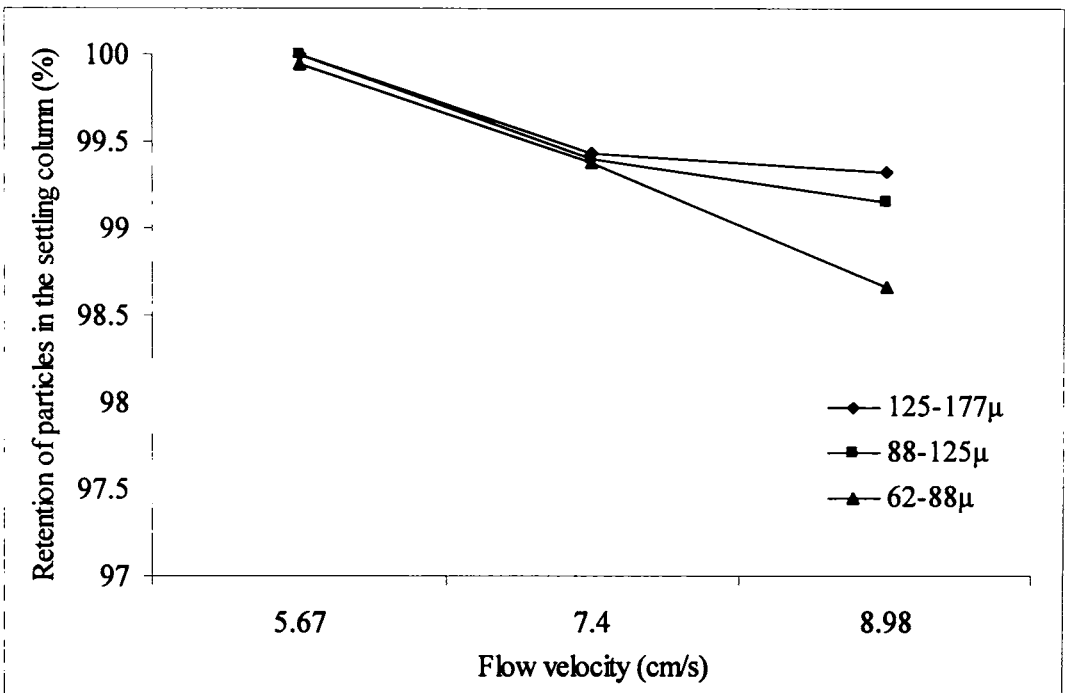


Figure 4.11 Retention vs Flow velocities for different particle sizes for MGAC 9 at a field strength of 49 G.

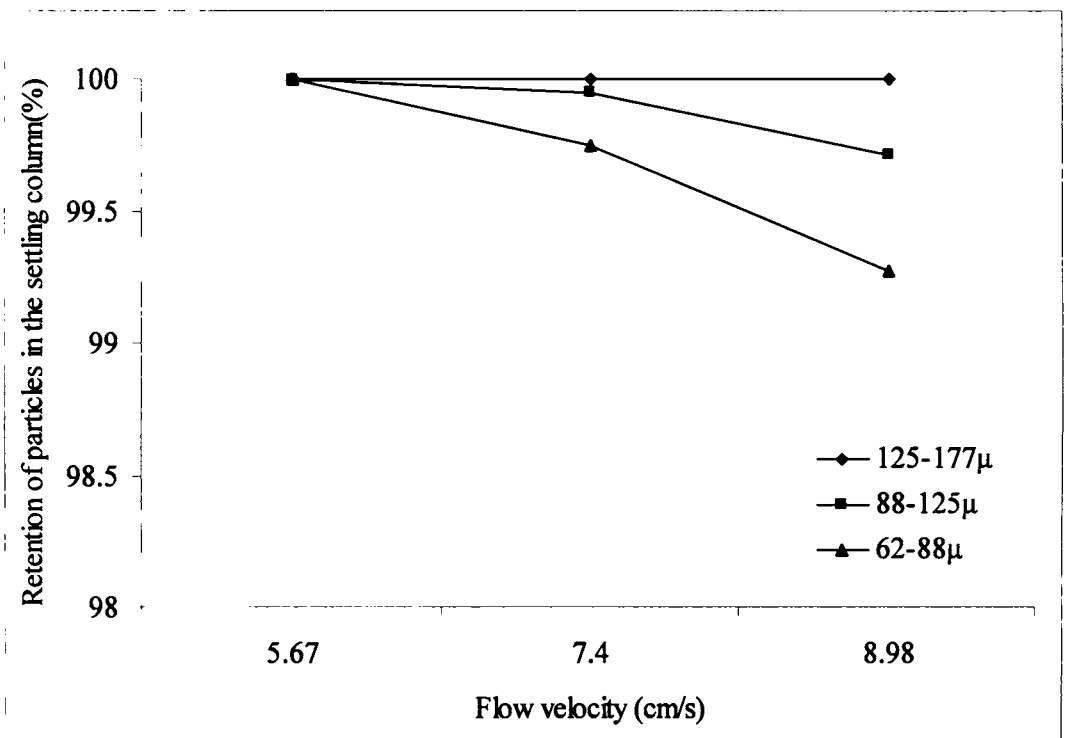


Figure 4.12 Retention vs Flow velocities for different particle sizes for MGAC 9 at a field strength of 99 G.

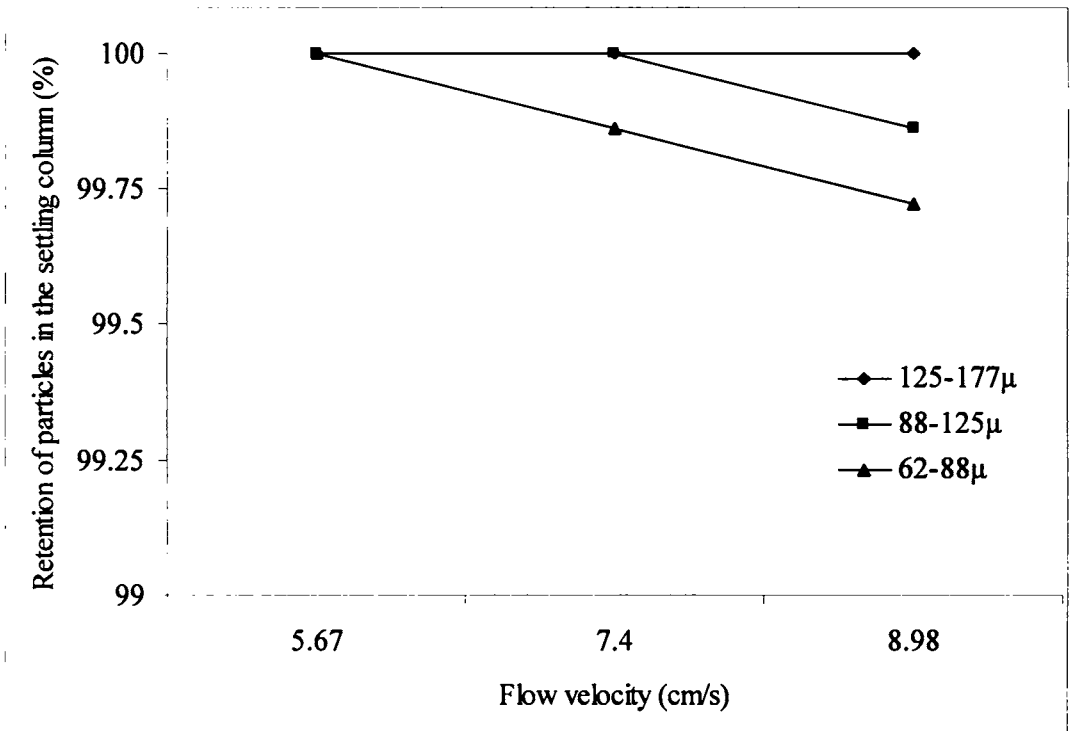


Figure 4.13 Retention vs Flow velocities for different particle sizes for MGAC9 at a field strength of 147 G.

the composite samples exerted a significant influence on the retention efficiency under different magnetic field strengths even when the particle size was reduced. The percentage retention obtained for MGAC5, which has the least iron oxide loading, varied between 60-100 % under different flow velocities and magnetic fields. The variations are given in Figures 4.5 - 4.7. The retention for MGAC7 varied from 80-100 % at different flow velocities and magnetic field strengths. Figures 4.8 - 4.10 gives the variation in particle retention at varying flow velocities and magnetic fields. More than 99% retention of the particles was achieved for MGAC9 for all the three particle size ranges. This was evident from Figures 4.11- 4.13. The overall retention capacity increased with magnetic iron oxide loading.

#### **Dependence of Retention Efficiency of Composites on Magnetic Field**

The dependence of separation efficiency of composite samples MGAC5, MGAC7 and MGAC9 on the magnetic field applied is drawn from Figures 4.5 - 4.13. Magnet number one, two and three has an effective magnetic field of 49, 50 and 48 Gauss respectively. It can be seen from these plots that higher the field applied greater the percentage of particles retained in the settling column. The influence of varying magnetic strength is more evident in the case of lower iron oxide loaded samples, MGAC5 and MGAC7 where the percentage retention depends on the magnetic field applied. For higher magnetic iron oxide loading (MGAC9) the variation in the magnetic field did not influenced the retention capacity significantly.

The effect of particle size on the retention efficiency at different magnetic fields was also studied. It can be seen from these plots that the influence of particle size on the separation efficiency was more visible for composite samples, MGAC5 and MGAC7. When the size of particles was decreased, the retention efficiency was

reduced. It is observed that irrespective of particle size, the retention capacity for MGAC9 was close to 100 % at all magnetic field strengths.

When the flow velocity was increased from 5.67 cm/s to 8.98 cm/s under different magnetic fields, a reduction in the retention efficiency was observed for MGAC5 and MGAC7. The reduction in the separation efficiency with increase in flow velocity is more predominant in the case of MGAC5 compared to MGAC7. And the influence of flow velocity on the composite sample, MGAC9 was only marginal under different magnetic fields. This suggests that for a higher magnetic iron oxide loading the flow velocity has little influence on the removal of particles from the stream at different magnetic fields.

#### **Dependence of Retention Efficiency on Flow Velocity**

The influence of flow velocity of the medium on the retention efficiency of carbon particles was studied at different particle sizes and magnetic field strengths. The dependence of retention capacity on the flow velocity in the settling column is shown in Figures 4.5 - 4.13. When the flow velocity of the medium was increased from 5.67 cm/s to 8.98 cm/s, the percentage retention decreased. The reduction was more significant for MGAC5. For higher magnetic iron oxide loaded carbons the influence of flow velocity on retention capacity was marginal and outweighed by the intensity of applied magnetic field.

The changes in retention capacity with particle size are significant at higher flow velocities. The capacity decreased with increase in flow velocity and decrease in particle size. Particles with smaller sizes are easily carried out of the settling column at higher velocities. However, under the influence of an applied magnetic field the influence of flow velocity on carbon particles of different size groups is reduced significantly. Separation efficiency of composite sample MGAC9 of different particle

sizes at varying flow velocities was not reduced significantly under the influence of varying magnetic fields.

The dependence of retention efficiency on the flow velocity and varying magnetic fields for each composite sample is given in Figures 4.5 – 4.13. The percentage reduction in the retention capacity varied as a function of applied magnetic field. An increase in the applied magnetic field reduced the dependence of separation efficiency on the flow velocity. But the gain in the separation efficiency due to higher applied magnetic fields against the flow velocity is felt more at higher iron oxide loading.

## CHAPTER 5

### SUMMARY AND CONCLUSION

The suitability of magnetic iron oxide loaded activated carbon for the adsorption and subsequent separation of the adsorbent by retention in a magnetic field were investigated. The effects of magnetic iron oxide (MIO) deposited on GAC on the physico-chemical properties were investigated using TG, SEM, Mossbauer spectroscopy, XRD and Vibration Sample Magnetometry were studied.

Mossbauer spectral results and XRD showed the presence of maghemite and other oxides of iron in various proportions. The structural environment and proportion of iron oxide varied depending on the sample. Equilibrium moisture uptake under ambient conditions varied with the proportion of iron oxide in the sample. TG further revealed the suitability of thermal desorption for the regeneration of spent adsorbent. In the middle range of temperature iron oxide facilitated increased mass loss. However, loss of carbon by burn-off was suppressed by iron oxide.

Evaluation of pore properties of magnetic iron oxide loaded activated carbons by nitrogen adsorption and micrographic images revealed that micro, meso and macro pores were affected by MIO to different extent. MIO was deposited inside and outside the pores. The crystallites of MIO had size distribution corresponding to the pore diameter. The surface area determined by the nitrogen adsorption and solution adsorption decreased with increasing MIO loading. The decrease in adsorption properties could not be directly correlated to the iron oxide content. This may be due to the variability in the chemical characteristics and particle size distribution of the mixed oxide.

Solution adsorption studies using phenol, 4-nitrophenol and methylene blue revealed some interesting aspects. Corresponding to the decrease in the surface area due to the MIO loading there is a decrease in the adsorption frequency for the solute loading. The Lagergren

plots revealed a decrease in rate constant for adsorption kinetics. The intra particle diffusion rate constant also reveals a similar trend. Thermodynamic parameters showed a modification in the parameters induced by the presence of MIO.

Regeneration of spent adsorbate using hot water showed a loss in adsorption capacity with increase in regeneration cycle. The advantageous property of MIO-GAC is that after effecting adsorption, the adsorbate could be conveniently retained in a flow through reactor using externally applied magnetic field. Hence the influence of particle size, flow velocity and strength of the scavenging magnetic field were investigated. Retention efficiency increased with increasing particle size and applied field strength and decreased flow velocity. Such changes were also influenced by the extent of loading GAC with MIO.

The studies and results presented in the thesis point to a new direction in the use of activated carbon. Such a flow through application can revolutionize the use of powdered activated carbon. The preliminary studies presented here is a modest contribution to separation science with a specific plausible application in the removal of organic gases in emissions and organic solutes in effluents.

The investigation also opens up some new challenges. These include studies on

- Influence of the method of preparation of MIO-GAC on the distribution of iron oxide phases, modification of pore size distribution and their bearing on adsorption properties.
- Adsorption of volatile organic compounds from gas streams onto MIO-GAC.
- Design and evaluation of devices for MIO-GAC adsorption, retention in magnetic field and regeneration of the used adsorbent.

## REFERENCE

- Achaerandio, I., Güell, C. & López, F. (2002) Continuous vinegar decolorization exchange resins. *Journal of Food Engineering* 51: 311-317.
- Achari, V. S. (1998) Modified carbons and wood dust: Evaluation of adsorption properties. PhD Thesis. Department of Chemistry, University of Kerala, India.
- Adamson, R. J. (1972) *Gold Metallurgy in South Africa*, Chamber of Mines of South Africa.
- Ahmedna, M., Marshall, W. E. & Rao, M. (2000) Production of Granular Activated Carbons from selected agricultural by-products and evaluation of their physical, chemical and adsorption properties. *Bioresources Technology*, 71, 2. pp. 113-123.
- Alaya, M. N., Girgis, B. S. & Mourad, W. F. (2003) Activated carbon from some agricultural wastes under action of one step steam pyrolysis. *Journal of Porous Materials*, 17, 4, pp. 509-517.
- Al-Duri, B. (1988) *Mass Transfer Processes in Single and Multi-component Batch Adsorption processes*, Ph.D thesis, The Queen's University of Belfast.
- Al-Duri, B. & McKay, G. (1991) Prediction of Binary System Kinetics of Batch Adsorption Using Basic Dyes onto Activated Carbon. *Chem. Eng. Sci.*, 46 (1), 193.
- Al Duri, B. (1995) Adsorption modeling and mass transfer. Chapter 7 in *Use of Adsorbents for the Removal of Pollutants from Wastewaters*. McKay, G. ed. CRC Press, Inc. Florida.
- Allingham, M. M., Cullen, J. M., Giles, C. H., Jaun, S. K. & Woods, J. S. (1958) *J. Appl. Chem.* 8, 108.
- Aly, O. M. & Faust, S. D. (1972) The Adsorption of Chlorinated Phenols by Activated carbon. Presented at the Kendall Award Symposium, American Chemical Society, 163<sup>rd</sup> National Meeting, Boston.
- Apblett, A. W., Al-Fadul, S. M., Chehbouni, M. & Trad, T. (2001) "Removal of Petrochemicals from Water Using Magnetic Filtration" Proceedings of the 8th International Environmental Petroleum Consortium.
- Armstrong, R. J., Morrish, A. H. & Sawatzky, G. A. (1966) *Phys. Letters*, 23, 414.

- Ashford, R. D. (1994) *Ashford's Dictionary of Industrial Chemicals*. London: Wavelength Publishers, Ltd.
- ASTM D 4607 (1986) Annual Book of ASTM Standards, Vol. 15.01.
- ASTM D 5159 – 91. (1991) Standard Test Method for Dusting Attrition of Granular Activated Carbon, Annual Book of ASTM Standards, Vol, 15.01.
- ASTM D 2866 (1994) Annual Book of ASTM Standards, Vol. 15.01.
- Arbuckle, W. B. (1980) *AICHE Symp.*, no. 197, 76, 61.
- Attia, A. A., Girgis, B. S. & Khedr, S. A. (2003a) Capacity of activated carbon to remove dyes and phenolics. *Journal of Chemical Technology & Biotechnology*, 78, 6. pp. 611-619.
- Attia, A. A., Girgis, B. S. & Khedr, S. A. (2003b) Capacity of activated carbon derived from pistachio shells by H<sub>3</sub>PO<sub>4</sub> in the removal of dyes and phenolics. *J. Chem. Tehnol. Biotechnol.*, 78, pp. 611-619.
- Aygun, A., Yenisoy-Karakas, S. & Duman, I. (2003) Production of granular activated carbon from fruit stones and nut shell and evaluation of their physical, chemical and adsorption. *Microporous and Mesoporous Materials*, 66, 2, pp. 189-195.
- Bacon, G. E. (1952) *Acta Cryst.*, 5, 392.
- Baker, F. S., Miller, C. E., Repik, A. J. & Tolles, E. D. (1992) Activated carbon. *Kirk-Othmer Encyclopedia of Chemical Technology* 4: 1015-1037.
- Banerjee, S. K., Reilly, W. O'. & Johnson, C. E. (1967) *J. Appl. Phys.*, 38, 1289.
- Bansal, R. C., Donnet, J. B. & Stoeckli, H. F. (1988) *Active Carbon*, Marcel Dekker, New York.
- Barton, S. S. (1987) The adsorption of methylene blue by active carbon, *Carbon*, Vol. 25, No. 3, pp. 343-350.
- Barton, S. S., Dacey, J. R., Harrison, B. H. & Sellors, J. R. (1979) *J. Coll. Interface Sci.*, 71, 367.
- Blanck, C. A. (1979) *J. Amer. Water Works Assoc.* 71, 525.
- Blyholder, G., & Eyring, H. (1957) *J. Phys. Chem.*, 61, 682.
- Boehm H. P., Heck, D. W. & Sappok, R. (1964) *Angew. Chem. Int. Ed.*, 3, 669.
- Boehm, H. P. (1994) *Carbon*, 32, 759.

- Bokros, J. C. (1969) In *Chemistry and Physics of Carbon*, Vol. 5. Walker, P. C. eds. John Wiley & Sons, New York.
- Booker, N. A., Keir, D., Priestly, A., Ritchie, C. D., Sudarmana, D. L. & Woods, M. A. (1991) *Water Sci. Technol.* 123, pp. 1703-1711.
- Boyd, S. A. (1982) Adsorption of Substituted Phenols by Soil. *Soil Science*, Vol. 134, No.5.
- Brady, M. & McKay, G. (1995) Characterization of Adsorbents. In chapter 4 of *Use of Adsorbent for the Removal of Pollutants from Wastewaters*. Edited by McKay, G. CRC Press.
- Brunauer, S., Emmette, P. H & Teller, E. J. (1938) *J. Amer. Chem. Soc.* 60. 309.
- Brunauer, S., *et al.* (1940) *J. Amer. Chem. Soc.* 62, 1723.
- Buschow, K. H. J., Long, G. J. & Grandjean, F. (1993) *High Density Digital Recording*. NATO ASI Series E, Vol. 29, Kluwer Academic Publishers, Boston.
- Calleja, G., Serna, J. & Rodriguez, J. (1993) *Carbon*, 31, 691.
- Cairo, P. R., *et al.* (1978) Development of Criteria for the Design of Full Scale Carbon Adsorption Systems. *Proc. Amer. Water Works Assoc. Water Quality Technol. Conf.*
- Caturia, F., Martin-Martinez, J. M., Molina-Sabio, M., Rodrigue-Reinoso, F. & Torregross, R. (1988) *J. Colloid Interface Sci*, 124, 528.
- Carrott, P. J. M., McLeod, A. I. & Sing, K. S. W. (1982) In *Adsorption at the Gas-Solid and Liquid-Solid Interface* (Edited by J. Rouquerol & Sing, K. S. W.). Elsevier, Amsterdam, pp. 403-410.
- Carrott, P. J. M., Roberts, R. A. & Sing, K. S. W. (1988) In *IUPAC Symposium on Characterization of Porous Solids* (Edited by Unger, K. K., Rouquerol, J., Sing, K. S. W. & Kral. H.). Elsevier, Amsterdam, pp. 89-100.
- Cheremisinoff, P. N. & Morresi, A. C. (1980) "*Carbon Adsorption Applications.*" *Carbon Adsorption Handbook*. pp. 1-54. Ann Arbor Science Publishers, Inc., Ann Arbor, Michigan.
- Chambers, R. W., Kajiwarra. D. R. & Kerans, J. (1974) *J. Phys. Chem.* 78, 380.
- Coughlin, R. W. & Ezra, F. S. (1968) *Environ. Sci. Technol.*, 2, 291.

- Coughlin, R. W. & Tan, R. N. (1968) *Chem Eng. Progr. Symp. Ser.*, 64, 207.
- Coughlin, R. W., *et al.* (1968) *J. Colloid Interf. Sci.*, 28, 386.
- Coughlin R. W. & Ezra, E. S. (1968) *Environ. Sci. Technol.* 2, 291.
- Crank, J. (1965) *The Mathematics of Diffusion*. Clarendon Press, London.
- Critoph, R. E. (1989) Activated carbon adsorption cycles for refrigeration and heat pumping. *Carbon*, Vol. 27, No. 1. 63.
- Daulan, C., Lyubchik, S. B., Rouzaud, J. N. & Beguin, F. (1998) Influence of anthracite pretreatment in the preparation of activated carbons. *Fuel*, Vol. 77. No. 6.
- Dalton, A. J. and S. Sircar. (1977) U. S. Patent 4,025,605.
- Dobbs, R. A. & Cohen, J. M. (1980) "Carbon Adsorption for Toxic Organics." EPA 600/8-80-023. Municipal Environmental Research Laboratory, U. S. EPA, Cincinnati, Ohio, 45268.
- Donmez, G. C., Aksu, Z., Ozturk, A. & Kutsal, T. (1999) *Process Biochem.*, 885.
- Dubinina, M. M. & Zaverina, E. D. (1936) *Acta Phys-Chim. U.S.S.R.*, 4, 647.
- Ererhardt, M., *et al.* (1979) Report No. 7. Engler-Bunte-Institute, Department of Water chemistry, Karlsruhe University, Federal Republic of Germany.
- Faust, S. D. & Aly, O. M. (1983) *Chemistry of Water Treatment*. Butterworths, Stoneham, Mass.
- Faust, S. D. & Aly, O. M. (1987) *Adsorption Processes for Water Treatment*, Butterworths, Stoneham, MA.
- Foersterling, H. U. (1990) Investigations of the adsorption of palladium on carbonaceous adsorbents modified with dimethylglyoxime – I. The adsorption of dimethylglyoxime on selected carbonaceous adsorbents. *Carbon*, Vol. 28. No.1, 27.
- Food Chemicals Codex Committee. (1996) *Food Chemicals Codex* (4th ed.). Washington: National Academy.
- Fernandez, N. A., Chacin, E., Gutierrez, E. & Alastre, N. (1995), *Bioresource Technol.*, 54, 111.
- Freundlich, H. (1926) *Colloid and Capillary Chemistry*. Methuen and Co., London.
- Fritz, W., Merk, W. & Schlunder, E. U. (1981) *Competitive Adsorption of Two Dissolved Organics onto Activated Carbon – II., Adsorption Kinetics, Chem. Eng. Sci.*, 36, 731.
- Fuderer, A. & Rudelstorfer, E. (1976) U. S. Patent 3,896,849.

- Garrido, J., Linares-Solano, A., Martin-Martinez, J. M., Molina-Sabio, M., Rodriguez-Reinoso, F. & Torgrosa, R. (1987) *Langmuir*, 3, 76.
- Giles, C. H., Greczek, J. J. & Nakhowa, S. N. (1961) *J. Chem. Soc.*, 93.
- Golden, T. C. & Sircar, S. (1990) *Carbon*, 28, 683.
- Gomez-Serrano, V., Valenzuela, C. C & Gonzalez-Martin, M. L. (1994) *Appl. Surf. Sci.*, 74, 337.
- Gonzalez-Martin, M. I., Gomez-Serrano, V. & Valenzuela, C. C. (1991) *Langmuir*, 7, 1269.
- Goyal, M. (2004) Adsorption of *p*-Nitrophenol by Surface Modified Carbons from Aqueous Solution. *Carbon Science*, Vol. 5, No. 2, pp 55-61.
- Graham, D. (1955) *J. Phys. Chem.*, 59, 896.
- Gray, E. L. (1940) *A History of the Discovery of the Witwatersrand Goldfields*, Chamber of Mines of South Africa.
- Greenwood, N. N. & Gibb, T. C. (1997) Chapter 10 in *Mossbauer Spectroscopy*. Chapman and Hall Ltd. London.
- Gregg, S. J. & Sing, K. S. W. (1982) *Adsorption, Surface Area and Porosity*. 2<sup>nd</sup> ed., Academic Press. London.
- Gulbransen, E. A. & Andrew, K. F. (1952) *Ind. Eng. Chem.*, 44, 1034.
- G<sup>u</sup>zel, F. & Tez, Z. (1993) *Separation Science and Technology*, 28, 8, 1609-1627.
- G<sup>U</sup>ZEL, F & UZUN, I. (2002) Determination of the Micropore Structures of Activated Carbons by Adsorption of Various Dyestuffs from Aqueous Solution, *Turk. J. Chem.*, 26, pp. 369-377.
- Hager, D. G. (1967) *Environ. Sci. Technol.* 1, 287.
- Harker, H., Jackson, C. & Wynne-Jones, W. G. K. (1961) *Proc. Roy. Soc. (London)*, A262, 328.
- Hassler, J. W. (1974) *Activated Carbon*. Chemical Publishing Co., New York.
- Hassler, J. W. (1974) *Purification with Active Carbon*, Chemical Publishing Co. Inc., New York, p. 326.
- Hedden, K., Huber, L. & Rao, B. R. (1976) VDI-Bericht Nr. 253, S. 37/42, VDI-Verlag, Dusseldorf.
- Henning, K. D., Keldenich, K., Knoblauch, K. & Degel, J. (1988) *Gas Sep Purif.* 2, 20-22.

- Henning, K. D. & Schäfer, S. (2003) *Impregnated activated carbon for environmental protection*. Available from: <<http://www.activated-carbon.com/enviro.html>> (Accessed 18 June, 2004).
- Ho, Y. S., Porter, J. F. & McKay, G. (2002) *Water Air and Soil Pollut.*, 141, 1.
- Honig, P. (1926) *Kolloid Chem. Beih.* 22, 345.
- Huang, C. P. & Ostovic, F. B. (1978) *J. Environ. Eng. Div. ASCE 104 (EES)*, 863.
- Hutchins, R. A. (1981) *In Activated Carbon Adsorption for Wastewater Treatment*, Edited by Jerry R. Perrich. CRC Press. pp. 29-37.
- Hyde, R. A. (1980) Removal of Haloforms and Pesticides by Granular Activated Carbon, Chapter 6 in *Activated Carbon Adsorption of Organics from the Aqueous Phase*, Vol. 2. McGuire, M. J. & Suffet, I. H. eds. Ann Arbor Science Publishers, Ann Arbor, Michigan, p. 137.
- Inhoffer, W. R. (1975) Use of Granular Activated Carbon at Passaic Valley Water Commission. Paper presented at the American Water Works Association Water Technology Conference, Atlanta, Ga.
- Inst. Merieux S. A. (1979) European patent appl., 16, 702.
- Jankowska, H., Swiatkowski, D., Gelbin, K. H., Radeke, K. H. & Seidel, A. (1986) *Proc. Carbon*, 86, conf. Baden, 397.
- Jiles, D. (1991) *Introduction to Magnetism and Magnetic Materials*. Chapman and Hall, New York.
- Juntgen, H., Knoblauch, K., Reichenberger, J., Heimbach, H & Tarnow, F. (1981) U. S. Patent 4,263,339.
- Kannan, N. & Sundaram, M. M. (2001) Kinetics and mechanism of removal of methylene blue by adsorption on various carbons—a comparative study. *Dyes and Pigments*, 51, pp. 25–40.
- Kaneko, K., Ishi, C., Ruike, M. & Kawabara, H. (1992) *Carbon*, 30, 1075.
- Keinath, T. M. & Weber, W. J., Jr. (1968) *J. Water Pollut. Cont. Fed.*, 40, 743.
- Kipling, J. J. & Wilson, R. B. (1960) *J. Appl. Chem.* 10, 109.
- Kistner O. C. & Sunyar, A. W. (1960) *Phys. Rev. Letters*, 4, 412.
- Kokando Co Ltd. (1978) *Kokai Tokkyo Koho.*, 80-78,965.
- Kruyt, H. R., & de Kadt, G. S. (1929) *Kolloid Z.* 47, 44.
- Kudo, K., Hosada, H., Honma, S. & Komatsu, M. (1973) *J. Fuel Soc. Japan* 52, 335

- Langmuir, I. (1915) *J. Amer. Chem. Soc.* 37, 1139.
- Lagergren, S. & Svenska, B. K. (1898) *Ventemskapaka Handl*, Vol. 24.
- Lawrence, C. H. (1968) *Water Wastes Eng.* 5, 46.
- Lee, P. E. (1974) Activated Carbon Removes Sulfide Odor. *Water & Sewage Works*, September. pp. 116-117.
- Lemin, D. R. & Vikerstaff, T. (1947) *Trans. Far. Soc.* 43, 491.
- Leon y Leon, C. A., Solar, J. M., Calemma, V. & Radovic, L. R. (1992) *Carbon* 30, 797.
- Linares-Solano, A., Lopez-Gonzalez, J. D., Molina-Sabio, M. & Rodriguez-Reinoso, F. (1980) *J. Chem. Tech. Biotechnol.* 30, 65.
- Liu, K. T. & Weber, W. J., Jr. (1981) *J. Water Pollut. Cont. Fed.* 53, 1541.
- Lorenzen, L. & Van Deventer, J. S. J. (1993) *The identification of refractoriness in gold ores by the selective destruction of minerals. Minerals Engineering, Vol. 6*, Nos. 8-10, pp 1013-1023.
- Lorenzen, L. (1995) *Some guidelines to the design of a diagnostic leaching experiments. Minerals Engineering, Vol.299*, pp.247-2256.
- Lovett, W. D. & Poltorak, R. L. (1974) Activated Carbon Used to Control Odors. *Water & Sewage Works*, August, pp. 74-75.
- Lounici, H., Aiouche, F., Belhocine, D., Drouiche, M., Pauss, A. & Mameri, N. (2004) Mechanism of Phenol adsorption onto electro-activated carbon granules. *Water Research*, 38, 1, pp. 218-224.
- Lussier, M. G., Shull, J. C. & Miller, D. J. (1994) Activated carbon from cherry stones, *Carbon*, Vol. 32. No. 8.
- Mahajan, O. P., Moreno-Castilla, C. & Walker, P. I., Jr. (1980) *Sep. Sci. Technol.* 15, 1733.
- Maggs, F. A. P. (1953) *Research*, 6, S13.
- Mall, I. D. & Upadhyay, S. N. (1998) *Indian J Environ Hlth.*, 40(2), 177.
- Mantell, C. L. (1968) *Carbon and Graphite Handbook*. John Wiley and Sons, Inc., New York.
- Mantell, C. L. (1979) *Carbon and Graphite Handbook*. Robert E. Krieger Publishing Co., Huntington, N.Y.
- Marsh, H. & Wynne-Jones, W. F. K. (1964) *Carbon*, 1, 281.
- Matsumoto, A., Zhao, J. & Tsutsumi, K. (1997) *Langmuir*, 13, 496.

- Mattson, J. S. & Mark, H. B., Jr. (1970) *J. Colloid Interface Sci.*, 33, 284.
- Mattson, J. S. & Mark, H. B., Jr. (1971), *Activated Carbon*. Marcel Dekker, New York.
- Mattson, J. S. (1973) *Ind. Eng. Chem. Prod. Res. Devel.* 12, 312.
- Mattson, J. S., Mark, H. B., Jr. & Weber, W. J., Jr. (1969) *Anal.Chem.*, 41, 355.
- Mattson, J. S. & Mark, H. B. Jr. (1971) *Activated Carbon, Surface Chemistry and Adsorption from Solution*. Marcel Dekker, New York.
- McBain, J. W. (1932) Chapter 5 in *The sorption of Gases and Vapours by Solids*, Routledge, London.
- McCarty, L. B. (2002) Activated charcoal for pesticide deactivation. University of Florida Cooperative Extension Service. [http://edis.ifas.ufl.edu/BODY\\_WG065](http://edis.ifas.ufl.edu/BODY_WG065).
- McEnaney, B. (1987) Estimation of the dimensions of micropores in active carbons using the Dubini-Radushevich equation. *Carbon*, 25, 1, pp. 69-75.
- McKay, G. & Al-Duri, B. (1989) Prediction of Multicomponent Adsorption Equilibrium Data using Empirical Correlations. *Chem. Eng. J.*, 41, 9.
- McKay, G., Otterburn, M. S. & Sweeney, A. G. (1980) The removal of colour from effluents using various adsorbents – IV silica. Equilibria and column studies. *Water Res.*, 14, 21-37.
- McKay, G. (1996) *Use of Adsorbents for the Removal of Pollutants from Wastewaters*. CRC Press, Inc., Florida.
- McKinnon, R. J. & Dyksen, J. E. (1984) *J. Amer. Water Works Assoc.* 76, 42.
- Meijers, A. P., *et al.* (1979) *J. Amer. Water Works Assoc.* 71, 628.
- Metcalf & Eddy, Inc. (1991) *Wastewater Engineering. Treatment, Disposal and Reuse*. Revised by Tchobanoglous, G & Burton, F. L. 3<sup>rd</sup> edn. McGraw – Hill Inc. New York. pp. 315 – 329.
- Meunier, F., Guilleminot, J. J., Gurgel, M., Paye, G. & Pons, M. (1986) *Solar Powered Refrigeration Using Intermittent Solid Adsorption Cycles*. Internal paper, Campus Universitaire, Orsay, France.
- Miller, G. W., *et al.* (1980) Large-Scale Applications of Granular Activated Carbon with Ozone Pretreatment, Chapter 13 in *Activated Carbon Adsorption of Organics from the Aqueous Phase*, Vol. 2. McGuire, M. J. & Suffet, I. H. eds. Ann Arbor Science Publishers, Ann Arbor, Mich., p. 323.
- Mochida, I., Mizojiri, N., Fujitsu, H., Komatsubara, Y. & Ida, S. (1985) *Nippon Kagaku Kaishi*, 9, 1676.

- Molina-Sabio, M., Perez, V. & Rodriguez-Reinoso, F. (1994) Impregnation of activated carbon with chromium and copper salts: Effect of porosity and metal content. *Carbon*, 32, 7, pp. 1259-1265.
- Molina Sabio, M., Salinas-Matinez De Lecea, C., Rodriguez-Reinoso, F., Puente-Rutz, C. & Linares Solano, A. (1985) A comparison of different tests to evaluate the apparent surface area of activated carbons, *Carbon*, Vol. 23, No. 1, pp. 91-96.
- Moore, R. H. (1974) United States Atomic Energy Commission. U. S. Patent, 3848048, Nov. 12.
- Moreno-Castilla, C. & Rivera-Utrilla, J. (1995) Adsorption of some substituted phenols on activated carbons from a bituminous coal, *Carbon*, Vol. 33, No. 6, pp. 845-851.
- Morrison, R. T. & Boyd, R. N. (1983) *Organic Chemistry*, Fourth edition. Allyn and Bacon Inc., Boston, MA.
- Nemerow, N. L. & Dasgupta, A. (1991) *Industrial and Hazardous Waste Treatment*, Van Nostrand Reinhold, New York.
- Netzer, A. & Hughes, D. E. (1984) *Water Res.* 18, 927.
- Nishino, A. (1996) *J. Pow. Sourc.*, 60, pp. 137-147.
- Nouri, S. & Haghseresht, F. (2004) Adsorption of *p*-nitrophenol in Untreated and Treated Activated Carbon. *Adsorption*, 10, 1, pp. 79-86.
- Nuñez, L. & Kaminski, M. D. (1998) Magnetically Assisted Chemical Separation Process. *Filtration and Separation*, May, pp 349-352
- Oda, H., Kishida, M. & Yokokawa, C. (1981) *Carbon*, 19, 243.
- Oliveira, L. C. A., Rios, R. V. R. A., Fabris, J. D., Garg, V., Sapag, K. & Lago, R. M. (2002) Activated carbon/iron oxide magnetic composites for the adsorption of contaminants in water. *Carbon*, 40, 2177-2183.
- Oliveira, L. C. A., Rios, R. V. R. A., Fabris, J. D. & Lago, R. M. (2004) A Simple Preparation of Magnetic Composites for the Adsorption of Water Contaminants, *J. Chem. Educ.*, Vol. 81, No. 2, pp. 248-250.
- Okabe, T., Saito, K. & Hokkirigawa, K. (1996) *J. Porous Mater.* 2, 221.

- Orbell, J. D., Godhino, L., Bigger, S. W., Nguyen, T. M. & Ngeh, L. N. (1997) *J. Chem. Educ.*, 74, pp. 1446-1452.
- Paneth, F. & Radu, A. (1924) *Ber.Dsch. Chem. Ges.* B57, 1221.
- Peel, R. G. & Benedek, A. (1980) *Environ. Sci. Technol.* 14, 66.
- Peel, R. G., Benedek, A. & Crow, C. M. (1981) A Branched Pore Kinetic Model for Activated Carbon Adsorption, *AIChE J.*, 27(1), 26.
- Plank, R. & Kuprianoff, J. (1960) In *Die Kleinkaltemaschine*. Springer-Verlag. Berlin/Gottingen/Heidelberg.
- Pons, M. & Grenier, P. H. (1985) *Solar Ice Maker Working with an Activated Carbon – Methanol Adsorbent – Adsorbate Pair*. INTERSOL 85, Proc. ISES Conf. Pergamon, New York.
- Process Design Manual for Carbon Adsorption*. (1971) U.S. EPA, Technology Transfer, Programme 17020 GNR. Washington D.C.
- Puri B. R., Singh, D. D. & Sharma, L. R. (1958) *J. Phys. Chem.*, 62, 756.
- Puri, B. R. (1966) *Carbon* 4, 391.
- Puri, B.R. (1983) *Physicochemical aspects of carbon affecting adsorption from the aqueous phase. Treatment of water by granular activated carbon. Advances in chemistry series 202*. American chemical society, Washington D. C.
- Puri, B. R., Bhardwaj, S. S. & Gupta, U. (1976) *J. Indian Chem. Soc.*, 53, 1095.
- Rao, M. B. & Sircar, S. J. (1993) *Membrane Sci.* 85, 253.
- Rebstein, P. & Stoeckli, H. F. (1992) *Carbon*, 30 747-750.
- Reid, M. S. (1985) Ethylene in post-harvest technology, in A. Kadar (ed.) *Postharvest Technology of horticultural Crops*. Oakland: University of California.
- Resnick, H. & Walker, P. (1997) *Fundamentals of Physics*, Fifth Edition, John Wiley & Sons Inc, New York, NY.
- Rialdi, G. (1977) British patent, 1, 570, 801.
- Rice, R. G., *et al.* (1978) A Review of the Status of Preozonation of Granular Activated Carbon for Removal of Dissolved Organics and Ammonia from Water and Wastewater, Chapter 14 in *Carbon Adsorption Handbook*. Cheremisinoff, P. N. & Ellerbusch, F eds. Ann Arbor Science Publishers, Ann Arbor, Mich., p. 485.
- Roberts, A. R., Sing, K. S. W. & Tripathy, V. (1987) *Langmuir*, 3, 331.

- Robert, C. M. (1987) Evaluating the Cost and Performance of Field-Scale Granular Activated Carbon Systems. *Environmental Science and Technology*, Vol. 21, pp 573-80.
- Robert, P. & Don, G. (1997) *Perry's Chemical Engineering Handbook*, Seventh Edition, McGraw-Hill, New York, NY.
- Rodgers, S. J., Udavcak, R. J. & Mausteller, J. W. (1965) International Symp. Fission Product Release Transport Accident Conditions, Tennessee.
- Rudisill, F. N., Haeskaylo, J. J. & Levan, M. D. (1992) *I & EC Res.* 31, 1122.
- Ruthven, D. M. (1984) Principles of Adsorption and Adsorption Processes. John Wiley & Sons, New York.
- Safarik, I., Safarikova, M. & Buricova, V. (1995) *Collection*, 60, pp. 1448-1456.
- Sakoda, A., Kawazoe, K. & Suzuki, M. (1987) *Water Research* 21, 717.
- Sakoda, A., Suzuki, M., Hirai, R. & Kawazoe, K. (1991) *Water Research* 25, 219.
- Samaras, P., Diamadopoulose, E. & Sakellaropoulose, G. P. (1995) *Water Quality Res. J. Canada*, 30, 325.
- Schwertmann, U. & Cornell, R. M. (2000) Iron Oxides in the Laboratory. Preparation and Characterization. 2<sup>nd</sup> edition. Wiley-VCH. p. 188.
- Shull, R. D., Ritter, J. J., Shapiro, A. J., Swartzendruder, L. J. & Bennet, L. H. (1990) *J. Appl. Phys.*, 67 (9).
- Sinha, R. K. & Walker, P. (1972) *Carbon*, 10 754-756.
- Sing, K. S.W (1994) *Technology Profile, Ground Water Monitor*, 21, pp. 60-67.
- Sing, K. S. W. (1995) *J. Porous Mater.* Vol. 2, No.9.
- Sips, R. (1948) *J. Chem. Phys.* 16, 490.
- Sircar, S., Golden, T. C. & Rao, M. B. (1996) Activated carbon for gas separation and storage. *Carbon*, Vol. 34, No. 1, 1.
- Smith, A. (1863) *Proc. Royal Soc. (London)* A12, 424.
- Smith, J. M. (1968) Kinetics of Adsorption, Chapter 2 in *Adsorption from Aqueous Solution*. Advances in Chemistry Series 79. American Chemical Society, Washington, D.C.
- Snoeyink, V. L., *et al.* (1969) *Environ. Sci. Technol.* 3, 918.
- Solar, J. M., Leon y Leon, C. A., Osseo-Asare, K. & Radovic, L. R. (1987) *Carbon*, 25, 569

- Standard Oil Development Co. (1952) U. S. Patent, 2, 609, 882.
- Stanley, C. G. (1988) *The Extractive Metallurgy of Gold in South Africa*, Vol. 1 & 2, SAIMM / Chamber of Mines of South Africa.
- Steenberg, B. (1944) *Adsorption and Exchange of Ions on Activated charcoal*. Almqvist and Wiksells, Uppsala, Sweden.
- Studebaker, M. L. (1957) *Rubber Chem. Technol.* 30, 1400.
- Streat, M., Patrick, J. W. & Perez, M. J. C. (1995) *J. Water Res.*, 29, 467.
- Summers, R. S. & Roberts, P. V. (1983) Dynamic Behavior of Organics in Full-Scale Granular Activated Columns, Chapter 22 in *Treatment of Water by Granular Activated Carbon*. McGuire, M. J. & Suffet, I. H. eds. Advances in Chemistry Series 202. American Chemical Society, Washington, D. C., p. 503.
- Suzuki, M. (1994) Activated Carbon Fiber: Fundamentals and Applications. *Carbon*, Vol. 32, No. 4, 577.
- Symons, J. M., Stevens, A. A., Clark, R. M., Geldreich, E. E., Love, Jr., O. T. & DeMarco, J. (1981) Treatment techniques for controlling trihalomethanes in drinking water. *EPA-600/2-81-156*, Environmental Protection Agency, Cincinnati, OH.
- Sze, S. M. (1985) *Semiconductor Devices- Physics and Technology*, Wiley & Sons.
- Tanada, S., Nakamura, T., Xiaohong, M., Higuchi, T. & Shmoda. S. (1992) *International Contamination and Toxicology* 49, 112.
- Tanju, K., Schlautman, M. A., Kilduff, J. E. & Weber, W.J., Jr. (1996) Adsorption of Organic Macromolecules by Granular Activated Carbon: 2. The Influence of Dissolved Oxygen, *Environmental Science and Technology*, 30, 2195-2201.
- Tremblay, G: Vsotola, F.T. & Walker, P. L. Jr, (1978), *Carbon* 16, p.31.
- Tidjani, M., Lachter, J., Kabre, T. S. & Bragg, R. H. (1986) Structural disorder induced in graphite by grinding. *Carbon*, Vol. 24. No. 4.
- Usmani, T. H., Ahmed, T. W. & Ahmed, S. Z. (1996) Preparation and characterization of activated carbon from a low rank coal. *Carbon*, Vol. 34, No.1. pp. 77-82.
- U. S. AEC. (1967) U. S. Patent, 3, 356, 586.
- Valenzuela, R. (1994) Magnetic Ceramics. In *Chemistry of Solid State Materials*. Cambridge University Press.
- Vogel, A. I. (1939) *A text book of quantitative inorganic analysis; theory and practice*, Longman, Green & Co., New York.

- von Kienle, H. & Bader, E. (1980) *Enke-Verlag*, Stuttgart 100-116.
- Wagner, N. J. & Jula. R. J. (1981) Chapter 3 in *Activated Carbon Adsorption for Wastewater Treatment*, Edited by Jerry R. Perrich. CRC press, Florida.
- Walker, P. L. Jr., Cariaso, O. & Patel, R. L. (1968) *Fuel*, 47, 322.
- Walker, P. L., Jr. (1970) *Chemistry and Physics of Carbon*, Vol. 6, p. 246. Marcel Dekker, New York.
- Walker, P. L. Jr., Carioso, O. L & Ismail, I. M. K. (1979), *Carbon* 18, p. 377.
- Water Quality and Treatment*. (1971) 3<sup>rd</sup> ed. American Water Works Association, Denver.
- Wheeler, A. (1951) *Advan. Catal.*, 3, 250.
- Wellen, C. W., Stephens, D. K. & Wellen, G. R. (1997) Method of producing activated carbon. US Patent # 5,858,911.
- Weber, W. J., Jr., *et al.* (1980) Potential Mechanisms for Removal of Humic Acids from Water by Activated Carbon, Chapter 16 in *Activated Carbon Adsorption of Organics from the Aqueous Phase*, Vol. 1. Suffet, I. H. & McGuire, M. J, eds. Ann Arbor Science Publishers, Ann Arbor, Mich.
- Weber, W. J., Jr. (1967) Sorption from Solution by Porous Carbon, Chapter 5 in *Principles and Applications of Water Chemistry*. Faust, S. D. & Hunter, J. V. eds. John Wiley & Sons, New York.
- Weber, W. J. Jr. & Morris, J.C. (1962) Advances in water pollution research. *Proc. 1<sup>st</sup> Int. Conf. on Water Pollut. Res.*, Vol. 2, 231, Pergamon Press, Oxford.
- Weber, W. J., Jr. & Morris, J. C. (1963) *J. Sanit. Eng. Div. ASCE SA2*, 31.
- Weber, W. J., Jr. & Rumer, R. R., Jr. (1965) *Water Resources Res.*, 1, 361.
- Weber, W. J., Jr. (1967) *Sorption from solution by porous carbon. Chapter 5 in Principles and applications of water chemistry*. S. D. Faust and J. V. Hunter, eds. John Wiley & Sons, New York.
- Weber, W. J., Jr. (1972) *Physicochemical Processes for Water Quality Control*, Wiley-Intersciences, New York.
- Young, D. M., & Crowell, A. D. (1962) *Physical Adsorption of Gases*. Butterworths, London.
- Yugov, V. A. (1957) Russian Patent, 104, 838.

G8970

Zogorski, J. S. (1975) The Adsorption of Phenols onto Granular Activated Carbons from Aqueous Solutions. Ph.D dissertation, Rutgers University, Department of Environmental Science, New Brunswick, N. J.

Zogorski, J. S. *et al.* (1976) *J. Colloid Interf. Sci.* 55, 329.

